A Functional Magnetic Resonance Imaging Study Evaluating the Effects of Intranasal Insulin on Food Related Reward and Appetite

Wingrove, Jed Oliver

Awarding institution:
King's College London

A Functional Magnetic Resonance Imaging Study Evaluating the Effects of Intranasal Insulin on Food Related Reward and Appetite

Jed Wingrove

Thesis submitted to King's College London for the degree of Doctor of Philosophy in Neuroimaging
2018

Acknowledgements

I would like to thank all the participants that took part in this study. Without your time and co-operation this research could not have been performed. With this in mind I would like to extend my gratitude to the radiography team at the centre for neuroimaging sciences as well as all the administration staff who supported and facilitated this neuroimaging study. I must acknowledge my funders; the engineering and physical sciences research council (EPSRC) and Unilever UK for providing funds for my PhD studentship, the neuroimaging experiments and a generous travel allowance for international conferences. I would like to thank Dr Louise Brown from Unilever for sourcing additional funds for aspects of the study and for your help during the study design phase of this PhD.

A massive thanks has to be extended to Steph and Ndaba for helping me with the clinical aspects of this study. Your wealth of experience in running pharmacological research studies was immeasurably helpful. I have gained a considerable amount of knowledge and developed a great number of clinical skills from both of you. In terms of practical clinical support, I must also thank Andy Pernet, Dr Meera Lawda and Dr Muna Nwokolo from the diabetes research team for your time supervising me and also taking blood samples during the early scanning sessions. Furthermore, would like to thank Dr Pratik Choudhary and Dr Yee Cheah for their valuable input and pragmatic discussions during research meetings.

I am grateful to be surrounded by such a great group of people and am fortunate to say that I really enjoyed my time during this PhD at the centre for neuroimaging sciences. This is mainly because of my colleagues Amanda, Vasileia, Pete and Will who have helped keep the work life enjoyable throughout my time and provided the necessary distractions and laughs needed along the way.

I am thankful to Dr Owen O'Daly for being selfless in his efforts to pass on his fMRI analysis wisdom and to go above and beyond to help me with my data analysis. I

must thank Professor Ben Forbes, Dr Magda Swedrowska, Glynis Ivin and Martin Heasman for all their help in sourcing the nasal pumps, insulin formulation and distribution of study drugs, if it wasn't for you this study could not have been conducted.

I want to thank my two fantastic supervisors. Firstly, Dr Fernando Zelaya, who provided an environment with the perfect amount of support and guidance to bring the best elements out of my work. I truly appreciate our daily discussions, the friendship that we have developed and how you have always been there for me throughout this process. Secondly, Professor Stephanie Amiel for inviting me into the diabetes research team and developing me as a researcher in this field. I thoroughly enjoyed our discussions, and your excitement and passion for research has really motivated me throughout my time. Thank you both.

Finally, I would like to thank my committed partner, Sophie. This PhD has had its many challenges along the way and I can't thank you enough for your continual support, sacrifice and love. I am grateful for your patience and how you always made sure I was mentally and physically healthy through the tough, and what seemed like never ending, data collection and writing stages. I want to thank you for initiating insightful and critical discussions which have helped to keep me grounded and present throughout this entire experience. Thank you.

Abstract

Central insulin resistance is common to both Type 2 Diabetes and Obesity. Magnetic resonance imaging (MRI) studies that investigated the effects of intranasally administered insulin, have highlighted the involvement of insulin in homeostatic, hedonic and to a lesser extent cognitive regulation of appetite control.

This thesis documents a study that set out to explore the effects of intranasal insulin on brain function, using a pharmacological MRI protocol that probed the effects of insulin on resting state connectivity, resting state cerebral perfusion and the cerebral reward response to a food administration paradigm. This study was conducted in a group of healthy, male individuals, with normal and overweight participants. A drug delivery device optimised for efficient nasal delivery of insulin, was employed.

A customised, long-label pseudo continuous arterial spin labelling sequence was employed. It was shown that intranasal insulin leads to decreases in cerebral blood flow in the left insula, putamen, hippocampus and para-hippocampal gyrus. These decreases were limited to the overweight group. Furthermore, both hippocampal and putamen blood flow responses in the overweight group were associated with their dietary intake of saturated fat and sugar.

Functional, blood oxygen level dependent (BOLD) images acquired during a paradigm in which participants received glucose and artificial sugar solutions, highlighted group differences in response to intranasal insulin in prefrontal, cognitive regions of brain. The normal weight individuals showed greater engagement of the anterior cingulate cortex, ventromedial prefrontal cortex and nucleus accumbens compared to overweight individuals when presented with conditioned stimuli for sweet tasting rewards.

Resting state connectivity data was acquired with a novel, multi-echo pulse sequence, developed to minimise artefactual sources of temporal variance. A seed-

based connectivity analysis showed that connectivity between the left posterior hippocampus and the left fusiform gyrus was increased in response to intranasal insulin in normal weight individuals. Furthermore, normal weight group connectivity between the left posterior hippocampus and prefrontal regions was increased compared to overweight individuals following insulin administration.

The results from this pharmacological MRI study indicate differential insulin responsiveness in normal weight and overweight individuals. These differences in responsiveness show changes in brain function as a result of increased weight in otherwise healthy individuals. This work adds to a large body of knowledge on central insulin signalling and has provided further supporting evidence of the involvement of insulin in the cognitive modulation of appetite control.

Personal contribution

This thesis reports a pharmacological magnetic resonance imaging (MRI) study to observe the effects of insulin, administered intra-nasally, using a combination of functional imaging methodologies. After obtaining Good Clinical Practice accreditation I, with assistance from my supervisor's Dr Zelaya and Prof Amiel, wrote to the MHRA to obtain confirmation that the study was not classed as a clinical trial of a medicinal product. Following confirmation, I wrote an ethics application for this study, which was approved. All aspects of this study protocol were designed by me with assistance and reassurance from both supervisors. Alongside engineers and software technicians at the Centre for Neuroimaging Sciences a functional paradigm that delivers small amounts of liquid to the participants mouth whilst in the scanner was developed and optimised for this particular study which filled a large portion of the scanning time and also forms a large part of this thesis.

In terms of the practical procedures performed throughout the study, I recruited and screened every potential participant. At the start of the study I underwent a practical phlebotomy course in order to perform blood sampling using venepuncture techniques. For the early experimental sessions, I received assistance from members of the Diabetes team and also the centre for neuroimaging sciences clinical team with taking blood samples. Once competent in bloodletting I then carried out the blood sample collection protocol individually. I set up and ran all the imaging required stimuli and paradigms from the control room of the MRI console room, whilst the centre for neuroimaging sciences radiographers prescribed and acquired the MR data.

All data was analysed by myself, with some supervision and guidance from my supervisors. All interpretations are my own and this thesis was written and produced by myself.

Conference Presentations

Drug Delivery to the Lungs, International Meeting, Edinburgh, 2017

- Pat Burnell New Investigator Award Nominee – Oral Presentation, Traditional Poster - **Characterisation of a Human Nasal Pump for Nose to Brain Delivery of Insulin**. *JO Wingrove, M Swedrowska, M Parry, M Ramjeeawon, D Taylor, G Gauthier, L Brown, S Amiel, FO Zelaya and B Forbes.*

International Society for Magnetic Resonance in Medicine

- International Meeting, Paris, 2018 – Poster – **Evaluation of the Suitability of Hadamard Encoding Schemes for Pseudo-Continuous Arterial Spin Labelling.** *JO Wingrove, M Lebel and FO Zelaya.*

- International Meeting, Honolulu, 2017 – Traditional Poster – **Less may be better: comparison of Multi-Echo-ICA for denoising for three and four echo EPI acquisitions.** *JO Wingrove, O O'Daly and FO Zelaya.*

- International Meeting, Honolulu, 2017 – Electronic Poster – **Identification of BOLD and non-BOLD components using Multi-Echo ICA analysis: is native space better than MNI space?** *JO Wingrove, O O'Daly and FO Zelaya.*

- International Meeting, Singapore, 2016 – Electronic Poster – **Single vs Multi-Echo EPI: a head to head, within session crossover comparison for task evoked and seed-based connectivity analysis.** *JO Wingrove, S Wastling, P Kundu, O O'Daly and FO Zelaya.*

- British Chapter Meeting, UCL, 2016 – Oral Presentation – **High resolution arterial spin labelling combined with long duration labelling pulses**. *JO Wingrove, O O'Daly, M Lebel and FO Zelaya*.

Table of Contents

Table of Figures

Table of Tables

Chapter 1 The role of cerebral insulin in the modulation of food intake: investigations using imaging methods

This introductory chapter will outline the basis for the aims of my investigation and the experimental procedures conducted and presented within this thesis. Throughout this introduction the reader will be given sufficient information with which to understand the reasons for conducting this research and also the reasons for implementing certain methodologies and protocols. Following this introductory chapter, the reader will be guided through the main methods implemented in the study, along with their relevant supporting theories. Then the experimental design and protocol will be described in detail with reference to the rationale and reasoning behind why and how the protocol was created. Following these three chapters (introduction, methods and study design) the five main experimental chapters and their results will be presented. Each chapter will contain introduction, methods, results and discussion sections. The final chapter within this thesis will present a summary and discussion of the main findings of each chapter, methodological considerations, suggestions for future work and final conclusions.

1.1 Type 2 Diabetes Mellitus

Type 2 diabetes mellitus (T2DM) is major global health concern, and has been described as one of the "major challenges to human health in the 21st century" (Unnikrishnan et al. 2017). T2DM is a metabolic disorder characterised by high blood sugar levels and poor blood sugar regulation. Initially considered a 'western population' disease, T2DM has reached global pandemic status, with widespread prevalence in emerging economies in continents such as Asia, Africa and Latin America (Unnikrishnan et al. 2017). In 2017, approximately 425 million people worldwide suffered from diabetes and this number is set to increase to 629 million by 2045 (Atlas 2017). The prevalence and development of T2DM continues to grow due to the combination of a sedentary lifestyle and overconsumption of energy dense foods that are high in saturated fat and processed carbohydrates. The risk of developing T2DM is associated with a number of other factors; genetic and epigenetic (Poulsen et al. 1999), smoking and alcohol consumption (Manson et al. 2000; Cullmann, Hilding, and Ostenson 2012) and obesity; rendering T2DM a multi-factorial and highly complex disorder. T2DM causes increased risk of cardiovascular disease morbidity and mortality (Martín-Timón et al. 2014), microvascular effects that can lead to blindness and neuropathic pain (Fowler 2008), cognitive dysfunction and Alzheimer's Disease (AD) (Sridhar, Lakshmi, and Nagamani 2015) and some cancers (liver, pancreatic) (Giovannucci et al. 2010).

1.2 Obesity

Obesity is characterised and defined by a disproportionate body weight to height ratio that is coupled with accumulation of adipose (fat) tissue. Obesity is usually assessed by anthropometric measures such as body mass index (BMI) that uses the ratio between body mass and the square of the height. A BMI between 25-29.9 kg/m^2 classifies people as overweight and a BMI greater than 30 kg/m^2 classifies subjects as obese. (Normal weight BMI = 18.5 – 24.9 kg/m^2). More than 2 billion people

worldwide are classified as overweight or obese based on BMI (Gonzalez-Muniesa et al. 2017). Obesity is a complex disorder that is often accompanied by systemic inflammation and increased risk for development of T2DM, some cancers (Renehan et al. 2010), cardiovascular disease (Nordestgaard et al. 2012), cognitive impairments (Jauch-Chara and Oltmanns 2014) and mood impairments and is also a significant economic burden (Renehan et al. 2010; Nordestgaard et al. 2012; Wang, McPherson, et al. 2011; Jauch-Chara and Oltmanns 2014). In very simplistic terms, the increased fat deposition seen in obese individuals results from an imbalance between energy intake (in the form of calories); and energy expenditure. This difference is known as the 'energy balance'. In light of this simplistic view, obesity is a result of chronic increased food intake coupled with low physical activity.

The rise of T2DM and obesity during the 'modern' age is primarily a product of the changes in lifestyle and diet that have accompanied modern civilisation. Originally seen as western diseases, T2DM and obesity continue to affect countries in growing economies and even within tribal communities, for example the aboriginal natives of Australasia. The environment we live in is changing at an exponential rate, a rate much faster than genetics and physiology are capable of. The introduction of automation and technology has revolutionised the capabilities of knowledge and technical efficiency, but at a cost of a decrease in physical activity and health. The diet of the modern age has changed considerably from originally consisting of unrefined whole foods to an increase in cheap and highly accessible processed foods high in saturated fats and carbohydrates. Common to T2DM and obesity and their related diseases and disorders is dysregulation of insulin and the pathways and mechanisms that insulin determines.

1.3 Insulin

In 1869, Paul Langerhans, a German anatomy student explored the anatomy of the pancreas and described “islands of clear cells” that populated this organ. These clusters/islands of clear cells are now known as “the Islets of Langerhans” and were later found to be responsible for the endocrine properties of the pancreas (Baskin 2015). The islets boast a highly efficient vascular system and are also innervated by autonomic nerve fibres and terminals, that contain neurotransmitters such as acetyl choline and noradrenaline. Each islet consists of a mixture of cell types, the main types being the insulin secreting beta cells and the glucagon secreting alpha cells (Cabrera et al. 2006).

Insulin is a small peptide hormone produced and released into the bloodstream by the beta cells of the pancreatic islets of Langerhans. The beta cell functions to both store as well as produce and secrete insulin into the peripheral circulatory system, where it acts to lower blood glucose concentration (Roder et al. 2016). The beta cells are highly specialised to meet the metabolic demands of the body, characterised by rapid insulin release into the bloodstream in response to acute physiological changes (Song et al. 2013). The alpha cells of the islets of Langerhans secrete glucagon, which, in contrast to insulin, increases blood glucose levels (Goke 2008). Through the balanced secretion of both these hormones the pancreas is able to promote and maintain blood glucose concentrations between 4-6 mmol/L in healthy humans (Roder et al. 2016), despite wide fluctuations in energy availability and expenditure, a process known as ‘glucose homeostasis’.

This endocrine system is a key physiological system that requires a finite balance of hormone release in order to achieve tightly controlled glucose homeostasis. The following sections will focus on insulin’s role in this process, its functions within the brain; and novel experimental methods that have been implemented to better explore insulin action within the brain.

1.3.1 Insulin release

Insulin is secreted into the circulation from the pancreas in response to circulating metabolites (predominantly glucose) but can also be regulated by changes in other peripheral hormone species and fatty acids (Fu, Gilbert, and Liu 2013). An elevation in blood glucose concentration is known as *hyperglycaemia* and a low blood glucose concentration is known as *hypoglycaemia*. The beta cells of the pancreas are equipped to sense changes in physiological levels of glucose in the blood and to respond by releasing appropriate amounts of insulin in order to reach and maintain *normoglycemia (euglycemia)*, a state of normal blood glucose concentration.

During an increase in blood glucose, such as after a mixed meal (postprandial state), the glucose molecules enter the pancreatic beta cells via glucose transporters (GLUT-1,2 and 3) along a concentration gradient (Richardson et al. 2007). Inside the beta cell, the glucose is phosphorylated by glucokinase, which acts as a glucose sensor and controls the subsequent release of insulin. Glucokinase is also found in the liver as well as the hypothalamus where it plays a role in hepatic glucose metabolism and top down control of glucose intake, respectively (Massa, Gagliardino, and Francini 2011; Hussain et al. 2015). Insulin release in response to these glucose concentrations displays a biphasic profile: a rapid, but transient initial phase shortly followed by a more prolonged second phase (Caumo and Luzi 2004). The initial phase peaks approximately five minutes after pancreatic glucose sensing characterised by a large insulin burst, and the second phase releases the remaining insulin (Roder et al. 2016). The instantaneous availability of insulin is permitted through the recruitment of insulin storage vesicles close to the plasma membrane which are pivotal to the speed at which insulin can be secreted upon stimulation.

1.3.2 Peripheral insulin effects

The insulin receptor belongs to the tyrosine kinase family of receptors and is found on the plasma membrane of the target cells within the insulin-responsive tissue types. The main sites of insulin action comprise skeletal muscle, adipose tissue and the liver (Fulop, Larbi, and Douziech 2003). A major anabolic role of insulin in the body is to regulate and maintain normal blood glucose levels by promoting cellular blood glucose extraction, glucose oxidation and energy storage in skeletal muscle and adipose tissue (Wilcox 2005). The rate of glucose uptake into these cell types is dependent on the quantity of glucose transporters, predominantly glucose transporter type 4 (GLUT-4), present on the cell surface (Kido, Nakae, and Accili 2001). Insulin signalling at the cell surface, via the insulin receptor, and subsequent downstream interactions stimulates the translocation of GLUT-4 from the cytoplasm to the cell surface, thus rendering skeletal and adipose tissue glucose uptake, insulin dependent (Chang, Chiang, and Saltiel 2004). In the liver, GLUT2 is the predominant glucose transporter, and is not insulin responsive. Insulin acts within the liver where it stimulates glycogen synthase and inhibits glycogen phosphorylase, promoting glucose storage in the form of glycogen and inhibition of glycogenolysis, respectively (Rui 2014). The combination of these effects is key to glucose homeostasis and underpins the anabolic effects of insulin.

Aside from glucose stimulated insulin release, the release of pancreatic insulin is sensitive to other external factors. For example, the gut hormone glucagon-like peptide-1 (GLP-1), which is secreted in response to fructose, free fatty acid and glucose ingestion, potentiates pancreatic insulin release (incretin effect) (Kreymann et al. 1987).

1.4 Insulin Resistance

Peripheral insulin resistance is defined as a pathological state in which the ability of insulin to produce its homeostatic effects on normal circulating glucose concentrations is reduced (Sears et al. 2009). In other words, peripheral insulin resistance is an impairment in the ability of insulin to control hepatic glucose output or to maintain uptake of glucose into peripheral target tissues. Insulin resistance refers to an inefficient peripheral response to insulin, thus requiring a greater concentration of circulating insulin to extract glucose from the blood into the liver and muscle cells. This inefficiency leads to a prolongation of the second phase pancreatic insulin release which, over time, significantly strains the islet beta cells of the pancreas. Insulin resistance precedes the development of T2DM and obesity and contributes to many of the complications associated with other metabolic diseases, such as the metabolic syndrome (Stears et al. 2012). Insulin resistance is a major risk factor for cardiovascular disease (Trevisan et al. 1998) and is known to contribute to accelerated ageing (Ryan 2000).

The complexities of both T2DM and obesity are associated with similar dysfunctions in the brain and therefore the action of insulin in the brain has been explored in depth to understand the central impairments common to both these disorders.

1.5 Insulin in the Brain

For a long time the brain was considered to be an insulin “insensitive” organ (Gray, Meijer, and Barrett 2014). The brain relies predominantly on glucose as a fuel source, with the adult human brain, which accounts for only 2% of total body weight, consuming roughly 20% of the body’s total glucose and oxygen content (Mergenthaler et al. 2013). Glucose, as in the majority of cell types, is metabolised in neurons and glial cells to produce adenosine tri-phosphate (ATP), the basis of cellular maintenance and energy for neuronal function (Erbsloh, Bernsmeier, and Hillesheim 1958). As the brain is such an energy demanding organ, there are requirements for a

constant glucose supply which is facilitated by the selective permeability of glucose through the blood brain barrier (BBB) (Mergenthaler et al. 2013). Blood glucose passes through plasma membrane GLUT-1 transporters along a concentration gradient into the extracellular fluid of the central nervous system (CNS). Once here, cell specific uptake is facilitated by GLUT-3 transporters for neuronal and GLUT-1 for glial and endothelial cell uptake, respectively (Ghasemi et al. 2013). These transporters, unlike GLUT-4, do not require insulin to initiate uptake and therefore glucose uptake within the majority of brain tissue cells can be classified as insulin-independent. However insulin receptors do exist within the brain and may have a different role in the brain in comparison to its actions of peripheral tissue target sites (Plum, Schubert, and Brüning 2005).

1.5.1 Insulin receptor distribution

In humans, insulin receptors are found on neurons within the hypothalamus, amygdala, hippocampus, cerebellum and maintain the highest density within the olfactory bulb (Schulingkamp et al. 2000). Insulin action within the brain is regionally dependent and is involved in a number of key central functions, from metabolism, memory and mood to appetite control (Heni et al. 2015; Kullmann et al. 2013; Kullmann, Heni, Veit, Scheffler, Machann, Häring, et al. 2015; Guthoff et al. 2010; Kroemer et al. 2013; Winocur, Moscovitch, and Bontempi 2010).

1.5.2 Insulin transport to the brain tissue

Circulating insulin enters the CNS via a saturable receptor-mediated transport mechanism across the blood-brain barrier (BBB) into the cerebrospinal fluid and interstitial fluid compartment (Blázquez et al. 2014). Measuring this concentration of insulin within the central nervous system (CNS) is not straightforward, however, estimations in cerebrospinal fluid (CSF) can be used as a surrogate measure (Banks, Owen, and Erickson 2012; Wallum et al. 1987). CSF insulin concentrations are considerably lower than those measured from the peripheral circulation but show proportional rises following a meal or with peripheral insulin infusion (Kleinridders et

al. 2014). The rate of insulin transport across the BBB shows regional variation with greatest BBB transport rates occurring in the olfactory bulb (Banks, Kastin, and Pan 1999). It is also known that some regions of the brain have an inherent reduction in BBB integrity, such as the hypothalamus, that renders these regions 'leaky' thus permitting greater BBB transport of insulin across the BBB (Kleinridders et al. 2013). In people with obesity and AD, reduced insulin transport into the CSF has been demonstrated, resulting in decreased concentrations of centrally available insulin and subsequent reductions in central insulin signalling (Kern et al. 2006; Craft et al. 1998). Impaired brain insulin signalling is known as *central insulin resistance*, a physiological state that has been observed alongside peripheral insulin resistance (Heni, Schöpfer, et al. 2014). Transport of insulin into the brain decreases with age (Sartorius et al. 2015) and an association between increased dietary fat intake and reduced CNS insulin uptake has been observed in dogs maintained on a high fat diet for seven weeks (Kaiyala et al. 2000). The exact mechanism behind this disrupted transport across the BBB is not fully elucidated although some have suggested that this impairment is thought to occur due to fatty deposits lining the cerebral vasculature, physically blocking transport across the BBB (Kullmann, Heni, Veit, Scheffler, Machann, Häring, et al. 2015).

1.5.3 Brain insulin resistance

Much like the description of peripheral insulin resistance, central insulin resistance can be defined as the failure of brain cells to respond to insulin (Mielke et al. 2005).

1.5.3.1 *In utero*

As central insulin resistance is largely associated with peripheral insulin resistance, some of the causes may be considered common to both types. Studies have shown the link between *in utero* development of brain insulin resistance in fetuses of insulin resistant mothers (Linder et al. 2014; Linder et al. 2015). These studies showed that administration of an oral glucose solution (the oral glucose tolerance test) in insulin-

resistant mothers led to a slower fetal post-glucose brain response in comparison to insulin-sensitive mothers (Linder et al. 2014; Linder et al. 2015).

1.5.3.2 Diet

Saturated fat intake is associated with a decrease in brain insulin sensitivity seen from rodent experiments focused on the amygdala (Boghossian et al. 2009; Oh et al. 2013). These studies showed that intracerebroventricular (ICV) injection of insulin to the amygdala leads to a significant reduction in food intake in wild type rats. These animals showed reduced amygdala responsivity to ICV insulin injections after just 3 days of a high fat diet, which was not coupled with significant changes in peripheral insulin sensitivity (Boghossian et al. 2009). Interestingly, this amygdala specific central resistance could be reversed upon switching to a low fat diet, and the rate at which sensitivity could be regained was dependent on the duration of the initial high fat diet (Boghossian et al. 2009).

1.5.4 Increasing insulin concentrations in the brain

To understand the effects of insulin resistance in the brain, it is necessary to discuss, firstly, the actions of insulin in the brain and secondly, to what extent these actions are dysregulated in those with central insulin resistance. To this end, explorations of insulin action in the brain have relied upon increasing insulin concentrations in the brain, which can be achieved by modulating endogenous pancreatic release or by increasing exogenous insulin concentrations. The common methods used are presented in Table 1.5.1.

Methods for increasing peripheral and brain insulin concentration	
Method	**Brief description**
Mixed meal tolerance test	Consumption of a defined meal of different nutrients stimulates pancreatic insulin production ✓ similar reaction to that witnessed in 'real-life' ✗ Initiates a complex cascade of reactions and gustatory hormones to be released, therefore unable to dissociate insulin effects.
Oral Glucose Tolerance test (oGTT)	Oral consumption of 75g of glucose solution, leads to a large rise in blood glucose coupled with a rise in blood endocrine factors, such as insulin, in response to this glycemic increase. ✗ Initiates a complex cascade of reactions and gustatory hormones to be released, therefore unable to dissociate insulin effects.
Intravenous glucose tolerance test	Intravenous glucose bolus leads to a large insulin secretory response ✓ stimulates insulin release without an additional cascade of gustatory hormones ✗ Does not replicate 'real-life' situations
Hyperinsulinemic euglycemic clamp	Intravenous infusion of insulin leads to increased insulin concentrations within the brain and periphery. Requires simultaneous intravenous glucose infusion to maintain normal fasting glucose levels (euglycemia). ✓ Continuous supply of insulin to the brain ✗ Unable to dissociate insulin actions in the brain and periphery

Table 1.5.1 Laboratory methods commonly used to increase insulin concentrations in the periphery and the brain in humans. Light grey rows refer to those methods used to increase pancreatic insulin secretion, whereas the dark grey rows describe methods used to increase exogenous insulin concentrations.

In clinical settings the hyperinsulinemic-euglycemic clamp technique is considered the gold standard method for assessing insulin sensitivity (Kim 2009); and is a useful tool for increasing insulin concentrations whilst avoiding the gustatory response that occurs following a meal ingestion. This clamp technique requires maintaining fasting blood glucose levels (euglycemia) by glucose infusion, and the amount of glucose required to achieve this can be used as a determinant of whole body insulin sensitivity (for example, high glucose = high insulin sensitivity). This method involves intravenous (iv) infusions, making this an invasive technique which, used as a

research tool, is fairly labour intensive. Furthermore, by increasing peripheral and subsequently central insulin concentrations (Kleinridders et al. 2014) simultaneously, dissociating peripheral and central insulin effects becomes unachievable. A recent addition to the repertoire of methods that can be used to increase central insulin concentrations is intranasal administration.

1.6 Intranasal Insulin

Insulin administered via the nasal cavity is a method that permits direct brain administration of insulin, circumventing peripheral blood glucose regulation and control (Henkin 2010). This route bypasses the BBB, by diffusion across the olfactory epithelia into the subarachnoid space (Dhuria, Hanson, and Frey 2010; Spetter and Hallschmid 2015), effectively reaching CSF within 30-60 minutes (Born et al. 2002), increasing CNS insulin concentration without going through the peripheral circulation. This method requires deposition of insulin, either in solution or as a powder aerosol, to the superior-posterior region of the nasal cavity using a nasal spray device. The anatomical pathways and mechanical methods used for this administration technique will be detailed in Chapter 4.

Following Born's seminal study profiling intranasal insulin (IN-INS) kinetics (2002), research in this area has grown substantially in the last decade (Born et al. 2002). The discovery that IN-INS shows beneficial effects on memory and cognition in patients suffering from AD (Benedict et al. 2004; Freiherr et al. 2013; Ott et al. 2012; Spetter and Hallschmid 2015) was a pivotal factor for the growing application of this technique to other basic science and neurophysiological questions. IN-INS is an attractive tool for assessing insulin effects on brain function using functional magnetic resonance imaging (fMRI) (Schilling et al. 2014; Grichisch et al. 2012). A body of behavioural and imaging related published literature has shown a modulatory role of insulin in appetite control and food intake. The next sections will introduce the mechanism involved in the processes of food intake, that extend beyond survival and the detrimental effects that occur as a result of dysregulation of these systems.

1.7 Food Intake and Appetite Control

Appetite control and subsequent food intake are complex multi-faceted functions that combines a range of dynamic, semi-dissociable mechanisms regulated within the brain. The interplay of these systems and mechanisms ultimately control eating behaviour from when food intake will occur, through what constituents the meal will be comprised of and how much will be consumed in the time between the next meal and subsequent meals thereafter. Dysregulation of these systems is likely to lead to poor appetite control, seen from the increased body weight and increased fat mass that is observed in overweight individuals. A long-term positive energy balance (more energy consumed than expended) that may result from poor appetite control is coupled with an increase in risk of insulin resistance and development of T2DM and obesity (Gonzalez-Muniesa et al. 2017).

Traditional research into appetite control has focused on two main systems; the homeostatic and the hedonic system. The homeostatic system can be referred to as the metabolic system as it is characterised by a co-ordinated communication between peripheral hormonal and nutrient sensing molecules; and the brain, largely the hypothalamus and midbrain. The homeostatic system acts to maintain energy balance through the dynamic variations in signalling molecule concentrations throughout the body, and signals that convey metabolic needs to the brain. In contrast, the hedonic system operates and drives desire for food consumption based on the palatability of food and the natural rewarding aspects and pleasure associated with food consumption. The hedonic system, driven by these potent rewarding effects, is capable of overriding the metabolic needs of the body, leading to periods of positive energy balance. These two systems are somewhat dissociable but not entirely independent due to crosstalk between the neurochemical substrates across both systems (Berthoud 2006). For example, the palatability of high calorie energy rich foods is increased when hungry in comparison to periods of satiation (Goldstone et al. 2009).

Recent work into the modulation of appetite control and food intake argues that there is a third mechanism involved in this multi-faceted network of appetite control and food intake; the cognitive system (Higgs 2016). This cognitive system concerns processes such as inhibitory control of food intake, dietary restraint, as well as learning value from food rewards, creating memory of foods and driving attention towards aspects of eating. This mechanism or system is a relatively new addition to the appetite control theories and mounting evidence continues to grow within this field regarding the cognitive aspects associated with food appetite and reward.

This thesis explores the role of central insulin in appetite control. The following sections will describe the regulation of the three control systems (homeostatic, hedonic, cognitive) with an emphasis on intranasal insulin; and research based on the use of functional magnetic resonance imaging (fMRI). Furthermore, the known dysfunctions associated with these systems, that occur in obesity and T2DM will also be discussed; as well as how modulation of central insulin affects these dysregulations.

1.7.1 Homeostatic system

The complexity of the homeostatic system is beyond the scope of this chapter, but it is necessary to explain a selection key metabolic peptide and hormone signals involved in homeostatic regulation of food intake. For a thorough review Coll et al., is recommended (Coll, Farooqi, and O'Rahilly 2007). As described earlier, the homeostatic system works to maintain energy balance (where energy intake equals energy expenditure) and body weight by integrating circulating signals that promote food intake and those that supress food intake. Peripheral signals originate from the gastrointestinal (GI) tract, adipose tissue stores and also from the pancreas and are key to sensing changes in nutrient availability such as glucose, fatty acids and amino acids. These signals are integrated largely within the homeostatic centre of the brain, the hypothalamus, via the arcuate nucleus (ARC) and the connections between hypothalamic and extra-hypothalamic regions of the brain, for example the nucleus tractus solitarius. For the purpose of describing the homeostatic system within the context of this thesis only a selection of signals involved will be described. An example of the integrated and dynamic activity of these signals is presented in Figure 1.7.1 during fasting and in the postprandial state in healthy and obese individuals.

1.7.1.1 Leptin

Leptin is released by adipose tissue and is considered an ‘adiposity signal’ or marker. In normal weight individuals, leptin levels are relatively stable over time, but they are increased in overweight/obese individuals who possess high amounts of adipose tissue (Carlson et al. 2009). Leptin supresses food intake by inhibition of the neuropeptide Y/Agouti-related (NPY/AgRP) peptide-expressing neurons and stimulates the cocaine and amphetamine-related transcript (CART) and the pro-opiomelanocortin (POMC)-expressing neurons located in the hypothalamus. As mentioned, leptin levels are raised during obesity but the sensitivity of leptin as an appetite suppressant is significantly reduced in obesity (Myers et al. 2010).Leptin is a marker of adiposity and does not show large dynamic variations during low energy

(fasting) or high energy (postprandial) states (Korbonits et al. 1997), having little impact on food intake.

1.7.1.2 Peptide YY

Peptide YY (PYY) is an amino acid secreted in response to food ingestion from the endocrine L cells of the gut. PYY exists in two forms PYY_{1-36} and PYY_{3-36}, which are both metabolically active. Secretion of PYY rapidly increases during the postprandial state but is low during fasting. PYY has anorectic effects, suppressing food intake, by inhibition of NPY activity either through penetration across the BBB or through activation of the vagus nerve. Overweight and obese individuals show a PYY deficiency that is well correlated with reduced satiety (le Roux et al. 2006).

1.7.1.3 Glucagon-like Peptide-1

Glucagon-like Peptide-1 (GLP-1) is a peptide released by the L cells of the small intestine. GLP-1 is released in response to food ingestion. GLP-1 is an incretin peptide that stimulates glucose-dependent insulin secretion from the pancreas and acts to supress glucagon release. GLP-1 agonists are used in the treatment of T2DM and obesity and display glucose lowering effects as well as weight loss effects. There is evidence to suggest that GLP-1 exerts its weight loss inducing effects at the level of the hypothalamus (Chaudhri et al. 2006). GLP-1 secretion to glucose ingestion is attenuated in obese individuals but shows a normal secretory response to oral fat ingestion (Ranganath et al. 1996).

1.7.1.4 Ghrelin

In healthy normal weight individuals during periods of negative energy balance, for example between meals or following an overnight fast, there is an increase in ghrelin secretion from the oxyntic cells of the stomach (Coll, Farooqi, and O'Rahilly 2007). Ghrelin is an enteric hormone that stimulates appetite. Peripheral administration of ghrelin stimulates food intake through activation of the NPY/AgRP expressing neurones of the hypothalamus. Ghrelin levels are highest during fasting and are supressed following calorie intake in the postprandial state (Goldstone et al. 2014). In obese individuals ghrelin is lower or comparable during fasting conditions vs normal weight individuals, however there is a significant delayed response in ghrelin level reduction following meal ingestion in obese individuals compared to lean, which leads to a reduction in satiety (Erdmann et al. 2005).

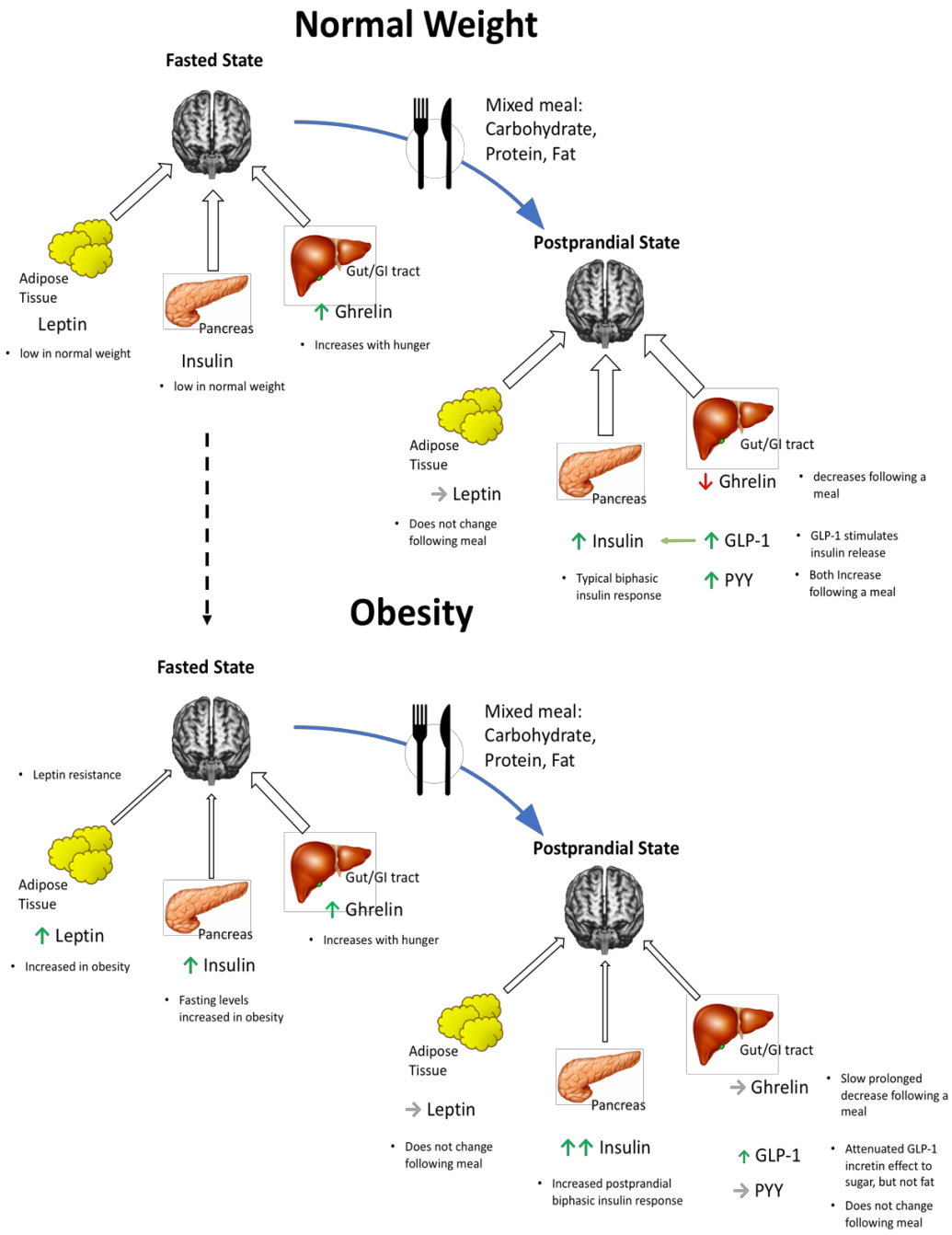

Figure 1.7.1 Schematic diagram showing a selection of homeostatic signals, described above, before and after a meal in normal weight and obese individuals. In normal weight individuals during the fasted state, ghrelin levels increase which promotes food intake. Following a mixed meal, ghrelin levels will decrease whereas GLP-1, PYY and insulin secretion will be increased. GLP-1 is an incretin and promotes pancreatic insulin release. All these signals will eventually reach the hypothalamus to supress further energy intake. In obese individuals, both leptin and insulin levels are higher in comparison to lean individuals but both brain leptin and insulin sensitivity is decreased. Ghrelin is largely unchanged between lean and obese during fasting. Following a mixed meal, there is a high increase in peripheral insulin (assuming no T2DM), postprandial ghrelin levels fall much slower in obese vs lean. GLP-1 response is attenuated to sugar but not fat. PYY levels remain largely unchanged following feeding. Insulin levels are high (during fasting and postprandial) due to decreased insulin sensitivity.

1.7.1.5 Insulin and its role in the homeostatic system

The presence of insulin receptors within the hypothalamus initiated the notion that insulin is key to the homeostatic control of food intake (Ott et al. 2012; Schulingkamp et al. 2000). Brain insulin receptor gene knockout mice (NIRKO mice) show increases in body weight and development of diet-sensitive obesity (Bruning et al. 2000), demonstrating a role of central insulin signalling in homeostatic weight regulation.

In humans, IN-INS administered four times per day for eight weeks resulted in significant weight loss (1.3kg) and a reduction in total adipose tissue in men (Hallschmid et al. 2004). However, this effect was not observed in women, which in contrast caused a small weight increase as a result of excess fluid retention (Hallschmid et al. 2004). However, the same treatment regimen in obese individuals did not lead to any differences in weight loss (Hallschmid et al. 2008). A suggested explanation for the absent treatment effect in the obese cohort is that obesity is associated with chronic endogenous brain insulin resistance and this route of administration, although effective in increasing CSF insulin, was not capable of increasing sensitivity to the weight reducing effects of insulin (Hallschmid et al. 2008).

Several studies have examined the effect of acute administration of IN-INS on responses to food intake. For example, three separate studies probing the differential gender effects mentioned above, showed that total food intake was reduced following IN-INS administration in men (Jauch-Chara et al. 2012; Benedict et al. 2008) but not in women (Hallschmid et al. 2012; Benedict et al. 2008). Firstly, following 40 international units (IU) IN-INS, men showed a significant reduction in food intake (breakfast *ad libitum* buffet), predominantly carbohydrate and protein based foods, in comparison to IN-PLA (Jauch-Chara et al. 2012). Secondly, in a sperate study, 160 IU IN-INS induced significant reductions in total food intake (breakfast buffet) in men (Benedict et al. 2008). These results suggest that central insulin in men has an appetite suppressant, anorexigenic effect. Benedict et al., further showed that the female comparator group were not sensitive to the anorexigenic effects of insulin, but, interestingly, presented with IN-INS related cognitive and memory

enhancing effects which were absent in the male group (Benedict et al. 2008). These differential effects have been seen in rodents, and research has shown that high brain oestrogen levels decrease insulin sensitivity, but in contrast increase leptin sensitivity (Clegg et al. 2006). The final study from these three studies mentioned showed a selective reduction of energy dense cookies, chocolate chip, in women following postprandial administration of IN-INS (160 IU) (Hallschmid et al. 2012). This postprandial reduction in cookie consumption was only in the cookies that were rated most palatable. This decrease did not result in a reduction in total calorie intake as intake of the other snacks available were slightly increased (not significant). These effects suggest that insulin may also interact with other satiety signals, thus restricting additional eating of palatable foods following a meal. The kinetics of endogenous insulin release from the pancreas to the brain CSF are slow (on the scale of 4 hours) and hence would render insulin an unlikely satiation hormone (Banks, Owen, and Erickson 2012; Wallum et al. 1987; Schwartz et al. 1990); however it can be seen that manipulation of central insulin concentration, via exogenous intranasal administration, could be an indirect method for reducing food intake in men and intensifying selective satiety of palatable foods alongside the plethora of metabolic signals released upon food ingestion.

fMRI studies implementing blood oxygen level dependent (BOLD) contrast have shown decreases in hypothalamic activity in response to glucose infusion and glucose ingestion (Opstal et al. 2017; Smeets et al. 2005). Importantly, the hypothalamic decrease in BOLD response is more pronounced followed glucose ingestion as opposed to glucose infusion, again suggesting a complementary role for insulin alongside other homeostatic signal molecules (Smeets et al. 2007). In keeping with this, the decrease in hypothalamic BOLD response (vs baseline) seen in response to glucose ingestion is augmented following elevation of central insulin concentrations via IN-INS (Opstal et al. 2017). Furthermore, an IN-INS triggered reduction in fractional amplitude of low frequency fluctuations (fALFF) (a measure of resting neuronal activity), was witnessed in the hypothalamus (Kullmann et al. 2018). Accumulation of these findings suggest an insulin-associated role in the hypothalamus supporting the role of insulin as a signalling molecule within the

homeostatic appetite control system. In contrast to the insulin sensitivity effects mentioned, Heni et al., showed measures of insulin resistance (using the homeostatic model assessment of insulin resistance (HOMA-IR)) to increase thirty minutes after IN-INS administration when compared to intranasal placebo (IN-PLA), which returned to comparable levels soon after (Heni et al. 2012). Heni et al., demonstrated that this increase in insulin resistance positively correlated with changes in hypothalamic fALFF measures (Heni et al. 2012). Insulin sensitivity was assessed by HOMA-IR using plasma glucose and plasma insulin concentrations. In this study a significant increase in plasma insulin and a significant decrease in plasma glucose was seen as a result of residual IN-INS absorption into the central circulation. HOMA-IR is typically used for measuring basal insulin sensitivity from fasting blood measures. This study implements a pharmacological challenge (IN-INS) and therefore cannot be considered basal conditions, especially given the significant changes in plasma glucose and insulin concentrations.

The BOLD responses reported from a selection of the aforementioned studies (Kullmann, Heni, et al. 2017; Kullmann et al. 2018; Heni, Wagner, et al. 2014; Heni et al. 2012) were acquired using traditional **whole brain** T2* weighted gradient echo Echo Planar Imaging (EPI) methods, which suffer from susceptibility-related signal dropout effects (Deichmann et al. 2003; Ojemann et al. 1997). Signal dropout due to magnetic field distortions at air-tissue boundaries, such as the orbitofrontal cortex and midbrain regions (hypothalamus), negatively influence image quality and therefore one must be slightly sceptical of these reported hypothalamic BOLD changes. Furthermore, the correlations reported between hypothalamic BOLD responsiveness and measures of insulin sensitivity, do not demonstrate a significant hypothalamic response when compared to IN-PLA and so these must also be viewed with caution.

In parallel with those investigations, studies using Arterial Spin Labelling (ASL), to assess changes in regional cerebral blood flow (CBF), have shown supporting evidence for insulin related changes in the hypothalamus. Using a high dose of IN-

INS (160 IU) Kullmann et al., presented an insulin-dependent decrease in hypothalamic cerebral blood flow (CBF) (Kullmann et al. 2018). Decreases in IN-INS related hypothalamic CBF have shown correlations with pancreatic insulin secretion, as measured with an oral glucose tolerance test (oGTT) performed on a separate day, illustrating a strong hypothalamus CBF decrease in individuals that secrete less pancreatic insulin to restore normoglycemia (Kullmann, Fritsche, et al. 2017), suggesting a link between hypothalamic and peripheral insulin sensitivity. Kullmann et al., also showed IN-INS associated decreases in hypothalamic CBF, compared to pre-administration measures in both lean (insulin sensitive) and overweight/obese (insulin resistant) individuals, highlighting that this insulin related response in CBF is also seen in those with peripheral insulin resistance. Furthermore, these significant CBF decreases from baseline in the hypothalamus following IN-INS (15 minutes after administration) correlated moderately (r=0.37, p = 0.015) with whole body MRI measurements of visceral adipose tissue (VAT) (Kullmann, Heni, Veit, Scheffler, Machann, Häring, et al. 2015). These findings suggest that those individuals with high amounts of visceral fat may have impaired hypothalamic insulin signalling, although the trend for this is arguably not very strong. Some ASL image acquisition schemes that do not use EPI readouts show good image quality in the regions typically affected by tissue susceptibility gradients in gradient-recalled EPI readouts. However, many of the ASL based studies did use EPI readouts and therefore the signal of hypothalamic change in these areas must also be interpreted with caution. In spite of this, the imaging evidence from both BOLD and CBF based studies is, at large, compelling; and suggests a role for insulin in the homeostatic control of food intake, primarily acting in the hypothalamus.

1.7.2 Hedonic mechanisms

Hedonic mechanisms underlying appetite and food consumption have been classically investigated through a conceptual framework that utilises two distinct reward concepts; liking (palatability of food) and wanting (motivation and drive for food) (Berridge 2004, 2009). 'Wanting' is predominantly governed by the dopaminergic (DA) neurotransmitter system which is comprised of midbrain and striatal structures and networks; the ventral tegmental area (VTA), substantia nigra (SN), nucleus accumbens (NAcc), caudate and putamen (Volkow, Wang, and Baler 2011; Berridge 2009) 'Liking', in the classical reward sense, can be defined by the hedonic properties of stimuli. With food, for example, the hedonic properties would be measured as palatability and appeal of certain food stimuli. This liking of food stimuli is considered to be underpinned by the opioid and endocannabinoid system (Pecina and Berridge 2005). Both systems show widespread receptor profiles that cover the striatum, midbrain, insula, thalamus, amygdala and regions of the prefrontal cortex too (Karlsson et al. 2015).

The hedonic control of appetite and food intake is posited to reflect the integration of these sub-systems and signals within cortical (insula, orbitofrontal cortex) and limbic regions (NAcc, caudate, putamen, amygdala, hippocampus). The dysregulation of these systems, scholars argue, underpins the disrupted appetite control and overeating of energy dense (highly palatable) foods that is associated with obesity (Volkow, Wang, Fowler, et al. 2008; Volkow, Wang, and Baler 2011; Drewnowski 2007). In general, the hedonistic value of food is underpinned by factors such as taste and flavour with high fat containing foods correlating with high palatability, which to some extent is supported by the overconsumption of fatty foods in obese populations (Dagher 2012; Drewnowski 2007). Consumption of palatable foods activates the mesolimbic system, a neural circuitry that mediates reward and motivation via dopaminergic (DA) neurons and neurotransmitters (Volkow, Wang, and Baler 2011). These systems are active when consuming palatable foods as well as during anticipation of sensory stimuli (Burger and Stice 2011a; Stice et al. 2008).

1.7.2.1 Insulin and the hedonic system

An intuitive example or argument for the involvement of insulin in hedonic processing of food is that during prolonged periods of negative energy balance (food deprivation) the responsiveness to food stimuli is increased. From our understanding of insulin's dynamic role in the body, during these times circulating insulin levels would be very low (Figlewicz and Benoit 2009) and these low levels could be associated with the drive and desire to seek food rewards. Likewise, increases in circulating insulin levels (such as that after a mixed meal) could attenuate the reward driven desires and motivations, a concept known as motivational salience. In healthy individuals, fasting increases motivational salience, whereas during food intake motivational salience decreases. In obese individuals, however, this motivational salience pattern is dysregulated, described throughout the sections below.

In humans, the hedonic value of food (liking) can be assessed behaviourally through questionnaires and ratings of palatability. 'Wanting' for food can be assessed by how much food is consumed and the amount of effort willing to exert to acquire certain food stimuli. Hallschmid et al., performed a study to investigate the effects of IN-INS on postprandial snack consumption in women (Hallschmid et al. 2012), which has been mentioned previously. In this study they evaluated snack intake (a choice of three types of cookies) two and a half hours after a substantial lunch (four mini pizzas). Shortly after lunch termination, participants were administered either IN-INS (160 IU) or IN-PLA. IN-INS did not show a reduction in total snack intake, however, IN-INS did evoke a significant reduction in palatability ratings for the most favoured cookie type (chocolate chip - measured under IN-PLA conditions) which was coupled with a significant reduction in chocolate chip cookie intake (Hallschmid et al. 2012). This result suggests that insulin does not inhibit postprandial intake as there was no difference between net snack consumption; but that insulin specifically reduced consumption of highly palatable snacks. Results like this might make the dissociation of 'wanting' and 'liking' effects more difficult. In theory, both 'liking' and 'wanting' of the highly palatable chocolate cookies decreased in the presence of central insulin

increases; suggested by the decrease in palatability ratings and reduced consumption for the chocolate cookies, respectively.

fMRI permits the assessment of behaviour in tandem with changes in neurovascular physiology, in response to changes in neuronal activity. 'Liking' of food stimuli can be assessed through the use of food cue responsiveness when participants are presented with a food related stimuli for example pictures of food, smells, tastes etc (Dagher 2012). Responsiveness to these cues is often processed by cortical structures in the brain; such as the insula, orbitofrontal cortex (OFC), fusiform gyrus and occipital regions (LaBar et al. 2001; van der Laan et al. 2011; Verhagen 2007). Food cues often engage sensory regions such as the insula, commonly known as the gustatory cortex, as well as regions involved in encoding stimulus value, for example the OFC (Gottfried, O'Doherty, and Dolan 2003).

Guthoff et al., were the first to show changes in food cue responsivity with increased central insulin concentrations, using IN-INS. Administration of IN-INS (160 IU) induced reduced cortical activity in comparison to IN-PLA in the fusiform gyrus, hippocampus, as well as the superior temporal gyrus (Guthoff et al. 2010). These decreases in BOLD contrast were exclusive to food pictures only suggestive of an IN-INS related decrease in salience or liking of the food picture stimuli presented. However, these findings must be carefully considered as the authors report these changes at a statistically liberal threshold ($p < 0.001$, uncorrected for multiple comparisons) and therefore these results could be suggestive of a trend, rather than a significant finding. Ferreira de Sa et al., did not provide complementary support to this finding, publishing a study that showed no central effect of IN-INS on food cue processing using an acoustic startle response technique (Ferreira de Sa et al. 2014). This study used a lower dose of IN-INS (40 IU) and a different technique and so it is difficult to directly compare these two studies. Despite this, with the same low dose (40 IU) Schilling et al., presented IN-INS related changes in CBF during the resting state (Schilling et al. 2014). They showed regional CBF (rCBF) increases in the insula and putamen, two key regions involved in gustatory integration and reward processing (Schilling et al. 2014). Although these individuals were not engaged in a

functional paradigm, the change in CBF might reflect a change in basal activity which could modulate engagement of these areas if recruited by a task. Resting-state fMRI-BOLD data that probed IN-INS (160 IU) related changes of fALFF in lean women observed a decreased in fALFF measures in the hypothalamus as well as the OFC (Kullmann et al. 2013). The OFC is a region with well documented involvement in palatable food reward valuation (O'Doherty et al. 2002) and could suggest that at rest, the sensitivity of this region is reduced following IN-INS, reducing reward sensitivity and thus reducing desire for food intake. However, it must be noted that both resting state studies (Schilling et al. 2014; Kullmann et al. 2013) were not designed to assess insulin related responses to food liking and furthermore there was no change in appetite ratings observed in response to IN-INS administration.

'Wanting' for food can be assessed by how much food is consumed and the amount of effort willing to exert in order to acquire certain food stimuli. Measures of motivation for rewarding or salient stimuli and 'wanting', are more easily measured from pre-clinical neuroscience experiments (Berridge 2009). In humans, however, these components of reward are often difficult to dissociate, given the significant overlap between liking and wanting, and the commonly self-reported measures used to ascertain these metrics (Finlayson, King, and Blundell 2007). Measures of motivation or desire for example could be sub-conscious or could be biased by self-reporting and therefore quantitative tools that use reactive measures, for example force grip, are being developed for implementation in neuropsychological research environments (Ziauddeen et al. 2014).

In regards to the effects of insulin on reward related behaviour, one must look to pre-clinical work in order to ascertain the modulatory effects of insulin on the dopaminergic system. Converging pre-clinical literature has suggested that insulin plays a role in modulating reward related circuitry and thus exerts much of its anorexigenic effects through modulation of the mesolimbic pathway. Firstly, in the rodent brain, insulin receptors have been found on DAergic neurons of mesolimbic regions such as the VTA, SN and also the NAcc, caudate and putamen (Figlewicz et al. 2003). In rats, direct administration of insulin to the VTA and hypothalamus resulted

in a concentration-dependent suppression of DA in the VTA due to an increase in DA transporter (DAT) reuptake of DA coupled with decreased sucrose self-administration (Mebel et al. 2012). This data suggests that insulin reduces DA signalling in limbic regions and therefore suppresses the rewarding effects usually obtained from eating, reducing the motivation and pursuit of food consumption. This data would suggest that 'wanting' of food as determined by self-administration is modulated via insulin's effects in the VTA, thus increased central insulin could lead to reduced hedonic drive thus terminating feeding. This would support a common hypothesis related to obesity, that obese compared to lean individuals, who present with lower insulin CSF levels (Kern et al. 2006), experience greater reward from food stimuli (hyper-responsivity) and therefore encourages increased food consumption (Davis, Strachan, and Berkson 2004; Dawe and Loxton 2004).

1.7.2.2 Hyper-responsivity to food cues

Some theories propose that greater reward evoked from food intake is a risk factor that contributes to the overeating associated with obesity (Stice et al. 2008; Davis, Strachan, and Berkson 2004; Rothemund et al. 2007). Evidence to support this theory comes from observations of greater activation in limbic (NAcc) and cortical regions (insula, OFC) from presentation of food picture stimuli in obese compared to normal weight individuals (Rothemund et al. 2007). Developing this further, overweight and obese patients with T2DM showed increased BOLD responses in the insula, OFC and caudate region upon presentation of food pictures in comparison to age and weight matched controls (Chechlacz et al. 2009). As the control group were weight matched it could be suggested that these hyper-responsive regions observed following food picture stimulation could be as a result of changes in insulin sensitivity both centrally and peripherally. An example of this aberrant cue responsivity is highlighted in Figure 1.7.3 as well as 'normal' responsiveness in Figure 1.7.2.

In contrast, there is a corollary hypothesis which postulates that obese individuals experience a decrease in mesolimbic reward activation from food intake in comparison to lean individuals, driving compensatory overeating and consumption (Comings and Blum 2000; Volkow, Fowler, and Wang 2002). This theory is known as the hypo-responsivity theory.

1.7.2.3 Hypo-responsivity to food intake

The hypo-responsivity theory, or sometimes referred to as the reward deficiency theory, posits that individuals who experience low reward effects or low engagement of reward circuitry are at risk of overeating (Stice et al. 2008). This reward deficiency thus drives repeated consumption or increased consumption of palatable foods to achieve equivalent reward. Brain regions known to encode reward upon consumption of food; insula, VTA, NAcc, caudate and putamen show decreases overtime that correlate with satiety (Small et al. 2003). Furthermore, DA levels within the NAcc, as measured by C-11 raclopride positron emission tomography (PET) are increased upon consumption of a pleasant meal, with the magnitude of release showing close association to subjective measures of meal pleasantness (Small, Jones-Gotman, and Dagher 2003). Support for this theory largely comes from observations of low dopamine receptor (D2 receptor) availability and lower DA levels in the NAcc in obese vs lean individuals, as measured with C-11 raclopride PET (Volkow, Wang, Telang, et al. 2008; Wang et al. 2001). An example of the hypo-responsive system can be seen in Figure 1.7.3.

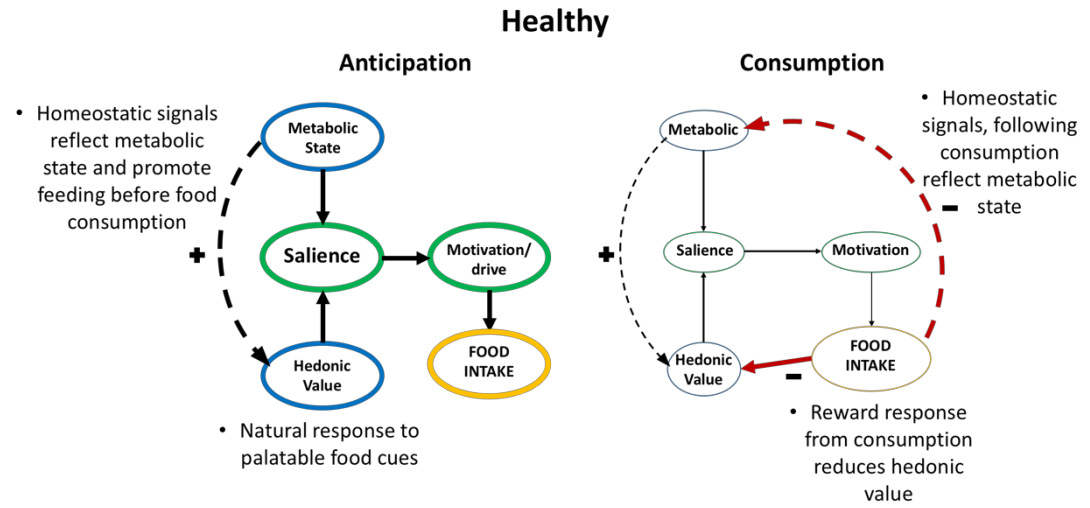

Figure 1.7.2 Simplified schematic models during anticipation of food intake and consumption in healthy individuals. Prior to food consumption the metabolic state can influence the hedonic value of foods, driving the salience of these foods, increased 'motivational salience'. Salience and attention increases motivation and drive which is essential for food intake. During consumption, homeostatic signals will update the metabolic state of the individual and the reward related response acts to reduce the salience or hedonic value of palatable foods, reduced 'motivational salience'.

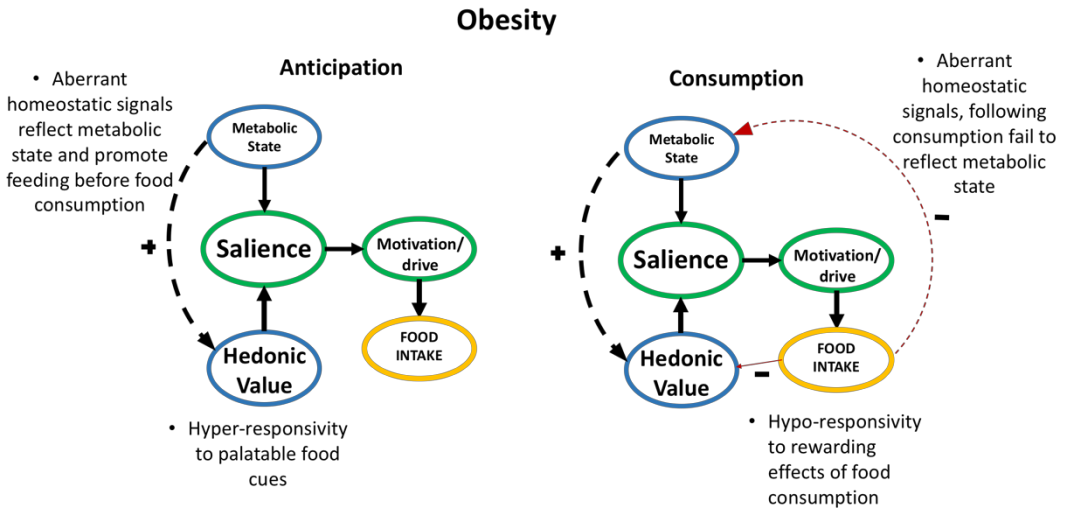

Figure 1.7.3 Simplified schematic models during anticipation of food intake and consumption in obese individuals. Prior to food consumption the metabolic state can influence the hedonic value of foods, driving the salience of these foods, increased 'motivational salience'. Salience and attention is hyper-responsive to food cues which increases motivation and drive for food intake. During consumption, aberrant homeostatic signals fail to update the metabolic state of the individual and the reward related response from food intake is largely blunted, 'hypo-responsive' consummatory reward. As a result the 'stop' eating signals are not effective or present which results in overconsumption.

1.7.2.4 Insulin and the hypo-responsivity theory

From the literature, there are lines of evidence that show how central insulin signalling agrees with this proposed theory. Firstly, *Stouffer et al.,* have recently shown that insulin enhances DA release from striatal (caudate and putamen) terminals and in the nucleus NAcc via an indirect mechanism involving insulin receptor expressing excitatory cholinergic interneurons (Stouffer et al. 2015). They further show that in obese mice this DA responsiveness is reduced compared to wild types and enhanced in food restricted mice (Stouffer et al. 2015). Finally, a PET study using a C-11 raclopride tracer, has shown that people with insulin resistance have decreased DA release in the NAcc after drinking a sugary drink in comparison to healthy individuals (Wang et al. 2013). This work was presented at a conference of which the methodological details cannot be gathered from the abstract. However, the data presented are suggestive of an increased modulation of insulin with regards to DA neurotransmission and limbic system reactivity.

A product of both the *hypo* and *hyper* responsivity theories is what many believe drives overeating seen in obese individuals. The increased (hyper) salience of food cues drives motivation to eat initially, however, upon receipt of food or consumption the rewarding effects are decreased (hypo). It is this discrepancy between the predicted reward value and the reward value encoded during consummation that is suggested to be a risk factor for overeating in obese individuals. This can be seen in Figure 1.7.3.

Limited human imaging studies have shown insulin related effects in the nucleus accumbens and striatal regions or explored these mechanisms. However, one study has observed functional BOLD responsiveness to food images (mixed high and low calorie) vs non-food images in insulin sensitive (normal weight) and insulin resistant (overweight and obese) individuals as measured using HOMA-IR (Tiedemann et al. 2017). This study showed that under placebo conditions the insulin resistant individuals displayed significantly lower BOLD responsiveness to food pictures vs non-food in the bilateral NAcc and left VTA compared to insulin sensitive individuals

(Tiedemann et al. 2017). This opposes the hyper-responsive food cue reward theory of obesity but with insulin resistant individuals. In this study, participants were also pharmacologically challenged with IN-INS (160 IU) administration. Following IN-INS the insulin sensitive group showed an IN-INS related decrease in NAcc and VTA activity, while the effect was reversed in the insulin resistant group who presented with increased IN-INS related activity of the NAcc and VTA (Tiedemann et al. 2017). Interestingly, this study also showed that preference ratings for the food items decreased under IN-INS reflecting a decrease in salience for these images in the insulin sensitive group. This effect was not seen in the insulin resistant group, but a trend (p = 0.09) towards significance was found, which presented a slight increase in food preference values following IN-INS. These data suggest that in healthy insulin sensitive individuals, insulin works to reduce reward related processing which is associated with reductions in palatability ratings of food. Yet, however, in those with differential peripheral sensitivity the effects of insulin show an opposing effect. Elucidating and exploring these effects in a more rigorous way, as well as investigating the opposing effects of changes in central insulin seen in those individuals presenting with peripheral insulin resistance, is imperative for future research.

The interplay between metabolic state and hedonic mechanism that drives overeating can be observed in healthy individuals and at times healthy individuals will 'binge' or overeat energy dense food or increase calorie intake significantly, in certain circumstances. However, the chronic overeating seen in metabolic disorders such as obesity or individuals at risk of developing metabolic problems is a result of an inherent dysregulation of these systems. Understanding whether this dysregulation precedes adverse metabolic manifestations or is an observation seen in obese individuals is largely unknown.

Understanding the role of insulin in this interplay has been illuminated in the last decade given the introduction of IN-INS and the increasing availability of functional imaging access for researchers in the field. The main relevance of hedonic dysregulation to T2DM and obesity is that the powerful systems that contribute to

hedonic hunger can override homeostatic signals promoting increased food and energy consumption. Dysregulation of the hedonic system coupled with a dysregulation in the homeostatic system arguably increases the risk of entering a pathological cycle of chronic positive energy balance, adipose storage, irreversible effects on health, increased risk for CVD and increased mortality. With homeostatic eating there are peptide signals such as ghrelin that act to promote eating, but there are also inhibitory satiety signals (PYY, GLP-1 etc). In contrast, the hedonic system which primarily describes a series of excitatory responses that drive and promote overeating does not describe a subset of inhibitory mechanisms. A large amount of research in humans has focused on the inhibitory control mechanisms that govern the hedonic system and the associated role these systems have in food intake dysregulation. These systems together are known as the 'cognitive mechanisms'.

1.7.3 Cognitive mechanisms

The homeostatic and hedonic system cannot completely account for all the processes involved in appetite control. On a primal level these systems do largely dictate energy regulation, which has been demonstrated by elegant animal model experimentations (Berridge 2004; Berridge and Kringelbach 2008). As humans operate at a higher cognitive level than primates and rodents, there exists an additional component to this integrative model of appetite control, which for a long time has been neglected by the classical theories of appetite dysregulation. The homeostatic and hedonic system present a restricted view on food intake that does not take into account the ability for restraint and inhibition of food intake (Higgs 2016). Examples of cognitive modulation of appetite control are seen in everyday situations, for example inhibiting the consumption of unhealthy, highly palatable foods, in pursuit of long-term healthier outcomes (Hare, Camerer, and Rangel 2009). Interestingly, evidence from behavioural tasks show that obese individuals display a preference for high immediate rewards at a cost of increased risk of future reward loss in comparison to normal weight individuals (Weller et al. 2008; Epstein et al. 2010). There is further evidence from imaging studies to suggest that high BMI impairs general cognitive

functioning, particularly executive function of prefrontal regions of the brain (Sellaro and Colzato 2017; Volkow et al. 2009). Regional brain glucose metabolic deficits measured with 2-deoxy-2 [18F] fluoro-d-glucose – PET (FDG-PET) negatively correlated with BMI in the ventromedial prefrontal cortex (vmPFC) , dorsolateral PFC (dLPFC), the anterior cingulate gyrus (ACC) as well as the medial OFC region (Volkow et al. 2009). Examples of cognitive inhibitory control can be seen in Figure 1.7.4.

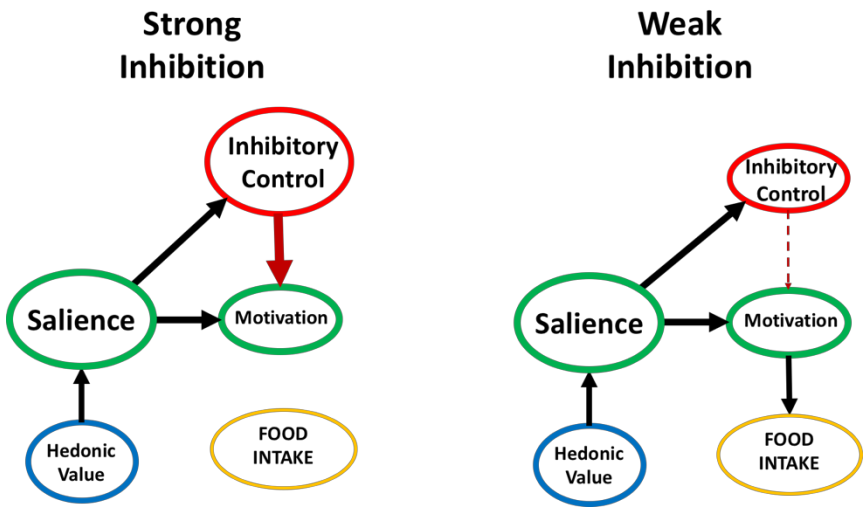

Figure 1.7.4 Simplified schematic highlighting how the cognitive inhibitory control mechanism is involved in food intake. In those with strong food inhibition the top down inhibitory effects are sufficient to reduce the motivation and drive to palatable, salient food. In those individuals with poor inhibitory control, salient food salience and subsequent motivation is too significant to inhibit and thus food is ultimately consumed.

1.7.3.1 Insulin and cognitive control of food intake

Imaging studies that have investigated the response to IN-INS administration have shown that effects within these prefrontal regions to be limited. Kullmann et al., showed that in lean women, IN-INS (160 IU) administration gave rise to an increase in resting fALFF within the ACC and superior frontal gyrus that was significantly associated with BMI (Kullmann et al. 2013). This study was limited to normal weight individuals and although the data suggests central insulin sensitivity increases with BMI, these interpretations must be restricted to BMI within the 'normal' range only. Additional resting state investigations, which also investigated the effects of IN-INS (160 IU) administration showed increases in regional fALFF within the lateral PFC

(Kullmann et al. 2018); and regional increases in CBF within the middle frontal gyrus in lean individuals (Kullmann, Heni, Veit, Scheffler, Machann, Häring, et al. 2015). In contrast to the IN-INS related increase in CBF mentioned above, the same study also highlighted a significant decrease in middle frontal gyrus CBF in response to IN-INS vs IN-PLA in overweight/obese insulin resistant individuals (Kullmann, Heni, Veit, Scheffler, Machann, Haring, et al. 2015).

The data from the limited studies presented provide grounds to suggest that IN-INS has a modulatory effect on prefrontal cortical regions. The role of insulin within these areas and the role of insulin as a central modulator of inhibitory control over the hedonic system remains to be elucidated. Higgs et al., provide an interesting presentation of when cognitive control and not just inhibitory control mechanisms are involved in appetite regulation. They argue that cognitive processes are involved in all aspects of food intake, from before a meal, during a meal and also periods after and between the next meal or energy intake periods (Higgs et al. 2017).

1.7.4 Cognitive processes involved before feeding

It is now thought that the cognitive system is required to make valuations of potential meal choices on the bases of taste, energy density and the health risks that might be associated with those decisions (Hare, Camerer, and Rangel 2009). These valuations are encoded within the vmPFC and based on these valuations decisions are made within the dLPFC and mOFC (Hare, Camerer, and Rangel 2009; Vassena et al. 2014). This prefrontal network provides humans with the ability to engage in goal directed behaviour as opposed to cue-driven behaviour. The ability to inhibit confounding cues such as palatable foods or smells and the desire for the long-term or short term goals must therefore require attention.

1.7.5 Cognitive processes involved during feeding

During a meal or food consumption it is generally well understood that the motivation and salience for specific food decreases over time, known as sensory specific satiety (Rolls et al. 1981) and also food in general, known as alliesthesia (decrease in motivational salience) (Stoeckel et al. 2007). In reality, these two mechanisms increase 'satiation' as opposed to satiety. These mechanisms are known to be associated with reductions in DA transmission, but also with increases in dLPFC activity that correlate with measures of satiety (Thomas et al. 2015). Attention also seems to form a significant component during the meal consumption phase. Being cognitively distracted during meal consumption such as by watching television leads to increased food intake (Braude and Stevenson 2014) and suggests the cognitive domains are important for selectively inhibiting the hedonic system to induce satiety.

1.7.6 Cognitive processes involved during feeding intervals

There is evidence to suggest that memory of a previous meal influences further eating behaviour (Higgs 2016). As an extreme example, people who suffer from amnesia and are unable to remember meal periods will often eat multiple meals with relatively short durations between them (Higgs et al. 2008). Within this work Higgs et al., also showed that sensory specific satiety was intact in amnesic patients thus providing evidence for intact dopaminergic transmission and potentially fully functioning hedonic systems (Higgs et al. 2008). In rats, inactivation of dorsal hippocampal neurons following a sucrose meal decreases the time interval between two meals, suggesting that this cognitive-memory association during postprandial and post-absorptive state are modulated by hippocampal-dependent processing (Parent 2016).

Taken together, these findings suggest that cognitive processes are a contributor to net food intake and that it is the integration of all three systems (homeostatic, hedonic and cognitive) that governs and controls food intake. Previous literature has

outlined insulin's involvement in homeostatic and hedonic pathways and to some extent the cognitive pathway too. The cognitive benefits of IN-INS on working memory, declarative memory in healthy individuals (Benedict et al. 2004; Benedict et al. 2008) and also in patients with mild cognitive impairment (MCI) and Alzheimer's Disease (AD) (Freiherr et al. 2013; Craft et al. 2012) suggest that insulin may have an important role in the cognitive pathways involved in food intake and appetite control.

1.8 Aims of Thesis

Given the evidence for insulin's involvement in the three systems engaged in appetite control, this thesis aims to explore these components further through a pharmacological neuroimaging framework. This investigation employs intranasal administration as a method to increase central insulin concentrations, hoping to give rise to a limited effect on peripheral hormone and peptide concentrations. This investigation has implemented a functional magnetic resonance imaging protocol to observe effects of intranasally administered insulin on the brain during rest as well as when engaged in a functional task probing the reward system. The studies set out to look at the effects of IN-INS in a group of healthy male individuals across a wide BMI range that included normal weight and overweight individuals. The study design and rationale behind the study are detailed in section 3.1.

The three aims of this thesis and exploratory investigation are:

1) To interrogate changes in Cerebral Blood Flow in response to IN-INS
2) To interrogate IN-INS related changes in functional connectivity between limbic and cortical regions and the rest of the brain
3) To interrogate the effects of IN-INS during engagement in a task that exposes the participant to primary food reward stimuli

Chapter 2 General Methods: Intranasal Insulin Imaging Study Protocol

The study that is being presented in this thesis is a pharmacological investigation of the effects of intranasally administered insulin on human brain function. In this study, I have implemented a range of functional Magnetic Resonance Imaging (MRI) techniques to explore the effects of intranasal insulin in comparison to intranasal placebo. This chapter will describe these imaging methods. The fundamental processes involved in functional image acquisition will be explained in a generalised format. The detailed parameters (and data analysis) of each methodology will be described in the individual chapters.

2.1 Nuclear Magnetic Resonance

The phenomenon of nuclear magnetic resonance (NMR) arises because of the quantum mechanical properties of nuclei and its constituent particles. Below I present a description of NMR based mainly on a classical rather than quantum mechanical formalism.

NMR refers to the interaction between magnetic moment and angular momentum, which occurs in atomic nuclei that possess an odd number of protons, for example hydrogen (^{1}H), carbon (^{13}C) and Fluorine (^{19}F). The effect occurs in the presence of an external magnetic field (Purcell, Torrey, and Pound 1946). The odd number of protons inherent within these nuclei produces a small magnetic character and their finite angular momentum around their own axis, is known as nuclear *spin*. This 'rotation' or *spin* produces a small magnetic field known as a magnetic dipole moment (MDM) (Figure 2.1.1). Although in principle, Nuclear Magnetic Resonance (NMR) signals can be obtained from any nucleus with a finite magnetic dipole moment; Magnetic Resonance Imaging (MRI) has predominantly exploited this physical property from hydrogen atoms, because their nuclei provide the strongest NMR signals and are ubiquitously abundant within the human body (Bloembergen, Purcell, and Pound 1948). Hydrogen nuclei are found in water, lipids ($-CH_2-$) and in most biological tissue.

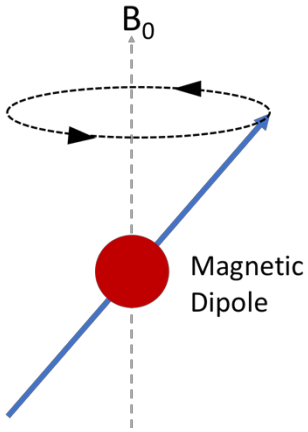

Figure 2.1.1 A Magnetic Dipole Moment precessing about an external magnetic field B_0.

When magnetic moments are placed in a strong external magnetic field, B_0, such as that produced by an MRI scanner, some of these magnetic moments will align with the magnetic field direction (B_0) and some will align in the opposing direction. For conventional MRI scanners and for this description, the main magnetic field direction refers to the z-axis and the orthogonal direction is the x-y plane. Exposed to this external magnetic field B_0, there will be a NET difference between spins that line up parallel and anti-parallel with the external field, giving rise to a NET bulk magnetisation vector (M_z) along the longitudinal (z) axis. Because of the angular momentum of this magnetisation vector, a finite torque between this vector and the external field causes these spins to undergo a motion known as *precession,* whereby the hydrogen spins rotate at a finite angle around the main magnetic field axis, M_Z, as if describing a 'cone'.

The *precession* frequency of the spins is known as the Larmor frequency, ω (Bloch 1946). The value of the Larmor frequency is governed by the product of the strength of the magnetic field (B_0, Tesla (T)) and the gyromagnetic ratio of the spin species (γ, MHz/T), which for hydrogen protons is 42.6 MHz/T (see below).

$$\omega = \gamma B_0$$

Detection of NMR signals is almost always achieved by establishing a resonance condition. In 'pulsed NMR' this is achieved by 'tipping' the net magnetisation vector from the longitudinal axis to the transverse plane, by delivering a radiofrequency pulse (RF) at the same frequency as the precessing spins (i.e. the Larmor frequency), via a RF transmission coil. The pulse of radio-frequency is delivered to the spins, for a time long enough to cause a 90^o rotation of the net magnetisation vector onto the axis of detection of the coil. The signal that is then detected by the coil is known as the "free induction decay".

For any arbitrary angle of rotation (i.e. not necessarily 90 degrees), the magnetisation can be defined by two separate components: 1) the remaining magnetisation along

the longitudinal axis (which experiences 'longitudinal' relaxation) and 2) the magnetisation along the transverse axis (which experiences 'transverse' relaxation).

2.1.1 Longitudinal relaxation

Immediately following a 90° flip of the net magnetisation vector into the transverse plane, the precessing spins will naturally begin to rotate back to their equilibrium state. The process by which this relaxation process takes place can be approximated by a simple exponential function:

$$M_{z(t)=} M_0 \left(1 - e^{t/T_1}\right)$$

where $M_{z(t)}$ is the instantaneous value of the longitudinal magnetisation, M_0 is its equilibrium value and the time constant of the exponential (T_1) is known as the 'Longitudinal Relaxation time'. The process of T1 relaxation is also referred to as spin-lattice relaxation, during which the spins simply 'return' the energy absorbed from the RF pulse into the surrounding lattice or environment. T1 relaxation is therefore driven by the ability of these spins to emit energy to the tissue and the dynamics of this process changes with tissue type. Therefore, images 'weighted by' or sensitive to differences in T1 provide a powerful mechanism to obtain T1 contrast in our images. As the magnetisation vector returns to the longitudinal axis, this process contributes to the loss of signal in the transverse plane (Figure 2.1.2)

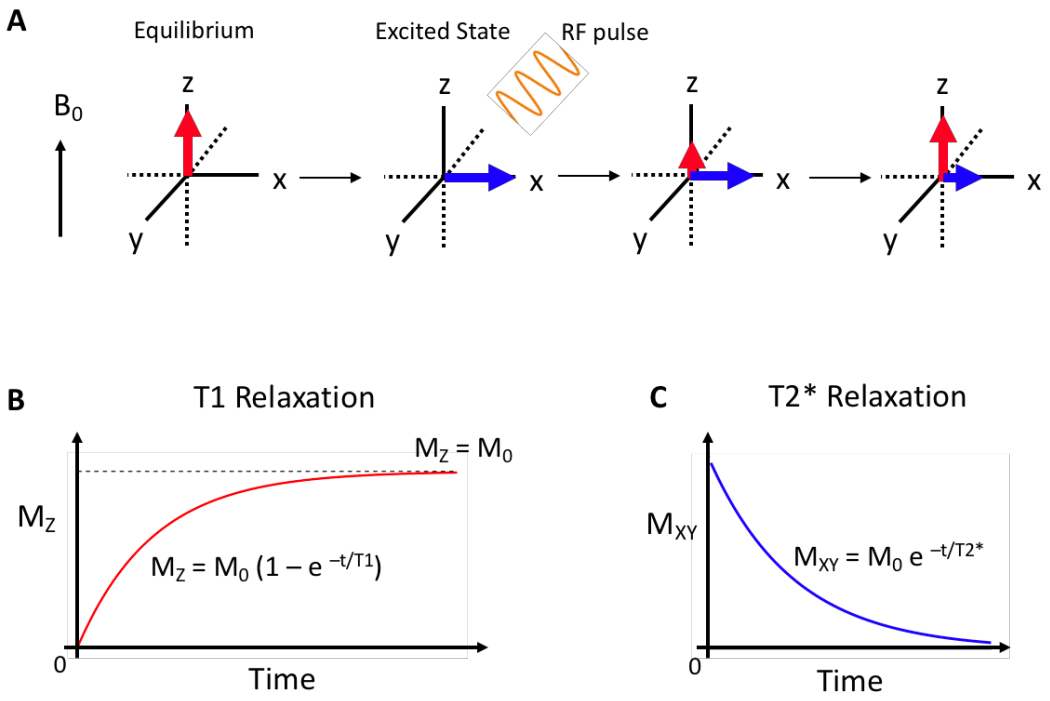

Figure 2.1.2 Longitudinal and transverse relaxation. A) Shows the longitudinal magnetisation vector (red arrow) and transverse magnetisation vector (blue arrow) in the rotating frame. During equilibrium the longitudinal vector Mz is aligned with B_0 in the z-axis. Upon excitation by a 90° RF pulse the bulk magnetisation vector is flipped into the transverse plane, and M_{XY} is maximal. The transverse magnetisation vector will decay exponentially as can be seen in figure (C) known as T2* relaxation. The longitudinal magnetisation vector will recover, known as T1 relaxation (B).

2.1.2 Transverse relaxation

Immediately following a 90° flip, the magnetisation vector is now in the transverse plane and the spins are in a higher energy state. The magnetisation is coincident with the axis of the detection coil and therefore the signal of the free induction decay is at a maximum. Over time, the net magnetisation vector will also decay with what is known as T2 relaxation. In the transverse plane the individual spin components will rotate around the longitudinal axis. During this rotation the spins will begin to dephase with respect to each other resulting in an overall decrease in the magnitude of the transverse magnetisation vector; and hence the signal. Two processes contribute to this decay (independent of T1). In this instance, the two main processes that contribute to this dephasing are: the interactions between spins and also the external magnetic field inhomogeneities.

The former dephasing mechanism is often referred to as spin-spin relaxation and is it a result of the interactions between individual spins. These local interactions reduce spin phase coherence which in turn reduces the net transverse magnetisation vector. For example, the differing density of tissue types affects the rate at which the spins dephase. Spins in dense tissues, that closely interact, dephase at a faster rate in comparison to those in less dense tissues. For instance, spins within white matter tissue will decay at a much faster rate (short T2) in comparison to spins within freely diffusing water, which will dephase more slowly (long T2).

The latter dephasing mechanism is in practice very relevant and describes additional spin dephasing in the transverse plane due to inhomogeneities in the external magnetic field. It is easy to see how if the field is different, the Larmor frequencies of spins will also be also different and therefore phase coherence between spins is reduced and eventually lost. The combination of both spin-spin interactions and the field inhomogeneities leads to a decrease of the free induction decay signal with a process that can be approximated by a single exponential function with a time constant known as T2* (see Figure 2.1.3)

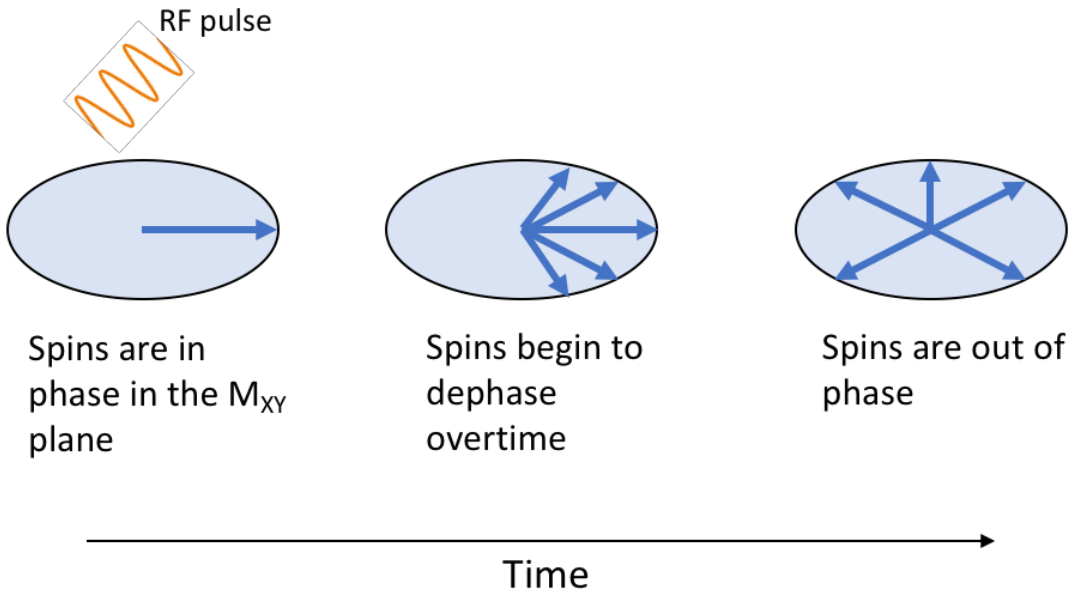

Figure 2.1.3 Schematic diagram of the rotating frame showing spin dephasing over time in the transverse plane following an RF pulse excitation

2.1.3 Free induction decay

In a frame of reference rotating at the Larmor frequency, and following the flip of magnetization from M_Z to M_{XY} , the spins will appear to be 'in phase' and precessing at the same frequency in the transverse plane. However, as the spins begin to dephase, the magnetisation vector M_{XY} will begin to decay with a time constant T2*. During this time, the magnetization vector rotates around the z-axis inducing an oscillating signal in the receiver coil. This oscillating signal is known as free induction decay (FID) and oscillates at the Larmor frequency and the amplitude of this FID decays exponentially with T2* ($e^{-\frac{t}{T2^*}}$) (Hoult and Richards 1975). The FID will decay exponentially with respect to T2* as seen in Figure 2.1.4

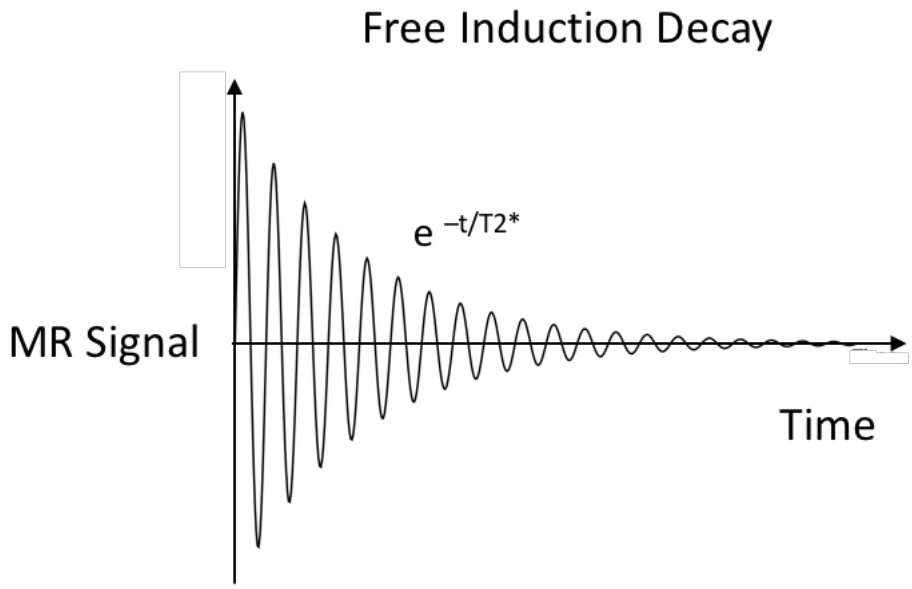

Figure 2.1.4 Free induction decay as a result dephasing in the transverse plane and external magnetic field inhomogeneities.

The duration of the FID signal depends obviously on the physical properties of the spins in each tissue type and the spatial homogeneity of the magnetic field. It is possible to see how imaging methods can exploit these differences in T2* to obtain additional tissue contrast. The duration of the FID can, in some instances, be very short (100ms or less) and in reality measuring the signal only from a single FID is not effective.

As will be explained below, there are methods that allow us to make further measurements by manipulating the evolution of the signal. Generally speaking, this is conducted using what is known as an MR pulse sequence. An MR pulse sequence describes a set of RF and gradient pulses that are applied to the object being scanned. Gradient coils are housed within the magnet and will be explained in later sections.

2.1.4 Spin echo

One of the earliest pulse sequences developed to eliminate the need to depend on measurements using the FID, is the spin echo sequence. A spin echo sequence consists of a 90° RF pulse that flips the net magnetization vector into the transverse plane. As shown in Figure 2.1.5 the spins will begin to dephase over time due to spin-spin interactions and external field inhomogeneities (T2* decay). However, after a short period of time (τ), a 180° RF pulse is applied, which inverts the direction of these dephasing spins. Through this inversion, the spins will travel in the opposing direction, in the direction they just came from, and begin to rephase. At time 2τ the spins will be refocused, in-phase, for a moment before dephasing again through T2*

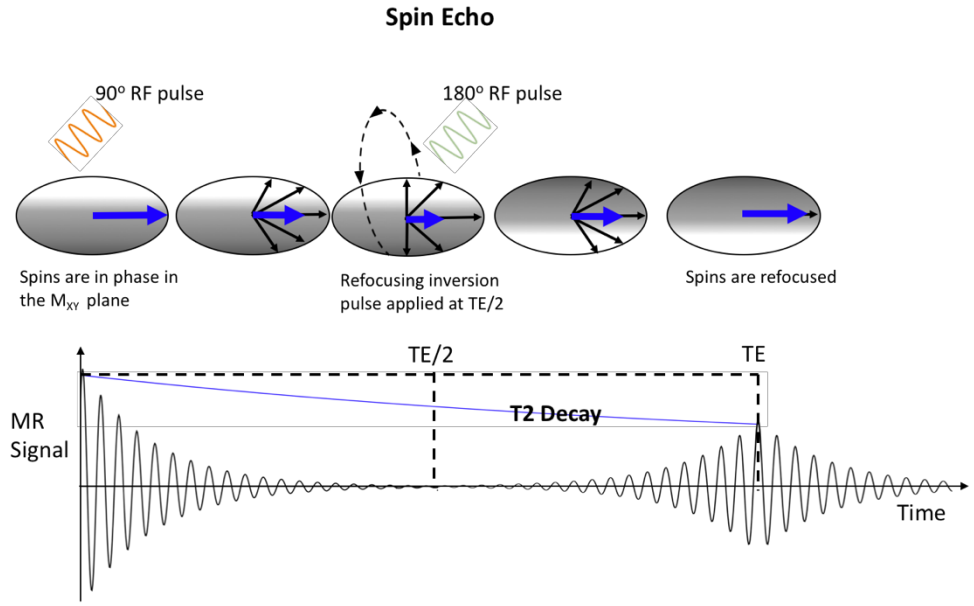

Figure 2.1.5 Diagram showing the spin echo sequence in the rotating frame as well as the MR signal produced and sampled. Spin echo uses a 180° refocusing RF after the spins have begun to dephase (TE/2). Following this refocusing pulse the spins begin to rephase producing an echo, with maximal signal intensity at TE. Not that the echo itself decays via T2* as an echo of the FID, whereas the peak of the echo decays with T2.

relaxation. The rephasing, in-phase (peak) and dephasing components following the inversion pulse are known as an 'spin echo'; and forms the basis behind many of the pulse sequences adopted for MRI (Hahn 1950).

As will be seen later, spin echoes are useful because they extend the time available for encoding spin frequencies in order to generate an image. It can also be seen that this approach makes the spin echo signals insensitive to the effect of differences in magnetic field homogeneity.

2.1.5 Gradient echo

A gradient echo sequence is another method of producing an echo-like signal, however, instead of using an inversion pulse to rephase and create an echo of the FID, one or more gradient pulses are used. Following a 90° RF pulse, the FID will begin to decay via T2* as the spins in the transverse plane dephase. At this point a finite gradient (dephasing gradient) is applied for duration, τ, which acts to accelerate the dephasing of the spins. Following this dephasing gradient, another gradient of opposite polarity but equal amplitude and duration (rephasing gradient) is applied which acts to refocus the transverse evolution of the spins. At time τ of the rephasing gradient, the spins will regain the phase evolution they would have had along the transverse plane before the application of the gradient pulses.

For both spin echo and gradient echo the time at which the echo peaks is known as the echo time (TE). For spin echo acquisition the inversion pulse is applied at TE/2.

2.1.6 Image formation

The FID and echo signals induced into the RF coil during image acquisition contain information regarding the entire brain or region of the brain excited. These signals do not contain any spatial information and therefore there are additional steps required to localise the origin of the tissue signals in space. This is achieved through

the use of external gradient coils that manipulate the magnetic field across the z, x and y planes in order to make the Larmor frequencies dependent on position. These gradient coils are housed in the MRI scanner. Each gradient coil is required during the MRI experiment to obtain spatial information and the gradients are commonly referred to as:

- Slice encoding gradient
- Phase encoding gradient
- Frequency encoding gradient

The gradient coils change the magnetic field most commonly in a linear manner and it is the combination of gradients applied across the imaging object, which imparts information about spatial location. Gradients are used to temporarily create non-uniformity across the magnetic field, which alters the spin frequency precession across the imaging object, thus creating spatial inhomogeneity across the magnetic field in a controlled manner.

2.1.6.1 Slice encoding gradients

The slice encoding gradient is used to selectively excite the spins within a finite region of space. Slice encoding gradients are applied during excitatory 90° RF pulses, which are designed to have a finite excitation bandwidth. In all instances, the excitation pulse used to flip the spins covers a range of radiofrequencies referred to as 'the bandwidth of the pulse'. By applying a gradient across the field the spins within the imaging object will precess at a range of frequencies above and below the Larmor frequency. A common 'RF pulse shape' employed in imaging sequences is the sinc function, whose corresponding envelope in the frequency domain is a rectangular profile. By virtue of the applied gradient, application of an excitatory RF pulse with a rectangular bandwidth of frequencies, will only excite those spins that correspond to a discrete portion of space in the direction of the slice encoding gradient, as opposed to the whole object. The thickness of the slice excited can be decreased by

increasing the strength of the slice encoding gradient or decreasing the bandwidth of frequencies excited by the RF pulse, or a combination of both.

2.1.6.2 Frequency encoding gradients

The frequency encoding gradient, sometimes referred to as the readout gradient creates a linear gradient across a chosen direction. The frequency encoding gradient is applied as the signal is captured (usually using an Analogue-to-Digital Converter (ADC) and so during this time, as long as the bandwidth of the receiver is sufficiently large, the MR signal that is collected contains information from all the frequencies of the object encoded by the 'frequency encoding' gradient.

The orthogonal dimension of the selected slice could also be encoded and acquired using a second frequency encoding gradient, but it turns out practically more difficult to achieve this. This is because magnetic field gradients add as vectors and the result of the simultaneous application of two gradients is in fact a single gradient along the direction of the vector sum of its components. Although this is the way in which MR imaging was originally achieved (Lauterbur 1973), a practical modification was later introduced which made imaging more practically achievable.

2.1.6.3 Phase encoding gradients

In 1980, Edelstein and colleagues (Edelstein et al. 1980) introduced the use of what was later known as 'phase encoding gradients'. A phase encoding gradient is a gradient across the orthogonal direction of the frequency encoding direction. The phase encoding gradient is usually applied any time before the application of the frequency encoding gradient. The phase encoding gradient effectively changes the phase at which the spins are precessing across its direction, within the slice that has been initially excited. Following the application of the phase encoding gradient, from the point of view of the frequency encoding axis, the spins will be resonating with different phases depending on their location along the phase encoding direction.

The combination of phase and frequency encoding gradients on the object being imaged provides the ability to now distinguish between individual signals of different phase and frequency by creating a measured signal which reflects the summation of multiple measurements and frequencies over time. A signal measurement is made along the frequency encoding direction for every value of the phase encoding gradient. Each of these sampled signals is collected into a data grid, which corresponds to the inverse domain of the object. This 'inverse space' of frequency encoding temporal signals is known commonly as k-space, because of its analogy with X-ray crystallography.

Conventionally, this data grid is filled 'line by line', known as Cartesian sampling although other methods for sampling trajectories are also used for MRI applications (Hennig 1999). Once the entire k-space grid (known as the data acquisition matrix) has been sampled, then the signals are reconstructed into an image by means of a discrete inverse Fourier transform which transforms the frequency components of the measured signal into real (Cartesian) space. In an MRI experiment each slice will be encoded by a single plane of its corresponding k-space.

2.1.7 Tissue contrast

T1 and T2 relaxation are inherent to individual tissue types and these relaxation differences are fundamental for differentiating between tissues. This is the basis of tissue contrast. Tissue contrast can be modulated and optimised through definition of two crucial imaging parameters; the repetition time (TR) and echo time (TE) (Damadian 1971).

TR is roughly defined as the time between two RF pulse excitations corresponding to different portions of k-space. A long TR will permit spins to relax fully through T1 relaxation, allowing the net magnetisation vector to align more closely to M_Z, whereas a shorter TR will prevent the M_Z vector for certain tissues to fully relax.

TE on the other hand is defined as the time between the excitation RF pulse and when the signal measurement from the transverse signal is taken. Dense tissues with shorter T2 values (due to increased spin-spin interactions) would require a shorter TE to capture the signal before the M_{XY} vector decays, whereas tissues with a longer T2, such as water, can be imaged with a longer echo time (see Figure 2.1.6).

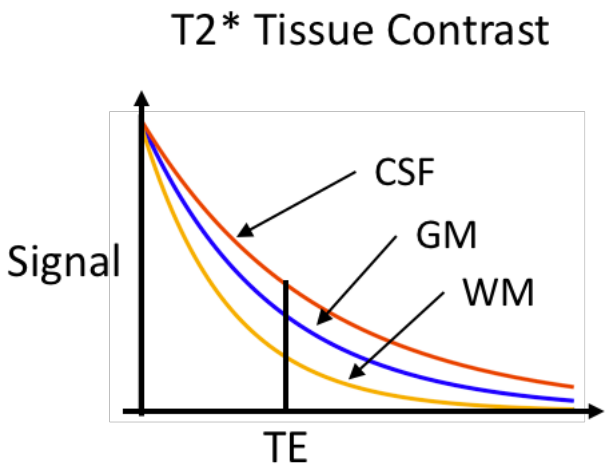

Figure 2.1.6 An example of how different tissues will decay at different exponential rates. By choosing an appropriate TE optimal contrast (difference in signal) between tissues can be obtained.

By defining both TR and TE parameters and with prior knowledge of the associated T1 and T2 relaxation rates of the tissues of interest, contrast of different tissue types within images can be achieved. For example, in a T1-weighted image acquired with a short TR (and a short TE), spins with a short T1 will provide a large signal. On the other hand, in a T2-weighted image acquired with a long TE (and long TR), spin species with a long T2 will exhibit larger signal amplitudes.

2.2 Functional Brain Imaging

Functional brain imaging using MRI, known as fMRI, has been vital to the present understanding of brain function and its modification in disease. fMRI adopts MRI techniques that are sensitive to neurophysiological and neurovascular changes that occur in response to neuronal activation (Attwell and Iadecola 2002). Although not a description of methods the next section will describe some of the key neurophysiological processes that occur during this neurovascular response.

2.2.1 Measuring neuronal activation – neurovascular coupling

The brain parenchyma is supplied with a fresh supply of oxygenated blood by cerebral arteries, arterioles and capillaries, this phenomenon is known as Cerebral Blood Flow (CBF) and is also referred to as brain tissue perfusion (Attwell and Iadecola 2002). Brain tissue perfusion is maintained at a relatively constant level; and as the brain is a highly metabolic organ, producing most of its energy through oxidative metabolism, any major disturbances or perturbations to this system can lead to severe gross pathology, for example stroke (Girouard and Iadecola 2006). Neural information is transferred throughout the brain via conduction along neuronal axons. The primary mechanism for information transfer between neurons across the synaptic cleft, is by the action of neurotransmitter molecules released from the pre-synaptic cleft which bind upon post-synaptic neurotransmitter receptors. These neurotransmission events are largely fuelled by oxidative glycolysis and therefore lead to metabolic changes within the neurons and surrounding glial cells as a result of a higher local demand for oxygen delivery. This close spatial relationship between the neurons, glial cells and the vascular system, which allows the local energy demands to be met by increasing regional blood flow at a cellular level, is known as *neurovascular coupling* (Attwell et al. 2010).

As previously mentioned, the brain has a very high level of resting metabolism, consuming approximately twenty percent of the body's total oxygen supply (Attwell

et al. 2010). The bulk of oxygenated arterial blood is delivered or supplied by two major groups of feeding arteries: the bilateral internal Carotid and Vertebral arteries. At the Circle of Willis, these cerebral feeding arteries bifurcate into smaller cerebral vessels known as pial arteries. These pial arteries are the anterior, middle and posterior cerebral arteries (Cipolla 2009). Pial arteries span across the surface of the entire brain parenchyma within the pia-subarachnoid space and perfuse all regions of the cerebrum. Surrounded by cerebrospinal fluid (CSF), the pial arteries advance into arterioles that 'penetrate' the brain tissue via the Virchow-Robin Space (Cipolla 2009). The vascular wall of arterioles is made of smooth muscle. Within the tissue architecture, the vessels are classified as parenchymal arterioles and are bounded by astrocytic end-feet which terminate on the outer layers of these arterioles. Downstream of these arterioles is the capillary bed, which forms a highly connected and dense network of vessels with a large surface area for efficient vessel to neuronal tissue nutrient exchange. Capillaries no longer have smooth muscle in their walls.
Exchange of nutrients is produced by an intra-capillary pressure gradient that when increased leads to enhanced tissue perfusion facilitated by specialised capillary endothelial cells (Begley and Brightman 2003). Therefore, an increase in nutrient exchange, in most cases oxygen and glucose, requires an increase in intra-capillary pressure.

The auto-regulatory control mechanisms that act to maintain sufficient blood flow and react in response to increased neuronal metabolism do so at the level of the parenchymal arterioles not at the capillary bed. However, this change in flow is accompanied by an increase in capillary pressure thus there are several mechanisms that must be achieved to increase oxygen supply to meet metabolic demands. These arterioles are comprised of three layers; the inner endothelial cell layer, the middle smooth muscle layer and the outer collagenous layer. The smooth muscle layer is capable of dilating and constricting the vessel walls, permitting increases and decreases in flow, respectively. Vascular resistance is governed by Pousille's Law which identifies the vessel radius as the main effective constituent. Vascular resistance is inversely proportional to radius (r) to the fourth power and therefore

any small change in vessel radius or lumen width is coupled with a dramatic change in flow (Washburn 1921).

Increases in synaptic transmission have been shown to directly influence the rate of regional brain tissue perfusion (Harris, Reynell, and Attwell 2011). A proposed mechanism suggests that, among the milieu of processes that occur during synaptic transmission, neuronal-astrocytic messenger molecules are generated that act to either modulate calcium (Ca^{2+}) ion channel activity on smooth muscle cells or to affect the sensitivity of contractile units to Ca^{2+} within the parenchymal arteriole smooth muscle cells (Attwell et al. 2010). In addition to interactions on Ca^{2+} channel activity there are agents or messenger molecules released during synaptic transmission that act on potassium channels (K^{+}) present on the smooth muscle cells of the arterioles. Opening of these channels causes cell hyperpolarisation, reducing intracellular Ca^{2+} and consequently leading to smooth muscle relaxation and an associated increase in flow (Buxton 2013). Furthermore, nitric oxide (NO) is known to interfere with the intracellular sensitivity of contractile units within smooth muscle to Ca^{2+} signalling (Buxton 2013) and is thought to be highly involved in this neurophysiological response.

This response to neuronal activity/metabolism can be termed functional hyperaemia as the increase in blood flow is coupled with an increase in oxygen supply. The two common fMRI techniques, used in the current study of intranasal insulin, and in most fMRI studies, are perfusion fMRI and blood oxygenation level dependent (BOLD) fMRI. Perfusion fMRI techniques permit assessment of neuronal activity through estimation of changes in cerebral blood flow (CBF). Blood Oxygen Level Dependent (BOLD) fMRI, however, permits the assessment of neuronal activity primarily by being sensitive to changes in the relative concentration of deoxygenated haemoglobin in the blood. This in itself is driven by changes in blood flow, oxygen metabolism and the changes in magnetic susceptibility that accompany this neurovascular response. The neurophysiology of the BOLD effect along with methods used to capture this effect will be outlined in section 2.3.

2.2.2 Cerebral blood flow and arterial spin labelling

Assessment of resting cerebral blood flow (CBF) for the SNIFAR study was conducted using a non-invasive perfusion imaging technique known as arterial spin labelling (ASL). Using blood water as an endogenous contrast agent ASL is a technique that can quantify regional CBF in traditional physiological units of ml / 100g of tissue / min (Petersen et al. 2006), it is a measure of the amount of arterial blood delivered to the brain tissue regardless of directionality.

In the simplest form, ASL requires the acquisition of a minimum of two images; one labelled image and one control image. The labelled image is produced in two steps. Step 1: water spins within arterial blood are magnetically labelled (inverted with respect to the static signal). Step 2: following this labelling period the spins are allowed to travel along the arterial cerebral tree to the capillary bed at which point an image is acquired. The control image is an image acquired in the same way as the label but without labelling of arterial blood (Detre et al. 1992). The control image theoretically contains signal contributions from flowing blood which are indistinguishable from the static signal; in turn, the static signal is also largely identical to that from the labelled image. Pairwise subtraction of these images (control – label) produces a difference image, known as a 'perfusion weighted image', with signal intensities that arise from the contribution of labelled, inflowing blood magnetisation. Acquiring and subtracting images in this manner achieves signal differences of approximately 0.5-1.5% (corresponding to the proportion of proton spins in the capillary volume relative to those of the rest of each voxel), but with multiple average acquisitions, sufficient signal to noise ratio (SNR) can be achieved (Alsop et al. 2014). The signal difference obtained from ASL is also dependent on factors such as T1 longitudinal relaxation of arterial blood, time taken for labelled spins to travel from the labelling plane to the imaging plane as well as haemodynamic properties such as cerebrovascular constriction and dilation (Petersen et al. 2006; Wang, Chen, et al. 2011a).

A huge benefit of ASL is that whole brain physiologically relevant information, CBF, can be ascertained that is easily interpretable and applicable to many research and clinical applications (Alsop et al. 2014; Wang et al. 2003). Another benefit is that unlike Positron Emission Tomography (PET), ASL does not require ionising radiation in order to generate perfusion contrast. In PET, this is normally achieved by injecting radiolabelled water ($H_2{}^{15}O$, due to the fact that ^{15}O is a positron emitter). This technique is still considered in some quarters as the 'gold standard' method for CBF quantification (Ramsay et al. 1993; Ye, Berman, et al. 2000). Due to the non-invasive character of ASL, serial ASL images and CBF maps can be acquired over the course of longitudinal MRI investigations, which is perhaps one of the main reasons why this method has become an attractive alternative in pharmacological investigations. The term pharmacological MRI (phMRI), coined by Jenkins et al., describes a methodology used to correlate changes in pharmacokinetic data (PK) with changes in functional MR signal (Jenkins 2012). Originally implemented with Blood Oxygen Level Dependent (BOLD) techniques, this concept has also been adopted with ASL through acquisition of serial measurements during an MRI experiment, for example in Paloyelis et al., (Paloyelis et al. 2014).

The next section will discuss in detail the fundamental physics of ASL and the evolved sophistication that this method has experienced, in order to provide more reliable quantitative estimates of CBF. Both the labelling and imaging components will be described in general and more specifically with reference to the technique used for the SNIFAR study.

2.2.2.1 Labelling

In general, there are three types of commonly used ASL techniques, classified depending on the nature of their labelling methods: pulsed ASL (PASL), continuous ASL (CASL) and a variant of CASL called pseudo-continuous ASL (pCASL) (Alsop et al. 2014).

PASL uses a single and relatively short (10-20ms) RF pulse to achieve labelling, through inversion of inflowing water spins in the region of the carotid arteries. CASL, which is the original ASL method realised in 1992 (Detre et al. 1992; Williams et al. 1992) requires application of a continuous RF pulse of 2-4 s duration as a labelling mechanism across a plane perpendicular to the feeding carotid arteries in the neck. Coupled with this pulse is a constant magnetic field gradient applied in the blood flow direction which causes flowing arterial (carotid) spins to experience slow moving variations of their resonance frequency as they move along this gradient, ultimately resulting in spin inversion (Williams et al. 1992).

The inversion of spins produced by the combination of an applied RF pulse and gradient vector in the flow direction is known as 'adiabatic inversion' or 'velocity driven adiabatic inversion', because it works as long as the target spins are moving, which is the case for arterial spins. Spins that flow through the labelling plane will possess a tendency to follow the slow rotating effective field producing an inversion of the magnetisation (Dai et al. 2008). The method works as long as the spins experience inversion at a rate faster than that at which they are losing magnetisation due to T2 relaxation; but slower than the rate of rotation of the effective field, hence the adiabatic character of the process. This condition can be summarised by the following expression

$$\frac{1}{T_2}, \frac{1}{T_1} << \frac{Gv}{B_{eff}} << \frac{\gamma}{2\pi}\left|B_{eff}\right|$$

where *G* is the amplitude of the gradient in the direction of flow and *v* is the flow velocity.

pCASL, a variant of CASL developed by *Dai* et al., achieves flow driven adiabatic inversion through application of a series of short (500-100 microsecond) Hanning shaped RF pulses coupled with a train of gradients with a small (non-zero) net value,

as opposed to a continuous RF pulse (Dai et al. 2008). The net amplitude of RF power in the presence of a net, finite magnetic field gradient, achieves flow driven adiabatic inversion. The Hanning shape of each pulse ensures that aliasing planes of the label fall outside of the desired image volume. The phase of each RF unit is incremented so that at the end of the RF train, the spins experience a net phase shift of:

$$\gamma G_{net} \Delta_z LD$$

Where G_{net} is the net gradient in the direction of flow, Δ_z is the position of the labelling plane relative to the magnet iso-centre and *LD* is the labelling duration.

In the control condition, the amplitude of each RF pulse unit is inverted and the gradient lobes are balanced so as to produce a net gradient of zero in the direction of flow. Therefore, the control condition has the same RF power deposition, the same magnetisation transfer contribution but no flow encoding.

The general scheme for a pCASL sequence is displayed in Figure 2.2.1

The net duration of the train of labelling RF pulses (labelling duration-LD) is an important parameter included in the CBF quantification calculation. The current recommended LD for pCASL, in healthy volunteers is 1800ms (Alsop et al. 2014).

2.2.3 Label duration

The effect of label duration (LD) has been explored by several groups in an effort to increase the ASL signal measured from pCASL experiments. The small amount signal provided from labelled arterial blood coupled with low capillary volume in the brain makes ASL a relatively low SNR technique (Buxton 2005). Explorative work with pCASL label durations has shown evidence that increased SNR can be achieved by increasing the labelling duration to 3.5 - 4s seen from both simulated and measured pCASL data (Zun et al. 2014). Any further increases are prevented by the hardware

constraints of the amplifier, the Specific Absorption Rate (SAR) limit and the need to have sufficient fresh inflowing blood for the next TR. Increasing the LD gives rise to a linear increase in the bolus width of the arterial label, which leads to greater perfusion induced signal difference in the perfusion weighted images. Selectively increasing the LD, with no change to the imaging readout parameters, provides an increase in contrast to noise ratio. With those values of LD, pCASL can be carried out without a significant increase in SAR (Dai et al. 2012).

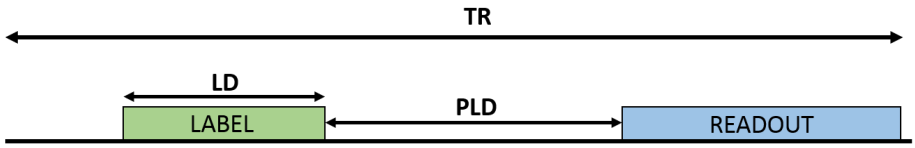

Figure 2.2.1 An example of a pCASL sequence. The labelling scheme (green) is applied for a set length, defined by the labelling duration (LD). Following labelling of inflowing arterial spins there is a delay period (PLD) to allow the labelled bolus to flow into the imaging volume an image is acquired (readout).

2.2.3.1 Imaging and post labelling delay

Immediately after labelling, the inverted spins will travel through the arterial vasculature to the capillary bed. The time between the end of the labelling pulse and the arrival of the labelled bolus to a voxel in brain tissue is known as the Arterial Transit Time (ATT) (Qiu et al. 2010); this is an important parameter for CBF quantification. In most pCASL protocols, a single delay period between labelling and image acquisition is used, sometimes also known as the post labelling delay (PLD). In an ideal ASL experiment, the PLD should match the ATT at every voxel so that image acquisition will be performed as the labelled spins are in the capillary bed. In reality this is of course impossible to achieve as the ATT is a physiological parameter that differs between subjects, it can vary with age, and also differs between brain regions and lobes (MacIntosh et al. 2010). If the chosen PLD is too short, labelled spins that are still within the arterial compartment will lead to signal hyperintensity in the arteries; whereas PLD times that are much longer than the ATT will lead to signal

corresponding to the venous compartment; and because of labelled signal decay via longitudinal relaxation (discussed in more detail below), this would lead a considerable loss in SNR. An optimal, single PLD for pCASL acquisition is one when most of the labelled bolus resides in the capillary domain. This value is approximately 1800 ms for young, healthy volunteers (Alsop et al. 2014).

The implementation of multi-PLD ASL acquisition schemes has seen an increase in popularity and development over the last few years. Multi-PLD refers to ASL acquisitions that acquire perfusion weighted images after more than one PLD time (Gonzalez-At, Alsop, and Detre 2000). In doing so, the inflow and outflow of labelled spins can be modelled more accurately. From this extra information, estimates of ATT can also be performed, in addition to measures of CBF for each voxel. Acquiring this additional information incurs a penalty on overall acquisition time. More complex methods to remedy this penalty, whilst still providing the gain in additional temporal information have been developed. One such method is known as Hadamard encoding ASL sequences (Dai et al. 2012; Wells et al. 2010; Gunther 2007).

2.2.3.2 Hadamard encoding

Typical pCASL or CASL perfusion weighted image formation requires the acquisition of a label image and a control image, which are subtracted to provide a perfusion weighted difference image. For Hadamard encoding acquisition the principle is to acquire a series of images following implementation of a labelling module that is constructed from several control and label sub-blocks (Wells et al. 2010). The labelling module oscillates between label and control sub-blocks of a set duration which produces an image that is composed of a mixture of control and label signals from these sub-blocks. The ordering of sub-blocks is determined by a Hadamard matrix which is then applied during image-processing to separate this mixture of signals through a linear combination of the images. Following image processing a set of perfusion weighted images with differing PLD times is created. To create a set of perfusion weighted images of seven different PLD's an 8 x 8 Hadamard matrix is used

that requires eight acquisitions. In comparison to conventional multi-PLD which would require fourteen total acquisitions (7 control, 7 label) to achieve seven PLD difference images (Dai, Shankaranarayanan, and Alsop 2013). In addition to this temporal benefit, Hadamard encoding also boasts an increase in SNR due to the way the images are linearly combined and also reduced number of acquisitions (Dai, Shankaranarayanan, and Alsop 2013).

For the SNIFAR study, we chose to employ a single-PLD pCASL ASL sequence. Following labelling of arterial blood, the inverted spins will decay with T1 during the PLD time; leading to a sub-optimal ASL signal difference, even in the presence of high RF inversion efficiency. Therefore, the readout imaging modules for ASL should ideally possess a high temporal resolution. Both 2D and 3D readouts can be utilised with pCASL. The main advantage of 3D readouts over 2D is that the entire imaging volume can be acquired during a single excitation permitting a single PLD to be used for quantification, as opposed to slice dependent PLDs that need to be adjusted for each slice location. Furthermore, suppression of background tissue signal (see below) is better executed because the inversion times of the background suppression module are relevant to the whole image volume.

2.2.3.3 Background suppression

Background suppression is a technique used to supress signal from tissues or components that are not of interest, to achieve higher contrast between the signals of interest (Garcia, Duhamel, and Alsop 2005; Ye, Frank, et al. 2000). In theory the perfusion weighted subtraction images should remove the static unwanted tissue signal however subject motion during ASL acquisition produces signal fluctuations proportional to the tissue of interest signal prior to this subtraction. By reducing the signal from the background, the sensitivity of pCASL can be improved dramatically (Garcia, Duhamel, and Alsop 2005). This is done using a combination of saturation, spatially selective and non-selective inversion pulses prior to labelling and readout to

essentially null the static signal at the start of the readout window (Garcia, Duhamel, and Alsop 2005).

2.2.3.4 Imaging readout

Readout modules should be considered independent of the labelling modules (see Figure 2.2.1). In the SNIFAR study, a single shot 3D fast spin echo (FSE) stack of spirals imaging readout was implemented (Ahn, Kim, and Cho 1986). In this sequence, the excitation pulse is applied to the entire imaging volume. Following a flip of magnetisation into the transverse plane a number of refocusing 180^{O} pulses are applied to produce a train of echoes, known as FSE sequence, originally called a Rapid Acquisition with Refocused Echoes (RARE) (Hennig, Nauerth, and Friedburg 1986). Each echo is sampled with a spiral trajectory, known as a spiral arm, with application of a phase encoding gradient along the slice direction between each of the echoes, so that each echo is sampled in an ascending slice order. As the peak of each echo within this train of sequential echoes (echo train) will decay with T2, there is a decrease in signal in the slice encoding direction, which leads to what is known as 'z-blurring' (Figure 2.2.3). A compromise between number of slices (which determines the length of the echo train) and the slice thickness must be considered in order to avoid deleterious blurring in the slice encoding axis (Glover 2012). This is most visible from coronal images.

Spiral imaging is a non-Cartesian method of sampling k-space that follows a spiral trajectory as opposed to filling k-space in a rectangular trajectory. This type of sampling is temporally efficient as using this trajectory, all the area of the k-space plane can be sampled within a single shot (Glover 2012). Spiral imaging sampling methods can be used to acquire data from the centre of k-space outwards or from the outside inwards. Both of these trajectories can increase the time taken to sample k-space by under-sampling the high frequency data points in the corner of k-space (Irarrazabal and Nishimura 1995; Glover 2012). Sampling in this way can provide a 21.5% reduction in overall acquisition time and by oversampling in the centre of k-space can provide some resistance to subject related movement (Liao et al. 1997).

Spiral readouts have been utilised in functional imaging experiments for these reasons (Glover 2012). To create a spiral trajectory in k-space the phase and frequency encoding gradients oscillate in a sinusoidal manner during the readout window (Ishimaru et al. 2007). This can be seen in Figure 2.2.2.

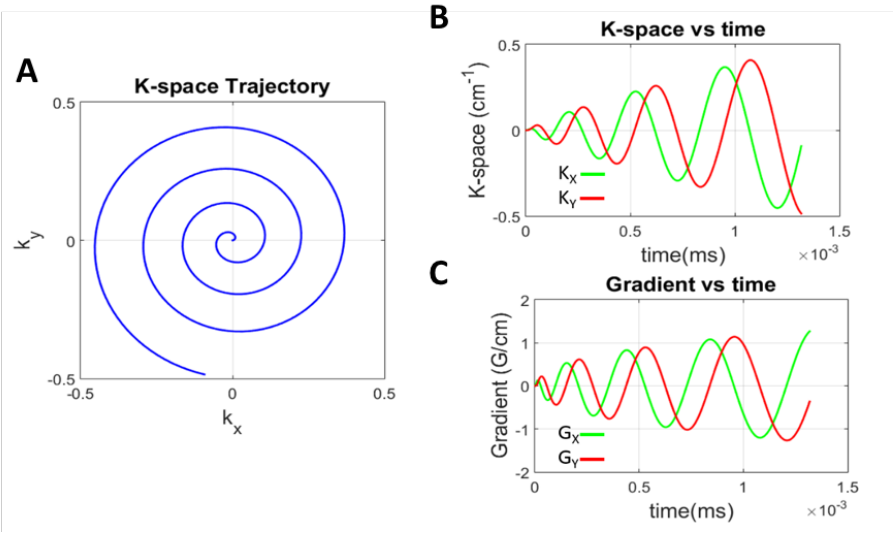

Figure 2.2.2 Example of a typical k-space trajectory adopted with a spiral readout sequence. A) The trajectory sampled in k-space with spiral readout. B) Depicts the K_x and K_y coordinates over time. C) The oscillating phase and frequency encoding gradients G_X and G_Y that are required for spiral sampling. Gradient amplitude increases over time as the spiral increases in diameter.

2.2.3.5 Decreasing the voxel size of CBF maps

Whilst the spatial resolution of a 2D image in MRI is dictated by the inverse of the area sampled in k-space, the ability to resolve the higher spatial detail encoded by higher gradient amplitudes, depends on being able to acquire information from smaller voxels with sufficient SNR. For spiral acquisitions, this can be achieved by increasing the number of points sampled per arm in k-space, and in the orthogonal dimension by increasing the number of frequency encoding steps. In the plane of the image, higher spatial detail can be obtained in two ways; by increasing the number of spiral arms acquired and by also increasing the number of points sampled per spiral arm. Increasing the number of arms leads to an associated increase in overall scanning time as each additional spiral arm requires an additional TR. Furthermore,

increasing the number of data points sampled per arm increases the echo spacing; and therefore the effective echo time of the through-plane sample, introducing greater T2 signal loss across the slice encoding gradient direction and consequentially exhibiting a greater degree of 'T2-blurring' along the z-axis.

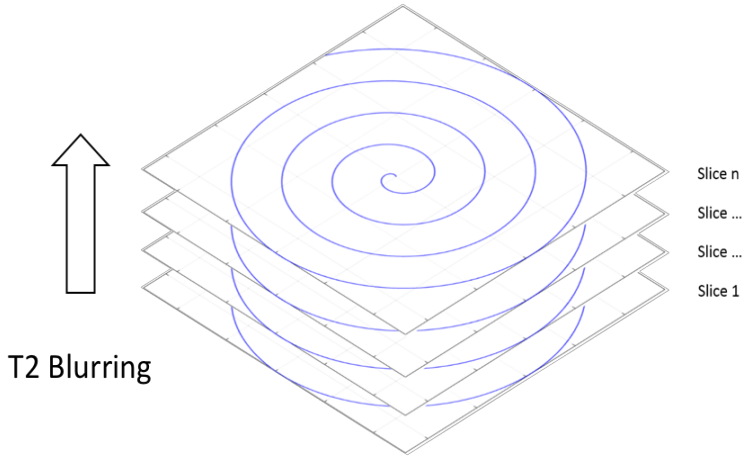

Figure 2.2.3 An example of the 3D spiral sequence trajectory. Each echo is sampled along a single spiral arm. In between each echo a slice encoding gradient moves to the next plane of k-space to acquire the subsequent echo and so on. As the sequence acquires from bottom to top there will be a blurring effect in this direction due to T2 decay of the echo train.

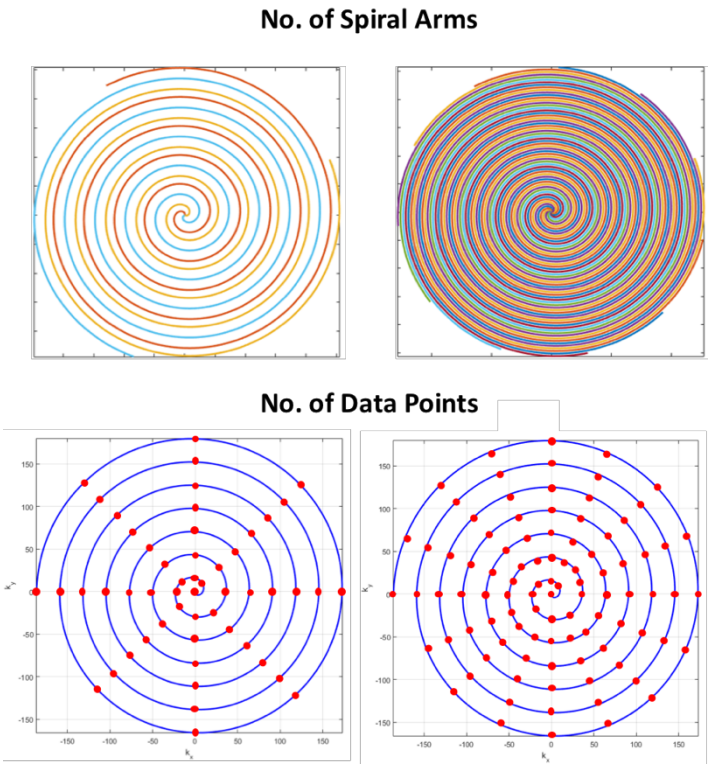

Figure 2.2.4 Examples of k-space spiral trajectories and how the sampling density can be increased by additional spiral arms or additional data point per spiral arm.

From previous work conducted as part of my MRes project, this 3D-pCASL FSE stack of spiral sequence was implemented in a pCASL sequence package that possessed the ability to deliver long label durations (up to 4s, in comparison with the 1.5s default duration of the conventional package). In this work, a pCASL sequence was optimised using a long LD to increase SNR within the perfusion weighted image acquisition. Increasing the LD from a standard label duration (1.5s) to 3-4s displayed a significant gain in SNR (approximately 30%, at in plane resolution of 3.4 x 3.4 mm^2), when compared with identical readout parameters, which turned out to be highly beneficial in spite of an overall decrease in temporal resolution (increased TR). Using this gain in signal, the project explored the effect of increasing the spatial resolution (decreasing the voxel size) in an effort to acquire pCASL images and CBF maps with sufficient resolution to better resolve small anatomical structures and better define

the cortical gyri. As mentioned in the previous chapter, increasing the resolution requires increasing the spiral sampling density which was achieved through obtaining an optimal combination of spiral arms and points sampled per arm. The optimal combination based on image quality and taking into consideration the overall scan time, was selected to be an isotropic resolution of $3mm^3$. This sequence was used throughout the pharmacological investigation of intranasal insulin which will be presented in this thesis.

2.2.3.6 Partial volume averaging

The average adult CBF for grey matter (GM) is approximately 55 – 65 ml/100g/min whereas the average CBF for white matter (WM) is considerably less, roughly 20 ml/100g/min (Parkes et al. 2004). CBF tends to show a decline with age independent of cerebral GM atrophy (Chen, Rosas, and Salat 2011). From ASL acquisition, a measure of CBF for each voxel can be obtained. Voxels at the boundaries between grey matter and white matter will contain signal contributions from both of these tissue types reflecting a signal average of both tissue (Chappell et al. 2011). This is known as a partial volume contamination (PV) effect and is inherent to imaging techniques but is accentuated in acquisitions with large signal differences between tissue types and techniques with low spatial resolution, such as ASL (Asllani, Borogovac, and Brown 2008). Similarly, these PV effects also arise at the GM and cerebrospinal fluid (CSF) boundaries. PV effects for CBF mapping leads to an underestimation of CBF within these boundary regions which is particularly problematic in studies looking at ageing where the cortical GM ribbon is largely reduced due to cortical atrophy processes (Creasey and Rapoport 1985). There are a number of PV correction methods that are available (Asllani, Borogovac, and Brown 2008; Chappell et al. 2011) which have struggled to be adopted in general ASL processing practices. Given the lack of an accepted and standardised PV correction approach we have opted to increase the SNR as much as possible to reduce the voxel size to an optimum dimension.

2.2.3.7 Cerebral blood flow calculation

A crucial advantage of ASL as a functional brain imaging tool is the ability to create quantitative maps of CBF. Assuming the static tissue signal from control and label images has been subtracted effectively the perfusion weighted image signal (difference) will be proportional to the efficiency of inversion, the amount of labelled arterial blood delivered to each voxel during the PLD and the specific capillary volume at each location. All these factors contribute to the computed regional value of CBF. Quantification of CBF is conducted through a voxel-wise calculation of perfusion weighted images (control – label) and also a reference scaling image (commonly a proton density (PD) image) along with additional parameters (Buxton 2005; Buxton et al. 1998) which depend on the specific pulse sequence employed.

There are several methods and models that can be used for CBF quantification, but the simplest model is the single compartment model which will be presented and for single PLD ASL data has been shown to be appropriate (Alsop et al. 2014). This model of CBF assumes that the entire labelled bolus has entered the target tissue. In healthy individuals, this assumption can be largely satisfied by selecting a PLD that is longer than both the longest ATT and tissue transit time (Alsop et al. 2014). Liu et al., showed that a typical tissue transit time was approximately 1900ms for healthy individuals and that a PLD of approximately 2s is hence sufficient to allow for arterial labelled spins to completely enter the tissue space (GM) (Liu, Uh, and Lu 2011). Additional parameters required in this model are calibration factors that take into account the T1 relaxation time of arterial blood ($T1_{blood}$), the labelling efficiency of the ASL label (α) and also the proportion of proton spins in blood vs the proton spins in tissue, known as the blood brain barrier partition coefficient (λ). The model also requires the value of the temporal width of the labelled bolus duration (τ); which in pCASL and CASL corresponds to the duration of the labelling pulse.

The formula, for pCASL using a single PLD is presented below:

$$CBF = \frac{6000.\ \lambda\ .\ PW\ .\ e^{\frac{PLD}{T1blood}}}{2\ .\ \alpha\ .\ T1blood\ .\ PD\ .\ (1 - e^{\frac{-\tau}{T1blood}})}$$

The PLD and τ are prescribed parameters of the sequences whilst the other parameters in the equation can be measured or, are known from reference values. For example, the T1blood set to 1650ms at 3T (Lu et al. 2004), α for pCASL is 0.85 (Dai et al. 2008) but the efficiency of background suppression also has to be taken into account (in our sequence this value was 0.8). λ is 0.9mL/g (Herscovitch and Raichle 1985). The PD image, used in the quantification is acquired with the same readout parameters as the control and label images, is employed as a scaling factor. The 6000 in the above equation is a conversion factor to produce CBF measurements as ml of blood per 100g of tissue per minute (Alsop et al. 2014).

This single compartment tissue model assumes that all labelled spins diffuse from the capillary compartment to the tissue compartment immediately, and therefore the signal contribution from each tissue voxel is from spins within the tissue space, assuming a long enough PLD. In reality this exchange is not immediate and furthermore, not all labelled spins will diffuse from vessel to tissue thus leading to inaccuracies in CBF estimation. *Parkes* et al., developed a kinetic CBF model that accounts for these two issues, which they call the *T1 effect* and *outflow effect* (Parkes and Tofts 2002; Parkes 2005). Although more accurate estimations of CBF can be obtained using those models, these were not employed in this work.

2.3 Blood Oxygen Level Dependent Contrast

The origin of the BOLD signal stems from the differential magnetic properties of haemoglobin which when oxygenated is diamagnetic and when de-oxygenated is paramagnetic; and from the uncoupling of blood flow and oxygen utilisation as a result of changes in neuronal activity. The paramagnetic properties of deoxyhaemoglobin alter the local magnetic susceptibility in its vicinity, both within and outside of the venous capillaries, ultimately producing a reduction in the regional transverse MR signal, as result of additional loss of phase coherence. As stated above, the origin of the BOLD effect exploited in fMRI experiments stems from a neurophysiological phenomenon that occurs in response to increased neuronal activity. Increases in neuronal activity are almost always associated with local increases in CBF as a result of the phenomenon of neurovascular coupling. Upon changes in neural activation this regional increase in CBF is *proportionally* much greater than the relative increase in cerebral metabolic rate of oxygen ($CMRO_2$) and this results in a decrease in oxygen extraction fraction (OEF) coupled with a decrease in the relative concentration of deoxyhaemoglobin in the venous domain (Fox and Raichle 1986). Because the blood, localised to the neuronal activation, is (as a whole) now more oxygenated than deoxygenated, the net magnetic field distortions are decreased and there is hence an increase in the local transverse MR signal. This dependence of the MR signal on the neurophysiological response of the tissue, also known as the 'haemodynamic response', is more strongly reflected in imaging methods that are sensitive to local field distortions, such as the case of gradient echo, T2* weighted echo Echo Planar Imaging (EPI) (Mansfield 1977).

The BOLD effect signal is a therefore the result of the sum of contributions from changes in CBF, $CMRO_2$ and Cerebral blood volume (CBV) partially mixed over the course of this haemodynamic process, and it is known as the 'haemodynamic response function' (HRF) (Buxton et al. 2004). A detailed description of the underlying mechanisms of the neurophysiological phenomenon of the BOLD effect is elegantly described in Buxton et al., (Buxton et al. 2004). The next section will guide

the reader through the BOLD effect in response to task-based stimulus, common to fMRI experiments and how these effects are measured.

Pioneering work by Turner et al., and Ogawa et al., initially showed how decreases in the MR signal surrounding cerebral blood vessels (following changes in blood oxygenation levels from respiratory gas challenges) could be observed in the cat and rodent brain, respectively (Turner et al. 1991; Ogawa et al. 1990). This work suggested that deoxygenated blood, in other words rich in deoxygenated haemoglobin, could be used as an intrinsic contrast agent when acquired with gradient echo imaging sequences. Shortly following these findings, Ogawa et al., showed that these MR signal changes could be observed in the human occipital region and calcarine fissure while the subject was presented with a bright visual stimulus (Ogawa et al. 1992). This evidence highlighted the sensitivity of rapid gradient echo sequences to local changes in deoxyhaemoglobin that could be perturbated by external stimuli and opened the door to a new field which we now know as BOLD contrast fMRI. Bandettini et al, (1992) also showed how similar changes could be measured in primary motor cortex in response to a 'finger tapping' task (Bandettini et al. 1992).

Fundamental to the ability to observe BOLD contrast changes in the human brain during a task requires a gradient echo scanning protocol that fulfils certain acquisition qualities. Firstly, to capture these temporal effects, the acquisition needs to be conducted rapidly, in order to capture signatures of these neurophysiological changes with sufficient accuracy and reliability (Turner et al. 1998). Secondly, images need to be acquired with sufficient spatial resolution in order to resolve local changes in BOLD contrast that are reflective of the underlying anatomy in small structures. And finally, to permit explorations of functional stimuli on the whole brain, an acquisition scheme capable of acquiring multiple slices during the BOLD contrast event is necessary. As indicated earlier, a rapid acquisition sequence known as gradient recalled Echo Planar Imaging (EPI) (Mansfield 1977), possesses these qualities and has been the 'workhorse' of the fMRI BOLD contrast research conducted over the last 26 years. EPI readouts are rapid (~40-100ms) but carry a cost

of spatial resolution and therefore a compromise between temporal and spatial resolution is required.

2.3.1 Echo planar imaging

With this method, it is possible to acquire whole brain data (20-30 T2* weighted images) in a single TR, which is approximately 2s for most conventional fMRI protocols. The term TR in this instance refers to the time taken to acquire all the slices as opposed to the time between subsequent RF excitations. A readout scheme known as blipped EPI is commonly used. This type of readout fills the entirety of k-space in a rectangular trajectory, following a single RF excitation pulse. As outlined in the beginning of this chapter, application of an excitatory RF pulse generates a Free Induction Decay (FID) signal. In the blipped EPI sequence, the FID decay is initially accentuated by application of a large phase and frequency de-phasing gradient. Following this, the receiver coil is opened and the first lobe in a train of frequency encoding gradient is applied, generating a gradient recalled echo from which a single line of k-space is sampled. A frequency encoding gradient of the same strength and duration is applied in the opposite direction preceded by a small phase encoding gradient (blip) to acquire another, the next, line of k-space. This frequency encoding gradient switching and blipped encoding sequence is repeated until the entire matrix of k-space data is 'filled'. Once filled, a slice encoding gradient is applied to excite the next slice and the same sequence is followed until all data for the next slice has been acquired. This process is repeated over an fMRI experiment producing a serial collection of T2* weighted images, known as a 'a functional timeseries'. From this time series, the haemodynamic response can be measured by obtaining a sufficiently large number of time points for each voxel. Several analysis methods can then be used to model the haemodynamic response function, in response to sensory or cognitively induced neuronal activation.

2.3.2 Task based fMRI and the haemodynamic response

Task based fMRI describes an MRI experiment where a participant is required to execute a paradigm whilst in the scanner; during which a functional time series of MRI data is acquired. Actions can range from basic sensory stimulations such as visual stimuli to more cognitively demanding tasks that involve learning, decision making or memory related functions (Amaro and Barker 2006). The series of actions within a task are known as 'the paradigm' and compiled using a pre-defined playlist of actions with explicit timings and duration for all the actions.

A convenient property of the HRF is that it is additive when more than one stimulus is applied within the temporal width of the HRF. Hence, a useful design for paradigms is what is known as a 'block periodic design'; in which images collected within periods of a certain type of sensory or cognitive engagement are contrasted against those collected within a 'reference' condition.

In response to a stimulus, the haemodynamic response function (HRF) can be observed as a temporal change in MR signal. The HRF can be broken down into three parts; the initial dip, the peak and the post stimulus undershoot. (HRF shown in Figure 2.3.1)

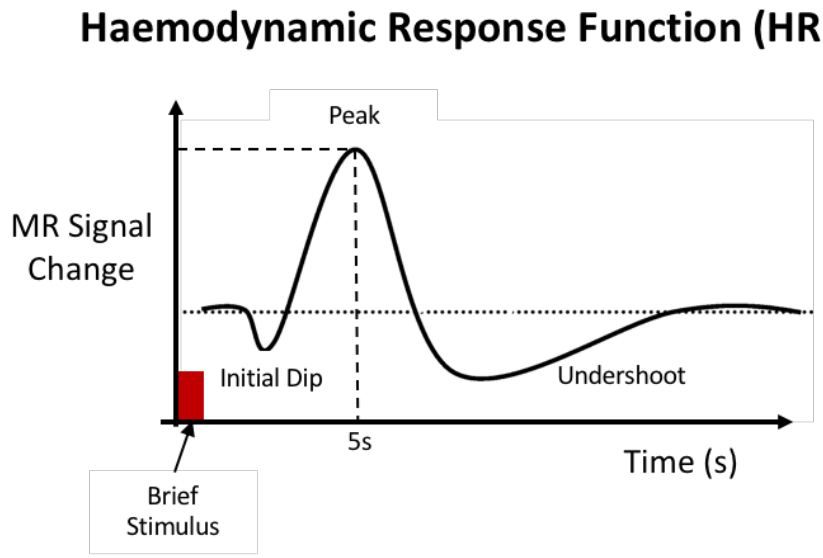

Figure 2.3.1 The haemodynamic response function.

2.3.2.1 The initial dip

A somewhat controversial topic, the initial dip reflects a transient dip in MR signal that occurs following neuronal stimulation (Hu and Yacoub 2012). This dip in signal is attributed to a transient increase in Oxygen metabolism ($CMRO_2$) in the absence of an increase in CBF, that leads to an increase in deoxyhaemoglobin concentration; and therefore a decrease in local MR signal (Menon et al. 1995; Hu and Yacoub 2012).

2.3.2.2 The peak

The haemodynamic response evolves over time, characterised by a local increase in both CBF and in the ratio of oxy to deoxyhaemoglobin concentration; as well as an increase in blood volume, which together give rise to an increase in the MR signal. The evolution of this response is slow compared with electric and magnetic field signatures observed with other techniques; and peaks at approximately six to eight seconds following stimulus presentation (Logothetis and Pfeuffer 2004).

As seen in data from block design studies, in which a stimulus or action is preformed repetitively over a period of time (for example 20s), the magnitude of this response will grow until a plateau is reached (Logothetis and Wandell 2004; Glover 2011). As stated earlier, in a block design paradigm the periods of stimulation, known as epochs, are contrasted with control epochs where the participant is not engaged (rest) or performing a less demanding action (Amaro and Barker 2006). In contrast, paradigms in which a single stimulus is presented for a brief period of time (as seen in Figure 2.3.1) (but repeated several times with a time interval longer than the full width half-maximum of the HRF), are known as event-related paradigms. This type of paradigm presentation is possible as a result of the speed at which T2* weighted data can be acquired with EPI based techniques. This design permits more cognitively demanding paradigms which, for example, involve learning or neuronal responses that may change over time, i.e. as a result of habituation.

2.3.2.3 The BOLD signal 'undershoot'

After stimulus evoked neural activity, the BOLD response peak begins to decrease, returning to a baseline, eventually passing beyond the baseline level, producing a small decrease in MRI signal (Buxton 2013). This is supposed to occur in response to a sustained increase in $CMRO_2$ coupled with a reduction in CBF, increasing the deoxy/oxy-haemoglobin concentration ratio (van Zijl, Hua, and Lu 2012).

Debate and controversy can be found in the neurophysiological literature regarding the physiological underpinnings of both the 'initial dip' and the 'undershoot'. This debate exists largely because the BOLD response is a product of at least three variables (CBF, CBV and $CMRO_2$); and trying to decipher or disentangle the effects of each of these responses is problematic and can lead to discrepancies. Despite this, the wealth of knowledge the BOLD contrast phenomenon has provided the neuroimaging community with, has been substantial.

2.3.3 Resting BOLD: image acquisition and analysis techniques

Building on from task based fMRI, BOLD data acquired during the resting-state, or better put, in the absence of an administered task of cognitive or sensory engagement, has grown in popularity and importance over the last decade. Measures of resting functional connectivity, i.e. the identification of regions that show synchronous activation (or deactivation), is a very useful alternative to investigate brain function. Its application has found utility in pharmacological MRI (phMRI) studies, as well as being a complementary tool alongside task-based fMRI experimentation (Murphy and Mackay 2010). Resting state connectivity analysis permits the interrogation of resting activity at a whole brain network level, allowing the researcher to infer and interpret changes beyond those recruited by cognitive engaging tasks (Lv et al. 2018). Furthermore, resting fMRI offers a significant pragmatic benefit since no task-administration is required, and therefore it is easier to make acquisition conditions more consistent across different studies. The main requirement from the participant is to stay awake and keep still, removing

performance bias or non-compliance often found in task-based studies, which can also lead to significant variability (Murphy, Birn, and Bandettini 2013). Biswal et al., first reported synchronous fluctuations in the BOLD signal that occurred during rest between the left and the right sensorimotor regions and the supplementary motor area (Biswal et al. 1995). These synchronous MR signals were observed at frequencies below 0.1Hz and since this initial observation considerable work has been conducted to better understand, observe and analyse these low frequency signal fluctuations during rest. Through this work a number of well-defined low-frequency networks have been characterised (Smith et al. 2013) and examining the modulation patterns on these fluctuations has been and continues to be a great tool for pharmacological MRI (Mehta and O'Daly 2011; Jenkins 2012).

2.3.3.1 Functional connectivity

Functional connectivity is defined by the degree of temporal correlation within the BOLD timeseries across different brain regions. Those regions that share a statistically significant degree of temporal correlation are labelled as being 'functionally connected'. The identification of these regions of functional connection is almost always made by identifying the independent frequency components of the time series and back-projecting those components onto the regions from which they are detected (see section 2.3.3.3). The validity and interpretation of this concept remains controversial.

2.3.3.2 Seed based functional connectivity analysis

There are a number of different ways to assess this degree of functional connectivity across the brain (for a review see (Cole, Smith, and Beckmann 2010) but one of the simplest in terms of both implementation and interpretation is 'seed-based connectivity' analysis (Biswal et al. 1995). Seed based analysis requires the selection of a 'functional seed' region, based on an *a priori* hypothesis or rationale, for which the BOLD time course for this seed is extracted, and used as a regressor within a whole brain General Linear Model (GLM) analysis, to derive whole-brain correlation

(connectivity) maps (Cole, Smith, and Beckmann 2010). This type of approach is considered *hypothesis*-driven as the researcher will select a seed or number of seeds based on one or more hypotheses.

2.3.3.3 Independent component analysis

In contrast, independent component analysis (ICA), is a *data*-driven tool that is also commonly used for resting state analysis (McKeown, Hansen, and Sejnowsk 2003). ICA for resting-state purposes is used to identify and decompose a functional BOLD timeseries into a set of spatially segregated components or maps, combined with the time course for each component (Cole, Smith, and Beckmann 2010). This type of decomposition processing is popular for defining discrete resting state networks and can be used at the single subject level as well as within a group analysis protocol. ICA uses the entire dataset in comparison to seed based analysis which restricts the analysis to just a single time course selected by the researcher thus is capable of finding effects that may be missed. With ICA, constraints can be imposed upon the decomposition to reduce the number of components that may be 'unmixed' from the data.

2.3.3.4 Resting state data quality

In contrast to task based fMRI data, with which a model of haemodynamic activity can be created and correlated with the time series data, resting state data lacks an 'input function' and has no prior knowledge regarding which signals are related to the BOLD contrast and which might be likely to derive from other sources. As the ICA method does not use prior information regarding resting state network components, the decomposition can also find spatial components that are attributable to non-neuronal source or noise. The BOLD response originating from neuronal activity within resting state data comprises 2-5% of the overall signal measured, which is sometimes largely corrupted by artefactual sources of signal change. Artefactual signal changes can arise as a consequence of (for example) involuntary head motion, cardiac pulsatile motion, breathing related motion, breathing related changes in

arterial carbon dioxide, scanner drift and thermal noise (Caballero-Gaudes and Reynolds 2017; Murphy, Birn, and Bandettini 2013). The corruption of data through artefactual perturbations severely affects the functional connectivity analysis of resting-state fluctuations in the BOLD signal, which are typically measured in the 0.01 to 0.1Hz frequency range. Some of these effects can be removed from the time series through temporal filtering processes, for example application of a bandpass filtering to restrict the time series data to only a defined frequency range (for example, removing those frequencies below 0.01Hz and greater than 0.1Hz) (Murphy, Birn, and Bandettini 2013). Given the large number of sources of signal corruption observed in resting-state data, there exists a need to perform denoising/cleaning methods prior to functional connectivity analysis.

A benefit of ICA is that non-constrained decomposition is useful for spatially defining these sources of corruption into spatially independent components (Salimi-Khorshidi et al. 2014). Several methods exist to identify nuisance components following ICA decomposition, one of which requires a different acquisition approach and therefore must be considered prior to protocol commencement (Kundu et al. 2012). ICA based denoising methods that use conventional acquisition protocols require identifying and defining the decomposed spatial components into neuronal origin (BOLD) or artefactual origin (non-BOLD) components. This can be done by subjective operator involvement, which is not typically recommended, or by the assistance of algorithms based on machine learning classifying techniques; for example: ICA-based X-noiseifier (ICA-FIX, 'Functional MRI laboratory (FMRIB), (Salimi-Khorshidi et al. 2014)) and FMRIB's ICA-based Automatic Removal Of Motion Artefacts (ICA-AROMA, (Pruim et al. 2015)). Both of these nuisance component identification methods show good denoising capabilities, however a comparative resting state study published in 2017 (Dipasquale et al. 2017) provided evidence to suggest that a technique known as multi-echo ICA (Kundu et al. 2012) was superior for noise removal compared to the two former machine learning ICA based methods. This technique requires a different acquisition approach to the conventional gradient echo methods described so far; and uses ICA coupled with a different signal analysis method for characterising components based on the nature of their corresponding T2* decay characteristics

(Kundu et al. 2013; Kundu et al. 2012). This technique was implemented in the current study of intranasal insulin and is described in detail below.

2.3.4 Multi-Echo ICA: acquisition and processing

As stated earlier, conventional BOLD contrast fMRI data is commonly acquired using gradient-echo echo planar imaging (EPI) using a single echo time (TE) for each image volume. BOLD contrast is maximal from gradient echo acquisition when the TE is equal to or close to the T2* value of grey matter (Howseman and Bowtell 1999), typically found to be 30 -35ms for acquisitions made at 3T. The TE set is a suitable compromise value so as to be able to acquire a sufficiently appropriate number of slices for the whole brain. However, the T2* of grey matter is not uniform throughout the brain and therefore some regions will inevitably display sub-optimal BOLD contrast. For example, gradient echo EPI image acquisition with a long TE will lead to susceptibility artefacts and greater signal dropout particularly in prefrontal regions (Deichmann et al. 2003), whereas a short TE will be associated with high global signal intensity, less signal dropout but a reduction in BOLD sensitivity in those regions with larger T2* values (Howseman and Bowtell 1999).

Multi-echo, gradient echo EPI (ME-EPI) acquisition is an acquisition approach that acquires multiple whole brain EPI images with increasing TE within a single TR (Posse et al. 1999). With this approach, every time point within the time series will have multiple whole brain volumes or better put, the data will consist of multiple time series each acquired with a different TE. The signal intensity across the echo acquisitions in each voxel will typically show an exponential T2* signal decay described in Figure 2.3.2.C and presented visually in Figure 2.3.2.A,B.

The use of this technique has been made possible through the advancement and development of rapid functional image BOLD contrast acquisition approaches. ME-EPI was initially implemented in an effort to reduce susceptibility related signal dropout whilst gaining maximum T2* contrast (Posse et al. 1999). This was achieved

by firstly, fitting the data to an exponential decay curve to attain the T2* value of that of each voxel and with this information average the signal across the different echoes together using a weighted approach, optimal for the T2* of the tissue within each voxel (Posse et al. 1999).

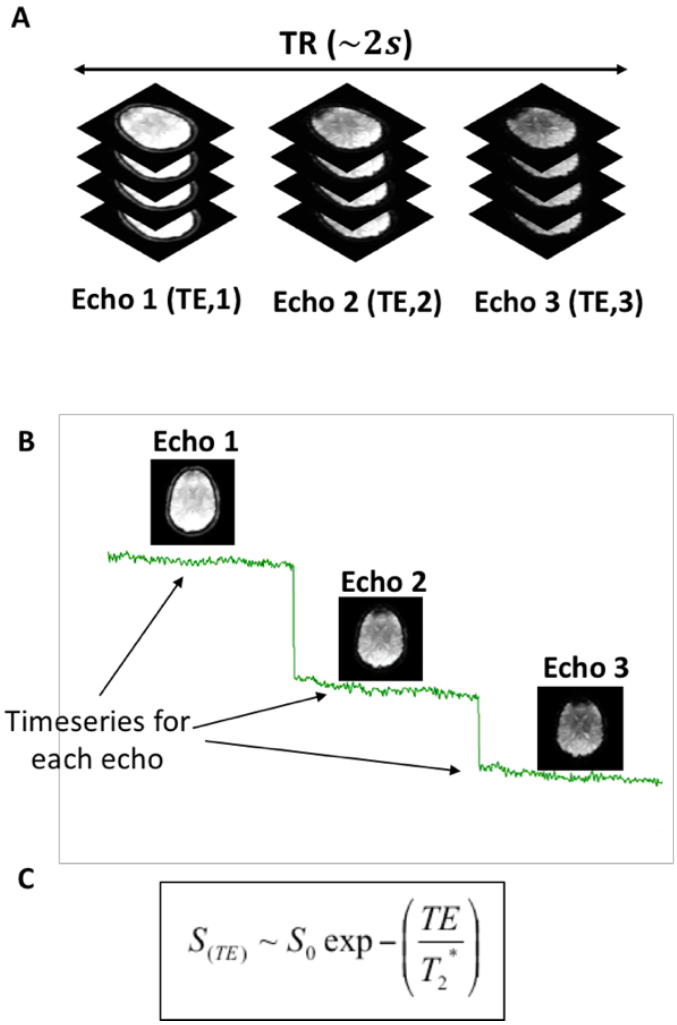

Figure 2.3.2 An example of a multi echo EPI acquisition with three echoes. A) for each TR three whole brain EPI images are created. B) The final output can be divided into three timeseries each acquired at a different TE. C) the signal intensity for each echo will decay as a function of T2* and initial signal intensity, S_0.

ME-ICA is a pre-processing technique developed to reduce the impact of noise and artefacts present in resting state data (Kundu et al. 2012), made possible through the combination of both acquisition and pre-processing techniques. Very simply, the multi-echo ICA processing employs a more sophisticated de-noising approach by assessing the T2* decay that is observed across the echoes, classifying signals that decay in an exponential fashion with T2* as 'BOLD-like' and those that do not show this relationship as 'non-BOLD-like' (Kundu et al. 2012). The appeal of this approach is that the independent components are classified based on their inherent T2* relaxometry characteristics; and attempts to identify BOLD components as opposed to simply identifying only the noise components. For this reason and also the superiority compared to other de-noising techniques (Dipasquale et al. 2017) the implementation of this technique is growing in the field of resting state functional connectivity analysis; as well as in task-based fMRI BOLD (Dipasquale et al. 2017; Kundu et al. 2013; Kundu et al. 2017; Lombardo et al. 2016; Power et al. 2018; Gonzalez-Castillo et al. 2016).

The method, proposed and developed by Kundu et al., (Kundu et al. 2012), bases this approach on the idea that within a small range of TE's the BOLD signal measured from tissue will decay exponentially with the T2* time constant of that tissue. In response to a change in neural activity the change in oxy/deoxy-haemoglobin concentration reduces the local susceptibility effects, increasing the apparent T2* value of that region and ultimately leading to an increase in MR signal (measured with gradient echo EPI). It has been shown that this signal difference increases when acquired at longer TE's (Bandettini et al. 1994) and therefore the change in MR signal displays a scaling factor that is dependent on TE. Therefore, confirmation of this type of TE-dependence can be considered a good marker of signal changes of a 'neuronal origin'.

On the other hand, observations of a change in MR signal could also arise from non-BOLD origins, such as those caused by motion. Following head movement for example, the tissue signal in the underlying voxel will be different and therefore the "spin-history" of the signal, will be also be different. This can be seen in Figure 2.3.3.

In this figure, the two voxels show different levels of steady state magnetisation due to differing T1 relaxation rates between voxels, however have a similar T2* value. As a result of the different steady state vectors the initial signal intensity (S_o) in the transverse plane will be different between these two voxels and therefore the signal within these voxels will decay differently according to the equation presented in Figure 2.3.2.C. In response to neural activity in Voxel B, a change in T2* is observed and in increase in T2* constant leads to a signal difference measured between sequential TR's if acquired at a suitable TE. However, in response to motion there is a displacement of the voxels and now Voxel A is located where Voxel B was. As Voxel A had a larger magnetisation vector in the steady state, the initial signal intensity, S_0, following RF excitation will be greater now that this displacement has occurred. This is an example of a 'spin history' effect. Given a higher S_0, the MR signal sampled at the same TE will exhibit very different changes in MR signal between successive TR's. The changes in MR signal between a true change in T2* (BOLD-effect) and those coming from a change in S_0, are essentially indistinguishable when using a single TE. In this scenario, spurious changes in MR signal are likely to be observed as a result of motion and changes in S_0 , thus corrupting the data.

Interestingly, the MR signal change produced from this change in S_0 does not show a linear relationship with increasing TE, therefore it becomes TE-independent. This crucial element therefore permits the use of fitting to model the TE dependence of the time series (or independence) and to use it as the basis for identifying components as BOLD and non-BOLD origin (Kundu et al. 2012).

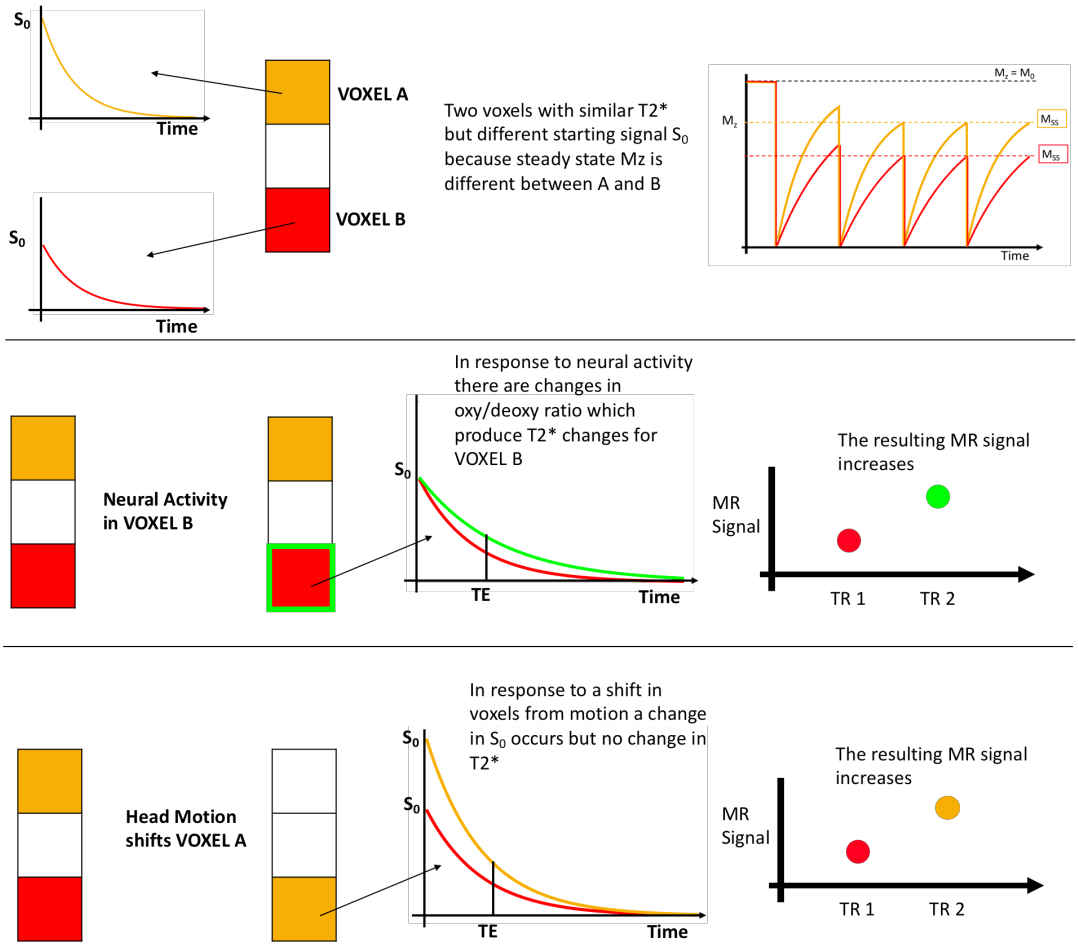

Figure 2.3.3 A diagram showing the effects of neural activity and motion on T2* decay and MR signal. Top panel shows two voxels, the associated steady state magnetisation curves and the T2* decay profile for both voxels when acquired with gradient echo EPI. Note the two voxels have differing S_0. Middle panel shows that in response to neural activity in Voxel B there is a change in T2* constant which could be observed if detecting changes between TRs. Bottom panel shows how if there is a motion displacement that shifts voxel A to Voxel B location then a change in S_0 will show a MR signal increase of measured with a single TE. This is known as a spin-history effect.

The ME-ICA approach has been widely used and has several steps which will be described in sequence:

Step 1:

An average T2* map is produced based from the echo signal intensities at each voxel, averaged over the entire time series. Based on this T2* value, the signal intensities from each voxel and each echo are combined using a weighting scheme that is optimal for the T2* value assigned for that voxel (Posse 2012). The combined echo time series is thus optimal for the T2* value of each voxel (Posse et al. 1999) with optimal contrast to noise ratio (CNR). In their software, this is known as the 'optimally combined' dataset.

Step 2:

The optimally combined dataset is run through a spatial ICA. The ICA algorithm is unconstrained, so the total number of components extracted can range between subjects.

Step 3:

Within each identified component, the algorithm assesses the degree to which the signal intensity represents T2* decay (by characterising its TE-dependence) or whether the signal change across echoes does not arise from an exponential T2* decay (TE-independence). This process is conducted at each time point by fitting the TE signal change as a function of TE to a TE-dependence model and also to a TE-independent model. For each time point a goodness of fit value is assigned for both of the models and a summary measure for the TE-dependence and TE-independent models is assigned for the component. These summary measures are defined as kappa, κ, and rho, ρ. A high κ value signifies a component that correlates well with TE-dependence in an exponential fashion. A low ρ value signifies a component that correlates well with the TE-independence model. A component defined with a high κ and low ρ value would be deemed to correspond to signal decay indicative of a 'true- BOLD' origin (of greater probability of arising from genuine changes in neuronal activity). Conversely, a low κ and high ρ component is deemed to exhibit signal

changes that are likely to arise from non-neuronally driven sources (e.g. motion or physiological nature) and likely to be artefactual.

Step 4:

Based on the distribution of the κ and ρ values, the ME-ICA algorithm defines thresholds for each component; and those components that show κ and ρ values greater and lower, respectively, (than the calculated thresholds) are then classified as having the appropriate TE-dependence. Those that fall outside of an established range of κ and ρ values, are classified as TE-independent and some that fall in the middle are classified as "unidentified" (Kundu et al. 2012).

Step 5:

Timeseries of components classified as non-BOLD (low κ and high ρ) are then regressed from the optimally combined echo time series in a similar way to which motion parameters are regressed in a General Linear model. The regressed time series is considered to be "de-noised". The main output from the ME-ICA de-noising process is therefore a single time series of functional volumes that have been optimally combined based on the T2* value and in principle 'cleaned' of non-BOLD components as described above (Kundu et al. 2012).

The next chapter will describe the application of these techniques for a pharmacological MRI study that explored the effects of intranasal insulin in healthy male volunteers.

Chapter 3 Study Design

3.1 Investigation of the Effects of Intra-nasally Administered Insulin on Food Appetite and Reward: The SNIFAR study

This is a double-blind, placebo controlled, crossover MRI study to investigate the effects of insulin in the central nervous system (CNS), using intranasal administration. This study was designed to evaluate the effects of intranasal insulin on both homeostatic appetite control and also hedonic food reward. A good proportion of investigations using intranasally administered insulin literature have focused on its effects on cognition, mood and also food related neural processing. This study aims to extend our understanding of the effects of this important compound by using a food administration paradigm that has not been reported in previous studies. This study also intends to contribute to the limited literature on resting state perfusion in response to intranasal insulin, through the implementation of an optimised arterial spin labelling sequence. Finally, the study reported here builds upon the current insulin related connectivity literature through the use of an artefact noise removal T2* weighted image acquisition and processing technique called multi-echo independent component analysis denoising (Kundu et al. 2012). Also included within this thesis is a chapter focused on work that was conducted to optimise a commercially available nasal pump, to provide optimal insulin delivery to the CNS. In this work (conducted using active insulin) I carried out key *in vitro* measurements that were made to determine the efficiency of nose-to-brain insulin delivery.

3.1.1 Participants

This study was approved the King's College London Psychiatry Nursing and Midwifery Ethics Committee (ethics no. RESCM-17/18-2282). Participants for this study were predominantly recruited through the King's College recruitment website although some were recruited through word of mouth. Participants liaised with the head researcher through email initially and also a short phone conversation to filter out participants who did not fulfil the immediate inclusion criteria. The study consisted of three visits in total. Visit one was a screening session and the remaining two sessions were experimental imaging sessions.

3.1.2 Screening and inclusion criteria

This study evaluated drug effects in healthy right-handed male volunteers (aged between 20-36 years of age). All participants provided informed written consent. Participants were screened to ensure they had no history of psychiatric illness or diabetes assessed by clinical interview, no cardiac-related complications (assessed at the screening visit by means of a 12-lead electrocardiogram (ECG)), no history of eating disorders, asthma or allergies associated with breathing difficulties and did not adhere to a vegetarian or vegan diet. During the screening, height and weight measurements were taken, as well as resting blood pressure and heart rate measurements in the supine and standing position.

During the screening session, participants answered three questionnaires to assess eating behaviours, to obtain an indication of weekly food intake and to assess how stable their eating behaviours were, using a three-factor eating questionnaire (Stunkard and Messick 1985), the dietary free fat and sugar subscale questionnaire (Francis and Stevenson 2013) and the council of nutritional appetite questionnaire (Wilson et al. 2005). These questionnaires are based on general eating behaviours and are highly unlikely to change during the length of the study; therefore, they were completed during the screening visit only. The council of nutritional appetite questionnaire (CNAQ) was used a screening tool. The CNAQ is commonly employed

to assess the likelihood of future weight loss, typically implemented in anorexia research (Wilson et al. 2005). The CNAQ consists of eight questions using a 5-point scale (1-5), total scores range from 8-40. Scores greater than 28 indicate a normal or good appetite, whereas scores ≤ 27.9 reflect poor appetite. Participants with scores representative of poor appetite were deemed not eligible for this study (Wilson et al. 2005).

The three factor eating questionnaire (TFEQ) and dietary free fat and sugar subscale questionnaire (DFS) was also used in the data analysis of the study. The TFEQ is commonly employed in obesity related research and measures three factors: dietary restraint, disinhibition and hunger (de Lauzon et al. 2004). The TFEQ is a 36 part questionnaire that uses both true and false questions as well as 4-point and 5-point Likert scales. TFEQ scores for each factor are calculated and severity ratings of 'low', 'medium' and 'high' for each factor can be ascertained.

Dietary restraint has an impact on weight control and how this can be achieved, for example by reducing food portions or restricting eating (Bryant, King, and Blundell 2008). High dietary disinhibition is reflected by a tendency to overeat, particularly at opportunistic moments within obesogenic environments. The final factor, hunger, explores the feelings of hunger and how these feelings can evoke food intake (Stunkard and Messick 1985).

The dietary fat and sugar (DFS) questionnaire provides an approximate guide to examine how often meals or food that contain high amounts of saturated fat and sugar are consumed. From the DFS the overall frequency of foods high in saturated fat, sugar as well as food that contains both high levels of fat and sugar can be calculated (Francis and Stevenson 2013). This questionnaire contains 26 food types for which the participant must mark on a scale how often that food type is consumed. The scale ranges from "less than once per month" to "5 + times per week" on a 5 point scale. The questionnaire is quick to complete and has been shown to produce valid and reliable measures of saturated fat and free sugar consumption when

compared with weekly food diaries which are also more arduous on the participant (Francis and Stevenson 2013).

During the screening session participants were given full details on what was required from them, familiarised with the study protocol, scanner paradigms as well as shown how to correctly operate the nasal administration pump.

3.1.3 Study cohort stratification

Participants with a body mass index (BMI) between 18 and 30 kg/m^2 were included. These subjects were then subdivided into two groups: below and above 25 kg/m^2 to examine differences between healthy and near-obese individuals.

This division allowed us to study individuals in a metabolic state between normal weight and obese, who are at risk of evolving into a condition of obesity along with its associated risks (González-Muniesa et al. 2017). In the UK approximately 40% of adult males are overweight as assessed by BMI, with 33% normal weight and 26% obese, therefore the majority of males in the UK are classified as overweight according to BMI (Barker 2018). Regarding the study of intranasal insulin, some reports have shown a lack of effectiveness in weight loss via long term intranasal insulin administration in obese men but not in normal weight men (Hallschmid et al. 2008). Therefore, the study of this group of individuals is important for establishing possible markers of brain function that may be associated with this 'at risk' population. Furthermore, overweight individuals represent an interesting study group as they are essentially healthy albeit 'less so' then normal weight individuals (González-Muniesa et al. 2017).

Furthermore, this study recruited men only. As described in the introduction central insulin has some differential gender effects as a result of interactions of central oestrogen on insulin anorexigenic effects (Clegg et al. 2006; Benedict et al. 2008). To avoid or limit these potential confounding effects of oestrogen males were exclusively recruited in this study.

For this repeated-measures design a sample size of sixteen was required to detect changes in cerebral blood flow (CBF) of 3 ml/100g/min, based on a standard deviation of 4 ml/100g/min and an effect size of 0.75 with a two tailed, paired t-test (α = 0.05, 1-β= 0.8). (G*Power, (Faul et al. 2007)). Therefore, this study aimed to recruit sixteen subjects within each group for a total of thirty-two subjects in the entire study (lean plus overweight). This specific change in CBF was used as a guide for this power calculation based on research by Kullmann et al., who presented changes in the hypothalamus of this magnitude from this dose of intranasal insulin (Kullmann et al. 2018)

3.1.4 Post absorptive state

Participants were instructed to follow an overnight fast, with their last meal to be consumed no later than 10pm the night before (approximately a 12-hour fast). As this study probed the effects of insulin on homeostatic and hedonic food related processing, it was important for the participants to be in a fasted/post absorptive state. Participants were allowed to drink water throughout the morning.

By skipping breakfast, participants entered into a negative energy balance thus promoting hunger. Previous functional imaging research comparing the fed and fasted state has shown that in the fasted state the appeal of food imagery is increased (LaBar et al. 2001) and is also associated with increased preferences or bias towards foods high in calories in comparison to low calorie food pictures (Goldstone et al. 2009). Findings from studies like these have provided a methodological foundation for investigating functional brain responses to food cues and food stimuli by placing the participant or patient in a state of negative energy balance and therefore increasing responsiveness to task based paradigms focused on appetite and reward (Dagher 2012). We implemented an overnight fast as the goal was to observe how this negative energy balance would affect brain responsiveness following intra-nasal administration of insulin compared to placebo. By implementing an ‘overnight’ fast rather than a prolonged fasting period (> 24 hours)

the effect of ketone bodies on brain metabolism was avoided (Cahill 1970). Following all scanning procedures a 'standard' lunch was administered to the participants.

3.1.5 Abstinence of vasoactive substances

Participants were further instructed not to consume alcohol 24 hours prior to scanning and also not to have caffeinated drinks on the morning of scanning, only water was allowed. Both caffeine and alcohol are vasoactive substances leading to global decreases and increases in cerebral perfusion, respectively (Vidyasagar et al. 2013; Gundersen, van Wageningen, and Gruner 2013) and therefore would introduce significant variability in the study.

3.2 Imaging Sessions

The first imaging session was conducted no later than thirty days following the screening session and the second imaging session no later than 15 days following the first imaging session. The protocol for each imaging visit is shown in Figure 3.2.1.

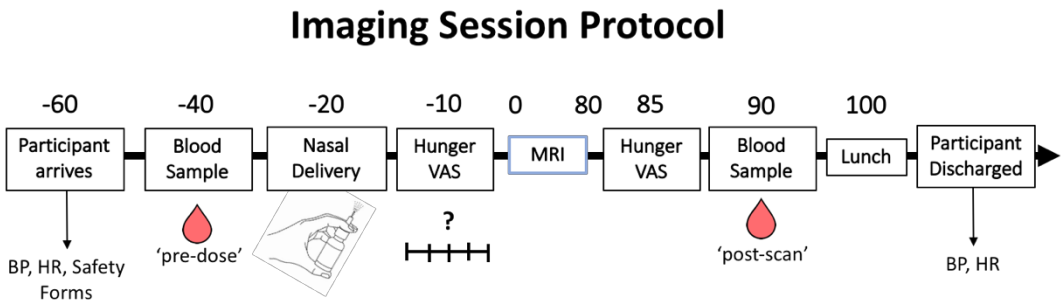

Figure 3.2.1 Protocol for the imaging sessions. All black boxes are considered non-imaging and the blue box will be referred to as the imaging component.

The next sections will discuss the non-imaging related components of the protocol using Figure 3.2.1 as a reference.

3.2.1 Participant arrival and physiological measurements

Participants arrived at the centre for neuroimaging sciences at 9am or 9:30am to begin scanning at either 10 or 10:30am, respectively. Upon arrival participants were required to fill out the necessary MRI safety forms and to relax before any physiological measurements were taken. After 20 minutes, seated blood pressure (BP) and heart rate (HR) were recorded. These vital physiological measurements are necessary to ensure that it is safe for the participant to start the full imaging session protocol.

Blood sampling was performed at two time points; before drug administration (pre-dose) and after scanning (post-scan). Using venepuncture techniques, blood samples were collected by filling one grey top (2.5 ml, Fluoride/Oxalate – for plasma glucose) and one gold top (serum separator tube – for serum insulin and C-peptide) Vacutainer (Becton, Dickinson U.K. Limited, Berkshire). In addition, a drop of blood from the butterfly needle was used to measure blood glucose concentration using a portable blood glucose monitor (FreeStyle Optium, Medi Sense, MPT Pharma Ltd, Walsall, UK). This measurement was recorded for safety reasons so that the researcher could be aware of the approximate baseline blood glucose concentration and if the participant felt unwell or showed signs of hypoglycaemia a second sample could be taken (via a pin-prick approach) and used to compare against the baseline measure permitting appropriate action to be taken in response to any adverse effects.

Samples were separated into plasma and serum by spinning the samples in a centrifuge at 4°C and 3000 rpm for 10 minutes. Plasma and serum were separated into 2.5ml aliquots and stored at -20°C until processed. These samples were processed and analysed for plasma glucose, serum insulin and serum C-peptide concentrations at the King's College Hospital clinical biochemistry department. All assays were conducted by a commercial contractor called ViaPath located within King's College Hospital site (King's College Hospital, Bessemer Wing, Denmark Hill, London, SE5 9RS).

3.2.2 Plasma and serum assays

Plasma glucose was determined using the glucose-oxidase method using an ADVIA 2400 Chemistry system (Siemens Healthcare Diagnostic Ltd, Newton House, Surrey, UK). Serum insulin and C-peptide concentrations were determined using a chemiluminescence assay using an ADIVA centaur system (Siemens Healthcare Diagnostic Ltd, Newton House, Surrey, UK).

3.2.3 Drug preparation and administration protocol

Twenty minutes prior entering the scanner, participants received a total dose of 160 IU insulin (Humulin®, 500 IU/ml, Eli Lily) or placebo (0.9% saline solution, Fresenius Kabi) by means of four intranasal applications (see details in the next section).

Insulin and placebo solutions were provided by KCL pharmacy department on the morning of each imaging session, in a plain white nasal pump device (SP270+ pump with 3959 actuator)(Nemera, La Verpillière, France), these contained 2ml of either insulin or saline solution.

The dosing protocol closely followed previous intranasal insulin dosing protocols reported in the literature (Guthoff et al. 2010). We employed a total of four nasal sprays over a four-minute period with each spray containing 40 IU of insulin (total dose = 4 x 40 IU = 160 IU). To employ this protocol, the insulin solution provided by pharmacy required dilution by the researcher. A single spray of the nasal pump contains 0.1ml solution. The insulin solution (500 IU/ml) dispensed by pharmacy was diluted with 0.5ml of saline solution to create a 2.5ml insulin solution with a new concentration of 400 IU/ml and the resulting insulin concentration per 0.1ml spray was 40 IU as per the protocol requirements. As this study was double blinded the dilution steps were performed for every imaging session.

Nasal spray administration was performed approximately thirty minutes prior to **functional** data acquisition (resting-state BOLD acquisition) in an effort to acquire data after insulin concentrations in the central nervous system have increased, in line with the pharmacokinetics of intranasal insulin previously reported(Born et al. 2002).

Participants were familiarised with the intranasal application procedure at the screening sessions and were then able to self-administer the dose under instruction from the head investigator at each of the imaging sessions. Participants received a total of 4 sprays, alternating between nostrils and leaving one minute between each spray to allow for sufficient diffusion time and to avoid the dose running out of the nostrils. Participants assumed a bent forward position and used their left hand to administer to the right nostril and vice versa (presented in Figure 3.2.2). Following each administration spray, participants were instructed to hang their head down and forward to prevent any fluid 'run out' and also to take advantage of gravitational forces, in an effort to facilitate droplets to travel towards the posterior regions of the nasal cavity (see Figure 3.2.2)

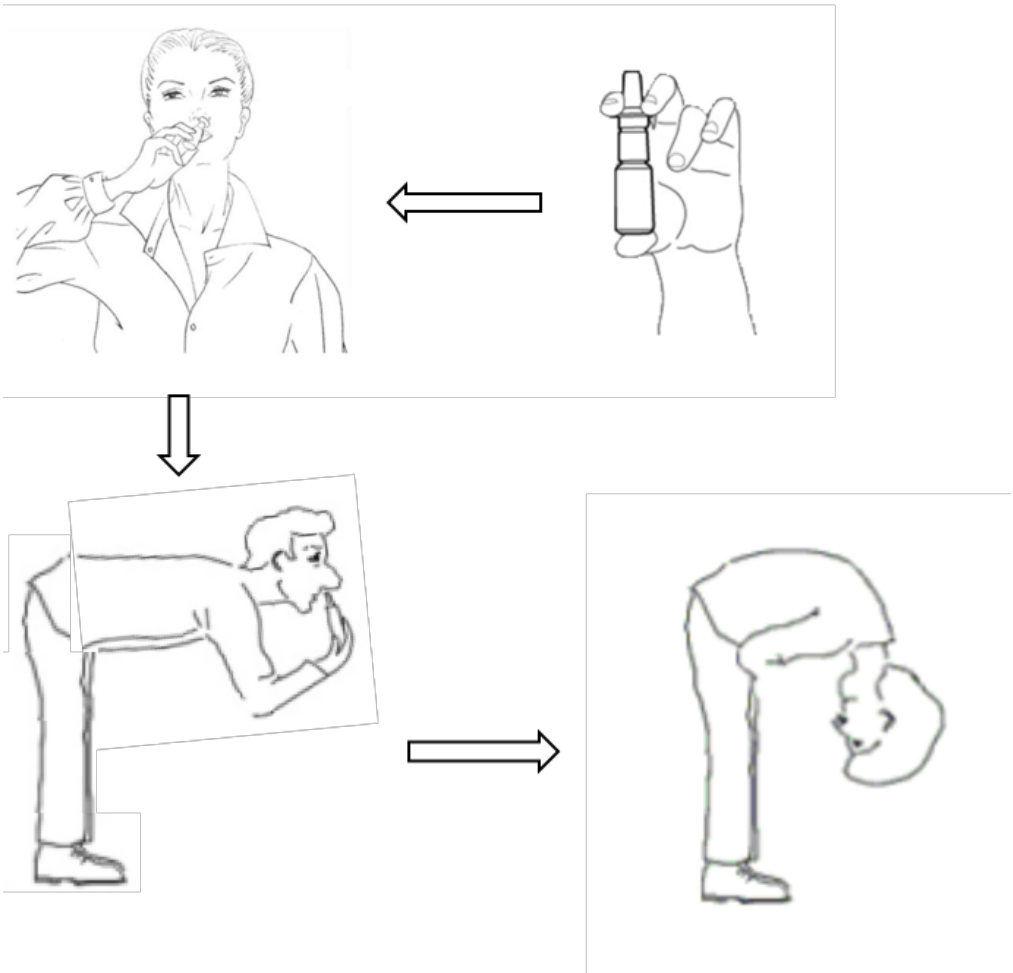

Figure 3.2.2 Nasal Self Administration process. The nasal administration process starts with the participant holding the spray between the thumb and fingers. The nasal pump nozzle is then inserted into the nose using the opposite hand, the image shows the right hand being used for the left nostril. The participant then bends forward, keeping the spray bottle upright and administers a single dose (spray). Immediately after administration the participant hangs there head down to prevent the dose running out of the nose and also to help the dose travel to the posterior region of the nasal cavity with the pull of gravity. Participants would only hang for 15-20 seconds or so, as instructed by the researcher.

The insulin solution carried a strong scent which was not replicated by the placebo solution. Prior to nasal administration the pump required 'priming'. Priming requires spraying the pump 3-4 times in the air in order to fill the pump and pump feeding tube with the solution. To avoid scent detection and potential unblinding by either the participant or the researcher a distraction protocol was implemented. Immediately before dosing the participant was given a 'dummy' pump defined as a "practice pump" which was filled with diluted TCP™ solution. The participant was instructed to spray the pump into the air 5-6 times with both right and left hands in preparation for dosing and to 'warm up' their hands. At the same time the researcher primed the nasal pump that was to be used for the study by spraying in the air 3-4 times. By spraying both fluids simultaneously, the scent of the solution under investigation was masked by the strong smelling TCP and thus both the researcher and participant remained blinded to the treatment.

3.2.4 Visual analogue scale (VAS) scores

Prior to entering the scanner and also imminently after scanning had terminated the participants completed visual analogue scales (VAS) to assess subjective hunger. This type of subjective rating is reproducible and a powerful marker of subjective appetite and hunger (Flint et al. 2000).

The question was "how hungry do you feel right now?" and each participant answered by placing a mark on a 10cm scale from "not at all" to "very". The first of the hunger score VAS assessments was performed after dosing and therefore these hunger VAS scores will be termed 'pre-scan' and not pre-dose from here on in.

3.3 Imaging Protocol

The SNIFAR study adopts a multi-modal MR imaging approach to investigate the effects of intranasal insulin on brain function. The following sections will provide the methodologies used for each component of the imaging protocol, the principles of each of these techniques are described in chapter 2. In an effort to aid the reader, the individual analysis techniques for each component will be detailed in each chapter. The following sections will highlight the main acquisition techniques and give information on the tasks that were implemented, and the equipment used in the functional paradigm. Furthermore, pre-processing that was common to all the functional imaging data will also be discussed.

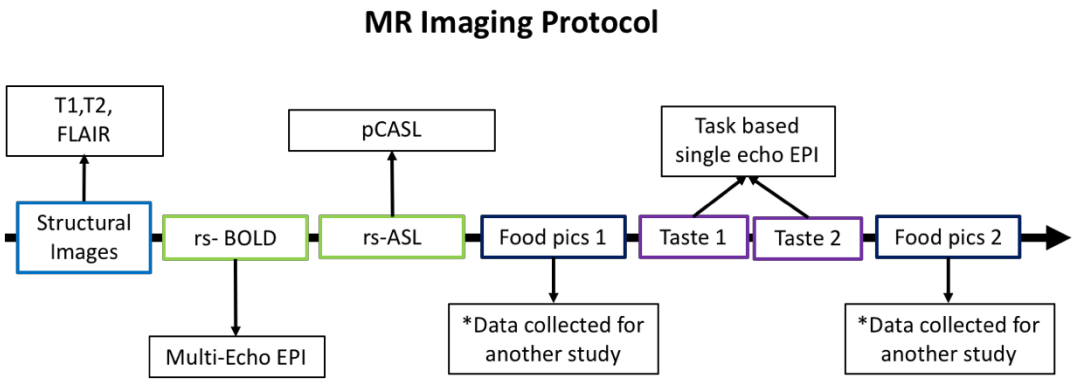

Figure 3.3.1 Imaging protocol for the SNIFAR study. Different colours refer to a different category of image acquisition, Blue = structural, Green = resting-state, Dark blue and purple = task based fMRI BOLD. * Food Picture fMRI data was collected for another study.

3.4 Image Acquisition

All scanning was conducted using a MR750 3 Tesla GE Discovery Scanner (General Electric, Waukesha, WI, USA) with a 32-channel receive only head coil. Each participant was provided with a button box (2 buttons, left and right), this device was placed in their right hand to allow for selections during task performance. Physiological data for each participant was also recorded for each participant using bellows (for breathing rate) wrapped around the diaphragm and a pulse oximeter (for heart rate) placed on the index or middle finger of the left hand.

3.4.1 Anatomical image acquisition

Structural images were acquired for each participant at the beginning of the scanning protocol. T2 and Fluid Attenuated Inversion Recovery (FLAIR) images were acquired during the first imaging session. The Centre for Neuroimaging Science's local policy requires acquisition of a T2 weighted and FLAIR image for every participant studied, these are assessed by a radiologist in the event of any incidental pathological findings.

3.4.2 T2 weighted

For each participant an axial T2 weighted fast recovery fast spin echo (FR-FSE) image was acquired with the following parameters: slice thickness (Δz)=2mm, slices = 72, slice gap = 2mm, TR = 4380ms, TE = 65ms, flip angle = 111°, matrix size (DM) = 320x256 with a Field of View (FOV) = 24cm. Acquisition time 2:03 min.

3.4.3 FLAIR

For each participant an axial T2 FLAIR image was acquired with the following parameters: slice thickness (Δz)=4mm, slices = 36, slice gap = 4mm, TR = 8000ms, TE = 65ms, Inversion Time (TI) = 2000ms, flip angle = 111°, DM = 256x128 with a FOV = 24cm. Acquisition time 2:33 min.

3.4.4 T1 weighted

At the second imaging session a high resolution (1.1 x 1.1 x 1.1 mm) T1 weighted image was acquired at the beginning of the protocol. The T1 weighted image was used in the SNIFAR study for co-registration and normalisation of functional imaging data to Montreal Neurological Institute (MNI) standardised space.

This sequence used a T1 weighted 3D Magnetisation Prepared Rapid Acquisition Gradient Recalled Echo (MP-RAGE) with the following parameters: slice thickness (Δz)=1.2mm, slices = 196, TR = 7.312ms, TE = 3.016ms, inversion time (TI) = 400ms, flip angle (FA) = 11°, matrix size (DM) = 256x256 with a FOV = 27cm. Acquisition time: 5:37 min.

3.4.5 Resting state BOLD

For each participant a resting state BOLD timeseries was acquired using a multi-echo EPI sequence. The multi-echo EPI sequence was chosen for this part of the study due to documented effects of artefact removal that can be achieved through the implementation of the multi-echo independent component analysis (ME-ICA) denoising algorithm proposed by this approach (Kundu et al. 2012).

For the acquisition of these data in SNIFAR study participants were instructed to look at a white 'fixation' cross presented to them on a black projector screen. Participants were instructed to keep still for the duration of the scanning and to let their mind wander naturally. The projector screen was situated at the back of the scanner bore.

3.4.6 Resting state perfusion - Arterial Spin Labelling

Resting state Cerebral Blood Flow (CBF) data was acquired using a 3D-pseudo continuous (3D pCASL) sequence. The sequence was used with a long label duration of 3500ms to maximise the signal-to-noise-ratio of this measurement (see details of long labelling in section 2.2.3.

As in the case of the resting state BOLD scan, participants were instructed to look at a white 'fixation' cross presented to them on a black projector screen. Participants were instructed to keep still for the duration of the scanning.

3.4.7 Taste task

The taste paradigm was performed as the second functional task in the SNIFAR protocol. The taste task was designed to evaluate the effects of receiving three different taste stimuli whilst in the scanner. This task employed an MR compatible system capable of delivering a pre-defined volume (0.5mL) of liquid to the participants during fMRI-BOLD acquisition.

3.4.7.1 Taste delivery system

The taste delivery system is known as the "MR Fluid Liquid Automatic Vendor (MR-FLAV) and was designed and built by the Engineering Section of the Department of Neuroimaging, KCL. The device is an automated, high speed liquid delivery system that dispenses a calibrated bolus of 0.5mL. The dose is restricted to 0.5mL to minimise any swallowing difficulties that may occur with a larger bolus whilst laying down; and to prevent the possibility of the fluid blocking the subjects' airways. The MR FLAV system can be broken down into three constituent parts: 1) the Pneumatic control device which resides in the scanner control room, 2) the dispensing unit which houses the liquid reservoirs and calibrated dose syringes and 3) the delivery tube which extends from the main unit to the subject's mouth (see Figure 3.4.2 and Figure 3.4.1).

The pneumatic control device is located in the MR control room and is the driving force behind the delivery pump system. This unit translates the paradigm commands into a pneumatic programmed sequence. The device receives air inflow and pumps this out as pressurised air along the 4-metre long piping tubes to the dispensing unit which is located in the scanner room, at the foot of the scanner bed.

The dispensing unit itself is MR safe and for this study was situated under a pillow, underneath the participants' legs. The dispending unit contains four separate reservoirs linked to 4 different syringes. Upon a taste delivery trigger, the syringe which is calibrated to 0.5ml is pneumatically pushed from the pressurised air, expelling a 0.5mL bolus of fluid along the delivery tube (see Figure 3.4.3.B). After delivery the syringe mechanism retracts via pneumatic suction which draws up the next 0.5 mL bolus from the reservoir, ready for the next administration.

The delivery tube extends from the dispensing unit to the head coil. In the internal part of the head coil there is a custom designed cradle/holder that holds the delivery tube during the taste task. At the end of the delivery tube is a solid mouthpiece shaped like a baby bottle teat which is purposefully designed to fit disposable rubber baby bottle teats over its surface (see Figure 3.4.1).

The system requires filling each reservoir with the experimental taste liquids and preparing the system so no air bubbles are within the liquid containing pipes or syringes.

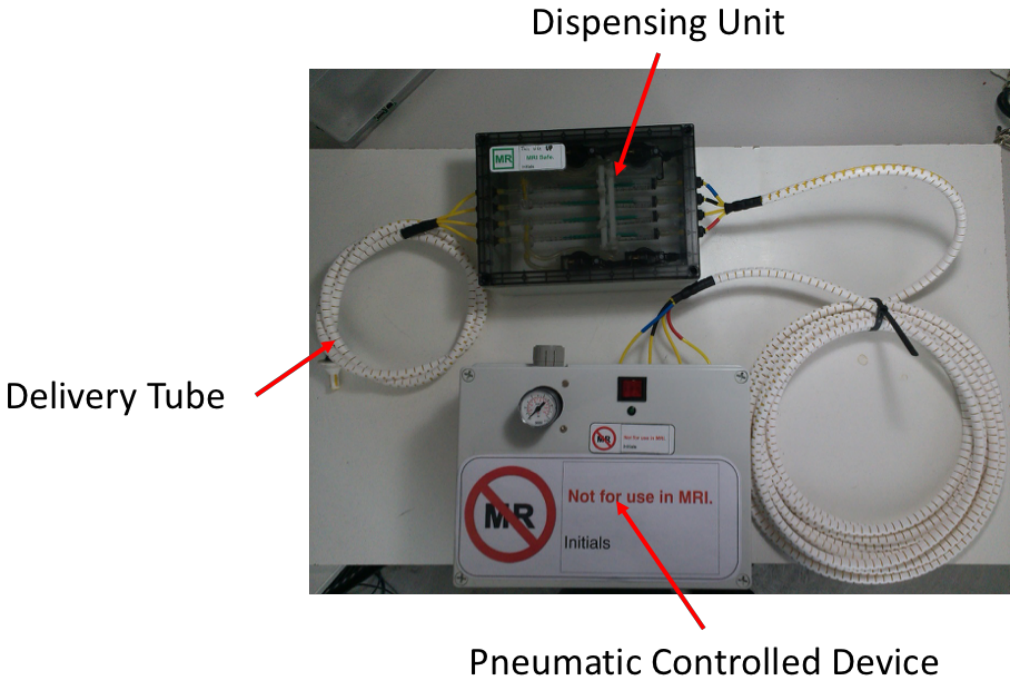

Figure 3.4.1 The pneumatic controlled device is not MR compatible and is located in the control room. The Dispensing unit is located in the scanner room and was placed underneath the participants legs in this study. The dispensing unit contains the calibrated syringes and reservoirs. The delivery tube extends from the dispensing unit into the bore of the scanner to the participants mouth.

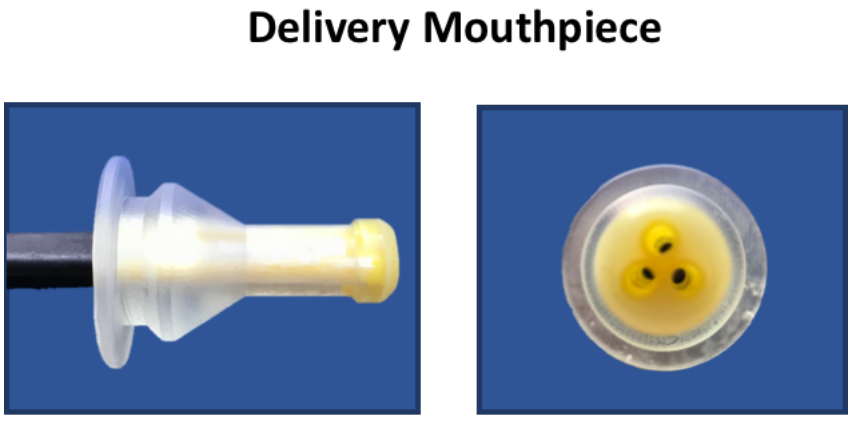

Figure 3.4.2 Taste bolus delivery mouthpiece. The mouthpiece is shaped like a baby-bottle teat and perfectly fits rubber disposable teats (left). The mouthpiece is an outlet for the three taste stimuli and has a separate outlet for each taste solution (right).

3.4.7.2 Taste stimuli

The taste stimuli used for this paradigm were selected to examine the primary taste response to sweet stimuli. Two sweet stimuli were used; a sucrose solution and a non-nutritive, low calorie, sweetener solution. In addition, a control mineral water solution was the third taste stimulus. Each taste stimulus was prepared the evening before scanning and was kept at 4°C in the fridge overnight. On the morning of scanning each taste stimulus was loaded in the designated reservoir prior to subject arrival, approximately an hour before scanning. The taste stimuli maintained a cool temperature by being in the reservoirs. For every visit, this protocol was followed and therefore one can assume that the temperature of stimuli was similar across all scanning sessions.

Water (control):

Bottled water ('Harrogate mineral water') was used as a control solution for this paradigm. Water is not tasteless and has been shown to activate the taste cortex (Zald and Pardo 2000). The taste of water however is markedly less intense in comparison to the two sweet stimuli, and therefore it is suitable in this instance as a non-sweet control stimulus.

Sucrose:

The sucrose solution was produced by diluting 12.5g (approximately 3 teaspoons) of table sugar (99.99% sucrose) (Caster Baking Sugar, Tate and Lyle) into 150ml of the mineral water (bottled Harrogate water - vehicle). This produced a 0.08g/ml (sucrose/water) stock solution. Each 0.5ml sucrose bolus delivered contained 0.04g of sucrose.

Stevia:

Stevia solution was created using a granulated sweetener made from the stevia leaf marketed as Truvia® (The Truvia Company LLC). In reference to the manufacturer's notes, Truvia® is three times sweeter than sugar. Therefore, stevia solution, the name that will be used herein, was produced by diluting 4.2g (approximately 1

teaspoon) of Truvia® into 150ml of bottled water. Each stevia solution stimuli contained 0.014g of Truvia® from a stock stevia solution of 0.028g/ml.

Stevia is a natural sweet-tasting non-nutritive (calorie free) extract from the *Stevia rebaudiana* leaves indigenous to South America (Goyal, Samsher, and Goyal 2010). Extracts from the stevia leaf are being used more regularly as alternative sweeteners to sugar. Interestingly, stevia has shown beneficial effects on postprandial blood glucose and plasma insulin concentration in humans (Anton et al. 2010). Furthermore, meals sweetened with stevia showed comparable satiation effects when compared with sucrose sweetened meals, in conjunction with decreased postprandial glucose and insulin responses (Anton et al. 2010). The main constituent of Truvia® is erythritol, a non-sugar carbohydrate that belongs to the family of polyols. Steviol glycoside and extract from the stevia leaf, is the other constituent within Truvia®. Truvia® is FDA approved and is one of the leading stevia based products on the market in the US with Companies such as Coca-Cola using stevia based extracts and sweeteners like Truvia® in some of their products as sugar free alternatives.

3.4.7.3 Taste dispenser setup *in situ*

The taste task occurs midway through the imaging protocol and therefore the researcher had to enter the scanner room for the setup of this paradigm. The participant was informed to remain as still as possible whilst the researcher positioned the MR compatible taste dispenser for the task.

The taste outlet mouthpiece was positioned into the right hand-side of the participant's mouth between the teeth and cheeks. This position ensured comfort for the participant for the duration of this paradigm. The taste outlet positioning was similar for all participants to ensure taste bud stimulation remained similar across all subjects. (shown in Figure 3.4.3.A).

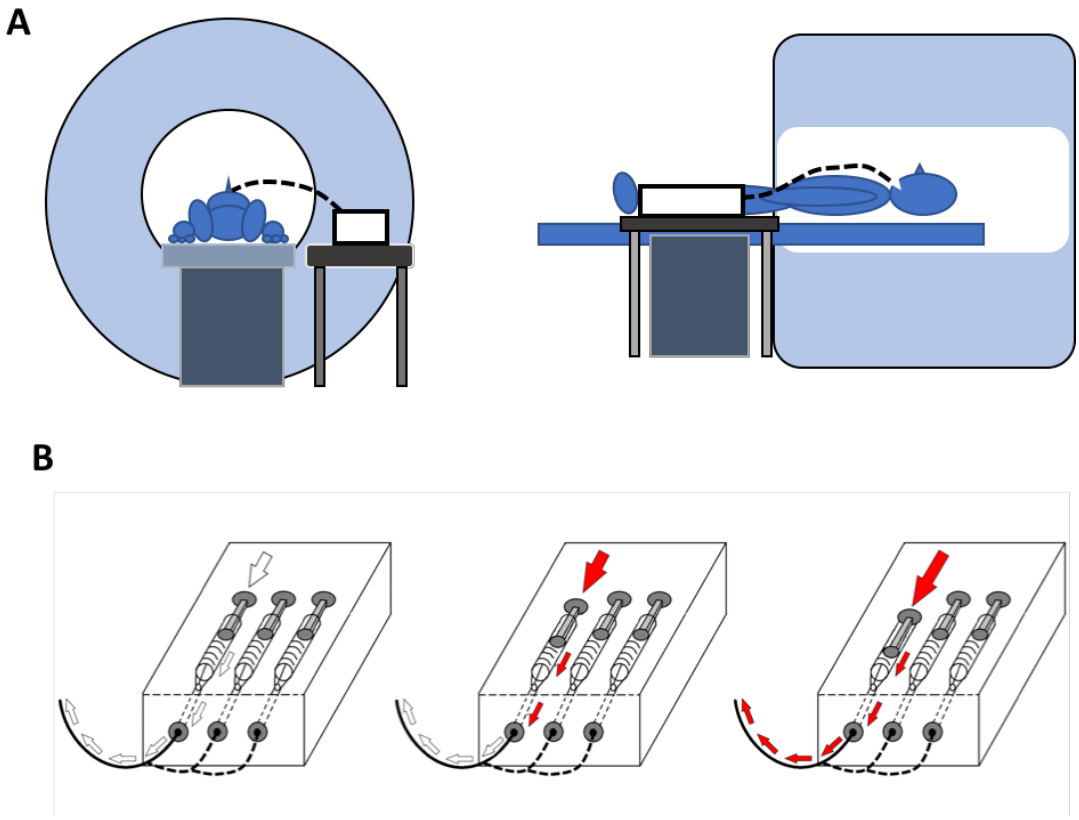

Figure 3.4.3 Schematic drawings of the taste dispenser in situ and during bolus delivery. A) The taste paradigm requires the taste dispenser box to be situated close to the bore of the scanner, either on a side table (seen from this picture) or under the participant's legs. The outlet tube and dispenser mouthpiece are positioned in the participant's mouth, inside the scanner. B) Schematic drawings of the syringe pumps that are used to administer the taste bolus, calibrated to 0.5ml. The three pictures (from left to right) show the evolution of a single taste bolus delivery.

3.4.8 Experimental paradigm

Participants became familiar with the experimental procedure at the screening session and completed a mock run of the paradigm outside the scanner without the taste stimuli. Furthermore, participants were reminded of the details of the paradigm prior to scanning by the researcher. The details of the paradigm and the three different trials are shown in Figure 3.4.4.

This was an 'event-related' paradigm. At the start, one of three abstract, arbitrary fractal images were presented at the beginning of each trial, with each fractal image being associated with either the water, sucrose or stevia stimulus. This relationship

between presented image and taste stimuli remained constant throughout the entire paradigm. This visual stimulus, referred herein as 'the cue', was presented for 2s either on the left or the right hand side a white fixation cross, positioned in the middle of the screen. Upon cue presentation, the participant was required to signal the direction of the cue presentation using an MR compatible button box. The period between the cue and impending taste stimulus delivery consisted of a white fixation cross and was set to 3s for every trial. Following this, the cross went from white in colour to green which signalled delivery of the taste stimulus. The delivery signal was present for 3s, however the taste stimulus (0.5ml delivery bolus) itself was delivered over the first 1.5s of this event. Following bolus delivery the participants were required to keep the liquid bolus in their mouth until the presentation of a "swallow now " prompt, known as a paired trial (Figure 3.4.4). The time spent with the stimulus in the mouth varied from 3 to 6s and began when the fixation cross returned to white in colour from green. The "swallow now" cue was presented for 2s which was followed by a fixed inter trial interval of 1.5s. Trials were presented in a pseudo-random order, so that each taste trial was never followed by the same taste. On 40% of the trials the taste stimulus was not delivered. This event is termed 'withheld delivery'. In these instances, the visual cue was presented, however when the cross turned green the taste stimulus was withheld, referred to as 'withheld delivery'. As there was no stimulus delivered the swallow prompt was not presented/required and the next trial started following the inter-trial interval (see Figure 3.4.4)

An entire run of this paradigm consisted of 45 trials, 9 delivery trials and 6 delivery withheld trials for each of the three taste stimuli. This paradigm consisted of 2 runs in total, performed in succession.

The first time each taste stimulus was delivered and swallowed two questions followed: "how much do you like the taste?" and "how sweet did you find this taste?", for which the visual analogue scale (VAS) ranged from "not at all" to "very" (0 to 100, respectively). The participant responded by pressing the left and right buttons of the button box, using their index and middle fingers, respectively, thus placing their chosen score in a visual analogue scale (VAS). These questions were

also presented following the final stimulus, at the end of the second run (VAS trial – see Figure 3.4.4), Fractal cues were different between visits and the paradigm playlist, which determined the order of presentation of the stimuli, also differed between visits.

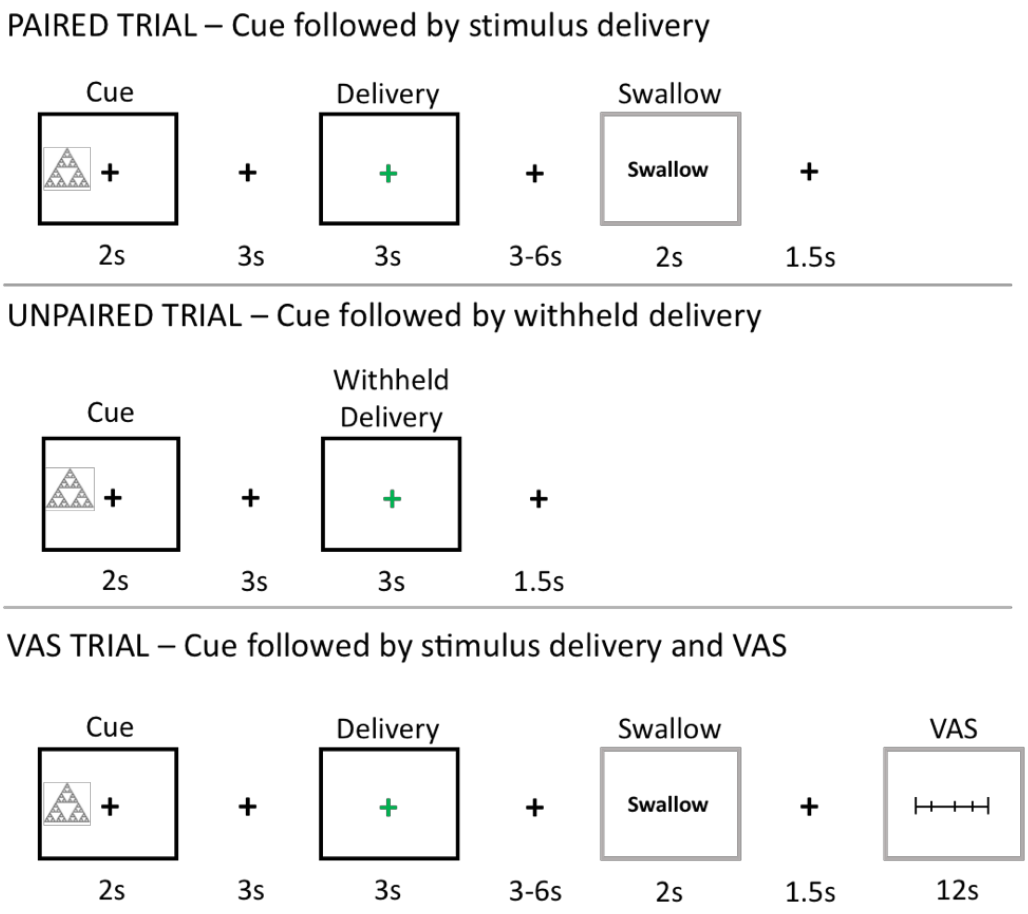

Figure 3.4.4 A diagram to show the three different trial types of the taste paradigm. Black boxes represent the events that are modelled as events of interest (cue, delivery and withheld delivery, respectively). Grey boxes represent events that are modelled in the first level model but not of interest or used for contrast creation (swallow and VAS scoring periods). A paired trial is the most common trial type and involves the delivery of a 0.5ml bolus/stimulus following visual cue presentation. An unpaired trial does not deliver the 0.5ml bolus as expected, instead nothing is delivered. A VAS trial is when the delivery of the bolus is followed by two VAS questions, this happens for each taste at the very beginning of the first run and at the very end of the second run.

3.5 Image Processing

3.5.1 Co-registration and normalisation of T1 weighted images

All the T1 weighted images from all subjects were used to create a group template using Advanced Normalisation Tools (Avants et al. 2014; Avants et al. 2011) (ANTs, templatecreate), which was registered to standardised MNI space using the FLIRT routine (Jenkinson and Smith 2001; Jenkinson et al. 2002) of the Functional Software Library (FSL, FMRIB, Oxford University, version 3.2, http://www.fmrib.ox.ac.uk/fsl). The parameters for co-registration of the T1 weighted image to the group template (T1 to template) and also from the template to MNI space (template to MNI) were saved as text files to be later used for functional image registration (see Figure 3.5.1). The MNI template had an isotropic resolution of $2mm^3$.

All functional imaging datasets were pre-processed prior to group level analysis. Specific details for image pre-processing differed between pCASL, multi-echo EPI and single echo EPI task-based datasets and therefore the individual pre-processing pipelines will be outlined in the respective chapters. However, all images whether CBF maps or time series data were co-registered and normalised to standard space Montreal Neuroimaging Institute (MNI) co-ordinates to facilitate group level inferences .

This involved creating a functional image to subject T1 co-registration (functional to T1) transform. And then the final stage involved application of three transformation parameters to the T1-weighted image using ANTs (Avants et al. 2011). The three transform parameters are defined as:

- Functional to T1
- T1 to Template
- Template to MNI

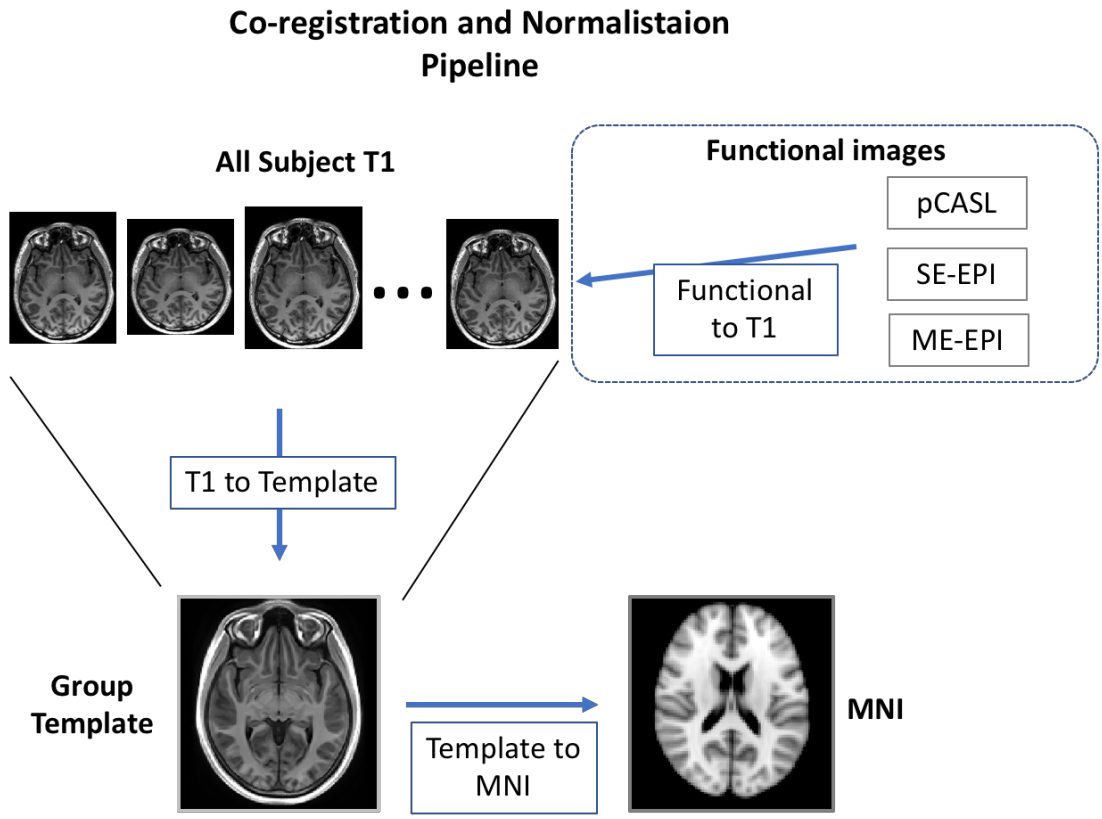

Figure 3.5.1 Pre-processing pipeline for co-registration and normalisation of images to MNI. The transformation files created at each point in the pipeline are outlined in blue. These three steps show the last of the pre-processing steps that would be taken for all the functional image acquired. The functional image datasets were pre-processed differently for each modality and is not shown in this diagram.

3.6 Lunch and Discharge

Following the final blood sample collection, participants were given a lunch meal which consisted of a sandwich, 'crisps' and a piece of fruit. The volume of food consumed was not assessed in this study. Participants discussed elements of the scanning with the researcher and after a final Blood Pressure and Heart Rate measurement, they were discharged.

Chapter 4 Nasal Pump characterisation

Nasal administration of insulin has been utilised as a drug delivery method and research tool to supply insulin directly to the brain; in order to study its effects with limited interference from systemic insulin-glucose interactions. Nose-to-brain delivery bypasses the blood brain barrier (BBB), by diffusion across olfactory epithelia and effectively reaches brain tissue within 30-60 min (Banks, Owen, and Erickson 2012). Thus, nasal insulin administration can be utilised as a tool for research in patients with diabetes, obesity and Alzheimer's disease where regular receptor mediated transport of insulin across the BBB to the brain tissue is disrupted (Craft et al. 1998; Kullmann, Heni, Veit, Scheffler, Machann, Häring, et al. 2015). For optimum delivery to the brain via this route, insulin must be deposited in the upper and posterior regions of the nasal cavity. Nasal cavity anatomy varies considerably between subjects and thus achieving maximal delivery for every subject is not always feasible using a single device. However, previous studies using both *in vitro* nasal cast experiments and computational modelling methods (Inthavong et al. 2006; Inthavong et al. 2008) have provided a general framework about nasal pump performance characteristics to achieve appropriate drug deposition in this region. This chapter will introduce the reader to some general aspects of nasal administration for drug brain delivery and the process by which I characterised and optimised a nasal pump to achieve successful nose to brain drug delivery.

4.1 Introduction

Delivery of therapeutic agents via the nasal cavity has long been utilised for treatment and research purposes alike (Ghori et al. 2015). The nasal cavity is a largely accessible route of drug administration and is well tolerated in most people and patient populations (Guastella et al. 2013). The nose is the main entrance point for inhaled air in humans and majority of land animals (Phalen 1976). The nasal cavity, which is situated just beyond the nostrils is the first anatomical landmark within the mammalian respiratory system. The nasal cavity acts primarily to filter and also modify inhaled air for efficient gas exchange within the lower airway structures. In addition to this air conditioning role, the nasal cavity contributes to many other functions such as olfaction, speech production and also taste which is permitted via the complex architecture and physiological functioning of the nasal cavity (reviewed thoroughly in (Geurkink 1983)).

The nasal cavity is a large structure that spans lengthways from the nasal vestibule to the nasopharynx (≈120-140 mm in length) and from the cavity floor to the cavity ceiling (cribriform plate) (≈40 mm in height) in adults (see Figure 4.1.1 and Figure 4.1.2). The nasal cavity is subdivided into two chambers by a cartilage wall called the nasal septum (Ghori et al. 2015). Within each of these chambers there are three further regional subdivisions: the vestibular, turbinate and olfactory regions, respectively (Cheesman and Burdett 2011). The vestibular region acts primarily to filter and remove large particles ($10\mu m$) within ambient air during inhalation. More posteriorly resides the turbinate region, which consists of upper, middle and lower turbinates' and are comprised of mucus secreting epithelial cells which serve to humidify incoming air and create flow turbulence effects for efficient gas exchange in the lower respiratory system (Kim, Kim, and Kwon 2018). The olfactory region, which is positioned just below the ethmoid bone and cribriform plate is responsible for odour recognition and comprises only 8% of the nasal cavity surface area (Ghori et al. 2015). The olfactory region consists of a mixture of cell types that have discrete

functionality which form several layers to bridge the gap between the nasal cavity and the CNS.

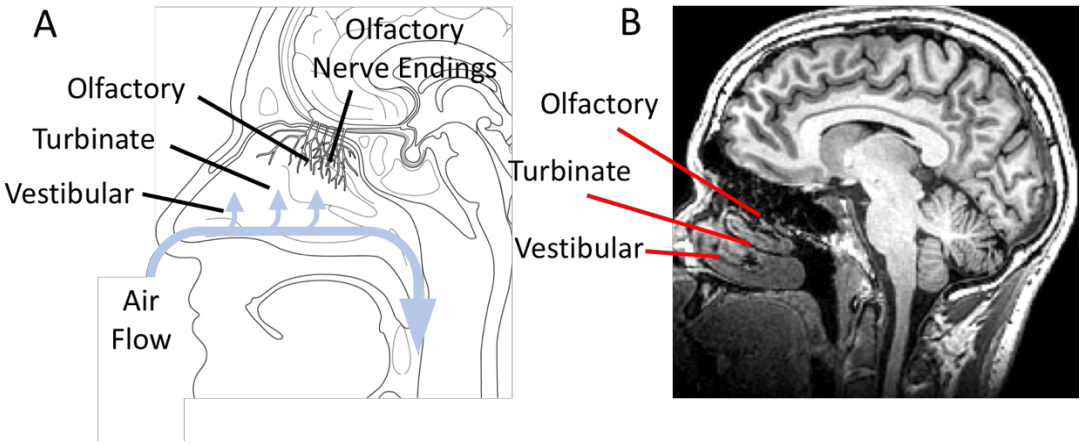

Figure 4.1.1 The anatomy of the nasal cavity. A) Schematic showing the nasal cavity from a sagittal view. Labelled are the vestibular, turbinate and olfactory regions of the nasal cavity as well as the olfactory nerve endings and air flow passage. B) Representative sagittal T1 anatomical MRI image showing the nasal cavity and the three nasal regions (vestibular, turbinate and olfactory, respectively).

The olfactory bulb sits on top of the cribriform plate which is a sieve like structure at the most superior region of the nasal cavity and has olfactory nerve endings that protrude through into the olfactory region of the nasal cavity.

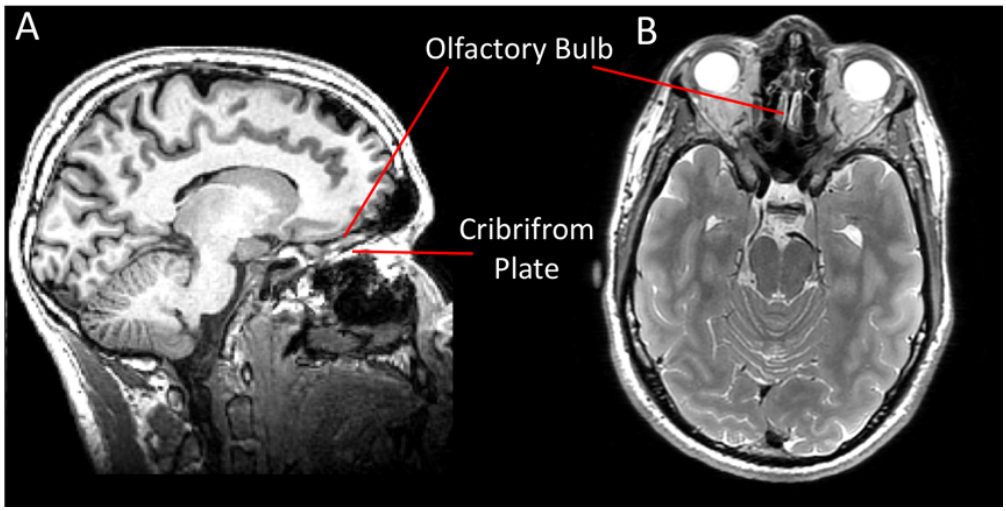

Figure 4.1.2 Representative MRI images showing the olfactory bulb and cribriform plate

The exact mechanisms of drug delivery via the nasal cavity to the CNS are not yet entirely understood, or agreed upon amongst the nose-to-brain drug delivery community. However, there is substantial agreement that the nerve cells and bundles connecting the nasal passages to the CNS (olfactory and trigeminal nerves) are heavily involved in this process (Pardeshi and Belgamwar 2013). It is most likely that nose to brain delivery is possible via several routes (olfactory nerve, trigeminal nerve, lymphatic and CSF pathways) and that specific drug delivery characteristics such as mode of delivery and formulation dictate which of these routes may dominate (Pardeshi and Belgamwar 2013). To this end, this chapter will briefly discuss the relevant olfactory and trigeminal nerve pathways as these are considered the most prominent and significant pathways for CNS drug delivery via the nasal cavity (Agrawal et al. 2018; Dhuria, Hanson, and Frey 2010).

4.1.1 Nose to brain drug penetration via nerve pathways

Whether through the olfactory or trigeminal nerve pathway, nasal drug delivery to the brain can be broken down into three distinct steps:

1. Drug transport across the nasal epithelial barriers
2. Drug transport to brain tissue entry points
3. Drug transport from brain tissue entry points to other brain tissue areas

For each of these steps there exist several potential mechanisms of which some are more validated and accepted than others. A thorough explanation of all the possible mechanisms is beyond the scope of this chapter and so the next sections will highlight only the most significant and accepted mechanisms. The reader should be aware that the majority of these mechanistic studies have been conducted in animal models which do not necessarily translate well to human models especially those conducted in rodents (Lochhead and Thorne 2012).

4.1.2 Olfactory nerve pathway

The olfactory nerve is comprised of the olfactory nerve endings, olfactory bulbs and olfactory tracts Figure 4.1.3 which connect the olfactory regions of the nasal cavity with the olfactory cortex (inferior pre frontal cortex) as well as the amygdalae and hippocampal structures (Dhuria, Hanson, and Frey 2010).

Olfactory nerve cells project from the olfactory bulb through the cribriform plate to the olfactory epithelium of the nasal cavity and are crucial for odour sensing. In combination with the columnar supporting cells and basal cells the olfactory nerve cells help to form the a blood brain barrier (BBB) at the level of the olfactory epithelium (Agrawal et al. 2018). Direct contact with peripheral toxins within the nasal cavity requires these olfactory nerve cells to regenerate every 3-4 weeks. This dynamic nature and constant regeneration results in immature cell formations (see Figure 4.1.3) that lack important protein components for BBB integrity and thus is

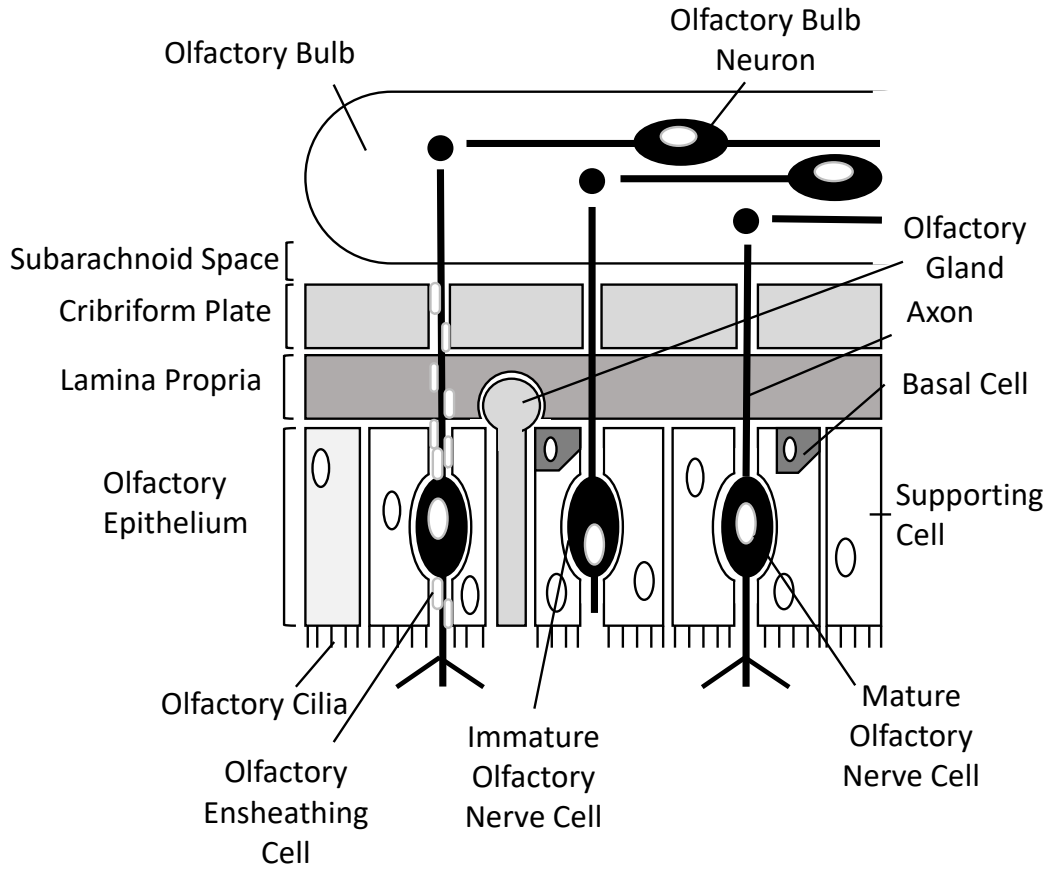

Figure 4.1.3 Olfactory bulb, nerves and epithelium.

considered a ‘leaky’ barrier (Balin et al. 1986). Furthermore, within this highly innervated region of the olfactory region there are myelinated cells, called olfactory ensheathing cells which wrap over the protruding olfactory nerve cell axons. As well as myelination, these ensheathing cells create fluid filled spaces between the olfactory nerve cells, peri-neuronal spaces, even during olfactory nerve cell regeneration (Lochhead and Thorne 2012).

4.1.2.1 Drug transport across the nasal epithelial barriers

Drug transport across the olfactory epithelium can occur via two mechanisms: the intra-neuronal and extra-neuronal route. The intra-neuronal route is extremely slow (up to 24 hours) and involves the transport of drug molecules along nerve bundles via intracellular and transcellular transport mechanisms (Kristensson and Olsson 1971). The extra-neuronal route on the other hand, is recognised as the predominant mechanism for nose to brain drug delivery of therapeutic agents. If sufficient drug molecules are deposited at the region of the olfactory epithelium these molecules can diffuse through the leaky barrier permitted by the creation of peri-neuronal spaces by olfactory ensheathing cells. Access via these peri-neuronal openings has been shown in rodents as well as non-human primates (Balin et al. 1986). Once successfully past the olfactory epithelium the molecules will have to cross the lamina propria to reach the subarachnoid space and CSF.

4.1.2.2 Drug transport to brain tissue entry points

Once in the lamina propria these molecules and substances could be absorbed or drained into the nasal vascular system or cervical lymph nodes, as a result of the rich vasculature and nasal lymphatics within the lamina propria (Dhuria, Hanson, and Frey 2010). Those substances that avoid uptake at this level can proceed through the peri-neuronal spaces from the lamina propria into the subarachnoid space and CSF beyond the cribriform plate. Furthermore, it has been shown that once in this space there are small openings for which some substances can enter into nerve bundle sheaths from the subarachnoid/CSF space (Faber 1937). Diffusion into the outer

nerve bundle compartments is thought to be established via a diffusion gradient and that sufficient quantities of substances can enter via these bulk movement effects (Jansson and Bjork 2002).

4.1.2.3 Drug transport from brain tissue entry points to other brain tissue areas

The peri-neuronal spaces connecting to nerve bundles are also surrounded by large amounts of blood vessels and can also provide suitable perivascular spaces for drug transport. The theory for drug molecule movement from the olfactory site to other regions on the brain relies on bulk flow within these perivascular and peri-neuronal spaces. This bulk movement is enhanced by the pulsatile motion of cerebral arteries (Ying 2008). Once at these more distal regions within the brain, substances can either diffuse into brain tissue or bind to cell receptors for cell mediated transport or as an agonist/antagonist. Studies have suggested that utilisation of this extra-neuronal route can produce adequate drug concentrations within the CNS in roughly 30 mins in rodents (Ichimura, Fraser, and Cserr 1991). With regards to insulin delivery to the brain via intranasal administration *Born et al.,* showed that a low dose of insulin (40IU) administered with a nasal spray device could produce an increase in insulin concentrations measured from CSF within 30 minutes in humans compared to baseline measures (Born et al. 2002). This seminal paper showed for the first time that intranasal delivery of neuronal active peptides show increased levels in the CNS compartment as measured via CSF (Born et al. 2002).

4.1.2.4 Trigeminal nerve pathway

In addition, the trigeminal nerve, which is the largest cranial nerve, has connections with the nasal cavity, oral cavity and eyelids via the V1, V2 and V3 branches of the trigeminal nerve, respectively. The ophthalmic nerve bundle (V1) and maxillary nerve bundle (V2) have processes that connect from the midbrain to the olfactory region and also the turbinate regions of the nasal cavity, respectively (Kamel and Toland 2001). The turbinate region of the nasal cavity is rich in ciliated mucous producing cells crucial for toxin clearance and so, it is unlikely that large amounts, if any, of drug molecules can enter the CNS at this entry point. It is therefore suggested that the

mechanisms of entry via peri-neuronal spaces at the olfactory epithelium and superior regions are present for this route also (Lochhead and Thorne 2012). Bulk movement of substances and pulsatile motion enhancements, as mentioned with the olfactory route, is likely to drive movement alongside the trigeminal nerve route. The overall trigeminal route, from nerve endings to midbrain entry sites, is greater in length than the olfactory route and is predicted that this route will take longer for compounds to travel along.

For both of these complex nose to brain administration routes the active pharmaceutical must first traverse beyond the vestibular and turbinate regions and deposit sufficient dose content in the olfactory region. Diffusion through these extra-neuronal pathways relies heavily on bulk movement and it is essential that these active substances have enough residence time within the olfactory region to facilitate movement into central nervous system compartments (Agrawal et al. 2018).

4.1.2.5 Nose to brain delivery considerations

This study formally characterises three commercially available nasal spray devices using the same dose of insulin solution that was implemented in the imaging phase of the study. Intranasal delivery of insulin solution in humans has previously been used in other research projects due to the quick onset of action in the CNS coupled with a limited effect on peripheral glucose concentrations (Born et al. 2002; Kullmann, Heni, Fritsche, et al. 2015). Most of these studies have used a nasal spray device and liquid solution which when sprayed (termed 'actuated'), produces a plume of liquid droplets that travels through the nasal cavity. Some of these droplets will deposit on the vestibular, turbinate and olfactory regions or if small enough can pass through to the lungs. Hopefully, the mechanistic definitions above illustrate the complexity of this administration to the reader. The next sections will highlight the relevant nasal anatomy, device mechanisms and formulation properties that must be considered for nose to brain drug delivery of insulin and will give the reader sufficient knowledge to understand the rationale and methodological aspects behind this characterisation study.

4.1.2.6 Nasal anatomy considerations

Firstly, the nasal cavity is architecturally complex with thin air filled passages that twist and turn from the nostrils through to the trachea. The narrowest region of the nasal cavity is called the nasal valve and is situated roughly 2-3 cm beyond the nostril entrance (Ghori et al. 2015). The nasal valve is the narrowest and most difficult of obstacles for any nasal delivery device to overcome (Haight and Cole 1983). Nasal valve cross sectional area is at its smallest during sharp inhalation through the nose and thus nasal administration is sub-optimal when sniffing or inhaling sharply through the nose. Optimal administration should be performed during light inhalation when the nasal valve is not minimal and there is a nasal air flow present (Djupesland 2013).

The nasal cavity undergoes dynamic cleaning and congestive swelling every 2-4 hours, alternating between the left and right sides, known as the nasal cycle. This autonomic mechanism results in one side being more congested (see Figure 4.1.4) and thus leads to a reduced cross sectional area within that nasal cavity passage, adding further hurdles for nasal spray droplet delivery (Djupesland 2013). There is little that can be done to avoid this, practically. However, implementing an administration protocol that alternates between nostrils will help to avoid either problems that might be encountered by using a single nostril.

Figure 4.1.4 Coronal View of Nasal Cavity in a healthy volunteer. Notice the congestion on the right hand side, which would be due to the nasal cycle.

4.1.2.7 Nasal pump

In this experiment, three commercial nasal spray devices were characterised. All the devices are known as 'metred nasal pumps', which means that the pump itself will dispense a pre-determined, fixed volume of liquid (dose) for every spray/actuation, permitted if actuation is performed correctly. All devices were metred to 0.1ml per spray, which is common for most nasal spray applications and is at the top end of the absorption capacity of the nasal cavity. Figure 4.1.5 shows a typical nasal spray pump, very similar to the pumps characterised in this study. The nasal device consists of three parts: The actuator, pump mechanism (and dip tube) and the bottle. To actuate the device, the actuator is squeezed down which produces a spray/plume that is released from the orifice at the tip of the actuator. After actuation, the pump will release naturally due to spring mechanism and will simultaneously draw up the next dose via the dip tube. Generation of a plume is key to the success of any nasal pump. Upon actuation the metred dose volume inside the pump (0.1ml in this instance) is put under sufficient pressure causing the dose to be propelled into

streams that run up the side of the nozzle. At the top of the nozzle these streams enter into a small cylindrical compartment called the swirl chamber via inlets. Within this chamber a vortex is created which is expelled into the air through an orifice at the tip of the nozzle. The plume itself goes through several stages of development: initial phase, stable phase and end phase, with the stable phase being the most relevant and important for *in vitro* nasal spray characterisation (Fung et al. 2013).

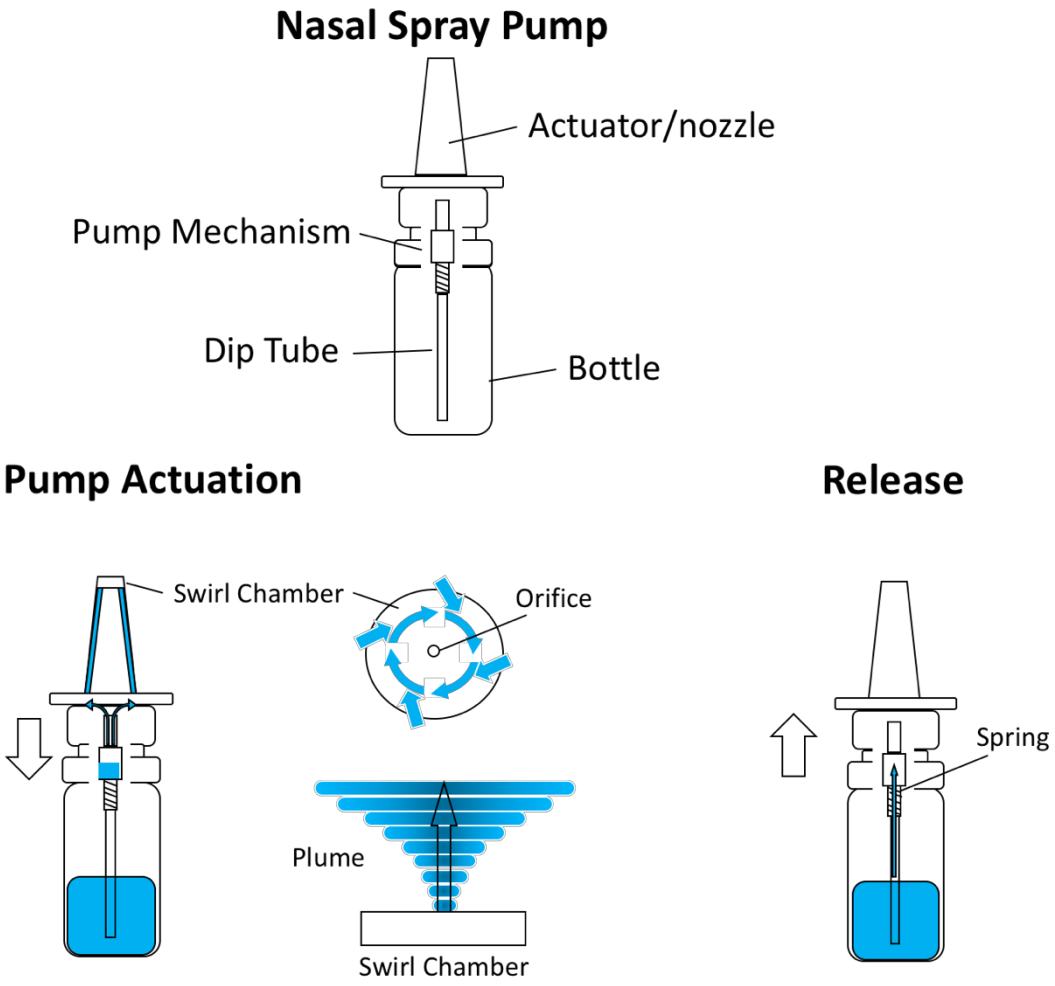

Figure 4.1.5 Nasal spray pump and actuation process. The nasal spray pump assembly consists of an actuator, the pump mechanism, dip tube and bottle. Pumps are actuated by applying a downward force onto the actuator which propels the liquid from the pump mechanism upwards. The liquid enters a swirl chamber and through this process produces sufficient force to propel out through the orifice, located at the top of the actuator, in the shape of a plume. Upon release, once a plume has been created, a spring mechanism returns the actuator back to its normal position and simultaneously a metred dose is drawn up via the dip tube.

Assessment of nasal cavity deposition pattern from nasal administration devices can be conducted *in vivo, in vitro* and *in silico,* using radiolabelled isotope imaging, human nasal cast model studies and advanced computational modelling, respectively (Suman et al. 2002; Inthavong et al. 2006; Pu et al. 2014). These types of evaluations are valuable for nasal delivery system assessment pipelines and observations from these datasets has provided a generalised framework of nasal pump characteristics that that are optimal for olfactory drug deposition leading to efficient nose-to-brain drug delivery with a typical nasal spray (Cheng et al. 2001; Inthavong et al. 2006; Newman, Moren, and Clarke 1988). Assessment of device characteristics such as the size of the droplets and plume shape can be assessed using more accessible *in vitro* techniques and therefore are useful as surrogate measures prior to or in the absence of nasal device deposition pattern analysis. These type of measures are also the first point of call for any device pipeline and are useful for determining reliability of spray performance.

A nasal pump plume will contain a mixture of small and large droplets. For nasal delivery of any kind, droplets must be between 30 and 120μm. Larger droplets will show very poor nasal cavity penetration and tend to deposit in the anterior regions of the nasal cavity due to the inability to travel with the air flow (Dayal, Shaik, and Singh 2004). Smaller droplets on the other hand, will travel and deposit within the olfactory regions whereas very small droplets (< 10μm) can travel beyond this and penetrate into the distal regions of the respiratory tract and lungs, which can be very harmful (Agrawal et al. 2018). The distance and degree a droplet or particle can travel is dependent on the interactions with the environment in which it is situated and the inertial components of that droplet within that environment. Smaller droplets have less inertia than large droplets and therefore will follow airflow streamlines and are more likely to avoid obstacles within the nasal cavity compared to large droplets (Inthavong et al. 2006). For olfactory epithelium deposition it is therefore crucial for a device to produce a consistent plume comprised of smaller droplets to reach this anatomically distal region within the nasal cavity.

The FDA released a guidance and recommendation document in 2003 that highlighted necessary parameter measurements and methodologies for in vitro characterisation of nasal sprays (FDA 2003). This was used as a reference for this study, and all methods were conducted to the standards set out in this guidance document.

Laser diffraction is a method recommended to measure droplet size (FDA 2003). This is an optical method that measures the size of droplets in flight (following actuation) (see Figure 4.1.6). A plume is actuated through a horizontal laser beam that runs between a laser source and detector. The plume will cause the laser light to diffract as it passes through the beam, reducing the signal detected (obscuration). Following this, a distribution of obscuration is measured from which the droplet size distribution can be calculated over the lifetime of a single actuation or during the stable phase (FDA 2003).

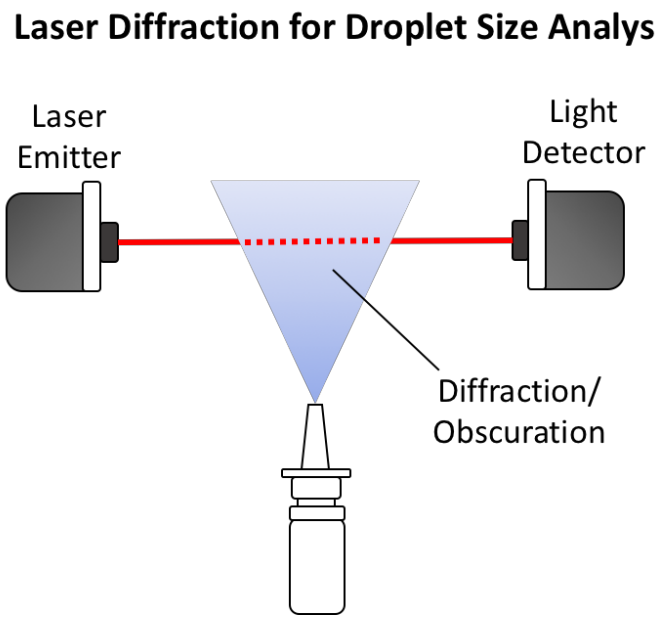

Figure 4.1.6 Schematic of the laser diffraction method setup.

Another aspect that needs to be considered for drug deposition inside the nasal cavity is the plume itself following actuation (Cheng et al. 2001). The plume is often cone shaped and a typical measure to assess the geometry of the plume is plume angle. This measure, which is conducted *in vitro,* is thought to be a useful determinant of penetration within the nasal cavity, particularly how much of the plume will penetrate past the nasal valve. One study showed that a narrow plume angle of 35° shows greater penetration beyond the nasal valve in comparison to a wider spray with a plume angle of 70° (Newman, Moren, and Clarke 1988).

Measuring plume angle requires a sagittal image of the plume (side view) during the stable phase, when the plume is at its largest. Recommendations for plume angle methodology is through the use of a high speed digital camera and laser light sheet combination. For this, a high speed digital camera is positioned to capture the nozzle pump and the impending plume. A laser light sheet is projected across the space above the nozzle. During actuation the plume is sprayed upright and is dissected by the laser sheet thus becoming illuminated and captured by the high speed digital camera (see Figure 4.1.7).

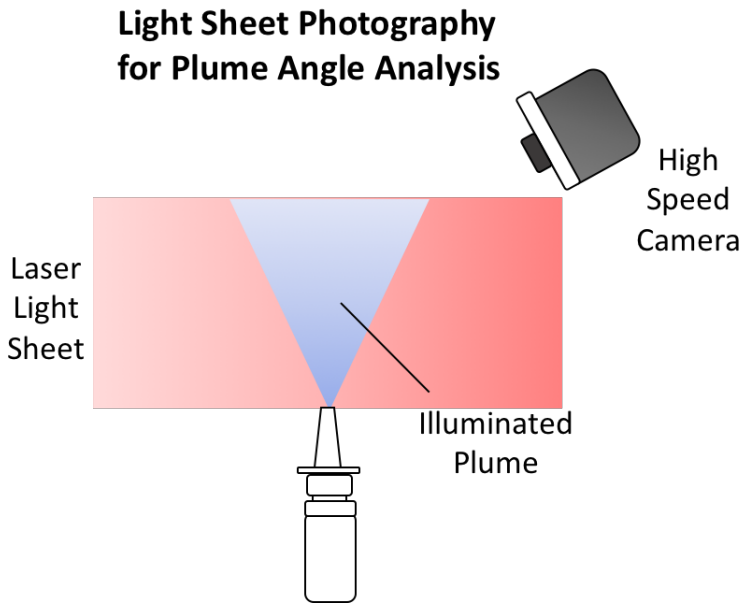

Figure 4.1.7 Schematic of the light sheet photography method setup.

Both droplet size and plume angle can be modified through the combination of the nasal delivery device and drug formulation (Dayal, Shaik, and Singh 2004). The drug formulation in this instance was the concentration of insulin that was to be used in the imaging phase of the SNIFAR study and therefore this aspect was not investigated or characterised in this study. In this study the primary objective was to characterise three nasal spray devices using *in vitro* measures of droplet size and plume angle with insulin formulation. Following this characterisation, the pump with the properties that best reflected olfactory deposition in humans would be adopted in this pharmacological investigation. Pump performance was compared to the generalised framework: a plume with a spray angle between 30° and 45° and droplets between 20 and 50 µm (Cheng et al. 2001; Inthavong et al. 2006; Newman, Moren, and Clarke 1988). The pump that has characteristics most similar to the generalised framework would be used in the SNIFAR study. In addition, testing a device is fit for purpose is very important and the current literature would suggest that this step is not routinely performed. This study is the first to report a preliminary nasal device testing stage with insulin, for use in a pharmacological human research study.

4.2 Materials and Methods

Human Insulin (Humulin®, 500 IU/ml) was purchased from Eli Lilly, USA (Eli Lilly and Company, Cambridge, MA). Three nasal spray pumps (100 µL) were provided by Nemera (La Verpillière, France), the SP270+® with two crimp on actuator types (3959 and 4290; Figure 4.2.1 A and B, respectively) and a new prototype device with a single crimp on nasal actuator (5701; Figure 4.2.1 C). An insulin stock solution was prepared by diluting the insulin with saline to create an insulin solution of 400IU/ml. The two SP270+® pump configurations and the prototype device were filled with 2.5 mL and 4.5 mL of insulin solution (400 IU/mL), respectively, due to different length dip tubes. With this stock solution there was enough to fill 5 bottles for each pump configuration. For ease of differentiation, the tested pump combinations will be labelled pump 1, 2 and 3:

- Pump 1 — SP270+® pump with 3959 actuator (n=5)
- Pump 2 — SP270+® pump with 4290 actuator (n=5)
- Pump 3 — Prototype device with 5701 actuator (n=5)

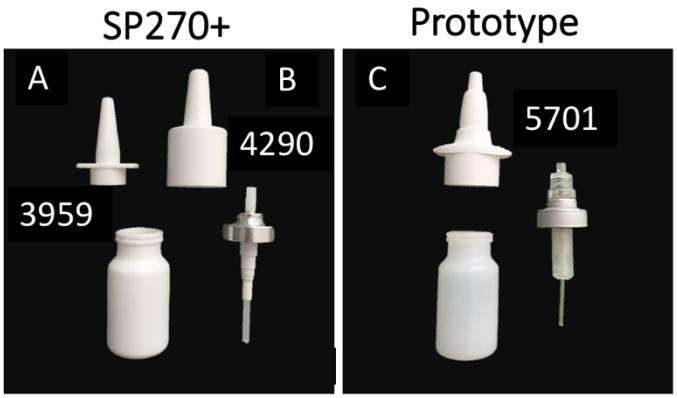

Figure 4.2.1 The three commercial pumps characterised with insulin formulation.

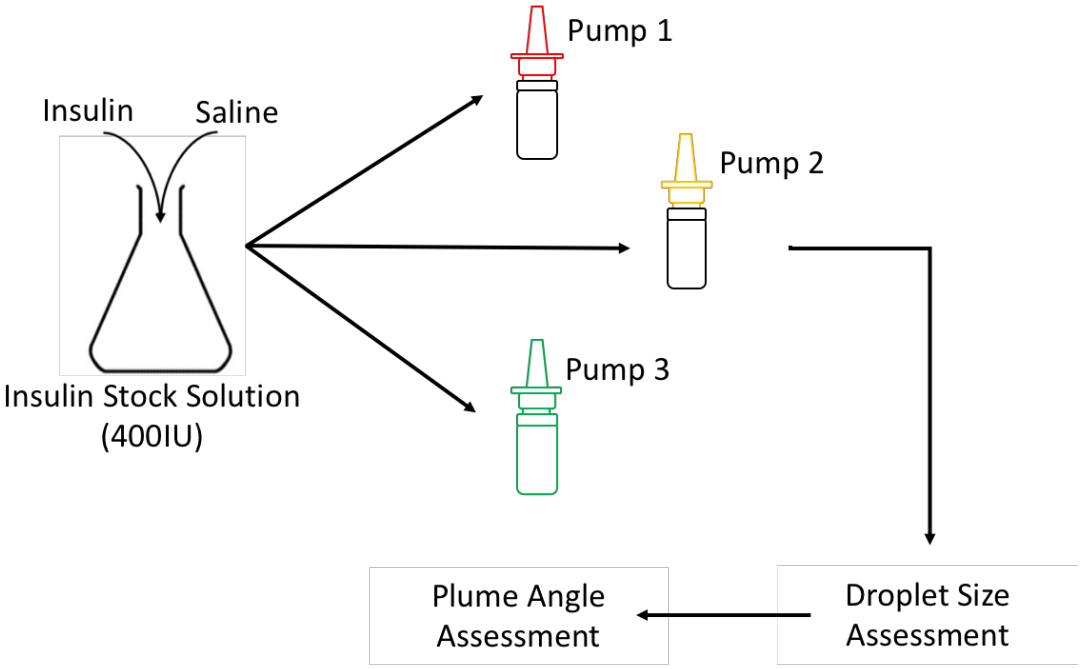

Figure 4.2.2 A schematic showing the nasal pump characterisation pipeline that was implemented.

All characterisation steps were performed in accordance with the Food and Drug Administration (FDA) guidance for industry document, that was designed to ensure nasal device analytical assessments were conducted to the highest quality (FDA 2003). The analytical procedures were performed personally at Intertek Melbourn, (Intertek, Melbourn, Cambridge, UK) according to good manufacturing practices as part of a collaboration with King's College London Institute of Pharmaceutical Sciences, Intertek Melbourn and Nemera.

4.2.1 Droplet size measurement

Droplet size was determined by laser diffraction using a Malvern Spraytec ® system (Malvern Instruments, Inc, Southborough, MA). A Proveris Vero® (Proveris Scientific Corporation, Malborough, MA) automated actuator was also used for reliable and automated actuation of each pump configuration and is recommended over manual actuation by hand (FDA 2003). Actuation force was kept constant for all experiments and pump configurations at 6.8 kg. The automated actuator was placed between the

laser emitter and the detector lens at 90° to achieve vertical spray actuation. Data was collected at a single distance from the tip of the actuator to the middle of the laser beam (30mm) and a single actuation at this distance for each pump was tested. Data was processed and analysed using the Malvern software (Malvern Instruments, Inc, Southborough, MA). Plots of obscuration over time were used to manually identify the stable phase of each actuation, when the plume is most constant, which was selected for analysis. From this phase the point in the size distribution up to and including 10, 50 and 90% of the total sample volume (known as Dv10, Dv50 and Dv90) , as well as the respirable droplets (<10 µm) were estimated for each pump and sample. Furthermore, a cumulative size distribution plot was created to help visualise the droplet size distribution and used to calculate the percentage of droplets that were in the range of 20-50 µm for each pump type.

4.2.2 Plume geometry and spray pattern measurement

A Proveris SprayView® setup and Proveris Vero® automated actuator (Proveris Scientific Corporation, Malborough, MA), actuation settings as above, were used to assess plume angle. The SprayView® setup couples a high-speed camera and a pulsed laser light sheet to capture high quality images of the insulin plume as it is emitted from the pump. For plume angle, the light sheet is positioned to dissect the centre of the plume, parallel to the plume flow. A single actuation is required for each pump sample.

For image assessment the Proveris software was used (Viota Software, Proveris Scientific Corporation, Malborough, MA). Axial plume images with maximal image intensity, i.e. when the plume is at its largest, were identified from signal over time plots and were used for analysis. From this image the tip of the nozzle was located and defined as the origin point. From this origin, two lines were aligned along the left and right edges of the plume using a manual threshold selection process. The angle (plume angle) created by these two arms was measured in degrees (°).

4.2.3 Statistical analysis

All processing and analysis for both droplet size and plume angle were measured individually for each pump sample (n=5) and then averaged together for each pump type. Data are presented as mean ± standard deviation. Unpaired t-tests were performed between data from all pump configurations for the measures obtained from droplet size, spray pattern and plume geometry analysis. P values were judged to $p < 0.05$ and $p < 0.01$ significance. All analysis was performed using R statistical analysis software (Rstudio - Version 1.1.453, Boston, MA, http://www.rstudio.org/).

4.3 Results

4.3.1 Droplet size distribution

Mean droplet size values for Dv10, 50 and 90 are presented in Figure 4.3.1. No significant differences in Dv10, 50 or 90 were seen between pump 1 or pump 2. Significant differences were seen between pump 1 – pump 3 (mean difference = -5.9, -22.9 and -50.8, for Dv10 (p < 0.05), 50 (p < 0.05) and 90 (p < 0.001), respectively). Significant differences were also seen between pump 2 –and pump 3 (md=-7.8, -26.2 and -55.6, for Dv10 (p < 0.001), 50 (p < 0.001) and 90 (p < 0.001), respectively). Respirable droplets (data not shown) for all pump configurations were very low (less than 0.7% for all devices), with no significant differences.

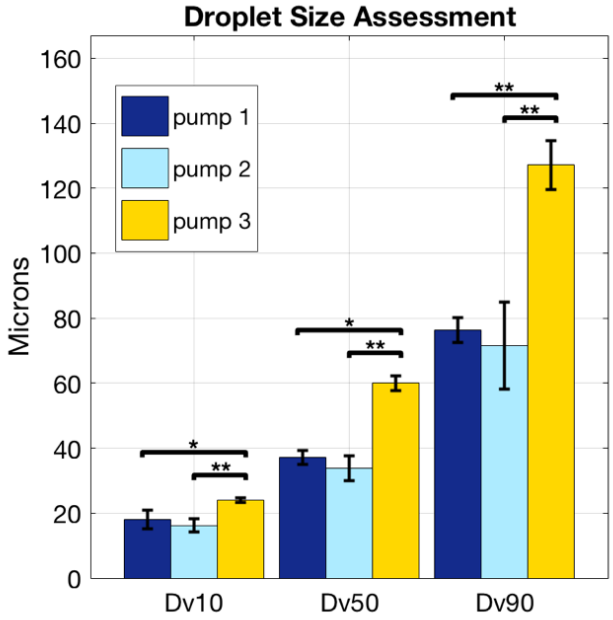

Figure 4.3.1 Bar graph displaying the droplet size measures recorded. All measures were taken at a 30mm distance. Values plotted are mean ± SD (n=5, for each pump). * p < 0.05, ** p < 0.01, unpaired t-test.

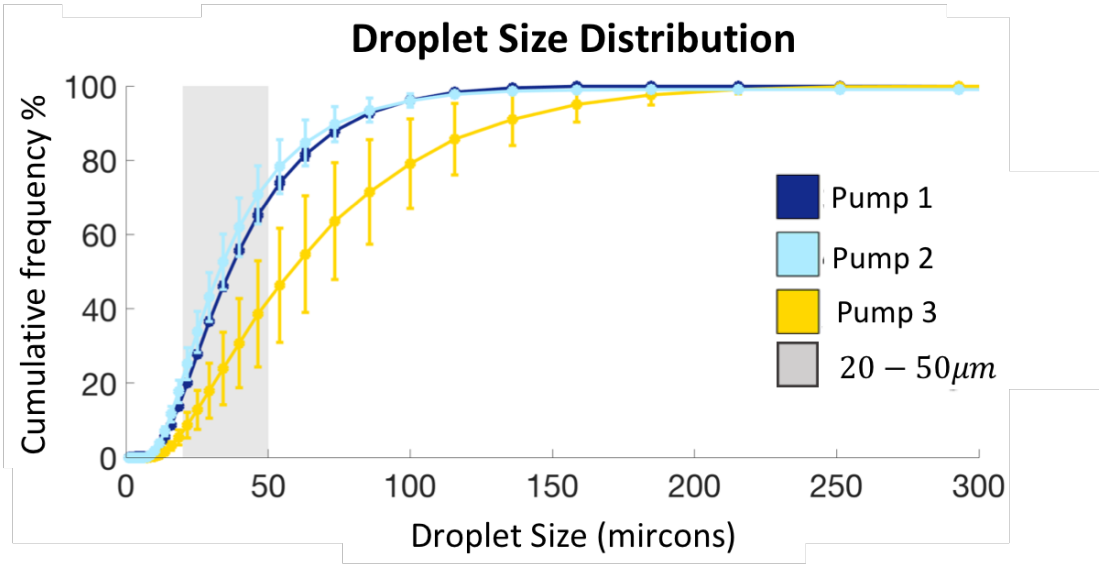

Figure 4.3.2 Droplet size distribution curves for each pump. This graph shows the cumulative frequency (%) of droplet sizes created from each pump. The grey shaded area represents the desired size range of droplets (20-50 µm). From the graph it is clear that both pumps 1 and 2 have a greater proportion of droplets that fall within this range compared to pump 3. Values plotted are mean ± SD at each point (n=5, for each pump).

	Median Droplet Size (µm) (sd)	% of droplets between 20-50 µm (sd)
Pump 1	37.2 (3.20)	48.88 (2.06)
Pump 2	33.83 (3.74)	51.38 (5.32)
Pump 3	60.06 (2.27)	29.76 (11.58)

Table 4.3.1 Median droplet size values for each pump as well as the % of droplets that are between 20-50 µm. Values shown are mean SD.

From the droplet size distributions the proportion of droplets between 20-50μm was measured and has been presented in Table 4.3.1. Although not statistically tested, pump 3 showed the smallest proportion of droplets in this range (29.76 ± 11.58%) with pump's 1 and 2 showing larger proportions (48.88 ± 2.06% and 51.38 ± 5.32%, respectively) (this can also be seen graphically in Figure 4.3.2).

4.3.2 Plume angle

Plume angle was measured for each device using light sheet high speed photography. Mean angle values are presented in Figure 4.3.3 as well as some representative images displaying the spray profile Figure 4.3.3. No significant differences were seen between pump 1 (37.8 ± 3.9°) or pump 2 (42.7 ± 3.7°). Plume angle was significantly different between pumps 1 and 3 ($p < 0.05$) as well as pumps 2 and 3 ($p < 0.01$) (pump 3: 27.5 ± 7.8°).

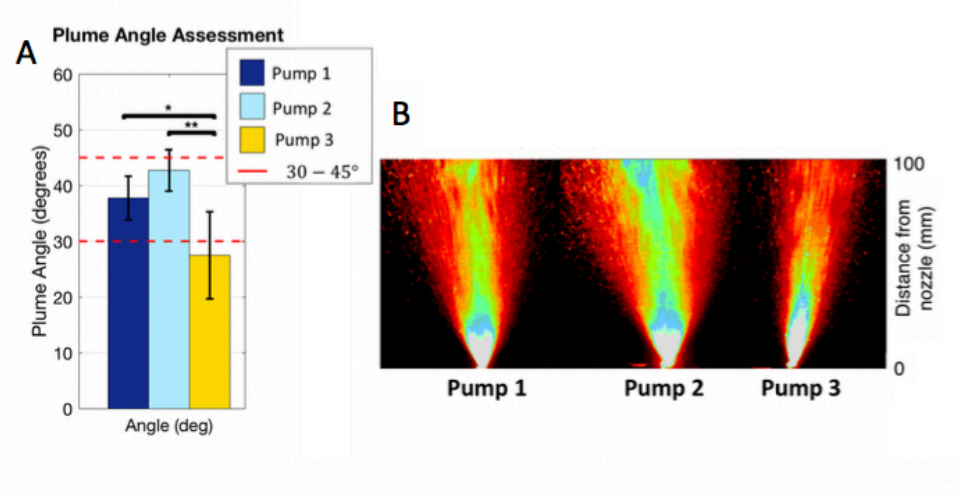

Figure 4.3.3 Bar graph displaying mean plume angle values and example images of plumes generated by each pump taken using light sheet high speed photography. A) The bar graph displays the mean ± SD plume angle calculated for each pump (n=5). The red dashed lines represent the desired plume angel range. * $p < 0.05$, ** $p < 0.01$, unpaired t-test. B) High speed photography images of representative plumes acquired during maximal plume creation. Pump 3 visibly creates a narrower plume than that of both pumps 1 and 2.

4.4 Discussion

This was a comparative study that analysed the performance of three commercial, nasal pump delivery devices and configurations with insulin solution. This study has provided information on pump performance that can be used to help predict the nasal deposition profile that may be achieved for the SNIFAR MRI study. The data reported here was collected to, firstly, see if any of the tested commercial nasal spray devices with insulin solution were capable of producing deposition suitable for nose to brain delivery in humans. And, secondly, to provide sufficient information for the researcher to make an informed decision about which pump, if any, to implement in the SNIFAR study. From previous flow dynamic modelling and *in vitro* cast model results, the optimal pump should have the following characteristics: small droplets (between 20µm and 50µm), contained in a narrow plume (between 30° and 45°) (Cheng et al. 2001; Inthavong et al. 2006; Newman, Moren, and Clarke 1988).

The respirable fractions for all the pumps were very low and therefore any of these could be implemented in a human study. From droplet size data it was clear that both pumps 1 and 2 had smaller droplets within the stable phase of the plume when compared with pump 3. Pumps 1 and 2 were not statistically dissociable from any of the droplet size measures assessed. All measures were assessed from the stable phase, when the plume is fully developed, based on obscuration thresholds. Within this stable phase, roughly 50% of that volume contained droplets that were within the desired range (20-50 µm) for pumps 1 and 2. Pumps 1 and 2 were comprised of the same pump mechanism but with different actuators, which would suggest that although physically quite different, these two actuators have similar plume creation properties. This is slightly surprising given that published data show changes in orifice size as well as actuator shape and length have significant impact on the size of the droplets produced (Dayal, Shaik, and Singh 2004).

The analytical data reported here with insulin further showed significant differences in plume angle between the three tested pumps. Pumps 1 and 2 both produced wider plumes as shown by both a larger angle from the nozzle orifice compared to pump 3.

It is known from previous work that increased droplet size leads to a narrower plume generation and given the smaller droplets produced from pumps 1 and 2 the associated wider plume was expected (Trows et al. 2014). No significant differences were seen between pump 1 and 2, a similar result as seen from the droplet size data. After gathering and analysing this data it can be concluded that pump 1 and pump 2 both displayed characteristics that were closest to the *a priori* metrics identified to be important for nose to brain delivery. The large droplets generated by pump 3 coupled with a very narrow plume < 30°, would be unable to penetrate past the anterior portion of the nasal cavity and thus not fit for purpose in this instance. A very narrow plume with big droplets acts more in the fashion of jet/hose then a mist which is sub-optimal for nasal cavity dispersion and likely lead to drug run out of the nose and would not be efficient for olfactory drug delivery. Both pump 1 and pump 2 produced more favourable results in comparison. Both of these pumps would be suitable for the SNIFAR study, however are not dissociable following this simple characterisation of each. Therefore, the physical and ergonomic characteristics of the two pump actuators were used to help decide between these two pumps. The term 'fit for purpose' in this context covers more than just the plume profile. A major consideration is that the device has to be user friendly for first time nasal spray users and have sufficient design flexibility to cater for individual differences, in for example nasal anatomy and hand sizes. The user friendliness was not explored through by a quantitative experimental approach and so has been based on qualitative assessments and backed by rationale specific to the intended use: a pharmacological MRI study in humans.

The actuator for pump 1 is narrow in shape and boasts lateral finger grips to aid manual actuation and manoeuvrability. Pump 2 has a slightly shorter and thicker actuator nozzle compared to pump 1, and does not have such obvious finger grips, rather a thick ring at the base of the nozzle.

In this study actuation of nasal sprays were controlled using an automated device, which is recommended for *in vitro* characterisation of nasal devices. The actuation force used was set to 6.8kg as per standard operating procedures (SOP) within the

laboratory this analysis was conducted at. Interestingly, this setting is slightly higher than the average adult actuation force, which was recorded as 5.82kg (range = 2.44-8.64kg) from a group of 20 inexperienced adults (Doughty et al. 2011). Actuation force has been shown to affect the size of droplets emitted within the generated plume, with stronger forces producing smaller droplets (Dayal, Shaik, and Singh 2004). Therefore, the finger grips in the case of the pump 1 would hopefully provide the participant to actuate with sufficient force, close to the 6.8kg described by the automated actuator implemented during characterisation.

Furthermore, as mentioned in the Chapter 3 (section 3.2.3), the participants administered the nasal spray in a 'forward leaning' position to aid olfactory deposition whilst keeping the nasal pump bottle upright. The participants will be required to insert the nozzle at least 1.5cm into to the nostril and roughly at a 60° angle, as recommended for olfactory deposition (Guastella et al. 2013). The slightly narrower and longer actuator would be beneficial in this situation due to increased insertion depth and degree of angular movement once inside the nostril compared to pump 2.

The ergonomic benefits of pump 1 is believed to have greater translatability for the use in the SNIFAR study. Therefore pump 1, the SP270+ and 3959 actuator, was chosen for the imaging phase of the SNIFAR study.

Chapter 5 Demographics, blood analysis, ratings and questionnaires

This chapter will present demographic data from the cohort investigated during the SNIFAR study as well as results from peripheral blood samples taken during each scanning session and questionnaires conducted both at screening and during scanning visits. Every participant enrolled in the SNIFAR study completed all three visits, however, four participants were excluded entirely from the analysis due to protocol non-compliance and other issues that warranted exclusion, which will be discussed in this chapter. The format of this chapter will present methods and results together followed by explanations of the findings for each component in the discussion section. This chapter will touch on how the findings impacted the SNIFAR study and how these data were used to supplement the imaging results.

5.1 Methods and Results

5.1.1 Participants

Forty one healthy male participants attended screening sessions for this neuropharmacological MRI investigation. Of these, thirty one fulfilled all the eligibility criteria, could commit to the study and were recruited for the imaging phase of the SNIFAR study. Those participants who were not eligible were excluded as a result of either baseline blood pressure issues (hypertension), electrocardiogram irregularities, logistically unavailable or deemed unsuitable for the research investigation by the researcher due to poor punctuality and communication difficulties. Participants were recruited in two groups, based on body mass index (BMI), in order to explore the effects of intranasal insulin (IN-INS) compared to intranasal placebo (IN-PLA) in both normal weight, referred herein as lean, and overweight (OW) individuals (lean BMI = 18.5 – 24.9 kg/m^2, overweight BMI = 25 — 29.9 kg/m^2).

5.1.2 Screening questionnaires

Three questionnaires based on eating behaviours and diet composition were completed by each participant at the screening session, which was at least seven days prior to the first imaging session.

5.1.2.1 Council for nutrition appetite Questionnaire

One of these questionnaires was used primarily as a screening tool: the council of nutrition appetite questionnaire. All of the forty one participants who attended the screening session scored above the threshold score (score = 28) for exclusion from the council of nutrition appetite questionnaire. The council of nutritional appetite questionnaire is used predominantly to look for poor nutrition, and from this questionnaire a low score (< 28) gives an indication of poor nutrition and appetite as well as a risk of at least 5% weight loss within six months (Wilson et al. 2005). This

test was used as a screening tool as the SNIFAR study aimed to assess central insulin effects within a cohort of male individuals that had a stable weight and appetite. The two remaining questionnaires (three factor eating questionnaire and dietary fat and sugar questionnaire) were implemented in order to assess eating behaviour and diet composition between groups as opposed to a screening tool, the results of which are presented below.

All statistical analysis performed was conducted using R statistical analysis software (Rstudio - Version 1.1.453, Boston, MA, http://www.rstudio.org/).

5.1.2.2 Three factor eating questionnaire

The three factor eating questionnaire (TFEQ) provides an assessment of dietary restraint, disinhibition and hunger as explained in Chapter 3 (section 3.1.2). Upon questionnaire marking a score for each factor is ascertained. The higher the mark the greater the severity, which ranks low, moderate and high. To test differences between BMI groups, unpaired t-tests were performed across groups for each factor using the factor scores as opposed to the severity category (judged to $p > 0.05$ significance). TFEQ scores are presented in Table 5.1.1 and graphically in Figure 5.1.1

Average TFEQ scores (mean ± SD)			
	Lean (n=12)	OW (n=15)	*p* value
Restraint	9.08 ± 4.81	9.26 ± 4.46	0.92
Disinhibition	4.25 ± 2.00	5.93 ± 2.37	0.06
Hunger	4.75 ± 4.33	5.67 ± 3.11	0.53

Table 5.1.1 TFEQ scores for lean and OW groups and associated *p* values produced from unpaired t-tests comparing groups.

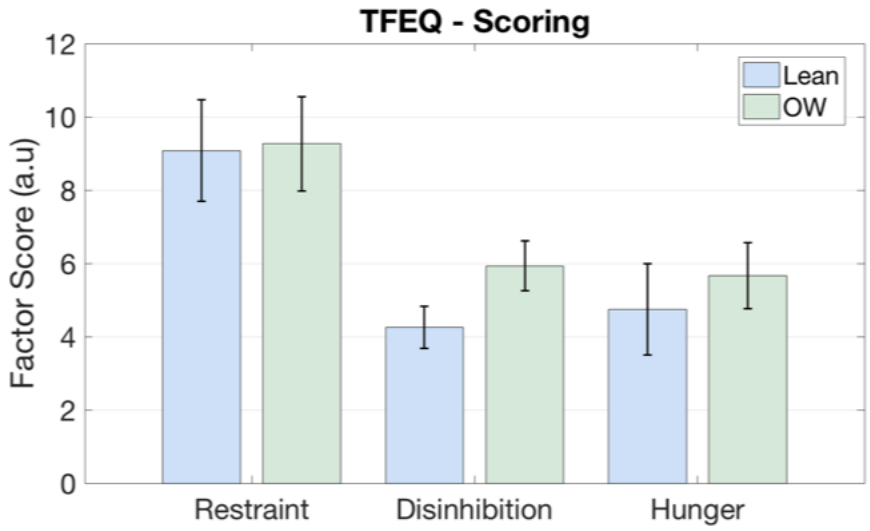

Figure 5.1.1 Three factor eating questionnaire scores. Scores for each factor are presented as mean ± SEM for lean (n=12) and OW (n=15) groups.

There were no significant group differences between the dietary restraint, disinhibition or hunger factors. For each factor the OW group displayed a higher score compared to the lean group with the biggest difference seen for the disinhibition factor (see Figure 5.1.1) In terms of severity category both lean and OW groups showed medium severity for dietary restraint and low severity for disinhibition. For the hunger factor, the lean group averaged a low severity score, whereas the OW group averaged a medium severity score.

5.1.2.3 The dietary fat and sugar questionnaire

The dietary fat and sugar (DFS) questionnaire provides an approximate guide to examine how often meals or food that contain high amounts of saturated fat and sugar are consumed, within an average week. From the DFS the overall frequency of foods high in saturated fat, sugar as well as food that contains both high levels of fat and sugar can be calculated. For each food category unpaired t-tests were conducted to interrogate group differences between the lean and OW groups.

Data are presented in Figure 5.1.2. There were no statistically significant group differences found for any of the three food categories tested (saturated fat, $p = 0.27$,

sugar p = 0.31, sugar and fat p = 0.26). However, similar to the TFEQ scores there was a slight group trend seen for all food types, that showed the OW group displaying slightly higher frequency scores for all three food categories; saturated fat, sugar and both sugar and fat, respectively.

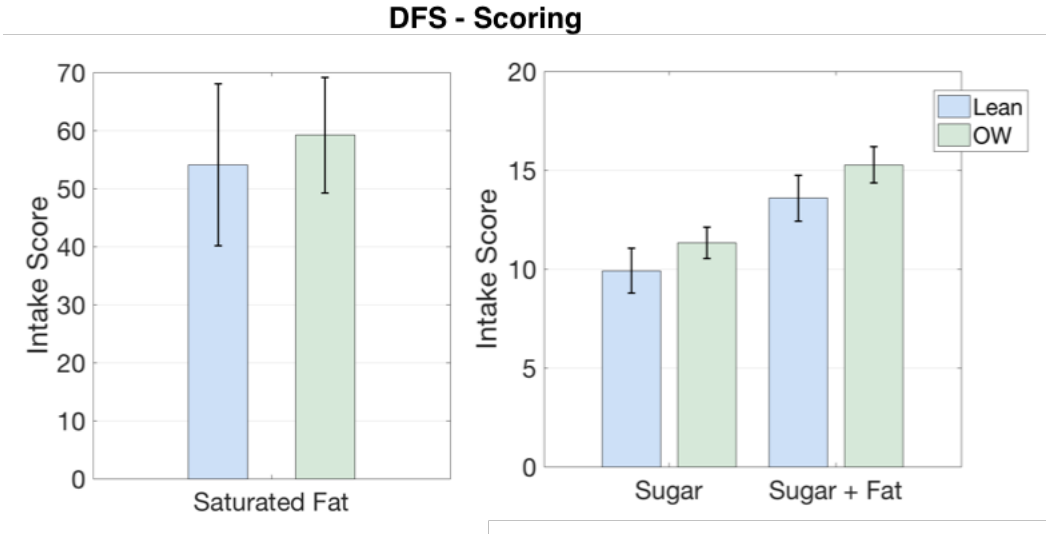

Figure 5.1.2 Dietary fat and sugar scores. Intake scores describe the frequency with which food containing saturated fat and sugar are consumed per week. Presented are scores for both lean (n=12) and OW (n=15). Data is presented as mean ± SEM.

5.1.3 Pre scan requirements

Participants were required to undergo an overnight fast and instructed to consume their last meal, which should be a regular size meal, no later than 10pm the night before. Furthermore, they were instructed to abstain from alcohol use the evening before and to avoid caffeinated drinks on the morning of scanning.

5.1.4 Blood analysis: as a screening tool

Blood samples were taken prior to dosing (defined as the pre-dose sample), once acclimatised, and immediately following the conclusion of the scanning protocol (post-scan sample) on both visits. Blood samples were spun and plasma separated on-site, for analysis conducted in batches off-site. Subject blood samples were collected to primarily measure the effects of IN-INS on plasma glucose, serum insulin and serum C-peptide concentrations over time and comparatively with IN-PLA sessions.

Having attained these particular metabolite and hormone measures, additional analyses were conducted to benefit the study. Firstly, blood samples were used to assess participant compliance with the study protocol. For example, abnormally high 'pre-dose' blood metabolite and hormone concentrations suggested the subject was not fully fasted. In this instance, a serum insulin concentration of > 50 mIU/L was used as a marker of non-compliance and any participant who exceeded this threshold, pre-dose, was excluded from the analysis. Using pre-dose insulin measures as a compliance measure was added to the SNIFAR protocol following data collection completion. In many cases blood analysis results were not analysed until the participant had completed both of the imaging sessions and therefore exclusion based on compliance was performed retrospectively at the data analysis stage.

As a result of high fasting insulin, three participants were removed from the analysis due to non-compliance with the fasting protocol. Furthermore, a fourth participant was excluded entirely from the analysis as a result of attending the final scanning session with only 1-2 hours sleep as a result of work related activity and stress. This lack of sleep was highlighted and coupled with a very low appetite rating from subjective measures of appetite. Thus the revised total number of participants included in the analysis of the SNIFAR study was twenty seven (n=27). Of those included twelve were normal weight (lean), fourteen were overweight (OW) and one was obese (BMI=31.4) but was included in the OW group. The two groups differed significantly for BMI but did not differ in age as assessed through unpaired t-tests ($p<0.05$ significance). Mean BMI and age are presented in Table 5.1.2 .

Age and body mass index of cohort		
	Age (years ± SD)	BMI (kg/m^2 ± SD)
All (n=27)	25.70 ± 4.89	25.38 ± 3.30
Lean (n=12)	27.00 ± 5.44	**22.40 ± 1.89 *** **
Overweight (n=15)	24.67 ± 4.30	**27.76 ± 1.92 *** **

Table 5.1.2 Age and BMI for the whole cohort and for the lean and overweight group. *** $p < 0.0001$, unpaired t-test.

Whole body peripheral insulin resistance was ascertained using the homeostasis model assessment of insulin resistance (HOMA-IR) (Levy, Matthews, and Hermans 1998; Matthews, Hosker, et al. 1985).

5.1.5 Blood analysis: as a measure of insulin resistance

Baseline measures (pre-dose) of insulin sensitivity/resistance for each participant were calculated using the HOMA-IR 2 model (Matthews, Hosker, et al. 1985) for each visit. HOMA-IR can be calculated using plasma glucose and serum insulin concentrations or plasma glucose with serum C-peptide concentrations. Given that there was a significant difference in baseline (pre-dose) serum insulin levels within the lean group, but C-peptide levels were highly comparable between sessions, the HOMA-IR calculation using serum C-peptide was used. The online, publicly available HOMA-IR 2 calculator v2.2.3 was used (https://www.dtu.ox.ac.uk/homacalculator/). Measures of HOMA-IR were calculated for both visits. The average HOMA-IR score for each participant (visit 1 + 2 / 2) was calculated and compared between groups (unpaired t-test). Furthermore, a correlation analysis was performed to look at the association between HOMA-IR and BMI for each group, using Pearson's correlation coefficient. Correlation coefficients (r) greater than 0.4 or less than -0.4, with an associated p value < 0.05 were deemed significant. Correlation coefficient thresholds were set to only look for 'moderate to very strong' correlations (i.e. 0.4 to 1.0) based on *Evans'* guide to correlational analysis (Evans 1995).

Participant HOMA-IR values did not significantly differ between groups (lean: 0.88 ± 0.22, OW: 1.07 ± 0.37, p = 0.12). Pearson's correlation analysis did not reveal a relationship between BMI and HOMA-IR in the lean group, however, a significant strong positive correlation was identified between BMI and HOMA-IR in the OW (r = 0.70, p = 0.003, Pearson's)(presented in Figure 5.1.3).

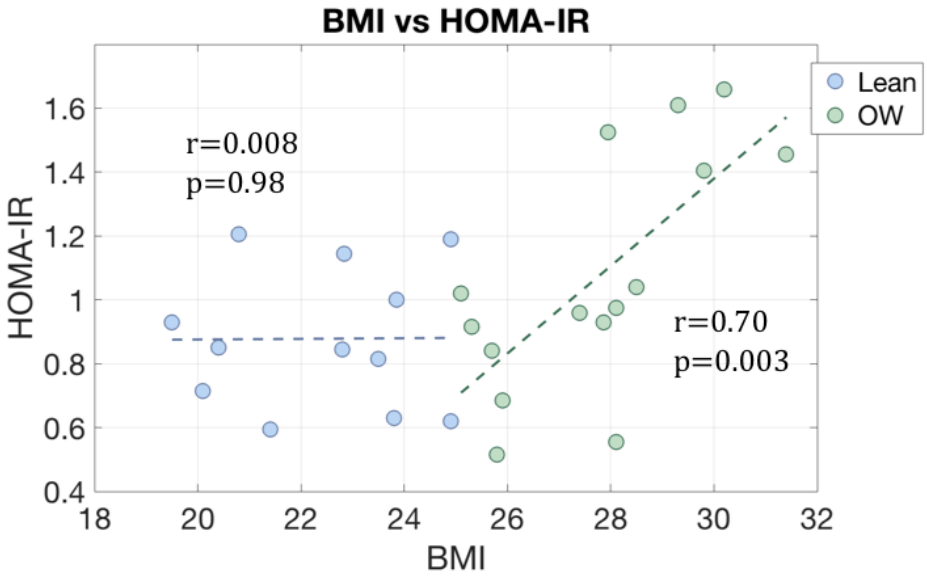

Figure 5.1.3 BMI vs HOMA-IR scores. The OW group HOMA-IR scores (averaged pre-dose across visits) show a strong positive correlation with BMI.

Through observing Figure 5.1.3, it can be seen that the lean group display a fairly tight range of HOMA-IR scores ranging from approximately 0.6 to 1.2, whereas the OW group display a much larger variation ranging from approximately 0.5 to 1.7. The strong positive correlation seen between OW BMI and OW HOMA-IR scores is interesting. There appears to be a BMI threshold of approximately 28 kg/m^2 at which HOMA-IR scores split into 'lower' and 'higher' HOMA-IR groups. This observation suggests that while BMI across the entire range does not correlate well with HOMA-IR, the increases in peripheral insulin resistance are observed from the upper end of the overweight BMI strata.

5.1.6 Blood analysis: to assess the effects of IN-INS

Plasma and serum blood concentrations were assessed to document the effects of IN-INS on plasma glucose concentration. Measuring serum C-peptide simultaneously with serum insulin permits the assessment of whether increases in serum insulin are attributed to endogenous pancreatic insulin release, which would be coupled with an increase in C-peptide, or from exogenous insulin increases, i.e. from overspill of IN-INS into the systemic circulation (Kullmann et al. 2018).

Pre-dose and post-scan blood concentrations for both placebo and insulin conditions were entered into a within-group repeated measures analysis of variance model (ANOVA), to look for main effects of treatment and time as well as interaction effects for plasma glucose, serum insulin and serum C-peptide concentrations separately. In light of a significant main effect of drug or time ($p < 0.05$), two planned comparison t-tests (paired) were conducted to ascertain from which time point or which treatment was driving this main effect, respectively, as post hoc tests (using a $p < 0.05$ statistical threshold). In response to an interaction effect, a post hoc Tukey test was performed to assess where the differences lay (applying a $p < 0.05$ statistical threshold). In the OW group, one participant did not provide a full set of blood samples, due to blood sampling issues that were encountered and therefore the OW blood analysis was conducted on fourteen participants.

Data are presented graphically in Figure 5.1.4. Within both groups there was a slight decrease in plasma glucose concentrations over time on both the placebo and IN-INS visit. The decrease in glucose following IN-INS was, in both BMI groups, visually greater compared to placebo albeit did not yield any significant effects of time or treatment on ANOVA. Within the lean group there was an IN-INS related decrease in glucose of 0.21 ± 0.22 mmol/L and in the OW group a decrease of 0.17 ± 0.46 mmol/L. In the lean group there was a significant main effect of treatment ($F_{1,23} = 5.75$, $p = 0.021$, ANOVA). Planned comparison t-test revealed a significant difference in serum insulin concentrations between placebo and IN-INS pre dose ($t(11) = -2.28$, $p = 0.04$, paired t-test, placebo (pre): 5.18 ± 2.51, IN-ins (pre): 13.98 ± 12.18) but no significant treatment effects from post-dose serum insulin measurements ($p = 0.14$). In the OW group there was significant main effect of treatment ($F_{1,27} = 9.15$, $p = 0.003$, ANOVA). Planned comparison, post hoc t-tests showed significantly higher post-scan serum insulin levels in the IN-INS condition compared to IN-PLA ($t(13) = -3.13$, $p = 0.008$, paired t-test) but no pre-dose differences were detected in the OW group.

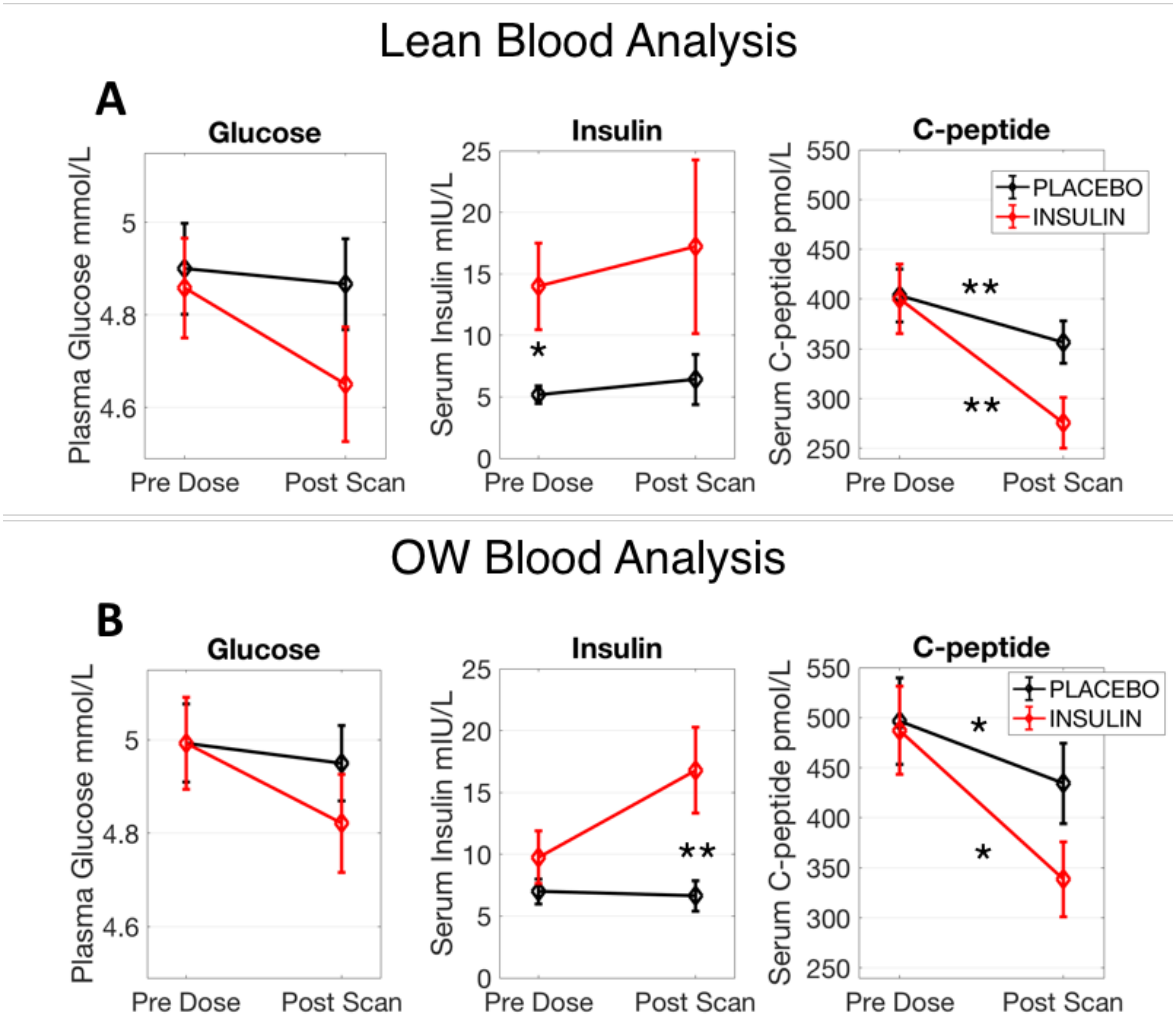

Figure 5.1.4 Lean and OW Blood analysis plots. A) Blood analysis shown for the lean group show the measured concentrations of plasma glucose, serum insulin and serum C-peptide for both IN-PLA and IN-INS sessions over time (n=12). B) Blood concentrations for the OW group are plotted (n=14). A significant increase in post scan serum insulin for IN-INS vs IN-PLA, as tested using paired t-test. Plots illustrate a significant decrease over time of serum C-peptide concentration. * $p < 0.05$, ** $p < 0.01$, plots show mean ± Standard error of the mean (SEM).

		Pre Dose		Post Scan	
		Lean	**OW**	**Lean**	**OW**
Plasma Glucose (mmol/L)	***IN-PLA***	4.9 ± 0.34	5.01 ± 0.31	4.86 ± 0.29	4.98 ± 0.30
	IN-INS	4.85 ± 0.37	5.03 ± 0.37	4.65 ± 0.43	4.78 ± 0.37
Serum Insulin (mIU/L)	***IN-PLA***	5.18 ± 2.51 *a*	6.94 ± 3.85	6.41 ± 7.06	6.76 ± 4.62 *b*
	IN-INS	13.98 ± 12.18 *a*	10.95 ± 10.12	17.21 ± 24.40	17.52 ± 14.44 *b*
Serum C-Peptide (pmol/L)	***IN-PLA***	403.58 ± 91.47 *c*	504.86 ± 177.15 *e*	356.75 ± 74.60 *c*	454.14 ± 168.50 *e*
	IN-INS	400.33 ± 120.89 *d*	489.38 ± 179.05 *f*	275.67 ± 88.63 *d*	319.54 ± 126.20 *f*

Table 5.1.3 Blood analysis values for both lean and OW groups. Data are displayed as mean ± SD lean (n=12), OW (n=14). *a,b* – significant treatment effect lean ($p < 0.025$) and OW ($p < 0.01$), respectively. *c,d* and *e,f* – significant effect of time lean ($p < 0.01$) and OW ($p < 0.001$).

In both groups there were significant main effects of time (pre-dose – post-scan) on serum C-peptide concentration (lean: $F_{1,23} = 9.70$, $p = 0.003$; OW: $F_{1,27} = 5.47$, $p = 0.02$, ANOVA). In the lean group planned comparison t-tests revealed a significant effect of time in both treatment conditions (IN-PLA: $t(11) = 3.17$, $p = 0.009$, IN-INS: $t(11) = 4.47$, $p = 0.001$, paired t-test). Similarly, in the lean group significant differences over time were found in both conditions (C-peptide: IN-PLA: $t(13) = 2.79$, $p = 0.015$; IN-INS: $t(13) = 2.89$, $p = 0.013$, paired t-test).

5.1.7 Subjective hunger scores

Prior to entering the scanner (but after dosing, pre scan) and also imminently after scanning had concluded (post scan) participants completed visual analogue scales (VAS) to assess subjective hunger. This type of subjective rating has been shown to be a reproducible and powerful marker of subjective appetite (Flint et al. 2000). These appetite ratings were an additional point of assessment within the protocol that was implemented after the first four participants had completed all sessions and therefore only available for twenty three participants. The appetite scores were assessed individually for each group; firstly, within treatment appetite ratings were compared over time (pre vs post) and, secondly, changes in hunger over time (post minus pre), were compared across treatment (insulin vs placebo) using paired t-tests ($p < 0.05$, significance).

Within the lean group there were no significant differences between pre and post measurements of appetite following either IN-PLA or IN-INS. There was a trend towards significance ($p = 0.06$, paired t-test) for an increase in appetite over time in the placebo condition. There were no significant differences seen from comparing the changes over time following each drug treatment within the lean group.

In the overweight group, there was a significant increase in appetite ratings over time between the pre and post scan measurement within the placebo condition (pre: 55.0 ± 16.5, post: 73.85 ± 15.25, $t(7) = -2.94$, $p = 0.01$, paired t-test). No drug related differences were observed within the OW group between any of the hunger change measurements. Data presented in Figure 5.1.5.

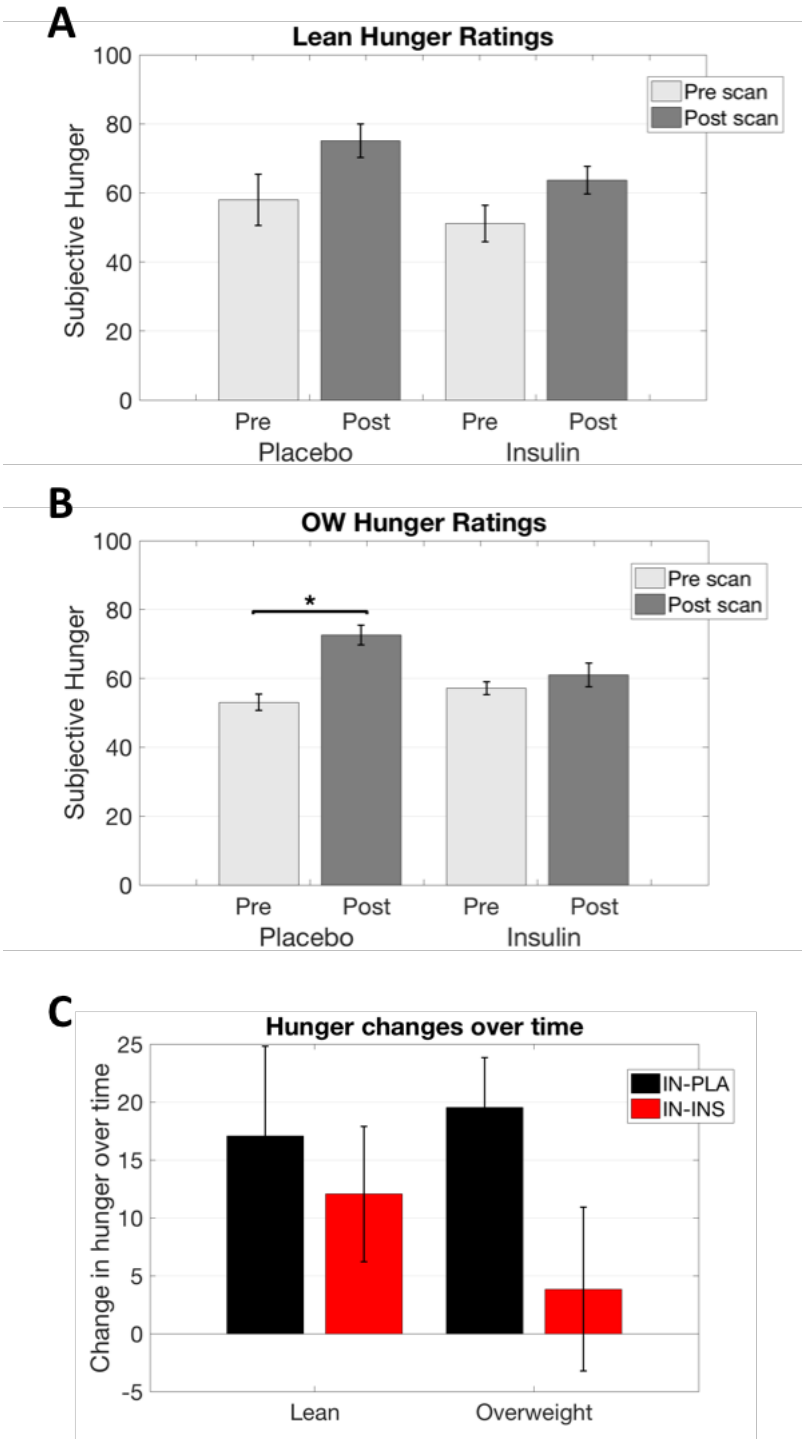

Figure 5.1.5 Pre and post-scan hunger VAS ratings for lean and OW groups. A) Lean hunger ratings did not show a statistically significant increase in hunger over time under both treatment conditions (n=8). B) Within the OW group, following IN-PLA administration there was an increase in hunger over time (n=12) (pre vs post-scan). C) Change in hunger over time following each treatment. There was no difference in change in hunger between treatment conditions. * $p < 0.05$, bars represent mean ± SEM. Light grey bars = pre scan, Dark grey bars = post scan, black bars = IN-PLA change in hunger and red bars = IN-INS change in hunger over time.

5.2 Discussion

The results from the non-imaging data are very informative and even within such a small sample there are some trends that can be observed. It is worth initially mentioning that the exclusion of four participants was unfortunate and even more unfortunate that both visits had been completed before this exclusion decision was made. In retrospect, issues of non-compliance such as fasting could be avoided by either bringing participants in to stay overnight or by conducting studies later in the day and controlling their meals or lack thereof. However, implementation of study protocols like this are time-consuming and more labour intensive for both the researcher and the participant and is not always feasible as was the case for this study, which was conducted predominantly by a single researcher.

5.2.1 HOMA - Insulin Resistance

HOMA-IR scores are useful for assessing peripheral insulin sensitivity and often used to correlate with some other physiological measure such as BMI (Vogeser et al. 2007). The HOMA is a tool to asses pancreatic beta cell function as well as IR (Wallace, Levy, and Matthews 2004) and as it is based on fasting measures, the latter primarily reflects hepatic insulin sensitivity rather than peripheral. It has been suggested that implementing C-peptide alongside glucose concentrations for HOMA calculations is better for predicting beta cell function, whereas predicting IR or insulin sensitivity is better conducted with glucose and insulin entered into the calculation (Wallace, Levy, and Matthews 2004). However, the scores in this case were calculated using the pre dose C-peptide blood measurements for the following reasons. There was a large amount of variability within the serum insulin data, as seen from the large standard deviation values (see Table 5.1.3). Furthermore, several participants had levels below the lower limit accepted by the HOMA-IR 2 online calculator used (Levy, Matthews, and Hermans 1998). These two points reflect the inherent variability in the insulin assay adopted in this study. Concerns regarding insulin assay standardisation do exist (Robbins et al. 1996), which is beyond the scope of this discussion but do support the justification in using C-peptide in this measurement.

Furthermore, these measures were not used clinically and were purely for research purposes and supplementation. Even with the more reliable c-peptide measure, there were no formal differences in HOMA-IR scores between the lean and the OW group. HOMA-IR has been shown to positively correlate with BMI (Vogeser et al. 2007) as well as many other factors, including age (Karakelides et al. 2010). The cohort enrolled and investigated as part of the SNIFAR were young, and otherwise healthy, which may explain the lack of difference between these two groups. A strong positive correlation was observed however between HOMA-IR and BMI which was exclusive to the OW group. From the BMI x HOMA-IR plot (Figure 5.1.3) a trend can be seen that shows a slight group separation in HOMA-IR at approximately a BMI of 28 m/kg^2. The absence of a correlation in the lean group may reflect a narrow range of BMI measures in this group, but may also reflect a healthy phenotype across the range of lean values, while a phenotype above the BMI threshold of 28 shows an impact of BMI on insulin sensitivity.

Previous imaging studies have assessed HOMA-IR in an effort to stratify study cohorts into insulin sensitive and insulin resistant groups in order to make inferences based on peripheral insulin sensitivity (Tiedemann et al. 2017). This was not possible in this case and therefore pre dose HOMA-IR scores primarily benefited the study through providing these values as 'covariates of interest' into the design matrix for whole brain second level random effects statistical models for functional imaging data analysis, as will be presented in the chapters to follow. This additional physiological information may in some cases help to account for some of the between subject and also within-subject variance inherent to the functional imaging data collected.

Blood was sampled on only two occasions during the present protocol. Sampling serial blood measurements throughout the duration of the scanning protocol might have been preferable and is used for pharmacological fMRI research, as drug activity can be closely correlated with pharmacokinetic data (Mehta and O'Daly 2011). In this instance, however, temporally rich blood sampling was not feasible and was also not a primary aim of this study. Furthermore, it was considered desirable not to disturb the participant during scanning. As such, only pre-scan (before dosing) blood

concentrations and HOMA-IR measures were employed as covariates for imaging data analysis. The addition of blood concentration and HOMA-IR covariates was purposely restricted to the resting state blood oxygen level dependent and the resting state cerebral blood flow data, which were acquired at the beginning of the functional imaging protocol.

5.2.2 Effects of IN-INS on blood glucose and hormone concentration

An acute 160 IU dose of IN-INS was implemented in this study via two nasal administrations in each nostril. A recent meta-analysis (Schmid et al. 2018) has formally looked at the safety aspects and concerns regarding hypoglycaemia and other adverse events in response to IN-INS. This meta-analysis reports 17 separate research papers that have studied the acute effects of a single dose of 160IU of IN-INS. From all of these studies there were no reports of severe hypoglycaemia (although not explicitly defined by the authors (Schmid et al. 2018)) but there were reports of IN-INS related decreases in blood glucose of approximately 0.24 mmol/L (Benedict et al. 2008), 0.2 mmol/L (Heni et al. 2012) and 0.48 mmol/L (Santiago and Hallschmid 2017) in response to a 160IU dose. For the SNIFAR study an explicit definition for a 'hypoglycaemia alert' was set to $\leq$ 3.9 mmol/L as defined in Seaquist et al., (Seaquist et al. 2013). From the data reported above a mean IN-INS related dip in plasma glucose concentrations of 0.21 mmol/L and 0.17 mmol/L in lean and OW groups, respectively, similar to those reported previously (Benedict et al. 2008; Heni et al. 2012; Santiago and Hallschmid 2017).

The trend towards a decrease in plasma glucose levels is very likely due to increased peripheral insulin concentrations from the IN-INS administration. In the OW group IN-INS administration was coupled with a significant increase in post scan serum insulin concentrations in comparison to IN-PLA. This increase was, however, not coupled with a rise in C-peptide levels which suggests that this increase detected is a result of exogenous insulin increases in the periphery from IN-INS administration. In the lean group however, there is a surprising statistically significant difference

between pre dose serum insulin levels between the IN-INS session and IN-PLA session. One might suspect that this difference has resulted from some participants not having been fasting on the IN-INS sessio . However, the increased pre dose serum insulin concentration seen on IN-INS sessions vs IN-PLA is not coupled with an associated increase in serum C-peptide. In fact the serum C-peptide levels between sessions are very similar pre dose and as alluded to before the discrepancy may be a consequence of an unreliable assay. Nevertheless, although all participants confirmed verbally to the researcher that they were fasted at the start of each study, the very high insulins of three participants did lead to their exclusion from the data analysis, on the basis that a non-fasted state could not be ruled out.

As mentioned the OW group displayed an increase in serum insulin concentrations after IN-INS compared to IN-PLA. Interestingly this increase was coupled with a slight but insignificant decrease in plasma glucose concentration. This lack of significant blood glucose decrease given the insulin rise may be reflective of a BMI related peripheral insulin insensitivity. Even though none of the OW participants were classified as IR this lack of significant glucose decrease could be an early sign of decreased peripheral insulin sensitivity within the OW group. The increase in post scan serum insulin seen within the OW group is strongly suggested to be as a consequence of drug absorption into the peripheral circulation. This is a consequence of using a high dose of insulin (160 IU) and also the route of administration. As described in detail in Chapter 4; the nasal cavity epithelium is highly vascularised. The nasal pump carefully selected for the SNIFAR study was superior to the comparator pumps tested against, but is arguably not fully optimal pump for nose to brain insulin delivery. In fact, given the complex architecture of the nasal cavity and large surface area of the nasal epithelium (Djupesland 2013) even a purposefully designed nose to brain nasal pump would lead to some residual drug deposition within the nasal epithelium which would subsequently be absorbed into the circulatory system. This spill over effect of IN-INS into the circulation was not however, coupled with any hypoglycaemic events or adverse reactions, similar to that observed from previous reports (Schmid et al. 2018). An exogenous insulin dose of 160 IU delivered intravenously would lead to severe hypoglycaemia. As there was a limited effect on

peripheral glucose levels following IN-INS there is strong evidence to suggest that a large majority of the 160 IU dose was delivered to the central nervous system (CSF) via olfactory and trigeminal nose to brain delivery routes (Djupesland 2013). It will be argued therefore, that imaging data differences seen within the SNIFAR data are due to central increases of insulin within the central nervous system (CNS) from nose to brain delivery of insulin solution.

C-peptide in all cases significantly decreased over time. The understating of this is that being in the fasted state for the duration of the protocol would not require pancreatic insulin release and subsequent C-peptide levels would drop over time as a result of C-peptide degradation (Matthews, Rudenski, et al. 1985). The larger drop after IN-INS is compatible with the systemic action of some of the exogenous insulin, presumably through a direct effect, as importantly the plasma glucose did not fall in any subject to or below 3.9mmol/l, the levels associated with the onset of the pancreatic homeostatic responses of reduced pancreatic insulin and increased pancreatic glucagon responses (Seaquist et al. 2013).

5.2.3 Hunger ratings

From subjective hunger ratings taken outside of the scanner it can be seen that there is an insulin related hunger blunting effect. In all cases hunger increased over time but was only significant in the OW group from the IN-PLA session. This may suggest the OW group are more susceptible to feelings of hunger during fasting. Comparing the change in hunger over time between intranasal treatments did not reveal any treatment related differences. The application of 160 IU IN-INS has been previously shown to reduce calorie consumption in healthy young men compared to IN-PLA (Benedict et al. 2008). Although ratings of hunger are physically different from food consumption it still serves as a good reflection of energy balance. One study looking at the effects of IN-INS on cerebral perfusion additionally reported no effect of IN-INS on self-reported subjective hunger following 40 IU IN-INS (Schilling et al. 2014) suggesting that the anorexigenic appetite reducing effects of IN-INS may be dose

dependent. These hunger ratings nonetheless showed a general trend towards an IN-INS related effect on hunger suppression in the OW group. These effects were subtle and do not suggest that IN-INS induces satiety but these observations are useful when interpreting the results from the functional imaging data collected which are subsequently analysed in the following chapters.

5.2.4 Questionnaires

Previous research has found that BMI correlates positively with both TFEQ disinhibition and hunger factor scores, but not dietary restraint (Zimmerman et al. 2017). These correlation results previously reported are in support of the trend seen from the data presented from the SNIFAR study. As the TFEQ questionnaire was completed at screening there are no drug related effects that can be attained from these scores. From previous research, the TFEQ has been used to good effect as a statistical regressor against functional imaging related data. For example, Kullmann *et al.,* showed that TFEQ disinhibition scores correlated with cerebral blood flow (CBF) responses to IN-INS within the prefrontal cortex (Kullmann, Heni, Veit, Scheffler, Machann, Häring, et al. 2015). The TFEQ scores gathered from screening may benefit and help to compound the understanding of imaging data collected via correlational analysis as has been described previously (Kullmann, Heni, Veit, Scheffler, Machann, Häring, et al. 2015) and were applied in this way when possible. The DFS is a rough marker of diet composition. The two groups differed by only one BMI category and therefore this might explain why a general trend was seen as opposed to formal statistical differences between the two groups. For all food categories the OW group showed slightly higher intake frequency scores suggesting that the OW group in general consume slightly more foods containing saturated fats, sugar and a combination of both sugar and fat. Similarly to the TFEQ scores, the use of these DFS scores will benefit the imaging data acquired through implementation of explorative correlational analyses. The SNIFAR study did not assess adiposity and therefore the self-reported saturated fat intake may serve as a partial surrogate for this.

All questionnaires performed at the screening were done so as to reduce the workload for the participants during the imaging visits of the study. Although the results from the questionnaires do not reveal differences between lean and OW groups, the information from these scores will be important additions to the imaging data analysis. The scores for the questionnaires were used within exploratory correlation analyses, particularly to supplement region of interest based analysis.

In conclusion, there are some interesting results from the demographic, questionnaire and blood concentration data. The SNIFAR study was implemented in an age matched group of healthy male volunteers who were stratified into two BMI groups; normal weight/lean and overweight. Differences in questionnaire scores were subtle and not statistically significant, as was also true of measures of insulin resistance. Therefore, these two matched cohorts were also matched for diet composition, dietary restraint, disinhibition and hunger permitting strong inferences to be made based on BMI.

Chapter 6 The modulatory effects of intranasal insulin on cerebral perfusion

This chapter will document the measurements of cerebral perfusion that I carried out in this study. Resting perfusion weighted imaging data were acquired using a 'work in progress' arterial spin labelling sequence that permitted the use of long labelling durations (> 1.5s). The sequence parameters chosen for this investigation of the effects of intranasal insulin on resting perfusion were chosen derived from a previous sequence optimisation project that I conducted during the MRes phase of this program, prior to the beginning of this PhD (Wingrove et al. 2015). The main focus of this chapter, therefore, will be the data analysis and results for the perfusion-related component of the SNIFAR study which will be presented and discussed with reference to the relevant literature.

6.1 Introduction

Arterial spin labelling (ASL) is an ideal imaging technique to explore regional changes in cerebral perfusion, or cerebral blood flow (CBF), in response to a pharmacological challenge (Wang, Chen, et al. 2011b). CBF measured through ASL is both quantitative (ml/100g of brain tissue/min) and physiologically relevant when examining drug induced effects in the brain (Mehta and O'Daly 2011). Regional CBF changes can be reflective of direct compound interactions on the cerebral vasculature, for example caffeine (Perthen et al. 2008), or as a result of increased metabolic demand required from neuronal populations due to neuroactive effects (see section 2.2.1). Previous work in humans using ASL has provided some evidence to suggest that exogenous insulin has little direct interaction with the cerebral vasculature (Grichisch et al. 2012) and that insulin-associated effects on CBF are driven by neuronal origins.

A small number of experiments looking at the modulatory effects of intranasal insulin have employed ASL to explore regional perfusion changes in healthy lean, obese, insulin resistant and also healthy elderly individuals (Schilling et al. 2014; Kullmann, Heni, Veit, Scheffler, Machann, Häring, et al. 2015; Akintola et al. 2017). The present study, however, is the first to explore these effects in a group of overweight individuals in comparison to an age matched normal weight group. Furthermore, within this interrogation, a pseudo-continuous ASL (pCASL) sequence with long labelling abilities was implemented, in an effort to acquire quantitative images of CBF with a voxel size adequate to resolve cortical and sub-cortical features with limited partial volume effects. CBF measurement with ASL is prone to image degradation effects, known as partial volume effects, as a result of the combined signal contribution from both grey matter (GM) and white matter (WM) (Asllani, Borogovac, and Brown 2008; Chappell et al. 2011). More often than not, an investigator is interested in GM perfusion, which is typically three times greater than that of WM. Voxels at GM/WM boundaries will inevitably comprise signal contributions from both tissue types, thus the WM contribution may introduce an underestimation of CBF. The sequence aims to limit the effects caused by partial volume through acquisition of images with smaller voxels in an effort to reduce CBF

underestimation. There have been no reported studies that have adopted a pseudo-continuous ASL (pCASL) sequence with long labelling abilities for use in a pharmacological MRI (phMRI) experiment. The sequence used has been optimised to achieve a balance between in-plane spatial resolution, temporal resolution, signal to noise ratio and blurring in the slice encoding direction (z-axis).

The aim of this experiment is to identify CBF changes in response to intranasal insulin administration in both lean and overweight individuals. The use of this pCASL sequence will permit the resolution of cortical and sub-cortical structures known to be insulin responsive and be sensitive to resolve significant insulin associated changes in regional CBF. We hypothesise that 160 IU IN-INS will produce significant changes in CBF within the limbic and cortical structures that possess insulin receptors. We predict that these changes will be decreases in CBF based on previous CBF literature with this dose (Kullmann et al. 2018) and that these decreases will be greatest in the lean group of individuals in comparison to the overweight group.

6.2 Methods

6.2.1 Participants and study protocol

As mentioned previously in Chapter 5 (see section 5.1.4) of the 31 participants scanned, 27 were included in the analysis of cerebral perfusion Three of these were removed due to possible non-compliance of the overnight fast and one was excluded due to a lack of sleep the evening before one of the scanning sessions. In total there were 12 lean participants (BMI = 22.40 ± 1.89 (mean ± standard deviation)) and 15 OW participants (BMI = 27.76 ± 1.92) that were included in this analysis of cerebral perfusion (groups did not differ in age, as mentioned in Chapter 5 (see section 5.1.1)).

6.2.2 ASL acquisition

Resting state ASL was performed directly after the acquisition of resting-state blood oxygen level dependent (BOLD) data and was the final resting acquisition within the SNIFAR protocol (see section 3.4.6). Given previous literature on intranasal insulin pharmacokinetics (Born et al. 2002) it is likely that CSF and interstitial brain insulin concentrations would be close to peak elevation levels at this time point.

All scanning was conducted using a MR750 3 Tesla GE Scanner with a 32 channel head coil. Whole brain resting cerebral perfusion images were collected using a 3D pseudo-continuous arterial spin labelling (pCASL) sequence acquired with a fast spin echo (FSE) stack of spiral readout. The following parameters were used; 10 spiral arms, 600 points per arm, in plane resolution 2.94 x 2.94 mm^2, slice thickness = 3mm, 54 slices, label duration (LD) = 3500 ms, post label delay (PLD) = 2025 ms, echo time/ repetition time (TE/TR) = 11.8 / 7325 ms, number of averages = 2, total time of acquisition = 5.22 mins. A background suppression module was applied, to null static signal, using default scanner calculated pulses. This consisted of one single selective saturation pulse applied to the imaging volume and an imaging selective inversion

pulse prior to labelling followed by four non-selective inversion pulses between the end of the labelling block and the readout window.

The labelling plane for this pCASL sequence is automatically set to 2 cm below the imaging volume. The imaging volume was positioned on the inferior surface of the cerebellum for all subjects to allow for both optimal labelling plane positioning and labelling efficiency, perpendicular to the carotid and vertebral arteries just below the Circle of Willis. The pCASL sequence automatically acquires a 3D proton density (PD) image using identical readout parameters for cerebral blood flow quantification purposes and was also used to aid co-registration. During resting pCASL acquisition participants were instructed to keep their eyes open and look at a fixation cross displayed to them via a projector screen.

6.2.3 Cerebral blood flow quantification

CBF maps were computed from perfusion weighted (PW) and PD images using the single compartment model using online GE scanner software, by performing the CBF calculation at each voxel, defined in section 2.2.3.7, of the acquisition methods chapter (chapter 2).

6.2.4 Image processing

PD images, which boast higher tissue contrast compared to both CBF maps and PW images were co-registered to 3D T1 images using epi_reg (FMRIB software Library, version 3.20, University of Oxford, UK, www.fmrib.ax.ac.uk/fsl - FSL (Jenkinson et al. 2002)). Subject CBF maps were registered to MNI space by applying the saved transformations (from the T1 normalisation steps, see section 3.5.1, in the study design chapter (chapter 3)) and warps using Advanced Normalisation Tools software (ANTs) (Avants et al. 2014). Normalised CBF maps were smoothed using a full width half maximum (FWHM) Gaussian kernel of 6 x 6 x 6mm^3 using the Statistical Parametric Mapping smooth function (SPM-12, Wellcome Trust Centre for

Neuroimaging, University College London, UK, www.fil.ion.ucl.ac.uk/spm). This smoothing kernel, approximately twice the acquired spatial resolution, was implemented in reference to recommendations for group statistical inferences with functional BOLD data (Worsley and Friston 1995).

6.3 Group level CBF Image Analysis

6.3.1 Whole brain analysis

Pre-processed CBF maps were analysed at the second-level using SPM. These maps were entered into a random effects second level voxel-wise repeated measures factorial model analysis with the three factors; subject, Drug (PLA, INS) and Group (LEAN, OW) (known in SPM as a flexible factorial model). The inclusion of the subject factor as an explanatory variable to encode the between subject-variability helps to reduce the amount of unexplained variance within the data and has been shown to increase detection sensitivity within pharmacological experiments (Mehta and O'Daly 2011). Mean grey matter (GM) CBF values, calculated from a liberal GM mask, were added to this model as a covariate to account for within-subject between session GM CBF variability. Analysis was constrained to those voxels within the GM by applying an implicit GM mask. Contrast T-maps for the main effect of PLA and INS were created as well as interaction effect contrasts (Drug X BMI) (see Figure 6.4.2). Voxel wise whole brain analysis results were set to a cluster forming threshold of $p < 0.01$. Significant clusters were classified based on cluster correction for multiple comparisons using a family wise error threshold (FWE) of $p < 0.05$. In response to a significant interaction effect ($p < 0.05$ FWE) or an interaction trend ($0.05 < p < 0.1$ FWE) 2nd level whole brain paired t-tests were created for each group for both main drug effects, INS > PLA and INS < PLA, using the same cluster forming threshold as mentioned above ($p < 0.01$) and again including the global GM mean CBF as a covariate.

To assess changes in global CBF whole brain median grey matter (GM) CBF values, constrained to a standardised GM mask, were extracted from the pre-processed maps using Analysis of Functional Neuroimage (Cox 1996) (AFNI, 3dmaskave) software. GM CBF values were entered into a repeated measures analysis of variance (ANOVA) model to test for main effects of drug group and interaction effects. Following a significant main effect of drug two paired t-tests were conducted to see if drug related changes were significant within the lean or overweight group, or both. Following a significant group effect two unpaired t-tests were conducted to explore whether these group differences in CBF were detected following placebo or insulin administration, or both. These t-tests will be referenced as planned comparisons and formed a post hoc analysis as opposed to testing all possible combinations. To correct for these two planned comparisons a Bonferroni multiple comparison correction was applied providing a significance threshold of $p < 0.025$. Following a significant interaction effect a Tukey test was performed post hoc to test all possible comparisons. Tukey tests inherently adjust for multiple comparisons and thus a significance threshold of $p < 0.05$ was employed.

Blood analysis results presented in Chapter 4 showed a degree of variability in baseline serum insulin concentrations in the lean group between imaging visits. This variability proved sufficient to produce significant differences in pre-scan serum insulin concentrations between the two imaging visits in the lean group only. In an effort to account for some of this variability, HOMA-IR scores, calculated and presented in chapter 4 for both INS and PLA, were added to the paired t-test model as a regressor of no interest (nuisance regressor) in the lean group only. The whole brain paired t-test was run both with and without the addition of the nuisance regressor.

6.3.2 Region of interest analysis

Small volume correction (SVC) analysis was conducted on whole brain t-maps to permit a more thorough exploration within pre-defined regions of interest (ROI). Bilateral anatomical regions were selected, as ROIs for this analysis. These regions

were defined *a priori* based on high insulin receptor density profiles and also from previous publications that have shown insulin induced responses within these ROIs and potential functions in food intake and behaviour (detailed in Table 6.3.1) (Schulingkamp et al. 2000; Schilling et al. 2014). Insulin receptor dense regions were defined as the hippocampus and amygdala (Schulingkamp et al. 2000) and the ROIs based on previous intranasal insulin literature were the insula and the putamen (Schilling et al. 2014).

Regions of interest	
Region	**Rationale**
Insula	• Observed CBF increases within this region with IN-INS (40 IU) (Schilling et al. 2014). • Region heavily involved in gustatory processing, potential link with insulin modulation (Frank, Kullmann, and Veit 2013).
Hippocampus	• Beneficial memory processes are regulated by insulin receptors within the hippocampus (Benedict et al. 2004; Benedict et al. 2008). • Region involved in cognitive processing of meals (Higgs 2016; Higgs 2005), potential role for insulin in cognitive aspects of food intake.
Putamen	• Observed CBF increases within this region with IN-INS (40 IU) (Schilling et al. 2014). • Region involved in hedonic reward processing, potential site for insulin modulation.
Amygdala	• Abundance of insulin receptors found within the amygdala (Schulingkamp et al. 2000). • Dysregulation of amygdala found in insulin resistance animals (Areias and Prada 2015).

Table 6.3.1 Regions of interest used in this cerebral perfusion analysis of IN-INS.

All subcortical bilateral ROIs were defined in SPM-12 using the Functional MRI tool of the Wake Forest University School of Medicine (http://www.ansir.wfubmc.edu) known as 'WFU pick atlas', implemented with automated anatomical labelling (AAL). The insula is a relatively large cortical structure with well-established functional roles in the processing of appetite related cues and reward (Frank, Kullmann, and Veit

2013). As a result of the size and diverse neural functionality of the insula was subdivided into the posterior and anterior subdivision in an effort to infer more specificity in reference to CBF related effects seen within the insula. These subdivisions used were based on publicly available cytoarchitecture data (Kurth, Eickhoff, et al. 2010). All ROIs are visually displayed in Figure 6.4.4.

SVC was applied to whole brain maps of both the main effects and interaction effects for the five ROIs described above. A significance threshold was calculated to correct for multiple comparisons by dividing the $p < 0.05$ by the number of ROIs used (ROIs = 5). The significance was set to $p < 0.01$ for SVC analysis.

Furthermore, median CBF values were extracted from the five bilateral ROIs defined above (Cox 1996) (AFNI, 3dmaskave). Median CBF values for each ROI were entered into a repeated measures ANOVA factorial model with two factors drug and group. Five ANOVA models were created to assess the five different ROIs. Main effects of drug and group were explored as well as drug by group interactions. Main effects and interactions were assessed to a significance threshold of $p < 0.05$. Following a significant main effect of drug two paired t-tests were conducted to see if drug related changes were significant within the lean or overweight group, or both. As with the median GM CBF analysis described earlier, following a significant group effect two unpaired t-tests were conducted to explore whether these group differences in CBF were detected following placebo or insulin administration, or both. A Bonferroni multiple comparison correction for two planned comparisons was applied providing a significance threshold of $p < 0.025$ (0.05/2). Following a significant interaction effect a Tukey test was performed post hoc to test all possible comparisons. Tukey tests inherently adjust for multiple comparisons and thus a significance threshold of $p < 0.05$ was employed.

6.3.2.1 Correlational analysis

As an additional exploratory analysis, drug induced changes in regional CBF within each group were assessed for correlations with dietary saturated fat intake and sugar intake measured through the dietary fat and sugar (DFS) subscale questionnaire that each participant completed during the screening. Insulin induced CBF changes from the five ROIs (Δ%) were defined as PLA – INS / PLA * 100, and self-reported dietary saturated fat and also sugar intake scores were in arbitrary units. Δ% CBF changes for each ROI were examined for associations with fat and sugar intake using Pearson's correlation coefficient. A relevant correlation was defined as rho (r)= > 0.4 or < - 0.4 with a *p* value < 0.05.

6.3.2.2 Statistical analysis

Descriptive parametric statistics were used to describe the results and noted as mean ± standard deviation unless stated otherwise. All ROI analysis was conducted using R statistical analysis software (Rstudio - Version 1.1.453, Boston, MA, http://www.rstudio.org/). Repeated measure ANOVA models were used to look for main effects of group and drug as well as interaction effects from the median extracted CBF values extracted from each of the ROIs defined. For within group and within treatment comparisons paired and unpaired t-tests were implemented, respectively.

6.4 Results

6.4.1 Grey matter cerebral blood flow

Median CBF (ml/100g/min) values extracted from GM voxels (presented in Table 6.4.1) revealed no significant effect of drug, BMI or interaction effect on global GM CBF.

Median Grey Matter Cerebral Blood Flow (ml/100g/min)		
	PLA	INS
All (n=27)	57.92 ± 6.84	58.23 ± 5.73
Lean (n=12)	56.33 ± 7.89	56.51 ± 6.34
Overweight (n=15)	59.19 ± 5.83	59.60 ± 4.98

Table 6.4.1 Median Grey Matter CBF. Data are presented as the average ± SD.

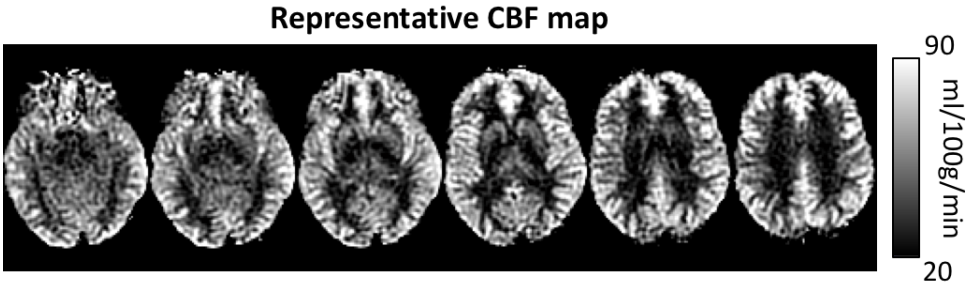

Figure 6.4.1 Axial CBF map slices from a representative volunteer acquired using the long label pCASL FSE stack of spiral readout sequence. The perfusion weighted data for this map was acquired with an in-plane spatial resolution 2.94 mm^2 with a 3mm slice thickness.

6.4.2 Repeated measures factorial model analysis

For the repeated measures factorial model four contrasts were created (Figure 6.4.2):

- INS > PLA
- INS < PLA
- Interaction 1 (LEAN INS > PLA, OW INS < PLA)
- Interaction 2 (LEAN INS < PLA, OW INS > PLA)

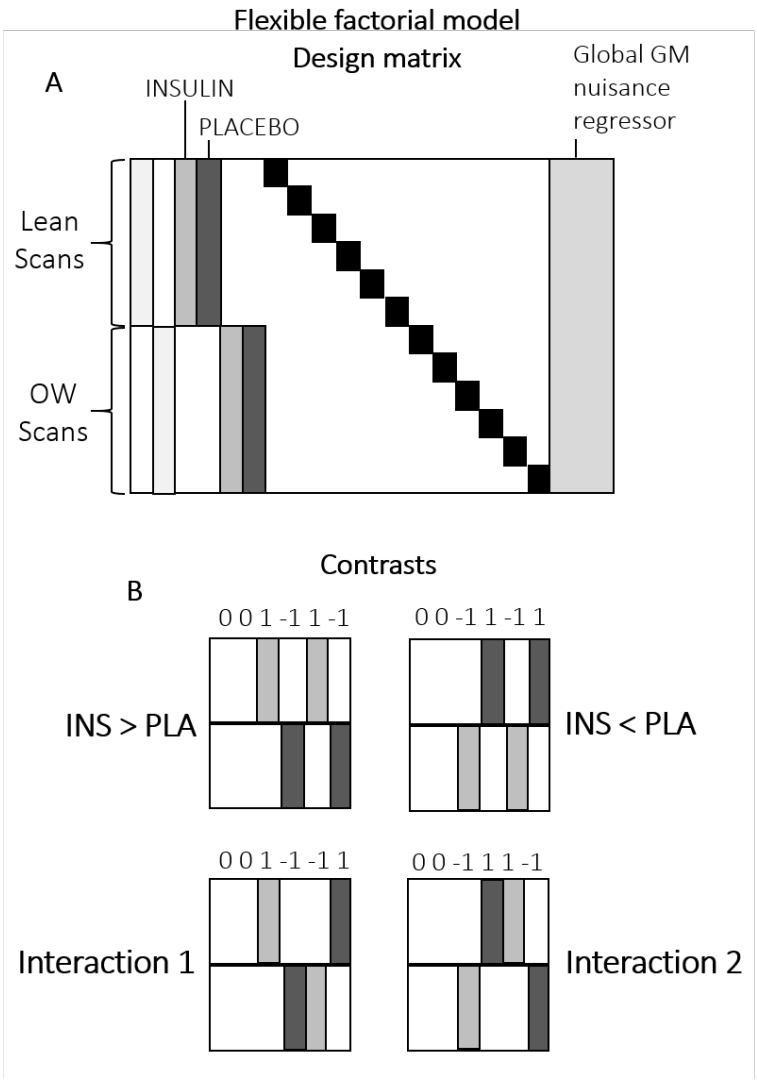

Figure 6.4.2 Repeated measures factorial model design matrix and contrasts. A) The design matrix for the repeated measures factorial model that was implemented for the 2nd level random effects analysis. Three factors (subject, drug and BMI) were used and the mean GM CBF (Global GM) was added as a regressor of no interest. B) Four contrast vectors were tested with this model, shown graphically.

This model was employed at the second level to identify clusters of significant change in regional CBF associated with the main effects of INS on CBF in both the lean and OW groups combined, and to search for any interaction effects or trends between these groups. The main effect of drug (INS > PLA), provided no significant clusters when corrected for multiple comparison (FWE $p < 0.05$ at the cluster level). Similarly, the opposite drug effect contrast, INS < PLA, did not reveal any significant clusters (FWE $p < 0.05$).

Two interaction contrasts were tested to look for any differential responses between lean and OW groups, noted above. Neither of these interaction contrasts revealed any significant clusters, when corrected for multiple comparisons at the whole brain level. However, for interaction 1 (Lean INS > PLA, OW INS < PLA) a trend towards significance was seen from a large cluster (1399 voxels) situated within the right middle temporal gyrus (p = 0.052, FWE-corrected) (MNI co-ordinates: *x = 52, y = -60, z = 6*) Figure 6.4.3.

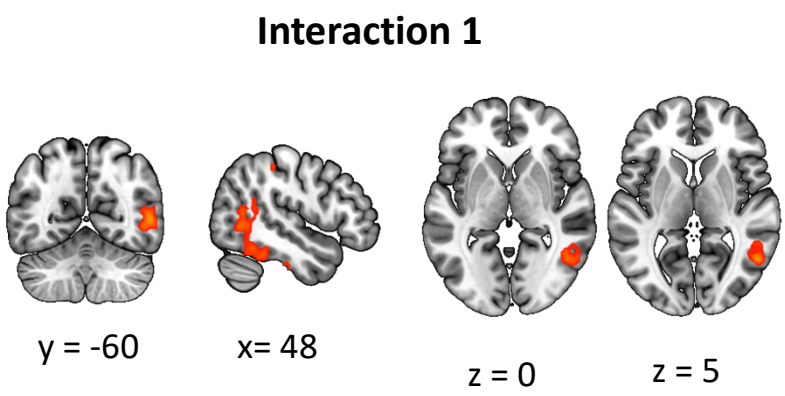

Figure 6.4.3 Interaction 1 trend (p=0.052, FWE) cluster seen within the middle temporal gyrus. Group level statistical parametric t-map overlaid onto an MNI template. Cluster forming threshold p < 0.01, cluster extent threshold 1000 voxels.

Five *a priori* defined anatomical ROIs (see Figure 6.4.4) were used for small volume correction (SVC) analysis on all contrast maps created from the factorial model analysis. All contrast maps were evaluated at a significance cluster forming threshold of $p < 0.01$ prior to SVC . A significance threshold for SVC of $p < 0.01$ was applied to correct for type I error inflation from multiple comparisons.

For main effects of drug defined as "INS > PLA" and "INS < PLA" none of the anatomical bilateral ROIs survived the significant threshold following SVC. For the interaction 1 contrast (see Figure 6.4.2) the bilateral posterior insula showed an interaction effect (p = 0.04) but did not survive Bonferroni correction. The origin of the interaction effect was the left posterior insula at MNI coordinates *x = -38 y = -6 z = -6,* and, *x = -38 y = -14 z = -6,* respectively (p = 0.040 and p = 0.041, t = 3.86, 3.85, respectively). Interaction 2 contrast did not provide any significant changes from SVC, from any of the five anatomical ROIs tested.

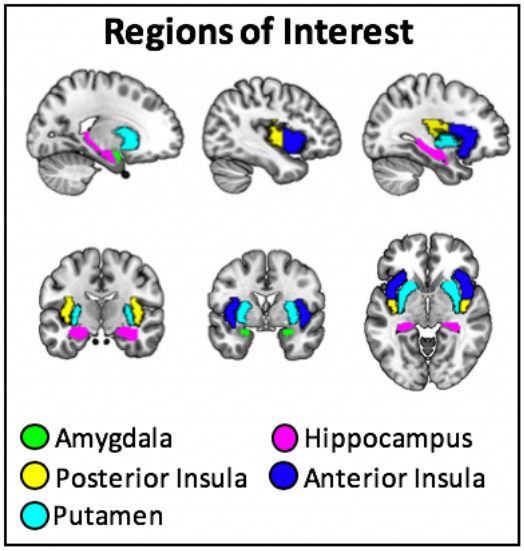

Figure 6.4.4 Regions of interest used for further analysis.

6.4.3 Whole brain, lean and OW voxel wise paired t test analysis

Whole brain results from the repeated measures factorial model showed a trend towards an interaction effect (interaction 1) within the right middle temporal gyrus (p = 0.052, FWE-corrected). As a result of this trend whole brain within-group paired t-tests were conducted post hoc to further interrogate this trend.

For the lean group both INS and PLA CBF images were entered into a whole brain paired t-test in SPM-12. Linear contrasts for drug effects were created (INS > PLA and INS < PLA). Mean GM CBF values were entered into the model, as described before, as a regressor of no interest. An additional paired t-test was created which added an additional regressor to the model. Measures of pre scan insulin sensitivity (HOMA-IR) calculated in chapter 5 (section 5.1.5) were entered into the model as a regressor of no interest for the lean group only.

For the OW group a whole brain paired t-test model was created and linear contrasts for both drug effects were created. Mean GM CBF values were entered in the model, as described before, as a regressor of no interest. Blood concentration covariates were not entered into the model as one participant did not have a complete blood sample profile.

Both paired t-tests had a cluster forming threshold of $p < 0.01$ applied. Clusters that survived a FWE-corrected significance threshold of $p < 0.05$ were reported as significant.

Finally, SVC analysis was employed using the five anatomical ROIs as described previously, with a significant threshold $p > 0.01$ for multiple comparison.

6.4.3.1 Insulin effects on CBF – lean

Whole brain voxel wise paired t-tests for both, INS > PLA and INS < PLA, contrasts revealed no significant changes in CBF at the whole brain level. Additionally, inclusion of HOMA-IR scores as a regressor of no interest did not yield any significant effects. SVC analysis was applied to the two contrasts with and without the additional insulin sensitivity regressor. No significant changes were seen in any of the ROIs tested for the paired t-test model without HOMA-IR scores for either of the contrasts. With HOMA-IR added as a nuisance regressor an effect was seen within the amygdala from the INS < PLA contrast created t map but did not survive the statistical significance threshold for multiple comparison correction (t(11) = 5.02, $p = 0.025$, paired t-test, MNI coordinates *x = 24 y = 2 z = -20*).

6.4.3.2 insulin effects on CBF - overweight

Voxel wise paired t-test for the INS > PLA contrast, revealed no significant CBF differences at the whole brain level. The INS < PLA contrast, however, revealed a large (1848 voxels) significant cluster of significant CBF change ((t14) = 6.00, $p = 0.017$, FWE-corrected, paired t-test). The spatial extent of the cluster was large and comprised three peaks within the left temporal lobe, corresponding to the left hippocampus, posterior insula/putamen and para-hippocampal gyrus (MNI co-ordinates and t-values are presented in Table 6.4.2, thresholded T-maps are presented in Figure 6.4.5).

INS < PLA whole brain results (OW n=15)		
Region	**T-score**	**MNI coordinates**
Left Hippocampus	6.00	-36 -22 -16
Left Posterior Insula/Putamen	5.92	-34 -4 -6
Left Parrahippocampal gyrus	4.72	-38 -18 -26

Table 6.4.2 Significant cluster found from whole brain paired t-test analysis in the OW group (INS < PLA) which comprised of three peak regions.

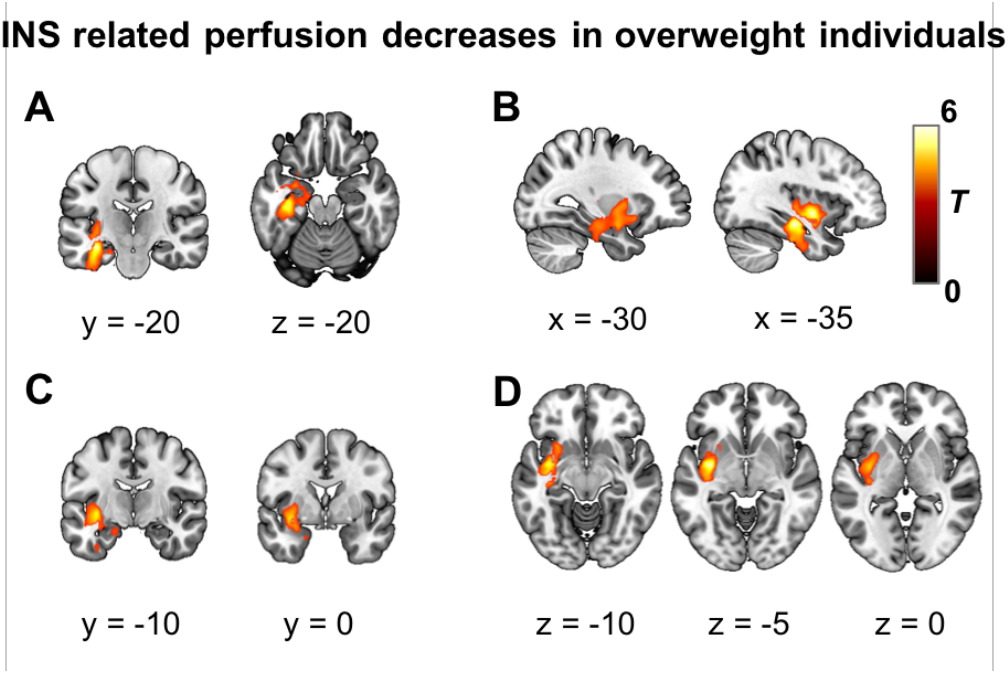

Figure 6.4.5 T maps overlaid onto structural images, illustrating insulin related perfusion decreases in overweight individuals. A) Coronal and axial sections displaying the left hippocampal region t-map cluster associated with an insulin induced decrease in CBF. B) Sagittal sections displaying both the left hippocampal and insula related decreases in CBF. C) Coronal sections showing insulin induced perfusion decreases localised to the left insula and putamen regions. D) Axial sections highlighting left putamen and posterior insula decreases in CBF in response to insulin compared to placebo.

For the contrast, INS < PLA, SVC revealed CBF differences within all five ROI regions (see Table 6.4.3). From these five regional differences in CBF only two were statistically significant when corrected for multiple comparisons, these were the hippocampus and posterior insula, $p = 0.008$ and $p = 0.007$, respectively.

INS < PLA small volume correction results (OW n-15)			
Region	**T-score**	**P value**	**MNI coordinates**
Bilateral Amygdala	3.80	0.036	-30 -2 -18
Bilateral Hippocampus	6.00	**0.008**	-36 -22 -16
Bilateral Putamen	5.10	0.025	-32 -4 -6
Bilateral Anterior Insula	4.88	0.042	-36 -2 -6
Bilateral Posterior Insula	5.77	**0.007**	-36 -4 -6

Table 6.4.3 Table showing the results from small volume correction analysis in the overweight group only. *P* values in **bold** correspond to ROIs that survived multiple comparison correction ($p < 0.01$).

6.4.4 Regional CBF assessment

SVC takes into account the model used at the second level and the regressors of no interest added (for example mean GM CBF and HOMA-IR). As an additive analysis method median CBF values were extracted from the five previously defined anatomical ROIs. These values (one value per subject) were compared across different drug conditions and also across groups to examine regional perfusion differences through creation of individual ROI repeated measure ANOVA models.

6.4.4.1 Insulin effects

No interaction effects were reported from any of the five ROIs tested and no drug effects were reported from any of the ROIs tested either.

6.4.4.2 Group Effects

Significant main group effects in CBF were seen within the insula cortex for both anterior ($F_{(1,26)}$ = 12.53, p = 0.001, ANOVA) and posterior regions ($F_{(1,26)}$ = 8.96, p = 0.004, ANOVA).

For the anterior insula CBF significant differences were reported from planned comparison t-tests following placebo (t(25) = 2.45, p = 0.0022, unpaired t-test) and insulin administration (t(25) = 2.48, p = 0.023, unpaired t-test). In both cases median anterior insula CBF was lower in the lean group in comparison to the overweight group (see Figure 6.4.6).

For the posterior insula, planned comparison t-tests reported significantly greater CBF in the overweight group compared to the lean group following placebo administration only (t(25) = 2.78, p = 0.0023, paired t-test) but not following intranasal insulin administration (see Figure 6.4.6).

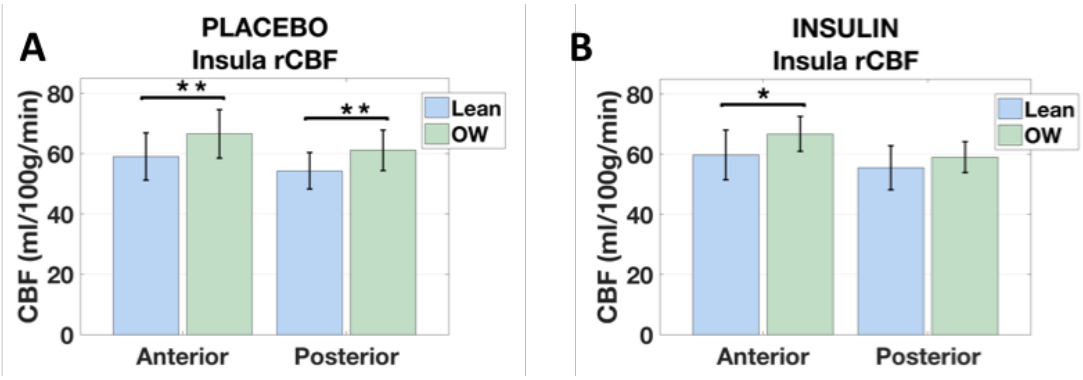

Figure 6.4.6 Regional CBF measures extracted from the insula A) Under placebo conditions both the anterior and posterior insula show increased rCBF in the OW group compared to the lean group. B) Under insulin conditions the anterior insula rCBF is significantly greater in the OW group compared to the lean group. * p < 0.025, ** p < 0.01, average median rCBF values plotted, error bars = SD, lean n=12, OW n=15.

6.4.5 CBF correlations with dietary measures

An assessment of the association between regional changes in CBF in response to INS vs PLA and self-reported saturated fat and sugar intakes were assessed as part of an exploratory correlational analysis.

Within the lean group, % regional CBF changes in response to insulin did not report any associations between any of the intake scores for any of the ROIs.

Within the OW group, the % change in hippocampal and putamen CBF had a strong negative linear correlation with saturated fat score (r = -0.58, p = 0.025 and r = -0.59, p = 0.020, Pearson's correlation coefficient, respectively) (see Figure 6.4.7). Additionally, % CBF changes in response to insulin measured from the hippocampus and putamen showed strong negative correlations with self-reported sugar intake scores (r = -0.58, p = 0.022 and r = -0.57, p = 0.026, Pearson's correlation coefficient, respectively).

No other ROI % change in CBF correlated with fat or sugar intake that survived the correlational coefficient thresholds set.

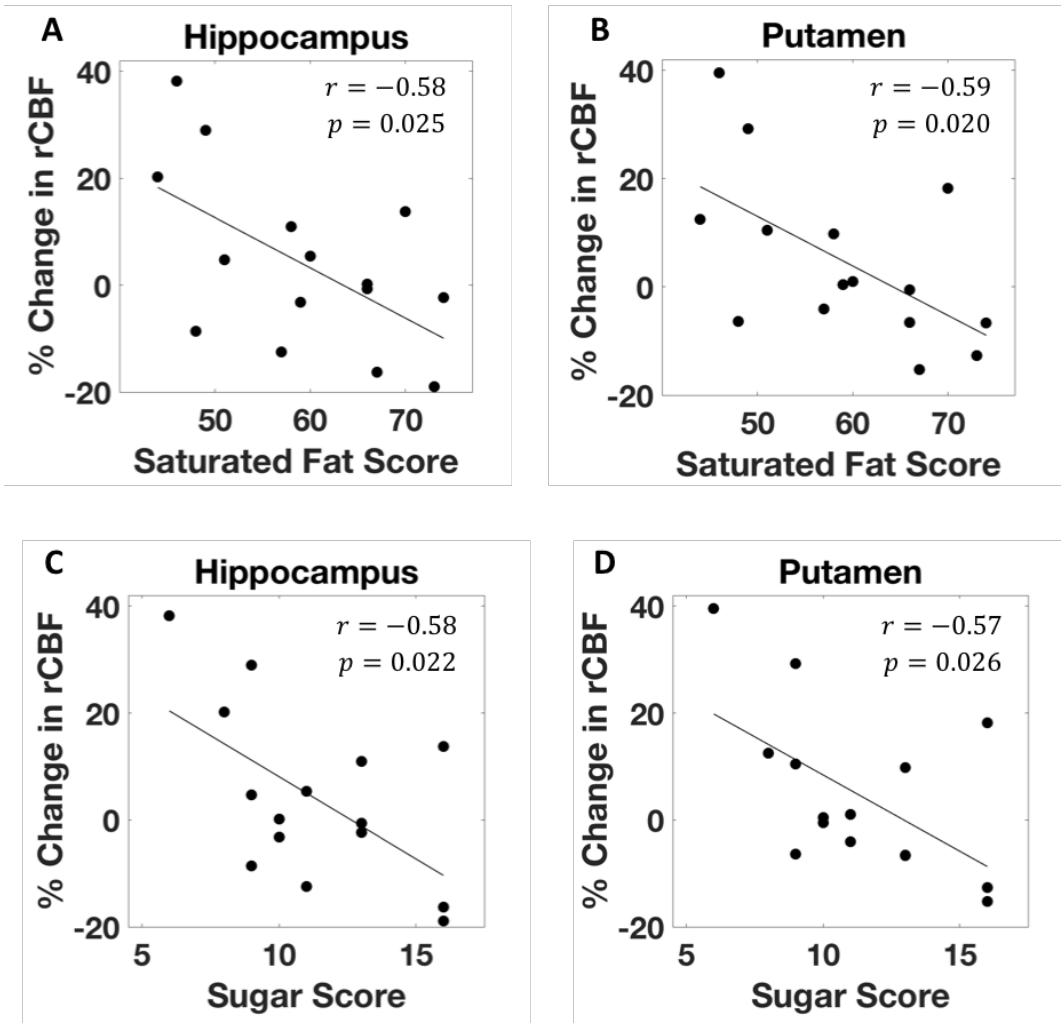

Figure 6.4.7 Association between % change in CBF and saturated fat and sugar scores within the OW group. A) % change in CBF in the hippocampus negatively correlates with saturated fat score (arbitrary units) $y = -0.94x + 59.71$. B) % change in CBF in the putamen is also modulated by saturated fat intake levels, $y = -0.92x + 58.80$. C) % change in CBF within the hippocampus negatively correlates with sugar intake (arbitrary units) $y = -3.07x + 38.84$, D) % change in CBF within the putamen negatively correlates with sugar intake $y = -2.85x + 36.93$, Significance was set to p< 0.05 and rho > 0.4 or < -0.4, n=15 (OW).

6.5 Discussion

The aim of this component of the study was to look at the effects of intranasal insulin administration on resting cerebral perfusion using arterial spin labelling. A 3D pCASL technique was used to acquire quantitative cerebral perfusion maps in a cohort of healthy males who had a range of BMI scores and were stratified into normal weight (lean) and overweight groups. The pCASL sequence implemented in this study adopted a long label duration (3.5s), to increase signal to noise ratio within the perfusion weighted images. To this end the voxel size of the acquired images was decreased to make use of this increase in signal from the larger labelled bolus. All other parameters used were in line with those recommended by the recent ASL consensus paper (Alsop et al. 2014). The sequence was successfully implemented and characterised for use in this pharmacological investigation. This study was able to provide observations of insulin induced decreases in CBF within the hippocampus, which has not been reported previously; as well as decreases in the insula and putamen, in contrast to regional CBF increases within these regions as previously reported (Schilling et al. 2014). Furthermore, this study showed that hippocampal and putamen CBF responses to nasal insulin are associated with self-reported dietary saturated fat intake and sugar intake in overweight subjects.

This study showed that long label pCASL provides sufficient sensitivity to detect changes in cerebral perfusion following intranasal insulin administration. Changes in perfusion were most apparent in the overweight group of individuals examined in this study, in comparison to the lean group who did not display a statistically significant or detectable change in response to intranasal insulin, at the whole brain level, but did show a reduction in the amygdala from small volume correction analysis, albeit did not survive statistical threshold applied for multiple comparisons. In this overweight group intranasal insulin also reduced CBF within the left hippocampus, left posterior insula, left putamen and also the left para-hippocampal gyrus, observed in the voxel-wise whole brain analysis. Post hoc analysis through the use of small volume correction also showed insulin induced CBF reductions within the amygdala and anterior insula, albeit these did not survive more stringent

statistical threshold (Bonferroni multiple comparison correction for the number of ROIs).

As detailed in previous chapters, cerebral perfusion is a surrogate marker for neuronal activity, due to the dynamic relationship between neuronal activity and neuronal vascular supply, known as neuronal coupling (Attwell and Iadecola 2002). Changes in CBF can be observed after administration of compounds that elicit direct effects on the vasculature. For example, caffeine an adenosine receptor (A2A) antagonist, elicits vaso-constrictive actions within the cerebral vasculature, reducing global CBF (Perthen et al. 2008; Liau, Perthen, and Liu 2008; Grichisch et al. 2012). There is compelling evidence to suggest that insulin has little direct vasoactive effect within the CNS (Grichisch et al. 2012) and therefore any perfusion differences seen from this reported experiment can be interpreted as very likely to be driven by changes in regional neuronal activity.

From an anatomical perspective the changes in perfusion presented are relatable to both previous literature from investigations of the effects of centrally acting insulin and also insulin receptor distribution in the brain. The decreases in CBF presented here are in contrast to the limited number of studies reported that have examined the effects of intranasal insulin on cerebral perfusion. These have reported both insulin induced decreases and increases which will be used in reference to the findings reported here (Grichisch et al. 2012; Schilling et al. 2014; Akintola et al. 2017; Kullmann et al. 2013; Kullmann, Heni, Veit, Scheffler, Machann, Haring, et al. 2015; Kullmann et al. 2018).

6.5.1 Hippocampus

The hippocampus is an area with a high density of insulin receptors (Plum, Schubert, and Brüning 2005). Subjects with conditions such as Alzheimer's disease (AD) and type 2 diabetes (T2DM) display central insulin resistance which is associated with cognitive and memory impairments, highlighting the role of central insulin in these cognitive functions and in hippocampal physiology (Ott et al. 2012; Benedict et al. 2004; Craft et al. 2012; Craft et al. 1998).

Whole brain statistical parametric maps in the overweight group displayed a large cluster of insulin induced CBF decreases with a peak in the left hippocampus. Visualisation of these maps shows that the cluster extends beyond the boundaries of the left hippocampus and encompasses regions of the para-hippocampal gyrus. These temporal lobe features are particularly important in memory related activity and formation (Braak et al. 1996). This is the first study that has examined CBF changes within the hippocampal formation following intranasal insulin administration. At the neuron receptor level, understanding how insulin exerts its central effects is becoming better understood. Electrophysiology studies in cultivated rat hippocampal slices and CA1 neurons show that an acute increase in insulin concentration induces recruitment of GABAergic receptors ($GABA_AR$) to these CA1 synaptic formations (Wan et al. 1997). In addition, insulin's effects on hippocampal neurons have previously shown an overall reduction in neuronal excitability through opening $GABA_A$ channels and thus establishes a state similar to tonic inhibition (Jin et al. 2011) within these cells. Furthermore, insulin action within the hippocampus has been shown to hyperpolarise neurons, reducing neuronal firing rate through interaction with potassium channels (O'Malley and Harvey 2007; O'Malley, Shanley, and Harvey 2003). An increase in GABA related activity and reduced firing rate within the hippocampus would arguably be sufficient to produce regional decreases in CBF as shown using pCASL in this report, and hence provide a mechanism for the results presented in the current study.

To complement these cerebral effects, this study also identified a relationship between insulin induced CBF changes within the hippocampus; and both dietary saturated fat and sugar intake, separately, in the overweight group. Saturated fat and sugar intake measured using the 'dietary fat and sugar subscale' questionnaire correlated with insulin related decreases in CBF. The relationship was negatively correlated implying that lower levels of saturated fat and sugar intake are related to greater insulin responses (decreases in CBF) within this overweight group. The modern western diet, characterised by high levels of saturated fats and refined carbohydrates, contributes significantly to weight gain and metabolic disease prevalence (Kanoski et al. 2010; Hu, van Dam, and Liu 2001). Overconsumption of

saturated fat in comparison to poly-unsaturated fat results in higher visceral adipose tissue deposition (Rosqvist et al. 2014). A previous cerebral perfusion imaging study which examined intranasal insulin responses showed that after insulin application a stronger decrease in hypothalamic CBF was witnessed in those individuals with lower levels of visceral adipose tissue (Kullmann, Heni, Veit, Scheffler, Machann, Häring, et al. 2015). High dietary saturated fat intake is associated with impairments in hippocampal memory related functioning (Pasinetti and Eberstein 2008) and an increase in metabolic disorders and incidence of Alzheimer's Disease (Pasinetti and Eberstein 2008). Some reports suggest that the modern western diet impacts blood brain barrier (BBB) integrity and that these memory related impairments are consequential to this process (Persidsky et al. 2006). From this collection of findings and the results reported in this study there is evidence to suggest an association between dietary fat intake and central insulin sensitivity within the hippocampus. Within this overweight cohort the sensitivity to insulin signalling in the hippocampus is decreased in those who consume higher amounts of saturated fat. Decreased hippocampal responsiveness to insulin signalling could be a marker of central insulin resistance that precedes peripheral insulin resistance, although more extensive research would need to be conducted to further explore this finding.

Furthermore, from studies looking at high sugar based diets, an accumulation of evidence has shown that peripheral insulin sensitivity is reduced in response to diets high in refined sugar (Macdonald 2016). A cross sectional study showed that a high fat and high sugar 'western diet' exhibited poor hippocampal-dependent memory function coupled with a reduction in sensitivity to interoceptive signals in humans (Francis and Stevenson 2011). Mice fed on a high fat and high sugar 'western diet' displayed BBB leakages in the hippocampus and dorsal striatum which was associated with poor performance in a learning task compared to chow fed mice (Hargrave et al. 2016). Findings like this support the correlation between increased sugar intake and reduced insulin responsiveness seen within the hippocampus and shed light on the effects of diet composition on the brain prior to severe metabolic dysfunction.

6.5.2 Insula

In the overweight group there was a large cluster of significant CBF change at the boundary between the left putamen and the left posterior insula cortex. A study of intranasal insulin in lean individuals showed a CBF increase in both the bilateral insula and the bilateral putamen (Schilling et al. 2014). The insula is known for its role as a hub for integration of visceral stimuli such as taste and odour, and commonly referred to as the primary gustatory cortex (Rolls 2006). Previous cerebral perfusion studies using ^{15}O-labelled water positron emission tomography (PET) have shown a relationship between hunger state and regional CBF within the insula, hippocampus, para-hippocampal gyrus and putamen (Tataranni et al. 1999). More specifically they showed regional perfusion increases in these areas following long fasting periods (36hrs), much longer than those implemented in this study (Tataranni et al. 1999). The data being reported here show decreases in these areas in response to increased central insulin concentrations. Centrally increased insulin concentrations in the brain has been shown to have anorexigenic effects, reducing food intake acutely and subsequent weight gain over time in mice (Air et al. 2002). Intranasal administration of insulin in humans has been shown to reduce appetite acutely (Jauch-Chara et al. 2012; Benedict et al. 2008). If cerebral blood flow in these limbic regions is closely linked to hunger states then the decreases seen from this ASL imaging study under an intranasal insulin challenge could be as a result of a mild change in appetite or hunger. A trend for an insulin associated change in hunger was seen from hunger questionnaires recorded prior to and after scanning in the overweight group. As described in chapter 4, subjective hunger ratings significantly increased during placebo sessions but there was no difference in hunger ratings pre and post scanning following intranasal insulin administration, suggestive of an appetite blunting response of insulin. To this end, *Tataranni et al.,* also showed that induction of satiety following a calorie dense liquid meal was associated with a selective reduction in perfusion within the insula, hippocampus, para-hippocampal gyrus and putamen (Tataranni et al. 1999). Although the results from the pCASL study being reported here did not show a satiation effect of intranasal insulin there is evidence of a hunger blunting effect seen from the intranasal insulin visits (reported in chapter 5 (see

section 5.1.7). Furthermore, *Tataranni et al* showed that decreases in CBF during satiety correlated with both plasma levels of insulin and plasma free fatty acid levels, which were increased and decreased following liquid meal ingestion, respectively (Tataranni et al. 1999). This is suggestive of modulatory metabolic mechanisms on neuronal activity within the insula region. It can therefore be proposed that insulin acts as a satiety signal, and that following meal consumption pancreatic increases in insulin reach the CNS where they impart an inhibitory effect on further food consumption. Insulin may have a direct effect on the hypothalamus or an indirect effect through its interactions with other hubs within the limbic system and prefrontal cortex and thus intranasal administration of insulin would mimic this effect.

It is also important to discuss the pharmacodynamics of insulin within the insula region, similar to the hippocampal mechanisms mentioned above. The insula boasts a high density of insulin receptors (Werther et al. 1987) and receives neuronal input from both the hypothalamus and amygdala (Allen et al. 1991). Electrophysiology studies have shown that acute insulin application to rat insula pyramidal neurons leads to an increase in repetitive spike firing rate (Takei et al. 2010) in comparison to control neurons. This increase was not however an increase in spontaneous firing but rather insulin had a neuromodulatory effect on neuronal firing. The authors propose that insulin increases neuronal excitability within the insula via sodium channel sensitivity changes and postulate that during times of increased insulin CSF concentrations, such as after eating, this increased firing rate is in response to increased interoception (Takei et al. 2010). Intranasal insulin related increases in the insula have been previously reported using a continuous ASL sequence (Schilling et al. 2014) in lean individuals. That study references *Takei et al.,* in support of the regional perfusion increase seen in the insula. Although the continuous ASL study mentioned and the present study used a similar imaging technique and analysis approach, there are several differences between experimental protocols which may explain the contrasting results. In the current study, a dose of 160IU was used in comparison to the 40IU used by *Schilling et al.* A dose dependent intranasal insulin effect has been identified previously from a multi-modal MR imaging investigation in

humans (Kullmann et al. 2018). CBF decreases within the hypothalamus showed a strong dose dependent effect on CBF with decreases being most prominent following 160IU administration vs placebo (Kullmann et al. 2018). Interestingly, following 40IU administration no significant changes in any of the imaging related measures (CBF or fractional amplitude of low frequency fluctuation) were identified in comparison to placebo. However, highly significant and opposing changes were seen between 40IU and 160IU, suggestive of intranasal insulin not only having a dose dependent effect but a differential dose dependent effect which may explain the opposing effects seen in this current study in comparison to Schilling et al., (Schilling et al. 2014). These differential effects were most prominent in the caudate, a region most commonly involved in dopamine signalling and closely connected to the putamen, often referenced together as the dorsal striatum (Kullmann et al. 2018).

6.5.3 Putamen

Putamen perfusion decreases were seen both at the whole brain level and also when assessed with small volume correction in the overweight group exclusively. Insulin plays a key role in reward behaviour and particularly food related reward (Figlewicz and Benoit 2009). As mentioned previously, the putamen has been shown to exhibit increases in CBF following nasal administration of insulin in humans (Schilling et al. 2014). As mentioned earlier, the results reported here differ in the direction of the perfusion change and could be as a result of the higher dose used in this study (160 IU) (Kullmann et al. 2018). The putamen, similar to the hippocampus, revealed a similar relationship between insulin induced changes in CBF and saturated fat and sugar intake. The association was negatively correlated, such that putamen decreases in CBF in response to insulin were higher in those who consumed less saturated fat and less sugar composed foods. In the absence of a rewarding stimulus, it is hard to make assumptions about how this change in putamen activity would be associated with reward. However, pre-clinical rodent work has shown reduced BBB integrity, more susceptible to leakage, at the level of the striatum in response to a high fat and sugar western diet (Hargrave et al. 2016). Furthermore, given that a high fat diet induces central insulin resistance (Arnold et al. 2014) it is perhaps intuitive

that this correlation between fat intake and IN-INS response exists. One can possibly suggest that the putamen and likewise the hippocampus are particularly susceptible to this high fat induction of central insulin resistance.

6.5.4 Amygdala

From whole brain paired t-tests, both lean and overweight groups showed a trend towards insulin related decreases in amygdala CBF from small volume correction. In both cases the difference was not sufficient to survive multiple comparison correction, but with a larger sample size this insulin associated effect on CBF within the amygdala may become apparent. The amygdala is an insulin receptor dense region and is a major component of the limbic system, commonly involved in fear and anxiety processing (Ohman 2005; Ressler 2010). However, there are several lines of research that support the notion for amygdala involvement with food intake and appetite control (Figlewicz, MacDonald Naleid, and Sipols 2007). Administration of insulin via injection to the amygdala in rats shows an acute decrease in food intake couple with a reduction in appetite (Boghossian et al. 2009). Insulin receptors in the central nucleus of the amygdala (CeA) are abundantly expressed and insulin binding within the CeA selectively increases both the amplitude and frequency of spontaneous inhibitory postsynaptic currents (sIPSCs) (Korol et al. 2018). It could be through this insulin-mediated mechanism in which the decrease in CBF seen in this study was realised. The amygdala is known to be responsive to visual food cues. Several studies have shown that in response to satiation the amygdala shows a decrease in responsiveness to food cue paradigms (Morris and Dolan 2001; Gottfried, O'Doherty, and Dolan 2003). Given that these decreases were seen during sensory manipulation, they might not be directly relatable to this study but highlight an involvement of the amygdala in appetite control and food intake.

6.5.5 Lean vs overweight

From the results reported in this study it is evident that there is a response within the overweight group to IN-INS which is not replicated within the lean/normal weight group. There was very little effect on CBF following intranasal insulin administration in the lean group, and to that extent there was no significant results to report from any of the whole brain analyses performed in the lean group. The failure to see an insulin induced response could be as result of the variability in baseline insulin levels witnessed in this weight group between sessions. Given this, pre-dose HOMA-IR measurements helped to account for some of this variability and highlighted a trend towards an insulin related reduction in CBF within the amygdala from small volume correction analysis.

Pharmacological decreases in CBF during rest are not entirely intuitive in comparison to increases in CBF which can be somewhat explained by an increase in neuronal activity, as a result of the neurovascular coupling phenomena, in the absence of direct effects on cerebral vasculature. Given the CBF differences in this study were selectively observed in the overweight group, it could be argued that this group showed an aberrant or increased CBF in the left hippocampus, insula, putamen and para-hippocampal gyrus. And that in response to insulin this aberrant activity was reduced. Given this study was placebo controlled it offered an opportunity to examine some differences between these two groups under both insulin and placebo conditions. To this extent the ROI extracted values were utilised to evaluate inter-group differences. There were no differences in global grey matter perfusion between groups from either placebo or insulin sessions. At a regional level, resting perfusion data showed CBF differences within both the bilateral posterior and anterior insula within the placebo condition. In both these insula regions, rCBF was higher in the overweight group in comparison to the lean group. Furthermore, following insulin administration the group differences in CBF within the anterior insula remained but were no longer observable in the posterior insula. Food cue tasks have highlighted the insula as a region involved in processing of high calorie visual food cues, and have also illustrated increases in insula BOLD activity in obese

individuals compared to normal weight (Rothemund et al. 2007). Furthermore, pre-meal resting state fMRI-BOLD data also supports an overactive insula in obese individuals vs normal weight individuals (Hogenkamp et al. 2016). The insula, as well as a region involved in gustation is also heavily involved in interoception. Perhaps not surprising is the finding that interoception sensitivity is reduced in overweight and obese individuals compared to normal weight individuals (Herbert and Pollatos 2014). The lack of an observable group difference within the posterior insula following intranasal insulin administration suggest that insulin may act to inhibit the overactivity of the insula in the overweight group. More work will need to be conducted to make more informative inferences from these results.

The results gathered from this interrogation of intranasal insulin's effects on cerebral perfusion has shown that insulin is centrally active in this group of overweight individuals eliciting regional decreases in perfusion. A lack of observable effects within the lean group was surprising given the profound effects seen within the overweight group. We cannot exclude that the lack of effect is possibly due to the variability seen within the baseline blood concentration measures and inclusion of these into the statistical model did help to reveal some insulin related effects but the alternative explanation, that in lean subjects these regions are already optimally active/inactive, remains attractive. These findings pose the question as to whether the regional perfusion observed in the lean group is fully (in)activated during fasting conditions, so the insulin challenge makes no difference, whereas in the overweight group the pathway is active and capable of being deactivated by intranasal insulin, and that this effect is impaired by poor dietary indiscretion.

This is the first time that insulin related changes in CBF have been reported in the hippocampus. The long label sequence implemented in this study was sensitive to demonstrate insulin induced changes within key regions of the brain involved in gustation, memory and reward.

Chapter 7 Taste task paradigm

This chapter will present the results from the taste paradigm that was employed within the SNIFAR protocol. The taste paradigm is a complex functional task that was conducted following the food pictures functional task. Participants were given clear instructions during the screening visit and also again on each scanning morning regarding the paradigm. In an effort to aid the reader the results for this paradigm have been divided into four separate sub-chapters. This first sub-chapter will provide the reader with detailed functional data acquisition parameters and overall paradigm details. The following sub-chapters will reference the specific analytical methods used firstly to, assess these functional data in an effort to best describe the main whole brain effects of the paradigm within each group and treatment, respectively; secondly, to examine whole brain treatment effects and group effects for each component of the paradigm and finally, to assess treatment effects through a thorough interrogation of the data with region of interest analysis and accounting for subjective changes in taste over time. I hypothesise that IN-INS will reduce the rewarding effects of each of the sweet taste stimuli and that these reductions will be greatest in lean individuals in comparison to the overweight group. Furthermore, in response to viewing the cue, I hypothesise that, the overweight will display a hyper-responsivity to these cues in comparison to the lean group, which will be reduced upon IN-INS administration.

7.1 Introduction

Intranasal insulin administration in humans has shown appetite reducing effects. In imaging studies using acute administration, significant reductions in food cue (food image viewing) responsiveness have also been observed (Guthoff et al. 2010). It is well established that there are three systems that interact to modulate energy intake: the homeostatic, hedonic and cognitive pathways (Volkow, Wang, Fowler, et al. 2008; Volkow, Wang, and Baler 2011; Berridge 2009; Berridge and Kringelbach 2008; Higgs 2016; Higgs and Spetter 2018; Higgs et al. 2017). Dysregulation of these systems is thought to be key to the development of obesity, insulin resistance and type 2 diabetes and therefore understanding this dysregulation is of great importance.

The homeostatic system controls energy intake and energy balance in response to metabolic demands and energy store levels in the body (see section 1.7.1). This pathway is regulated largely by peripheral hormones such as leptin, ghrelin, insulin and intestinal peptide YY 3-36 (PYY) that relay metabolic information from the periphery to the hypothalamus which processes and acts on these signals (Lutter and Nestler 2009; Karra, Chandarana, and Batterham 2009). Overproduction or underproduction of appetite inducing and appetite reducing hormones, respectively, has been associated with the weight gain seen in obesity (Goldstone 2006).

Additionally, there is a large body of empirical evidence suggesting that aberrant hedonic responses (supported by its corresponding functional networks) also contribute greatly to the dysregulation of energy intake associated with obesity (Volkow, Wang, and Baler 2011). 'Hedonic feeding', also known as 'non-homeostatic feeding', is characterised by the consumption of palatable food for its potent rewarding effects, as opposed to satisfying the metabolic demands of the body (see section 1.7.2). The hedonic system incorporates regions of the meso-limbic system (amygdala, hippocampus, nucleus accumbens (NAcc)) involved in learning and reward processing, as well as cortical regions (anterior cingulate cortex, orbital

frontal cortex, and insula) involved in motivation, decision making and gustatory processing, respectively (Volkow, Wang, and Baler 2011).

Finally, the cognitive systems involved in appetite control and top down modulation of inhibitory and valuation of food choices is an important and often neglected aspect in this discipline (Higgs 2016) (see section 1.7.3). Particularly, as a large amount of evidence regarding food consumption and the mechanisms that govern this action have been observed in pre-clinical animal models.

Insulin has been shown to be centrally active and a large amount of evidence shows that insulin has effects on both 'homeostatic feeding' and 'hedonic feeding' (Figlewicz and Benoit 2009), with much of this support coming from animal model literature. This investigation therefore seeks to examine the effects of increased central insulin concentrations on hedonic and cognitive brain responsivity to food/liquid stimuli administration in a cohort of normal weight and overweight individuals. This experiment will also probe the anticipatory effects, described as the time immediately before receiving a primary food stimulus, as well as the consummatory response, defined as the response to actual receipt of a primary food stimulus. Anticipation responses to receiving food reward stimuli have been shown to be increased in obese compared to lean individuals (hyper-responsivity) (Burger and Stice 2011b). In contrast, BOLD effects seen from the consummation response to food stimuli are decreased in obese compared to lean (hypo-responsivity) (Stice et al. 2008). Given these observations, some have hypothesised that these differential effects seen in lean and obese individuals are key features of obesity and may contribute to the development of this metabolic disease.

This experiment looks at two discrete responses, anticipation and consummation, for two sweet solutions, one of which contains calories (in the form of sucrose) and the other a non-nutritive artificial sweetener, ('stevia'). The use of non-nutritive sweeteners as replacements for calorie dense sweeteners such as sucrose has increased over the last decade (Anton et al. 2010). Many suggest non-nutritive sweeteners can provide a sweet palatable taste whilst negating the sugar load and

postprandial increase in insulin associated with many energy dense sweeteners. Some suggest that non-nutritive sweeteners may be useful for promotion of weight loss or weight gain prevention (Mattes and Popkin 2009), although this remains largely debated, with limited long term empirical evidence to support the former. Stevia (previously described in section 3.4.7.2), a relatively recent addition to the non-nutritive sweetener market, is thought to have beneficial effects on insulin sensitivity (Chang et al. 2005) and postprandial glucose and insulin levels in comparison to other popular sweeteners and sucrose (Anton et al. 2010). The hedonic effects of stevia however, have yet to be reported and this study sets out to examine the brain response to this non-nutritive sweetener.

7.2 Methods

7.2.1 Participants

Thirty one participants took part in this study. As mentioned in chapter 4, three of these were excluded due to evidence of non-compliance with the fasting protocol. Furthermore, two of the normal weight participants (lean, as stratified by BMI (kg/m^2)), were excluded from this analysis due to technical problems encountered with the scanner and taste dispenser apparatus. As a result, the sample size for this analysis has been reduced to 10 normal weight (BMI = 22.01 ± 1.81 kg/m^2, mean ± SD) and 15 overweight individuals (BMI = 27.76 ± 1.92 kg/m^2).

7.2.2 Taste dispenser setup

The researcher had to enter the scanner room for the setup of this paradigm. The participant was informed to remain as still as possible whilst the researcher positioned the MR compatible taste dispenser for the task. The taste outlet head was positioned into the right hand-side of the participant's mouth between the teeth and cheeks.

The taste paradigm has been described in detail in chapter 3 (see section 3.4.7). The participants were reminded of the details of the paradigm prior to the paradigm commencing by the researcher. The details of the paradigm and the three different trials are shown in Figure 7.2.2 and the fractal cues used for both visits are shown in Figure 7.2.1.

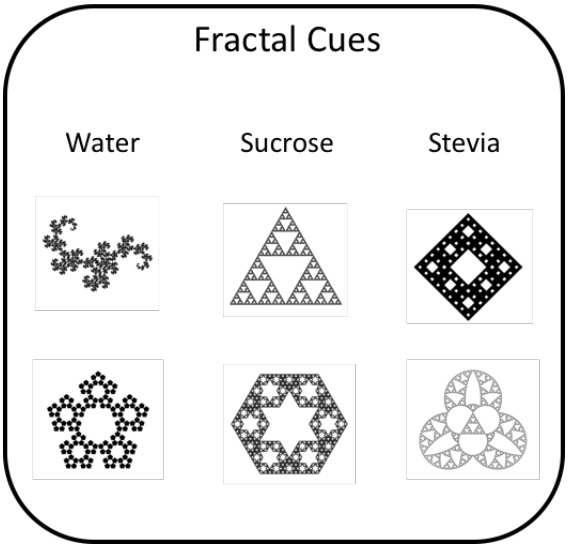

Figure 7.2.1 The fractal cue images that were used for the taste paradigm.

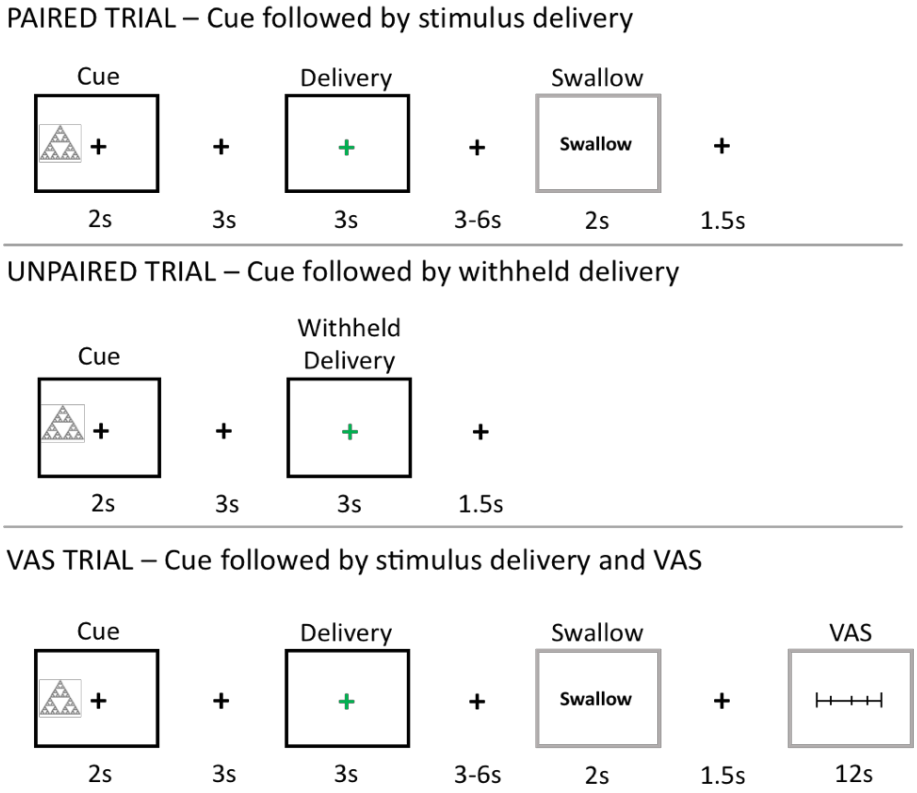

Figure 7.2.2 A diagram to show the three different trial types of the taste paradigm. Black boxes represent the events that are modelled as events of interest (cue, delivery and withheld delivery, respectively). Grey boxes represent events that are modelled in the first level model but are not of interest or taken through to the second level analysis (swallow and VAS scoring periods). A paired trial is the most common trial type and involves the delivery of a 0.5ml bolus/stimulus following visual cue presentation. An unpaired trial does not deliver the 0.5ml bolus as expected, instead nothing is delivered. A VAS trial is when the delivery of the bolus is followed by two VAS questions, this happens for each taste at the very beginning of the first run and at the very end of the second run.

7.2.3 Image acquisition

Whole brain functional images were acquired using a single-shot 2D T2* weighted gradient echo echo-planar imaging (EPI) sequence using parallel imaging (Array coil Spatial Sensitivity Encoding, ASSET). Slices were acquired in a sequential top down direction in the near- axial plane parallel to the anterior-posterior commissure (AC-PC) line (approximately 30°) with the following parameters: TR = 2000 ms, TE = 30 ms, flip angle = 75°, matrix size = 64 x 64, FOV = 211 x 211, slice thickness = 3 mm, slice gap = 0.3 mm, no. of slices = 41, in-plane voxel size = 3.3 x 3.3 mm^2. Four dummy acquisitions were acquired to achieve steady state magnetisation which were discarded, prior to analysis. The total number of imaging volumes was 324 acquired in 10:56 mins for each run. This experiment was conducted, as mentioned earlier, using two consecutive runs.

7.2.4 Image processing

Image processing was performed using a combination of neuroimaging software packages. Firstly, outliers were removed from the time series using 3dDespike (Analysis of Functional Neuroimages (AFNI) (Cox 1996)). To correct for subject motion images were realigned to a base volume using 3dVolreg (AFNI) and all volumes were subsequently corrected for slice timing differences using 3dTshift (AFNI). The base volume was co-registered to the subject specific T1 anatomical image using epi_reg (FSL, FMRIB, version 3.20, University of Oxford, UK, http://www.fmrib.ox.ac.uk/fsl). Normalisation warping parameters for the anatomical to standard MNI template were then applied using Advanced Normalisation Tools (ANTs)(Avants et al. 2011; Avants et al. 2014). Finally, spatial filtering of the images was applied using a full width half maximum (FWHM) gaussian kernel of 8 x 8 x 8 mm using the Statistical Parametric Mapping smoothing function (SPM-12, Wellcome Trust Centre for Neuroimaging, University College London, UK, http://www.fil.ion.ucl.ac.uk/spm). Furthermore, a high-pass temporal filter (filter width of 128s) was also applied as part of the first level model design.

7.2.5 Image analysis

Several different analyses were performed on this dataset. For ease of interpretation and to allow the reader to follow the results found from this task more clearly, this chapter has been broken into the following three sections.

A. Interrogating the functional effects of the taste paradigm

Within this section the reader will be guided through the BOLD response profiles to this complex paradigm for each taste and each event (cue and receipt of taste), respectively. This section will explore these responses through whole brain voxel wise analysis and also small-volume correction (SVC) from *a priori* selected regions of interest (ROIs). Within this section it is also appropriate to look at any group related differences using two sample t-tests at the whole brain level and also to further interrogate these through SVC analysis.

B. Formal comparisons between intranasal insulin and intranasal placebo

Within this section the main effects of intranasal insulin on brain modulation within this paradigm will be assessed. The analysis was conducted using both whole brain analysis and ROI analysis (not small volume correction) using extracted beta estimates. In addition to drug related effects, ROI analysis permitted the exploration of group related (BMI) differences in BOLD response for each taste and condition.

C. Time dependent effects of intranasal insulin: separate analysis of each functional series

Functional data for this paradigm was acquired over two runs. The temporal dynamics associated with this paradigm attributed through learning conditioned stimuli and due to sensitisation effects over time, were acknowledged and therefore analysis was conducted to evaluate any differences between runs. This analysis was conducted entirely through the extraction of ROI data (extracted contrast image estimates).

Each section will have a short introduction followed by the specific data analysis and statistical techniques implemented. This multiple analysis strategy was conducted in an effort to fully interrogate the vast amount of functional data that can be examined using this paradigm.

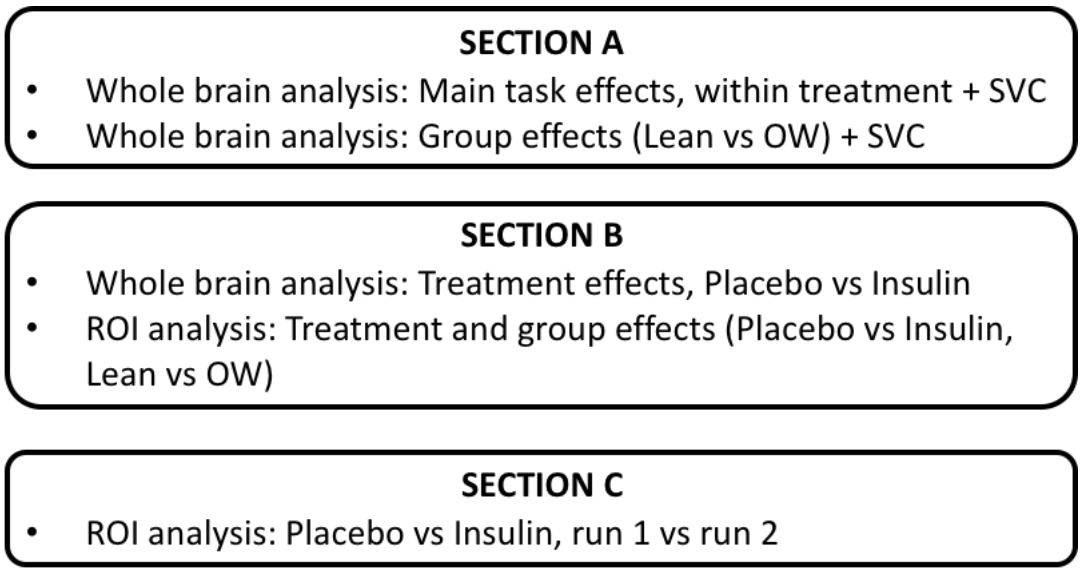

Figure 7.2.3 Diagram to show the structure of the three sections within this chapter

7.3 SECTION A. Interrogating the Functional Effects of the Taste Paradigm

SECTION A

- Whole brain analysis: Main task effects, within treatment + SVC
- Whole brain analysis: Group effects (Lean vs OW) + SVC

Within this subchapter the analysis methods and results used to explore the main task effects within each treatment will be described. Furthermore, with this methodology, the differences between BMI stratified groups within treatment were also interrogated from whole brain analysis.

In addition, the VAS rating analysis and results will be reported.

7.3.1 Analysis of VAS ratings

VAS ratings were collected at the beginning of run 1 and at the end of run 2.
Average run likeness VAS ratings for each taste were entered into a repeated measures ANOVA, with two factors drug (insulin vs saline) and substance (water, sucrose, stevia) for the whole group (n=25), to assess differences in ratings between substances and any drug related effects. Similarly, to assess the effect of drug or substance on sweetness, average run sweetness VAS ratings for each taste were entered a repeated measures ANOVA, with two factors drug and substance for the whole group (n=25). For each ANOVA model there were three taste stimuli, so statistically significant main effects and interaction effects were inspected using a Tukey post hoc test to look for significant comparisons.

Two further repeated measures ANOVA models were created that included just the two substances, sucrose and stevia, to examine drug and substance effects, for likeness and sweetness, which may have been missed from including water in the repeated measures ANOVA model described above. Following a statistically significant interaction effect a post-hoc Tukey test was implemented and following a

main effect of either drug or substance two paired t-tests, within substance and within drug, were conducted, as respective planned comparison tests. All ANOVA main effects and interaction effects were assessed at $p < 0.05$ significance. Tukey tests adjust for multiple comparisons and so were assessed to $p < 0.05$. Planned comparisons were assessed to $p < 0.025$ for multiple planned comparisons (0.05/2).

7.3.2 1st level model designs

For statistical analysis of whole brain data, SPM-12 software was used. A random effects analysis was implemented through creation of 1st level contrast images from a standard general linear model analysis. These contrast images were taken through to the 2nd level to interrogate group level effects.

For this paradigm each trial was modelled as having three conditions of interest:

- Cue presentation
- Stimulus (taste) delivery
- Stimulus delivery withheld

The paradigm was modelled as an event-related task with condition onsets and durations defined from the task. The duration of the cue presentation was set to 2s and both the stimulus delivery and withheld conditions were set to 3s, respectively. Each condition was modelled separately for each of the three taste stimuli, water, sucrose and stevia (see Figure 7.3.1). In addition, the swallowing periods were implicitly modelled with onsets defined when the swallow cue was presented, 2s duration. The swallow cue was modelled as a single condition as opposed to a taste specific swallow condition. Each condition was convolved with SPM's canonical haemodynamic response function (Worsley and Friston 1995). Furthermore, the six 'scan-to-scan' affine head motion parameters produced during motion correction were included as nuisance regressors in the model to account for subject head motion (see Figure 7.3.1.A).

This paradigm was acquired through two functional runs, with identical scanning parameters. Both run 1 and run 2 were combined at the first level (see Figure 7.3.1.B).

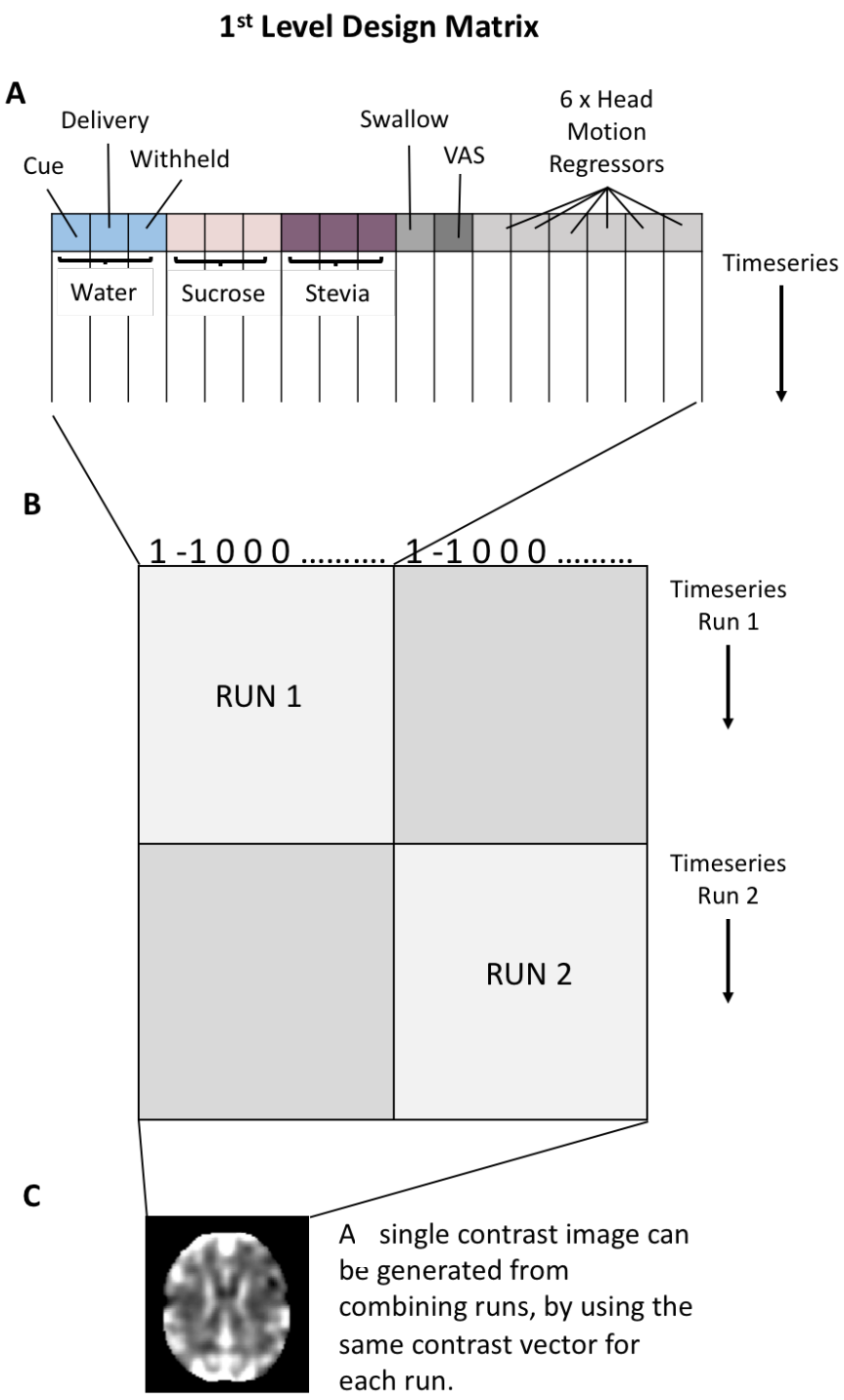

Figure 7.3.1 Diagram showing the first level model design matrix setup and an example output from this general linear model design. A) displays the three events of interest for each taste (water, sucrose and stevia) that were entered into the model along with the swallow, VAS and the six motion regressors included in this model. B) Both runs are combined into the design matrix. An example linear contrast vector applied to both runs is shown at the top of the design matrix. C) From the general linear 1st level model a single contrast image for each of the contrasts is created. An example of a single contrast image is displayed for the contrast vector applied to this model.

Linear contrasts were generated to examine the differences in BOLD response between each taste for the cue presentation. These linear contrasts were replicated for run 1 and run 2 so that a single contrast statistical parametric map was created for each contrast (Figure 7.3.1.C).

7.3.2.1 Cue presentation contrasts:

Contrast images were created by comparing the BOLD response to presentation of the cue assigned to one taste against the cue assigned to another. To be clear, the taste cues refer to the fractal images that are presented prior to the taste being delivered, or withheld, depending on trial type. In all cases the cue is 100% predictive of the taste that will be delivered, but is not predictive of whether the taste will be delivered or withheld. All cue presentation contrasts are shown in Figure 7.3.2.

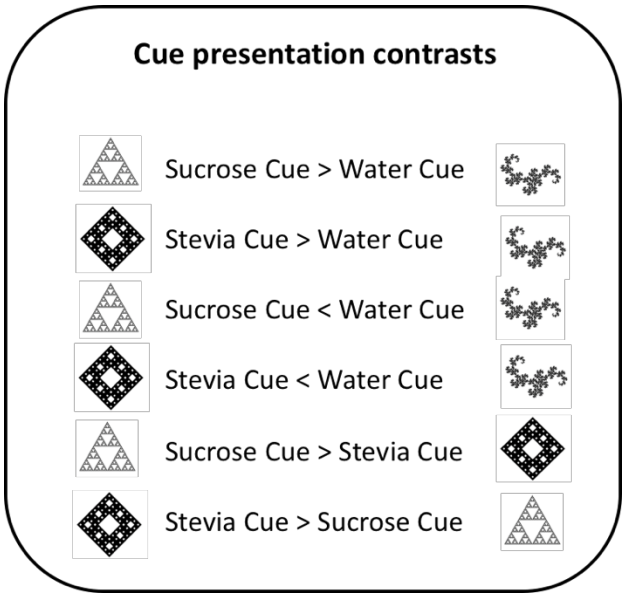

Figure 7.3.2 Cue presentation contrasts created from the 1st level statistical general linear model.

7.3.2.2 Stimulus Receipt contrasts:

Statistical contrast images were generated for the BOLD response to stimulus receipt for each taste, respectively. These images were created by contrasting the delivery event against the delivery withheld event. Contrasts were created independently for each taste and thus three taste dependent contrasts were created from 1st level statistical modelling:

- Water delivery > Water delivery withheld
- Sucrose delivery > Sucrose delivery withheld
- Stevia delivery > Stevia delivery withheld

7.3.3 Group level inferences

Random effects second level models were created to examine:

- Task related effects within each group and treatment; using one sample t-tests.

AND

- Group effects within treatment; using two sample t-tests.

Contrast estimate images for each contrast of interest created at the 1st level were entered into these group level models (lean (n=10) and OW (n=15).

7.3.4 Whole brain analysis

For both the one sample and two sample t-test models, whole brain analysis was carried out using a cluster defining threshold of $p < 0.001$ uncorrected. Significant clusters were deemed significant if $p < 0.05$ following a family wise error (FWE) correction for multiple voxel comparisons, using what SPM defines as the cluster extent threshold.

7.3.5 Small Volume Correction (SVC)

SVC was also employed for this analysis using a priori regions of interest (ROIs). For the cue event, four ROIs were used. These were the anterior cingulate cortex (ACC), the ventro-medial prefrontal cortex (vmPFC), nucleus accumbens (NAcc), and medial orbitofrontal cortex (mOFC). These regions were selected according to previous work which had examined the response to cues associated with conditioned primary rewards (O'Doherty et al. 2002) and have been also linked with insulin-related reward signals (Tiedemann et al. 2017). Bilateral ACC and mOFC masks were designed in SPM-12 using the Functional MRI tool of the Wake Forest University School of Medicine (http://www.ansir.wfubmc.edu) known as 'WFU pick atlas', implemented with automated anatomical labelling. The bilateral NAcc was defined from the Harvard probabilistic brain atlas in FSL (Desikan et al. 2006). The vmPFC was defined from *Manning et al.,* (Manning et al. 2015) as two 10mm radius spheres centred at MNI coordinates, x = 6, y = 30, z= -9 and x = -6, y = 24, z = -21. A multiple comparison correction was used to assess significance from SVC results. For the four comparisons/ROIs tested for BOLD responses during the cue presentation, a *p* value of 0.0125 was used (0.05/4 = 0.0125).

For the delivery phase, four bilateral anatomical regions of interest were used: the caudate + putamen (CPu), NAcc, anterior insula and the amygdala. Both the NAcc and CPu are part of the striatum and are involved in reward processing through dopaminergic neurotransmission (Schultz 2001). The amygdala is a region of the limbic system also involved in response to taste and heavily involved in the gustatory response (Breslin 2013). Finally, the anterior insula is heavily involved in taste processing, commonly referred as the gustatory cortex (Frank, Kullmann, and Veit 2013). The CPu structures and amygdala were defined using the WFU pick atlas tool. The CPu was created by combining the caudate head and body mask with the putamen mask. The anterior insula mask was defined using publicly available cytoarchitecture segmentations (Kurth, Eickhoff, et al. 2010). For four comparisons/ROIs assessed for BOLD responses during the stimulus delivery, a *p* value of 0.0125 was used (0.05/4 = 0.0125) to correct for multiple comparisons.

Regions of interest: Cue contrast	
Region	**Rationale**
Anterior Cingulate Cortex (ACC)	• The ACC appears to play a role in deciding necessary action that would be required to gain a rewarding stimulus and the effort that this would need (Vassena et al. 2014). • Active during the anticipatory phase of rewarding paradigms and is connected to other prefrontal regions active during anticipation (Vassena et al. 2014).
Ventromedial Prefrontal Cortex (vmPFC)	• Heavily involved alongside the mOFC in valuation of a number of different presented rewards (e.g food, money) (Vassena et al. 2014; Rushworth et al. 2011), as well as the prediction of outcomes.
Medial Orbitofrontal Cortex (mOFC)	• The mOFC is a key region involved in anticipation of primary food rewards, and has been shown to be responsive in similar fMRI study designs (O'Doherty et al. 2002).
Nucleus Accumbens (NAcc)	• The NAcc is a dopaminergic region, receiving input from dopaminergic nuclei in the midbrain. The NAcc is involved in encoding primary reward and salience of rewarding stimuli (O'Doherty et al. 2004; Schultz 2001; Schultz, Dayan, and Montague 1997). • Key region in dopaminergic reward theories (Burger and Stice 2011; Stice et al. 2008).
Regions of interest: Delivery contrast	
Region	**Rationale**
Anterior Insula	• The anterior insula is commonly known as the gustatory cortex (Frank, Kullmann, and Veit 2013). • A cortical hub for integrating tastes, odours.
Amygdala	• The amygdala, is limbic region connected with the insula and is also involved in taste processing (Veldhuizen et al. 2011). • Furthermore, a region with dense insulin receptor distribution (Schulingkamp et al. 2000).
Caudate-putamen (CPu)	• Caudate-putamen, region actively involved in food based conditioning fMRI paradigms (O'Doherty et al. 2004). • Both regions shown to be modulated by insulin receptor binding (Stouffer et al. 2015)
Nucleus Accumbens (NAcc)	• The NAcc, similar to the caudate and putamen is recruited in food conditioning paradigms (O'Doherty et al. 2004). • Involved in the initial taste response and modulates reward guided behaviour, and has been shown to be modulated by insulin receptor binding (Stouffer et al. 2015).

Table 7.3.1 Table of regions of interest used for the cue and delivery contrasts.

7.3.6 Correlation analysis with BMI

The effect of BMI on BOLD response for both cue and delivery conditions was assessed using a linear regression correlational analysis. Each ROI, defined above, was used as a mask to extract mean BOLD contrast estimates (from 1st level contrast maps) for each treatment condition (3dmaskave function, AFNI) for every participant. These mean values were regressed against BMI as part of a supplementary exploratory analysis.

Contrast estimates extracted from the ACC, vmPFC, mOFC and NAcc ROIs for the sucrose > water and stevia > water contrasts were correlated against BMI.

For the delivery > delivery withheld contrasts, only the two sweet delivery tastes were interrogated. Extracted values from the insula, amygdala, CPu and NAcc, under insulin and placebo conditions were regressed against BMI and correlations were estimated.

Correlations were estimated using Pearson's correlation coefficient. Correlation coefficients (r) greater than 0.4 or less than -0.4, with an associated p value < 0.05 were reported. Correlation coefficient thresholds were set to only look for 'moderate to very strong' correlations (i.e. 0.4 to 1.0) based on *Evans'* guide to correlational analysis (Evans 1995). However, within this exploratory analysis a total of 32 correlations were tested. Therefore, an adjusted statistical threshold of $p < 0.00156$ (0.05/32) was used to correct for multiple comparison testing and therefore correlations that fulfilled both the coefficient threshold and the p value significance will be reported as significant.

7.4 SECTION A. Results

7.4.1 VAS ratings

7.4.1.1 Likeness ratings

VAS ratings used to assess how much the participants liked each flavour revealed highly significant main effect of substance ($F_{2,24}$ = 45.85, p < 0.001, ANOVA). Post hoc Tukey test showed that following both placebo and insulin administration there was a significant difference between sucrose and water as well as stevia and water (p<0.001, adjusted for multiple comparisons Tukey test) for all within drug sweet taste vs water comparisons (see Figure 7.4.1). In all cases water was the least palatable substance. There were no differences between sucrose and stevia from this ANOVA analysis or drug related effects.

Furthermore, excluding the water scores from the ANOVA model did not reveal any significant differences between sucrose and stevia likeness or any treatment related effects on palatability.

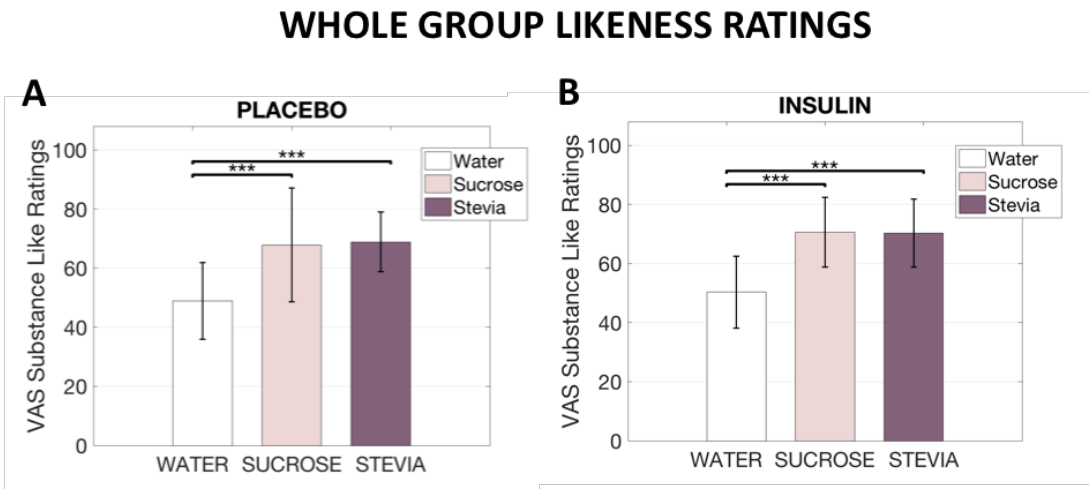

Figure 7.4.1 VAS likeness ratings averaged across runs for each taste and condition. A) VAS ratings recorded during the placebo session show that both sucrose and stevia solutions were 'liked' more in comparison to water. B) similarly, sucrose and stevia solution were liked more than water under insulin conditions. Mean ± SD *** p < 0.001, Tukey test for multiple comparisons, n =25 (whole group).

7.4.1.2 Sweetness ratings

With water included in the ANOVA model there was a significant substance effect ($F_{2,24}$ = 176.01, p < 0.001, ANOVA). Post-hoc analysis showed that across drug conditions both sucrose and stevia were rated sweeter than water (p<0.001, adjusted for multiple comparisons, Tukey test) for all within drug sweet taste vs water comparisons (see Figure 7.4.2).

Exclusion of water related sweetness scores from the ANOVA model provided a significant main effect of substance ($F_{1,24}$ = 4.47, p = 0.037, ANOVA). Within drug paired t-tests showed that sucrose (77.46 ± 10.42) was rated as sweeter than stevia (71.1 ± 13.75) **under insulin conditions only** (t(24) = 2.42, p = 0.023, paired t-test) (Figure 7.4.3).

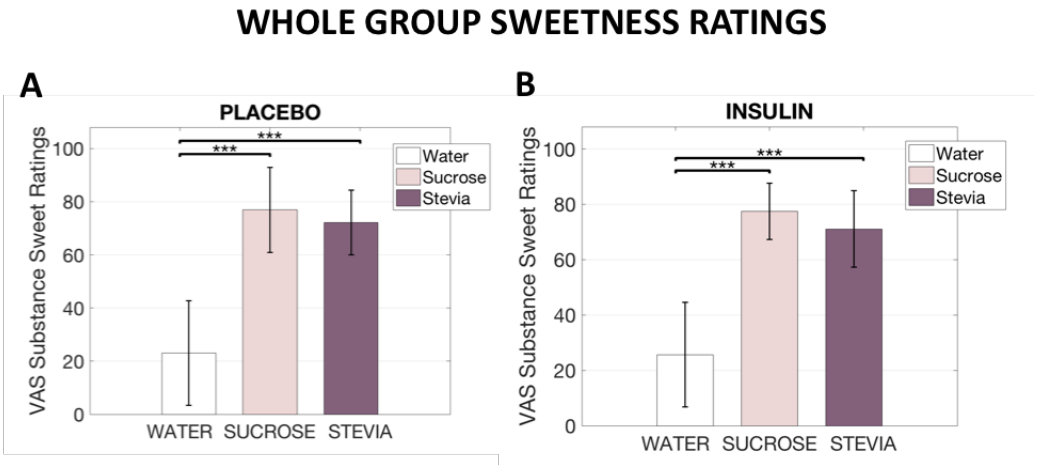

Figure 7.4.2 VAS sweetness ratings averaged across runs for each taste and condition. A) VAS ratings recorded during the placebo session show that both sucrose and stevia solutions were perceived to be sweeter in comparison to water. B) similarly, sucrose and stevia solution were reported as sweeter vs water under insulin conditions. Mean ± SD *** p < 0.001, Tukey test for multiple comparisons, n =25 (whole group).

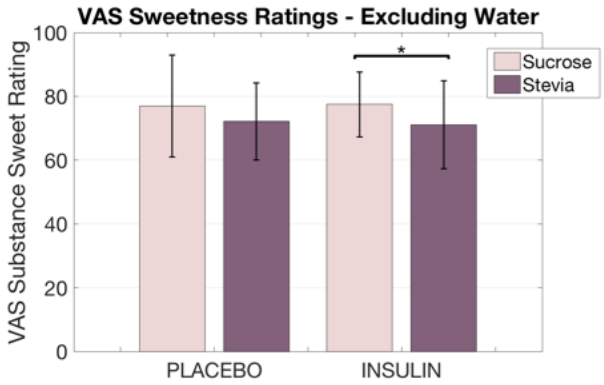

Figure 7.4.3 VAS sweetness ratings show an increase in sweetness for sucrose vs stevia under insulin conditions only. Mean ± SD , * $p < 0.025$ (multiple test correction), paired t-test, n=25 (whole group).

7.4.2 Cue presentation contrasts

Both 'sucrose < water' and 'stevia < water' contrasts revealed no significant clusters following both one sample and two sample t-tests.

7.4.2.1 Sucrose cue > water cue

Within the placebo session, both lean and OW groups showed activation within the visual cortex in response to the sucrose cue compared to the water (control) cue, see Figure 7.4.4 and Table 7.4.1.

There were no further significant regions after applying small volume correction with each bilateral ROI.

Within the insulin session, both groups showed areas of BOLD response within the visual cortex from whole brain analysis (see Figure 7.4.4 and Table 7.4.2). After applying small volume correction (SVC) to the lean group one sample t-test statistic maps there were significant areas of activation within the ACC, NAcc and mOFC. Only the NAcc and mOFC survived correction for multiple ROI comparisons (p = 0.0125)(results are shown in Table 7.4.3).

Furthermore, contrasting lean vs OW revealed no significant differences at the whole brain level or following small volume correction within the **placebo session**. Likewise the **insulin session** did not provide any whole brain differences between lean and OW groups. However, from SVC performed for the 'lean > OW' contrast there was a significant difference within the ACC, which did not survive multiple comparison correction (p = 0.042, t = 4.02).

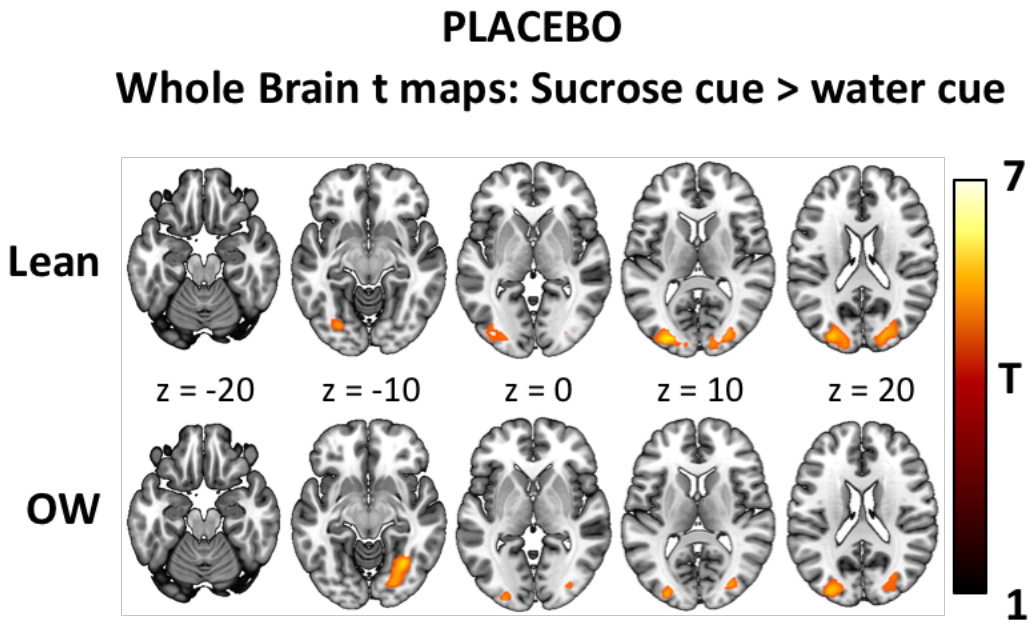

Figure 7.4.4 Statistical T-maps overlaid onto structural MNI images of one sample t-test statistical clusters for the sucrose > water cue contrast, following placebo administration for both lean (n=10) and OW (n=15) individuals. Both groups show statistically significant areas of activation within the occipital cortex, primary visual and visual association areas.

PLACEBO				
Lean Whole Brain Results sucrose > water: CUE				
Region	***p* value (FWE-corrected)**	**Cluster Size**	**T-score**	**MNI coordinates**
Left Visual Cortex	**0.008**	978	5.52 5.10 4.78	-20 -88 14 -30 -90 10 -28 -78 -6
Right Visual Cortex	**0.031**	644	4.99 4.64 4.37	18 -88 16 26 -84 12 24 -82 20
Overweight Whole Brain Results sucrose > water: CUE				
Region	***p* value (FWE-corrected)**	**Cluster Size**	**T-score**	**MNI coordinates**
Right Visual Cortex	**0.014**	824	5.15 4.96 4.54	34 -62 10 28 -74 -6 30 -82 12

Table 7.4.1 Whole brain statistics from one sample t-tests performed in lean (n=10) and OW groups (n=15) following intranasal placebo administration. All p values presented have been corrected for multiple voxel comparisons using a family wise error Bonferroni correction.

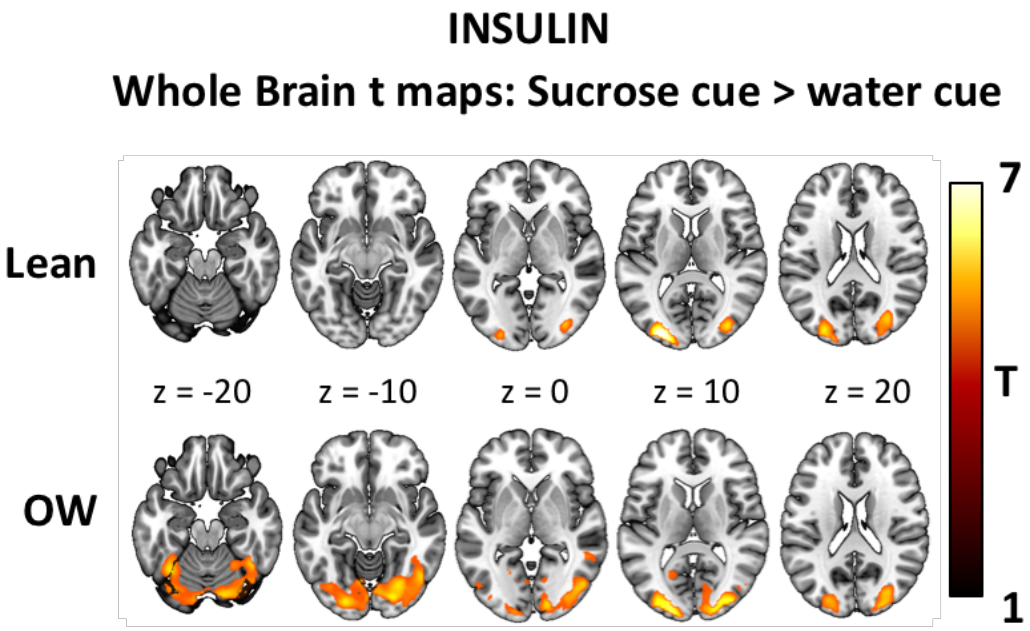

Figure 7.4.5 Statistical T-maps overlaid onto structural MNI images of one sample t-test statistical clusters following insulin administration for both lean (n=10) and OW (n=15) individuals. Both groups show statistically significant areas of activation within the primary visual cortex. OW maps display slightly more widespread activation into the occipital cortex.

INSULIN				
Lean Whole Brain Results sucrose > water: CUE				
Region	***p* value (FWE-corrected)**	**Cluster Size**	**T-score**	**MNI coordinates**
Left Visual Cortex	**0.009**	769	7.39 3.82	-26 -90 8 -20 -90 32
Right Visual Cortex	**0.000**	1454	5.57 5.06 4.61	32 -82 4 30 -80 28 22 -70 60
Overweight Whole Brain Results sucrose > water: CUE				
Region	***p* value (FWE-corrected)**	**Cluster Size**	**T-score**	**MNI coordinates**
Bilateral Visual Cortex	**0.000**	14680	6.36 6.24 6.09	16 -62 60 24 -62 58 -20 -98 -10

Table 7.4.2 Whole brain statistics from one sample t-tests performed in lean (n=10) and OW groups (n=15) following intranasal insulin administration. All p values presented have been corrected for multiple voxel comparisons.

INSULIN		
Lean: SVC Results stevia > water: CUE		
Region	***p* value (FWE-corrected)**	**T-score**
ACC	0.021	3.70
vmPFC	NA	NA
NAcc	**0.012**	3.89
mOFC	**0.010**	4.61

Table 7.4.3 Statistical results from small volume correction (SVC) analysis performed on one sample t-test parametric maps in the lean group. *p* values in bold indicate regions that survived correction for multiple ROI comparison. NA signifies that there were no results for that given region.

7.4.2.2 Stevia cue > water cue

For placebo, the stevia cue > water cue contrast provided significant increases in the BOLD response compared to water within the visual cortex and Crus I region of the cerebellum both within lean and OW groups (see Figure 7.4.6 and Table 7.4.4). Furthermore, the lean group also showed areas of significant activation within the right anterior pre-frontal cortex/lateral OFC.

SVC revealed significant effects which survived multiple comparison correction within all tested ROIs for the lean group. In the OW group the ACC and NAcc survived multiple correction significance but the mOFC did not (Table 7.4.5)

Under placebo conditions, there were no significant group differences from whole brain or SVC analysis.

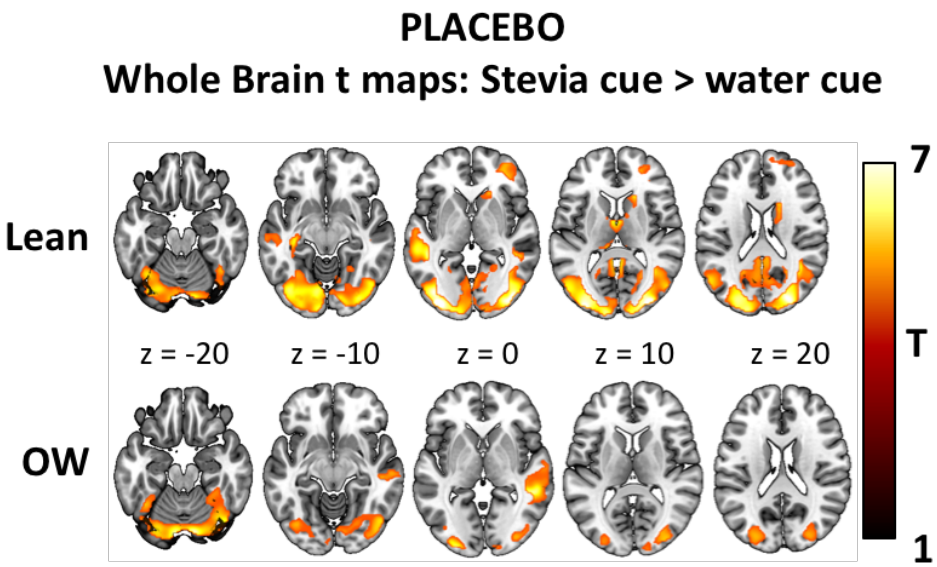

Figure 7.4.6 Statistical T-maps overlaid onto structural MNI images of one sample t-test statistical clusters following placebo administration for both lean (n=10) and OW (n=15) individuals for the stevia cue > water cue contrast. Both groups show regional BOLD related activity within the occipital cortex. The lean group further displayed cluster activation towards the right lateral OFC and left middle temporal gyrus. The OW showed increased BOLD activity within the right middle temporal gyrus in addition to the occipital regions.

PLACEBO				
Lean Whole Brain Results Stevia > water: CUE				
Region	***p* value (FWE-corrected)**	**Cluster Size**	**T-score**	**MNI coordinates**
Right Visual Cortex and Extrastriate Cortex	**0.000**	28639	9.12 5.60 5.57	-36 -90 2 32 -88 14 42 -84 2
Left Middle Temporal Gyrus	**0.007**	769	6.94 5.77 5.52	-46 -38 -2 54 -34 -2 -58 -16 -2
Right Lateral Orbitofrontal Cortex	**0.033**	494	4.47 4.11 3.94	24 48 6 36 44 0 36 54 -2
Overweight Whole Brain Results Stevia > water: CUE				
Region	***p* value (FWE-corrected)**	**Cluster Size**	**T-score**	**MNI coordinates**
Right Visual Cortex and Cerebellum	**0.000**	6124	7.28 6.78 6.44	-26 -82 -28 10 -82 -20 -10 -84 -22
Right Middle Temporal Gyrus	**0.002**	1009	6.59 6.43 5.21	46 -40 0 54 -38 2 44 -30 -4
Left Visual Cortex	**0.009**	719	6.05 4.64	-28 -96 0 -28 -92 16

Table 7.4.4 Whole brain statistics from one sample t-tests performed in lean (n=10) and OW groups (n=15) following intranasal placebo administration for the stevia cue > water cue. All *p* values presented have been corrected for multiple voxel comparisons using a family wise error Bonferroni correction.

PLACEBO		
Lean SVC Results Stevia > water: CUE		
Region	**P value (FWE-corrected)**	**T-score**
ACC	**0.003**	7.10
vmPFC	**0.012**	4.10
NAcc	**0.007**	4.05
mOFC	**0.005**	4.86
Overweight SVC Results Stevia > water: CUE		
Region	**P value (FWE-corrected)**	**T-score**
ACC	**0.001**	5.97
vmPFC	0.020	3.86
NAcc	**0.002**	4.54
mOFC	0.024	4.10

Table 7.4.5 Statistical results from SVC analysis performed on one sample t-test parametric maps in the lean and OW group in response to presentation of the stevia cue > water cue. *p* values in bold indicate regions that survived correction for multiple ROI comparison.

Under insulin conditions, whole brain analysis revealed significant activation in response to the stevia cue vs water cue presentation within the visual cortex, anterior cingulate cortex and precuneus regions in the lean group (see Figure 7.4.7 and Table 7.4.6). In the OW group, BOLD responses seen from this cue presentation contrast were found within the bilateral visual cortex.

For both groups, the ACC showed significant recruitment for the stevia cue but only survived small volume correction in the lean group (p =0.008, t = 4.20) and not in the OW group (p = 0.020, t = 4.35) following **insulin administration**. None of the remaining ROIs tested with SVC showed any statistical effects (data not tabulated). Furthermore, there were no significant group differences seen in the insulin condition for this contrast.

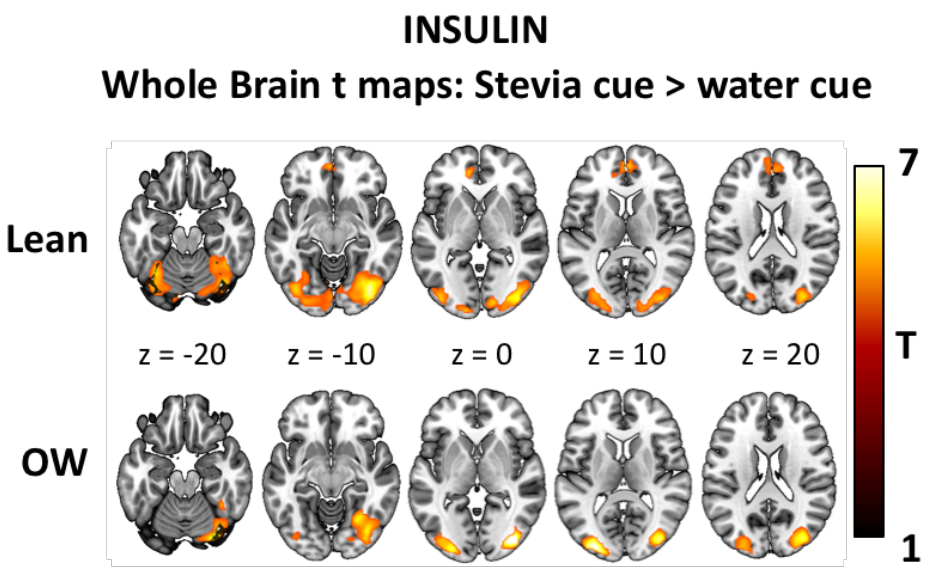

Figure 7.4.7 Statistical T-maps overlaid onto structural MNI images of one sample t-test statistical clusters following insulin administration for both lean (n=10) and OW (n=15) individuals for the stevia cue > water cue contrast. Both groups show regional BOLD related activity within the occipital cortex. The lean group further displayed cluster activation within the ACC.

INSULIN				
Lean Whole Brain Results Stevia > water: CUE				
Region	***p* value (FWE-corrected)**	**Cluster Size**	**T-score**	**MNI coordinates**
Visual Cortex	**0.000**	6856	6.84 5.70 5.51	38 76 -12 38 -86 -2 -40 -72 -16
Anterior Cingulate Cortex	**0.012**	794	4.80 4.62 4.56	2 54 10 -12 44 0 -4 52 -10
Precuneus	**0.003**	1112	4.50 4.28 4.16	18 -52 58 4 -50 54 -6 -58 64
Overweight Whole Brain Results Stevia > water: CUE				
Region	***p* value (FWE-corrected)**	**Cluster Size**	**T-score**	**MNI coordinates**
Left Visual Cortex	**0.002**	1156	7.28 6.78 6.44	-28 -92 8 -34 -82 -4 -24 -90 32
Right Visual Cortex	**0.000**	3010	7.46 5.93 5.90	38 -84 0 32 -80 -22 34 -82 18

Table 7.4.6 Whole brain statistics from one sample t-tests performed in lean (n=10) and OW groups (n=15) following intranasal insulin administration for the stevia cue > water cue. All *p* values presented have been corrected for multiple voxel comparisons using a family wise error Bonferroni correction.

7.4.2.3 Sucrose vs stevia cue

There were no significant changes in BOLD response when contrasting the cue for sucrose vs stevia under both **placebo and insulin conditions** for either sucrose > stevia or stevia < sucrose. Furthermore, there were no group effects for either **placebo or insulin** contrasts assessed at the whole brain level or through SVC.

7.4.3 Stimulus delivery contrasts

7.4.3.1 Water delivery vs water withheld

Under placebo conditions delivery of water stimulus contrasted with when the water bolus was withheld showed increases in the BOLD response within the somatosensory cortex, supplementary motor area and the cerebellum in the lean group (see Figure 7.4.8 and Table 7.4.7). In the OW group significant clusters were produced within somatosensory cortex, frontal operculum as well as in the VI region of the cerebellum (see Figure 7.4.9 and Table 7.4.7)

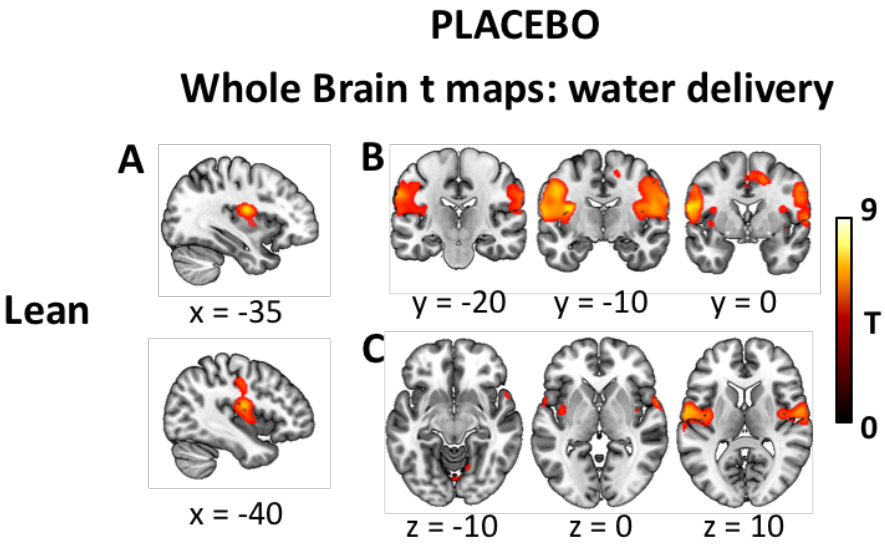

Figure 7.4.8 Whole brain statistical t-map overlaid onto a structural MNI image for the water delivery > water withheld contrast in the lean group (n=10). A) Sagittal sections display significant clusters within left middle insula cortex. B) Coronal sections illustrate significant BOLD related activity within bilateral somatosensory cortical regions, extending to the insula region. C) Axial images highlighting the bilateral insula and somatosensory BOLD increases for this contrast.

SVC analysis was performed and revealed significant BOLD responses contained within the anterior insula, CPu and amygdala for both groups (Table 7.4.8). No group differences were reported in the placebo session.

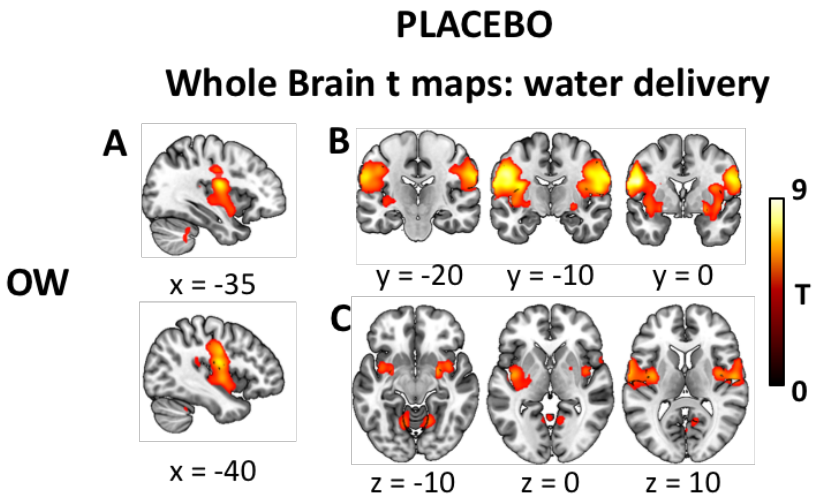

Figure 7.4.9 Whole brain statistical t-map clusters overlaid onto an MNI structural image for the OW group (n=15) from water delivery contrast. A) Sagittal sections and B) coronal sections show insula BOLD related activity. C) Axial images display bilateral insula clusters as well as clusters within the cerebellum.

PLACEBO				
Lean Whole Brain Results Water Delivery > Water Withheld Delivery				
Region	***p* value (FWE-corrected)**	**Cluster Size**	**T-score**	**MNI coordinates**
Left Somatosensory Cortex	**0.000**	3813	7.10 6.62 6.29	-64 -4 18 -36 -10 18 -48 -6 32
Right Somatosensory Cortex	**0.000**	3188	5.71 5.70 5.66	56 -8 22 68 -10 26 54 -8 14
Supplementary Motor Area	**0.024**	719	5.15 4.30 4.06	16 -2 48 -4 8 40 16 14 48
Cerebellum	**0.037**	618	5.12 4.78 4.56	18 -64 -22 12 -86 -34 22 -86 -38
Overweight Whole Brain Results Water Delivery > Water Withheld Delivery				
Region	***p* value (FWE-corrected)**	**Cluster Size**	**T-score**	**MNI coordinates**
Left Somatosensory and Operculum Cortex	**0.000**	5852	8.83 8.49 7.11	-52 0 22 -48 -6 28 -36 -10 18
Right Somatosensory Cortex	**0.000**	4688	7.65 7.59 5.98	62 -14 28 56 -6 24 36 -6 16
Cerebellum Right and Left VI	**0.001**	1987	6.74 6.20 4.28	20 -60 -24 -16 -58 -22 12 -58 -6

Table 7.4.7 Whole brain statistical results from one sample t-tests performed in lean and OW groups for the water delivery contrast. Cluster size = no. of voxels within the significant cluster.

PLACEBO		
Lean SVC Results Water Delivery > Water Withheld Delivery		
Region	***p* value (FWE-corrected)**	**T-score**
Anterior Insula	**0.000**	6.32
Amygdala	**0.002**	4.48
CPu	**0.002**	5.60
NAcc	NA	NA
Overweight SVC Results Water Delivery > Water Withheld Delivery		
Region	***p* value (FWE-corrected)**	**T-score**
Anterior Insula	**0.001**	5.63
Amygdala	**0.002**	3.85
CPu	**0.008**	4.76
NAcc	NA	NA

Table 7.4.8 SVC statistical results in the lean and OW group for the water delivery contrast following placebo administration. BOLD *p* values represent regions that survived multiple ROI correction.

Under insulin conditions, the delivery of water yielded significant increases in the BOLD response within the left and right somatosensory cortex for both lean and overweight groups. In the overweight group these large clusters centred around the somatosensory cortex and also span to cover the operculum cortex on the left side in the OW group (see Figure 7.4.10 and Table 7.4.9).

From lean group statistics, only the anterior insula survived SVC ($p = 0.001$, $t = 5.58$). In the OW group, the anterior insula ($p < 0.000$, $t = 8.53$), CPu ($p = 0.003$, $t = 5.88$) and amygdala ($p = 0.010$, $t = 3.86$) survived SVC (see Table 7.4.10).
No group differences were observed within the insulin session.

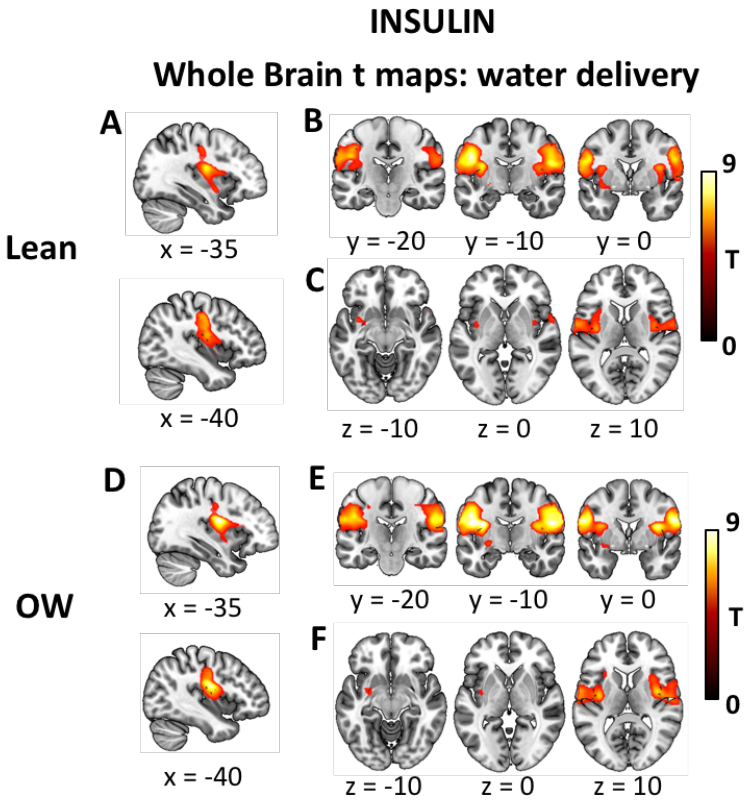

Figure 7.4.10 Lean and OW whole brain t-maps overlaid onto structural images following insulin administration. A) and D) display insula activity. B) and E)coronal sections highlighting bilateral somatosensory and insula significant clustering. C) and F) highlight similar patterns of insula activity in both lean and OW groups for this contrast.

INSULIN				
Lean Whole Brain Results Water Delivery > Water Withheld Delivery				
Region	**P value (FWE-corrected)**	**Cluster Size**	**T-score**	**MNI coordinates**
Left Somatosensory Cortex	**0.000**	3799	9.26 7.09 6.94	-48 -6 30 -34 -10 18 -62 -14 24
Right Somatosensory Cortex	**0.000**	3321	7.96 6.25 6.04	54 -8 22 64 -6 26 36 -4 18
Overweight Whole Brain Results Water Delivery > Water Withheld Delivery				
Region	**P value (FWE-corrected)**	**Cluster Size**	**T-score**	**MNI coordinates**
Left Somatosensory and Operculum Cortex	**0.000**	4418	10.40 9.69 8.92	-46 -12 22 -34 -10 20 -48 -6 28
Right Somatosensory Cortex	**0.000**	4368	9.63 9.34 9.34	64 6 24 56 -2 24 52 -10 22

Table 7.4.9 Whole brain statistical results from one sample t-tests performed in lean and OW groups for the water delivery contrast following insulin administration.

Lean SVC Results Water Delivery > Water Withheld Delivery		
Region	***p* value (FWE-corrected)**	**T-score**
Anterior Insula	**0.001**	5.88
CPu	0.047	4.04
Overweight SVC Results Water Delivery > Water Withheld Delivery		
Region	**P value (FWE-corrected)**	**T-score**
Anterior Insula	**0.000**	8.53
CPu	**0.003**	5.38
Amygdala	**0.010**	3.86

Table 7.4.10 SVC results from the water delivery contrast following intranasal insulin administration, for both lean and OW. BOLD *p* values represent those regions that survived multiple ROI comparison Bonferroni correction.

7.4.3.2 Sucrose delivery vs sucrose withheld

Under placebo conditions, the effect of sucrose solution delivery against withheld showed increases in BOLD response within the left somatosensory cortex in lean individuals. In the OW group there were significant responses in the left and right somatosensory cortex, as well as in the left operculum cortex (see Figure 7.4.11 and Table 7.4.11) .

Within the lean group the anterior insula survived SVC (p = 0.001, t=4.56). Within the OW group the anterior insula (p = 0.001, t = 6.05) and amygdala (p = 0.003, t=4.50) survived SVC analysis (Table 7.4.12).

There were no group differences found within the placebo session.

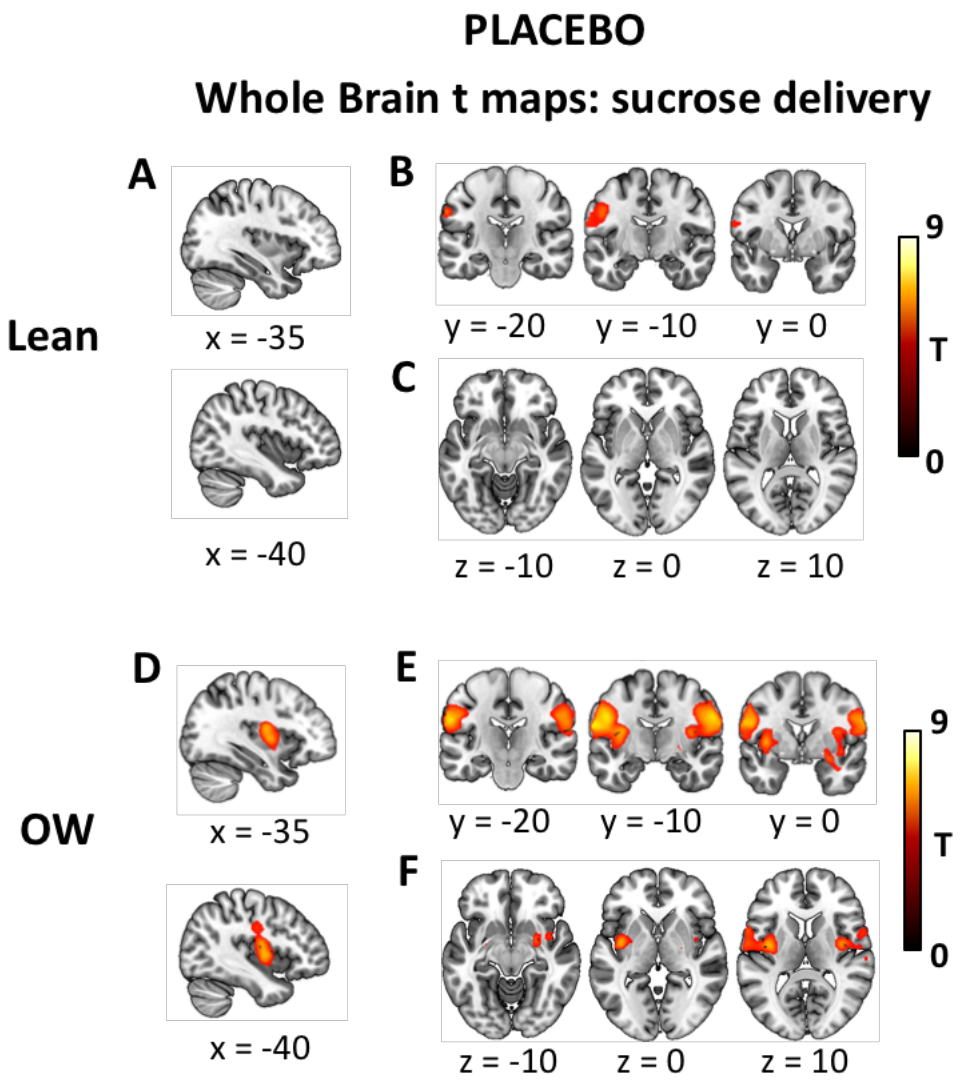

Figure 7.4.11 Statistical t-maps created from one sample t-test overlaid onto structural MNI images for the lean and OW groups following placebo administration for the sucrose delivery > withheld contrast. A) and D) sagittal sections for lean and OW respectively display large BOLD activation clusters within the left insula region for the OW group, with this observation being absent in the lean group. B) and E) coronal sections showing bilateral somatosensory and insula BOLD cluster recruitment in the OW group which is much reduced and lateralised to the left somatosensory cortex in the lean group. C) and F) show axial activation within the insula and regions of the left putamen in the OW group (F) but a lack of BOLD effects seen in the lean group.

PLACEBO				
Lean Whole Brain Results Sucrose Delivery > Sucrose Withheld Delivery				
Region	***p* value (FWE-corrected)**	**Cluster Size**	**T-score**	**MNI coordinates**
Left Somatosensory Cortex	**0.028**	640	5.04 4.85 4.78	-64 -20 34 -50 -8 32 -66 -6 20
Overweight Whole Brain Results Sucrose Delivery > Sucrose Withheld Delivery				
Region	***p* value (FWE-corrected)**	**Cluster Size**	**T-score**	**MNI coordinates**
Left Somatosensory and Operculum Cortex	**0.000**	3541	6.76 6.49 6.41	-62 -10 26 -36 -8 16 -42 -16 -4
Right Somatosensory Cortex	**0.000**	3119	6.41 5.82 4.86	60 -12 30 38 -6 14 40 6 -24

Table 7.4.11 Whole brain statistics produced from one sample t-tests in both the lean and OW groups.

PLACEBO		
Lean SVC Results Sucrose Delivery > Sucrose Withheld Delivery		
Region	***p* value (FWE-corrected)**	**T-score**
Anterior Insula	**0.001**	4.56
Overweight SVC Results Sucrose Delivery > Sucrose Withheld Delivery		
Region	***p* value (FWE-corrected)**	**T-score**
Anterior Insula	**0.001**	6.05
CPu	0.024	3.68
Amygdala	**0.003**	4.50

Table 7.4.12 SVC results for lean and OW groups following placebo administration for the sucrose delivery > withheld contrast. BOLD indicates regions where the *p* value calculated was less than the threshold for multiple ROI comparison.

Following insulin administration, the effect of sucrose solution delivery against withheld delivery, showed increases in BOLD response within the left and right somatosensory cortex in lean individuals. In the OW group there were significant responses in the left and right somatosensory cortex, right anterior insula cortex and also in the left and right cerebellum VI region (see Figure 7.4.12 and Table 7.4.13). Within the lean group the anterior insula ($p < 0.001$, t = 6.51) and CPu ($p = 0.002$, t = 5.53) showed significant changes. Within the OW group the anterior insula ($p = 0.001$, t = 4.61), CPu ($p < 0.000$, t = 6.51) and amygdala ($p = 0.007$, t = 4.01) survived SVC analysis (Table 7.4.14).

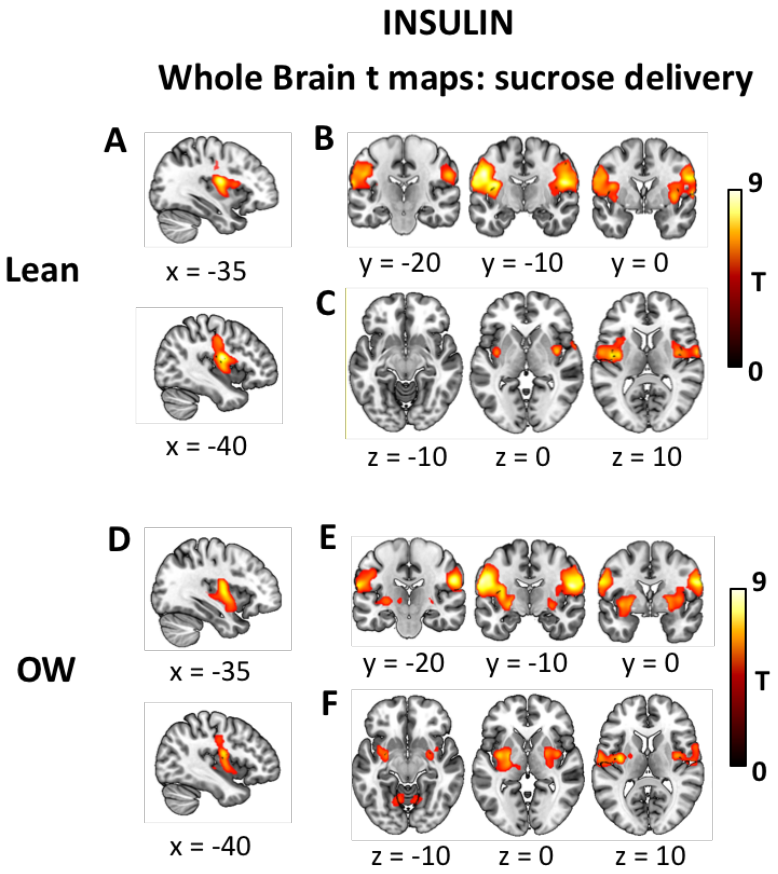

Figure 7.4.12 Whole brain statistical t-maps overlaid onto structural MNI images from one sample t-tests performed in lean and OW groups following insulin administration for the sucrose delivery > withheld contrast. A) and D) show sagittal sections with BOLD clusters within the insula region for lean and OW, respectively. B) and E) are coronal sections that display on both lean and OW groups somatosensory BOLD activity from this contrast. The OW group (E) display greater BOLD responses within subcortical regions around the putamen and caudate region. C) and F) axial slices that illustrate increased BOLD activity within the insula for the lean and OW groups, as well as BOLD responses in the putamen and cerebellum within the OW group.

INSULIN				
Lean Whole Brain Results Sucrose Delivery > Sucrose Withheld Delivery				
Region	***p* value (FWE-corrected)**	**Cluster Size**	**T-score**	**MNI coordinates**
Left Somatosensory Cortex	**0.000**	3951	8.87 8.61 8.39	-50 -10 32 -40 -8 18 -64 -16 20
Right Somatosensory Cortex	**0.000**	3433	8.56 8.53 6.86	52 -10 20 56 -4 26 64 -2 8
Overweight Whole Brain Results Sucrose Delivery > Sucrose Withheld Delivery				
Region	***p* value (FWE-corrected)**	**Cluster Size**	**T-score**	**MNI coordinates**
Right Somatosensory and Operculum Cortex	**0.000**	3554	8.95 8.75 8.54	60 -16 24 54 -10 20 58 -4 24
Left Somatosensory Cortex	**0.000**	3993	8.71 8.67 8.11	-64 -14 20 -60 -8 26 -52 -12 22
Cerebellum VI left and Right	**0.007**	924	6.90 6.33 4.48	18 -60 -20 -16 -62 -18 6 -64 -6

Table 7.4.13 Whole brain statistics from one sample t-tests performed in lean and OW groups following insulin administration.

INSULIN		
Lean SVC Results Sucrose Delivery > Sucrose Withheld Delivery		
Region	***p* value (FWE-corrected)**	**T-score**
Anterior Insula	**0.000**	6.51
CPu	**0.002**	5.53
Overweight SVC Results Sucrose Delivery > Sucrose Withheld Delivery		
Region	***p* value (FWE-corrected)**	**T-score**
Anterior Insula	**0.001**	4.61
CPu	**0.000**	6.51
Amygdala	**0.007**	4.01

Table 7.4.14 SVC results for lean and OW groups following insulin administration for the sucrose delivery > withheld delivery contrast.

There were no group differences seen following insulin administration.

7.4.3.3 Stevia delivery vs stevia withheld

Under placebo conditions, the effect of receiving stevia solution was contrasted against not receiving it. This gave rise to increased BOLD response within the left and right somatosensory cortex in lean individuals. In the OW group there were significant responses in the left and right somatosensory cortex, as well as in the left operculum cortex and left and right cerebellum VI (Figure 7.4.13 and Table 7.4.15).

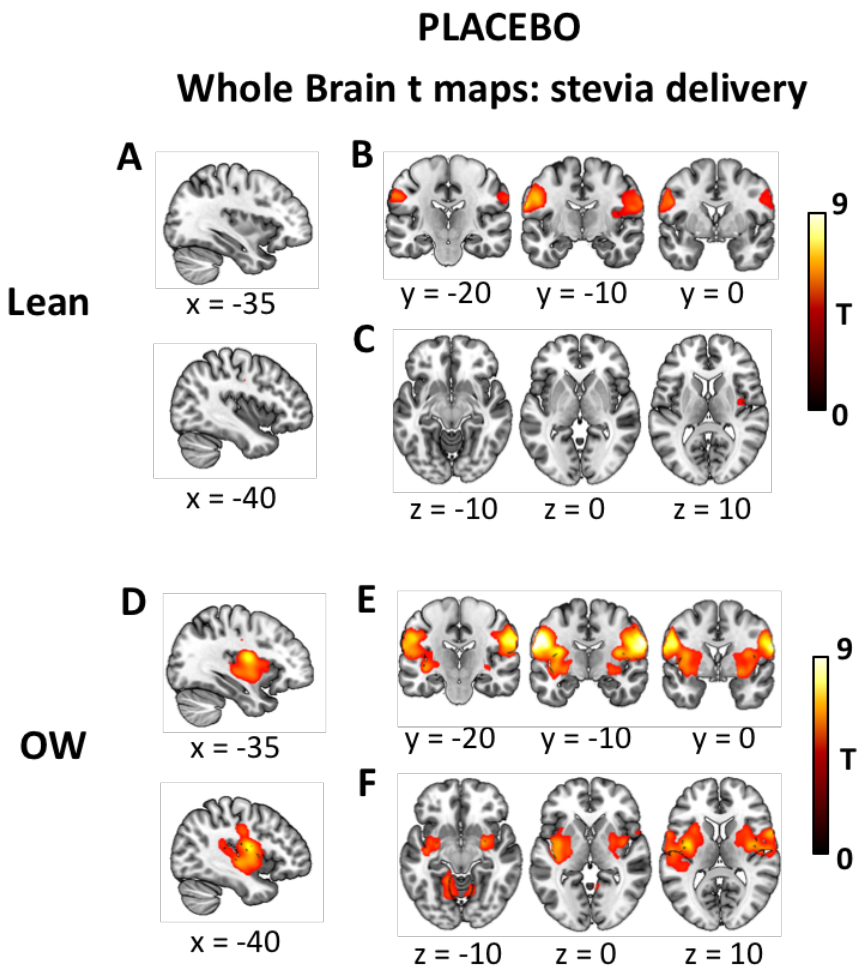

Figure 7.4.13 Whole brain statistical t-maps overlaid onto structural MNI images from one sample t-tests performed in lean and OW groups following placebo administration for the stevia delivery > withheld contrast. A) and D) show sagittal sections for lean and OW, respectively. The OW group show a large degree of BOLD related activity within the insula region which is absent in the lean group. B) and E) are coronal sections that display on both lean and OW groups somatosensory BOLD activity from this contrast. The OW group (E) display greater BOLD responses within subcortical regions around the putamen and caudate region also. C) and F) axial slices that illustrate a reduced response in the right insula of the lean group in comparison to the OW group who show bilateral increased BOLD activity within the insula, as well as BOLD responses in the putamen and cerebellum.

None of the ROIs tested survived SVC in the lean group. Within the OW group the anterior insula ($p < 0.001$, t = 6.32), CPu ($p = 0.002$, t = 65.60) and amygdala ($p = 0.002$, t = 4.48) survived SVC analysis.

There were no group differences within the placebo session for this contrast.

PLACEBO				
Lean Whole Brain Results Stevia Delivery > Stevia Withheld Delivery				
Region	***p* value (FWE-corrected)**	**Cluster Size**	**T-score**	**MNI coordinates**
Left Somatosensory Cortex	**0.002**	1512	7.87 6.86	-64 -8 24 -52 -8 32
Right Somatosensory Cortex	**0.004**	1239	5.39 5.32 5.15	68 -10 24 58 -10 20 66 -14 32
Overweight Whole Brain Results Stevia Delivery > Stevia Withheld Delivery				
Region	***p* value (FWE-corrected)**	**Cluster Size**	**T-score**	**MNI coordinates**
Left Somatosensory Cortex, Insula Cortex	**0.000**	6797	10.18 7.40 5.63	-62 -10 26 -36 -8 16 -42 -16 -4
Right Somatosensory Cortex, Insula Cortex	**0.000**	5534	9.51 8.81 8.76	62 -12 28 66 2 22 58 -8 20
Cerebellum Right and Left VI	**0.001**	1655	7.05 6.71 4.93	18 -60 -22 -16 -62 -18 8 -60 -6

Table 7.4.15 Whole brain results for the stevia delivery condition under placebo conditions for both lean and OW groups.

PLACEBO			
Overweight SVC Results Stevia Delivery > Stevia Withheld Delivery			
Region	***p* value (FWE-corrected)**	**T-score**	**MNI coordinates**
Anterior Insula	**0.000**	6.32	-38 -2 12
CPu	**0.002**	5.60	32 -6 12
Amygdala	**0.002**	4.48	24 -8 -10

Table 7.4.16 SVC results from the OW group under placebo conditions for the stevia delivery > withheld contrast.

Under insulin conditions (Figure 7.4.14 and Table 7.4.17) the effect of stevia solution delivery against withheld delivery, showed increases in BOLD response within the left and right somatosensory cortex, left and right cerebellum VI, left and right lingual gyrus as well as the supplementary motor area in lean individuals. In the OW group there were significant responses in the left and right somatosensory cortex, right operculum cortex, the left and right cerebellum VI region, left and right lingual gyrus and also the right putamen.

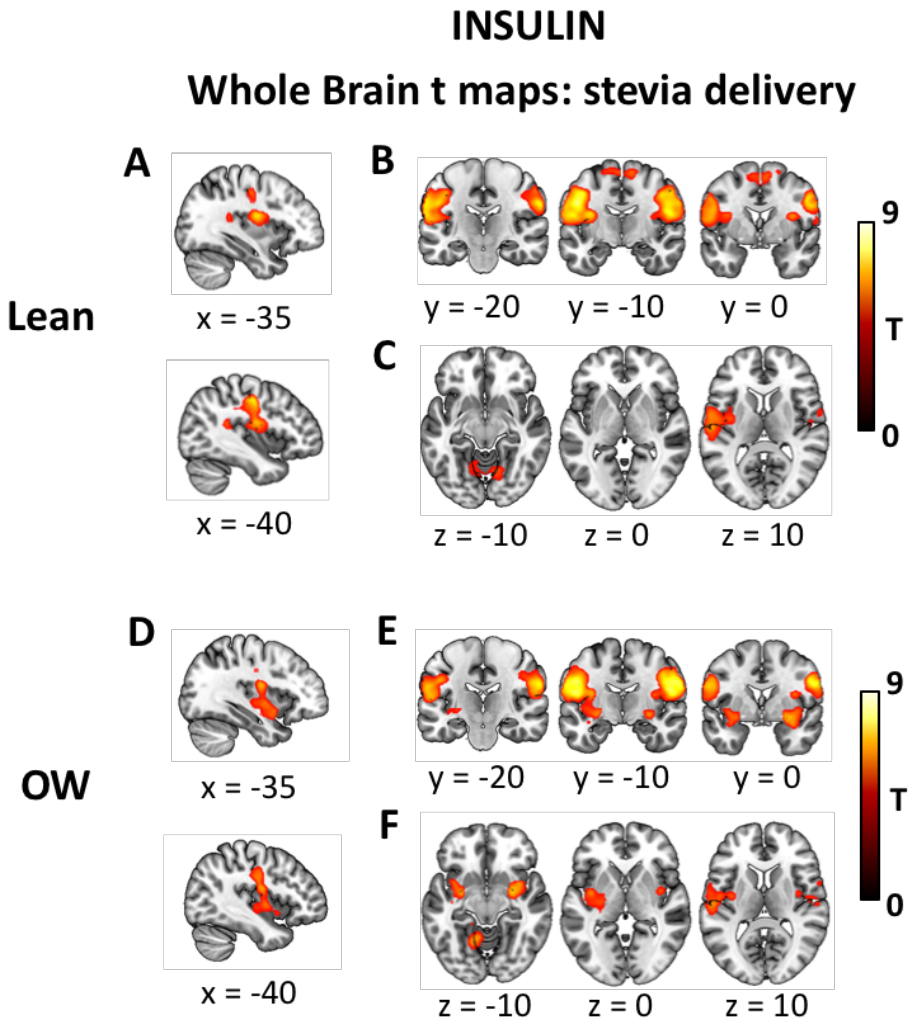

Figure 7.4.14 Whole brain statistical t-maps overlaid onto structural MNI images from one sample t-tests performed in lean and OW groups following insulin administration for the stevia delivery > withheld contrast. A) and D) show sagittal sections for lean and OW, respectively. Both groups show a large degree of BOLD related activity within the insula region and somatosensory cortex. B) and E) are coronal sections that display both lean and OW groups somatosensory BOLD activity from this contrast. The lean group (B) also shows increased BOLD related activity within the supplementary motor cortex. C) and F) axial slices that illustrate a reduced response in the right insula in comparison to the left in both lean and OW groups. Both groups display BOLD related increases in the cerebellum, and the OW (F) group show left and right putamen activity also.

INSULIN				
Lean Whole Brain Results Stevia Delivery > Stevia Withheld Delivery				
Region	***p* value (FWE-corrected)**	**Cluster Size**	**T-score**	**MNI coordinates**
Left Somatosensory Cortex	**0.000**	4314	7.98 7.47 6.93	-48 -8 32 -64 -16 26 -54 -8 18
Right Somatosensory Cortex	**0.000**	2819	7.43 7.40 7.39	50 -2 34 62 -16 32 52 -10 22
Left Lingual Gyrus/ Cerebellum V1	**0.009**	1230	6.11 5.62 4.14	-16 -62 -18 18 -64 -22 -4 -70 -14
Supplementary Motor Area	**0.010**	993	5.10 4.81 4.52	8 -4 62 -4 -6 64 -12 -12 68
Overweight Whole Brain Results Stevia Delivery > Stevia Withheld Delivery				
Region	***p* value (FWE-corrected)**	**Cluster Size**	**T-score**	**MNI coordinates**
Right Somatosensory Cortex	**0.000**	2790	8.70 7.80 7.79	62 -16 28 52 -10 22 56 -6 30
Left Somatosensory Cortex	**0.000**	3757	7.78 7.75 7.16	-52 10 18 -50 -10 30 -62 -14 22
Left Lingual gyrus/ Cerebellum V1	**0.009**	698	6.86 4.39 3.87	-16 -60 -14 -12 -28 -16 30 4 18
Right Putamen	**0.010**	691	6.16 5.56 5.46	18 -64 -22 12 -86 -34 22 -86 -38

Table 7.4.17 Whole brain statistic results from one sample t-tests performed in lean and OW groups under insulin conditions for the stevia delivery > withheld contrast.

Within the lean group the anterior insula (p = 0.002, t = 5.56), CPu (p = 0.003, t = 5.50) and amygdala (p = 0.10, t = 3.95) showed statistically significant changes. Within the OW group the anterior insula (p = 0.002, t = 5.56), CPu (p = 0.001, t = 5.97) and amygdala (p = 0.001, t = 4.96) survived SVC analysis (Table 7.4.18).

There were no group differences seen following insulin administration.

INSULIN		
Lean SVC Results Stevia Delivery > Stevia Withheld Delivery		
Region	**P value (FWE-corrected)**	**T-score**
Anterior Insula	**0.002**	5.56
CPu	**0.003**	5.50
Amygdala	**0.010**	3.95
Overweight SVC Results Stevia Delivery > Stevia Withheld Delivery		
Region	**P value (FWE-corrected)**	**T-score**
Anterior Insula	**0.002**	5.66
CPu	**0.001**	5.97
Amygdala	**0.001**	4.96

Table 7.4.18 SVC results for both lean and OW groups under insulin conditions for the stevia delivery > withheld contrast.

7.4.3.4 Correlation analysis with BMI

An exploratory correlational analysis was performed to examine the relationship between regional BOLD contrast estimates for cue presentation and stimulus delivery contrasts for both insulin and placebo sessions. From this analysis very few regional extractions correlated with BMI. However, a strong negative correlation between BMI and BOLD contrast estimates from the vmPFC during the stevia cue > water cue for the placebo session was observed (t = -4.1, p = 0.0005; r=-0.65, Pearson's) (see Figure 7.4.15). This correlation suggests that as BMI increases, BOLD related activity within the vmPFC upon presentation of the stevia cue decreases. For the same contrast (stevia cue > water cue), but following insulin administration the vmPFC extracted values regressed against BMI provided a negative correlation but did not fulfil the statistical threshold criteria for this analysis (t = -2.0, p = 0.055, r = -0.39, Pearson's, Figure 7.4.16). Finally vmPFC extracted contrast estimate values for

the sucrose > water cue presentation event provided a moderate negative correlation with BMI (t = -2.57, p = 0.017, r = -0.47, Pearson's). This negative correlation, however, did not satisfy the multiple comparison statistical threshold set for this analysis. No other correlations were observed that survived the threshold of significance set for this exploratory correlation analysis.

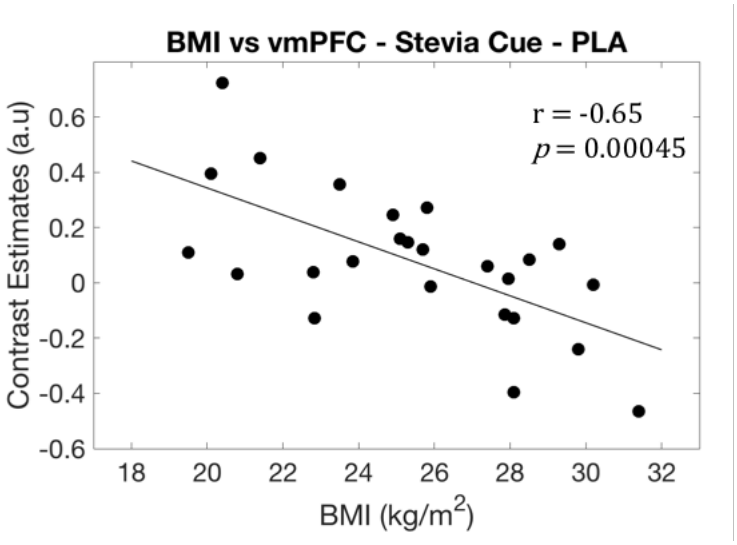

Figure 7.4.15 Plot of BMI vs vmPFC extracted contrast estimates for the stevia > water cue following placebo administration. Each black dot is a single participant (n=25) and the black line is the line of best fit. The plot shows a strong negative correlation and that vmPFC BOLD estimation from this contrast decreases as BMI increases.

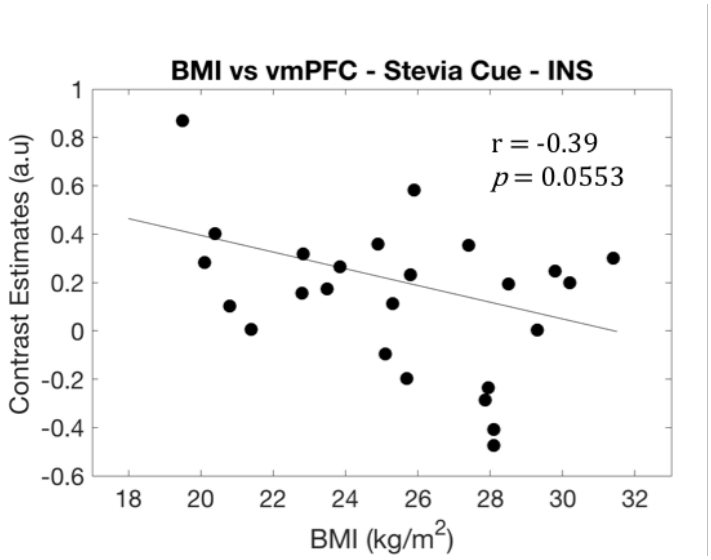

Figure 7.4.16 Plot of BMI vs vmPFC extracted contrast estimates for the stevia > water cue following insulin administration for comparison against. The plot shows an insignificant negative correlation between vmPFC BOLD estimation from this contrast vs BMI.

7.5 SECTION B. Formal Comparisons Between Intranasal Insulin and Intranasal Placebo

SECTION B

- Whole brain analysis: Treatment effects, Placebo vs Insulin
- ROI analysis: Treatment and group effects (Placebo vs Insulin, Lean vs OW)

Within this section the analytical methods used to assess the effects on intranasal insulin compared to intranasal placebo will be detailed along with the results. To explore these drug-related effects a whole brain analysis method and also a ROI based analysis method have been employed.

7.5.1 Whole brain analysis

A random effects repeated measures factorial model was constructed at the second level for each contrast to explore both the main effect of drug and the interaction between drug and group. Following the task related effects the analysis was focused on three cue contrasts of interest: sucrose > water, stevia > water and sucrose > stevia. Furthermore, only the two sweet taste delivery contrasts were assessed: sucrose delivery > sucrose withheld and stevia delivery > stevia withheld. Subject-specific contrast images created from the 1st level model for each condition were entered into a repeated measures factorial model with three factors; subject, drug and group using SPM-12 software. Four t-test comparisons (contrasts) were created from this 2nd level model; two drug effects and two interactions (see below).

1. Insulin > Placebo (Main effect of drug)
2. Insulin < Placebo (Main effect of drug)
3. Lean Insulin > Placebo, OW Insulin < Placebo (Interaction 1)
4. Lean Insulin < Placebo, OW Insulin > Placebo (interaction 2)

The resulting statistical parametric t-maps created from this second level model were set to a cluster forming voxel threshold of $p < 0.001$. Clusters which survived a FWE-correction for multiple comparisons ($p < 0.05$ FWE-corrected) were reported as significant. Following the detection of significant clusters in the interaction contrast a post hoc analysis was performed using two, whole brain, within group paired t-tests. Single linear contrasts within these paired t-tests were created depending on the directionality of the interaction contrast (interaction 1 or 2). Following significant cluster formations seen from main drug effect contrasts, within group whole brain paired t-tests were performed. Cluster forming thresholds and significant cluster thresholds were implemented as described above for all of the post hoc whole brain tests.

7.5.2 ROI analysis

ROI analysis was performed separately to look at regional effects of drug, group and also drug by group interactions. Mean parameter estimates for each contrast were extracted at the subject level within each ROI mask using 3dmaskave (AFNI). ROI mean BOLD estimates for each contrast were entered into a repeated measures Analysis of Variance (ANOVA) factorial model with two factors, drug and group. Significance, for either main effects of drug or group and also drug*group interaction effects was set to $p < 0.05$ from the ANOVA. Following a drug*group interaction a post-hoc Tukey test was used to assess which comparisons were driving the interaction effect. The Tukey post hoc analysis tests every possible comparison and adjusts the outcome accordingly for the number of comparisons. For significant main effects of drug and group, planned comparisons to explore this effect were conducted as post hoc tests. Therefore, a significant main effect of drug or group was interrogated through the use of two t-tests within group (paired) or within drug (unpaired), respectively. Significance for t-tests was set to $p < 0.025$, to correct for the two planned comparisons.

Bilateral ACC, vmPFC, mOFC and NAcc ROI masks, which have been defined and selected *a priori*, were used to assess drug and group differences during cue presentation conditions. Furthermore, for delivery contrasts, the anterior insula, CPu, NAcc and amygdala ROI masks were used to assess both drug and group differences, again previously defined.

7.5.3 Statistical analysis

All statistical analysis was conducted using R (Rstudio). Mean and standard deviation values are used as summary statistics unless stated otherwise.

7.6 SECTION B. Results

In a similar structure to the previous results section (section A), the whole brain and ROI analysis results will be considered for each contrast separately.

7.6.1 Sucrose cue > water cue

No significant drug related BOLD changes were seen assessed at the whole brain level. Furthermore, there were no differential drug related responses from either of the interaction contrasts.

ROI analysis revealed a significant group effect within the ACC ($F_{1,24}$ = 5.07, p = 0.029). Un-paired t-tests showed a greater contrast estimate in the lean group (0.73 ± 0.49 arbitrary units) compared to the OW group (-0.16 ± 0.87) following insulin administration ($t(23)$ = -3.28, p = 0.003) but not in the placebo session ($t(23)$ = -0.44, p = 0.67) (presented in Figure 7.6.1). Furthermore, ANOVA results from the vmPFC revealed a significant drug by group interaction effect ($F_{1,24}$ = 4.64, p = 0.037). Tukey test post-hoc analysis did not produce any significant comparisons, adjusted for multiple comparisons.

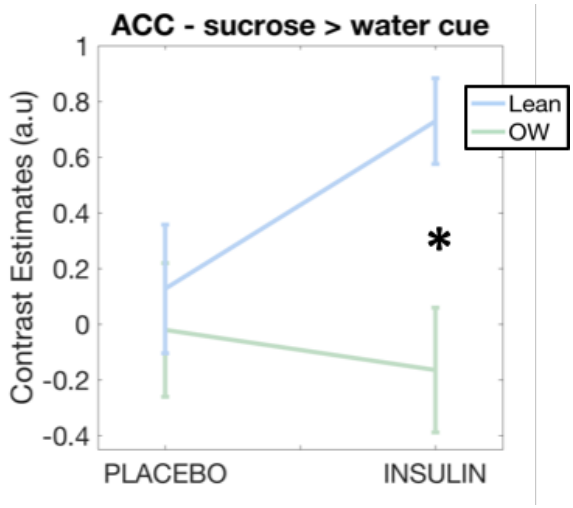

Figure 7.6.1 Plot showing extracted contrast estimates from the ACC in both groups and under both pharmacological conditions for the sugar > water cue contrast. Estimates are from contrast images. Unpaired t-test revealed a significant difference between lean and OW group contrast estimates in this region, exclusively under insulin conditions. Values are mean ± SEM, * $p < 0.025$, corrected for multiple comparisons.

7.6.2 Stevia cue > water cue

Whole brain voxel wise analysis produced no significant insulin effects or interaction effects.

ROI analysis showed a significant group effect within the ACC ($F_{1,24}$ = 5.62, p = 0.022). Unpaired t-test post-hoc analysis showed that this group effect was evident within the insulin session. Lean individuals showed significantly greater ACC BOLD responsiveness (0.88 ± 0.82) compared to OW individuals (0.15 ± 0.24) (t(23) = -2.27, p = 0.036)(Figure 7.6.2.A). Group effects were also seen in the NAcc ($F_{1,24}$ = 4.90, p = 0.032, ANOVA) which was significant within the insulin condition (t(23) = -2.66, p = 0.014, unpaired t-test) as a result of greater contrast estimates in lean individuals vs OW (0.29 ± 0.19 vs 0.06 ± 0.24, respectively) (Figure 7.6.2.C). Furthermore, significant group effects were seen within the vmPFC ($F_{1,24}$ = 12.02, p = 0.0012, ANOVA). Within the vmPFC these group effects (lean > OW) were significant in the placebo condition (lean: 0.23 ± 0.25, OW: 0.02 ± 0.21, t(23) = -2.63, p = 0.018 , unpaired t-test) but did not survive multiple correction for the insulin condition (lean: 0.29 ± 0.24, OW: 0.04 ± 0.31, t(23) = -2.63, p = 0.027, unpaired t-test) (Figure 7.6.2.B).

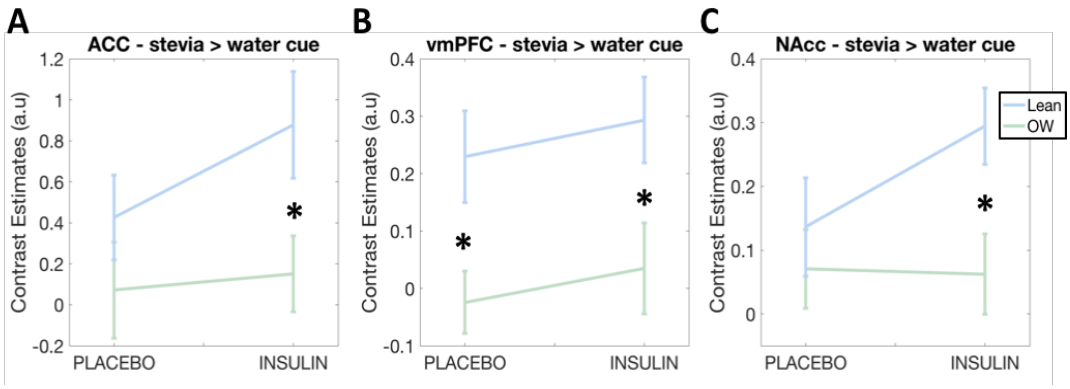

Figure 7.6.2 Plots showing contrast estimates and group differences for the stevia > water cue contrast for the ACC, vmPFC and NAcc. A) ACC - unpaired t-tests show a significant increase in the lean group vs the OW group under insulin conditions. B) vmPFC - unpaired t-tests show differences under both placebo and insulin conditions, and in both cases lean estimates are greater. C) NAcc - under insulin conditions the lean group display greater estimates under insulin conditions compared to the OW group. Values are mean ± SEM, * p < 0.025, corrected for multiple comparisons.

7.6.3 Sucrose cue > stevia cue

No whole brain effects of drug were seen from this contrast. ROI analysis showed a significant group effect within the vmPFC ($F_{1,24}$ = 6.38, p = 0.015), which was only significant within the placebo condition (t(23) = 3.30 , p = 0.005, unpaired t-test), with the OW group displaying a greater response in comparison to the lean group (lean: -0.23 ± 0.29, OW: 0.12 ± 0.19).

7.6.4 Sucrose delivery > sucrose withheld

No drug related effects were produced at the whole brain level or from ROI analysis from the delivery of sucrose solution.

7.6.5 Stevia delivery > stevia withheld

Receipt of stevia solution contrasted with when stevia was withheld, resulted in a significant interaction effect from the whole brain analysis (interaction 1). A single significant cluster was formed over Brodmann area 11 and Brodmann area 32, which covers parts of the mOFC, rostral ACC (rACC) and vmPFC anatomy (see Table 7.6.1 and Figure 7.6.3). To explore this interaction whole brain paired t-tests in lean (Insulin > Placebo) and OW (Insulin < Placebo) groups were computed. Neither of these whole brain comparison revealed any significant clusters that survived FWE correction for multiple comparisons.

ROI analysis did not reveal any other significant drug or group related effects, for any of the ROIs tested.

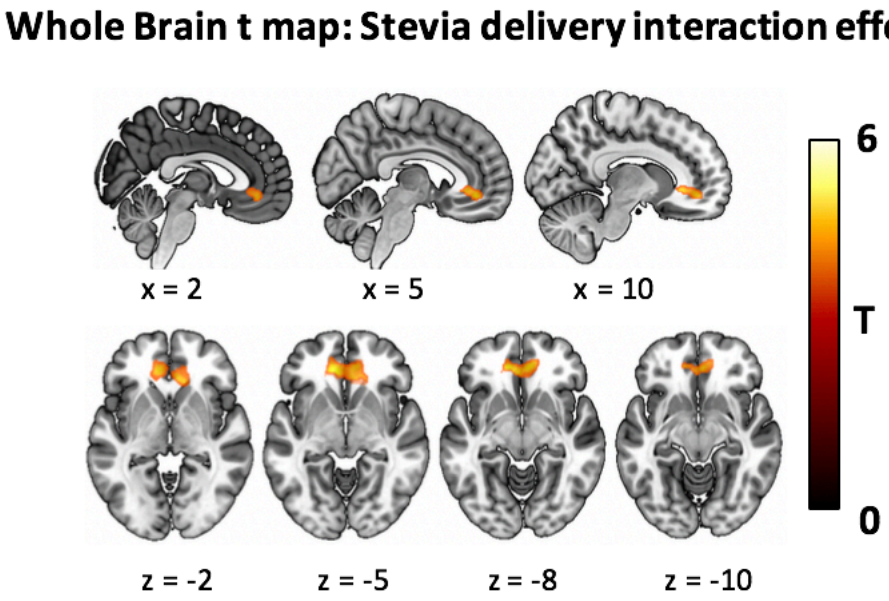

Figure 7.6.3 Whole brain statistical t-map overlaid onto an MNI structural template showing the statistical interaction effect cluster that was observed from a repeated measure whole brain ANOVA model for the stevia delivery > withheld condition. The significant cluster as seen from sagittal and axial slices is located within the region of the rACC and mOFC. This T-map has been cluster corrected using FWE threshold of $p < 0.05$.

Whole Brain Results Stevia delivery > Stevia withheld Interaction (L I > P OW I < P)				
Region	***p* value (FWE-corrected)**	**Cluster Size**	**T-score**	**MNI coordinates**
mOFC and rACC	**0.034**	550	5.03	-12 40 -6 14 30 -4 6 42 -8

Table 7.6.1 Whole brain statistic results from the interaction effect observed from the repeated measures ANOVA analysis conducted for the stevia delivery > withheld contrast. A significant cluster was identified following Bonferroni correction for multiple comparisons. Cluster size refers to the number of voxels within this significant cluster. Lean (n=10), OW (n=15).

To aid the interpretation of this result, the significant cluster seen in Figure 7.6.3 was used as a mask to extract contrast estimates from all participants under both placebo and insulin conditions for the stevia delivery contrast. The contrast estimates for each group (plotted as the mean) under both pharmacological conditions were plotted in Figure 7.6.4. These values are only used for observational purposes and no further statistical analysis was made on these extracted values. The plot in Figure 7.6.4 does display this interaction effect very clearly as the lean activity, measured via contrast image estimates, increases in response to insulin, whereas the OW group show a decrease in response to insulin.

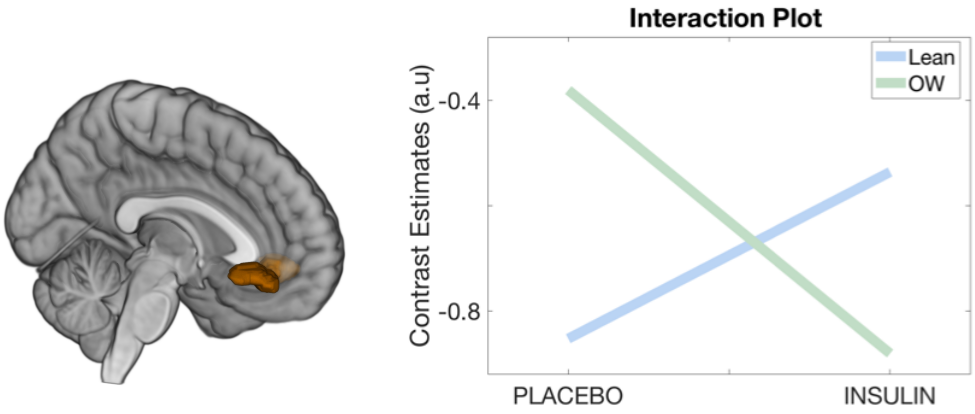

Figure 7.6.4 Sagittal view from a 3D rendered image showing the location of a cluster that survived the statistical significance threshold for the stevia delivery contrast. Plotted are the contrast estimates extracted from this cluster for both lean and OW groups for each treatment.

7.7 SECTION C. Time Dependent Effects of Intranasal Insulin: Separate Analysis of Each Functional Run

SECTION C

- ROI analysis: Placebo vs Insulin, run 1 vs run 2

The functional data collected for this paradigm were acquired over two runs. The previous analysis of this dataset has been conducted using both of these runs combined into a single 1st level model. The effects seen from the previous analysis are valid, however, it is necessary to address and explore the effects that might be seen across runs or from the individual executions of the paradigm. This paradigm was designed in a way that required the participant to learn the relationship between a visual cue and presentation of a taste stimulus. Previous work using predictive learning and temporal difference paradigms have shown that dopaminergic responsiveness shifts from the presentation of the reward stimulus to the cue presentation, once learnt (Gottfried, O'Doherty, and Dolan 2003; O'Doherty et al. 2003; O'Doherty et al. 2002). This shift has also been shown from fMRI studies, which demonstrate the BOLD response shifts from the stimulus presentation to stimulus cue, once learnt (O'Doherty et al. 2003), although not as clearly as that from single cell recordings in primates (Schultz 1998). Furthermore, the participants are presented with repeated taste stimuli which will likely to lead to either habituation and desensitisation effects within the primary taste receptors of the tongue (Li et al. 2002). Under these considerations, analysing the effect of each run is appropriate and permits a more thorough exploration of this functional data set.

7.7.1 VAS ratings

Subjective ratings of likeness and sweetness for sucrose and stevia were evaluated separately for differences between runs using paired t-tests within drug for the whole cohort (n=25). These paired comparisons were conducted within treatment. Within group comparisons were made to explore differences between the sweetness and likeness of sucrose and stevia across runs. A 2 x 2 within drug ANOVA was created to look at the effects of substance and run for ratings of likeness and sweetness. Main effects of run or substance were explored further with planned comparison t-tests and interactions using Tukey tests, respectively. Planned comparisons for main effect of run employed two within substance paired t-tests, for example sucrose likeness run 1 vs run 2, whereas planned comparisons for main effect of substance employed two within run paired t-tests, for example sucrose likeness run 1 vs stevia likeness run 1.

All planned comparisons were deemed significant if $p < 0.025$, adjusted for two comparison tests. Tukey tests were judged to $p < 0.05$ statistical threshold as this test automatically adjusts for multiple comparisons.

7.7.2 1st level model design

To assess BOLD related effects of both run and drug, two separate 1st level models were created in SPM-12; one for the first run and one for the second run. As before 1st level models were modelled with nine regressors of interest (cue, taste delivery and taste withheld for each taste), a swallow cue regressor (participant visually instructed to swallow) and also a VAS regressor. Six additional head motion regressors, saved following motion correction during pre-processing, were entered into the model Figure 7.7.1. For each run, there were 324 whole brain EPI images. Linear contrast images were created at the first level . Three contrasts were created for the cue presentation event: sucrose > water, stevia > water and sucrose > stevia. Two contrasts were created for the delivery minus withheld event for each sucrose and stevia (sucrose delivery > withheld and stevia delivery > withheld).

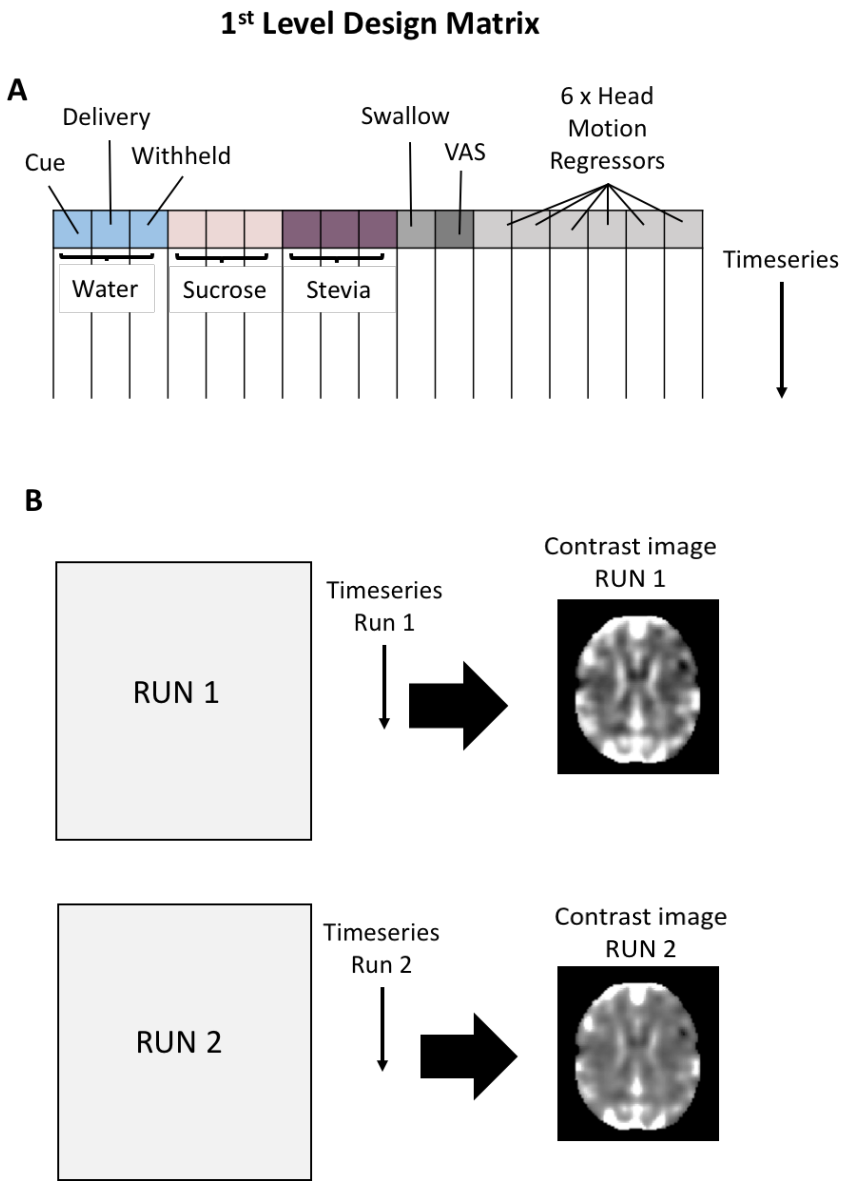

Figure 7.7.1 A) the 1st level model design matrix included all events of interest (cue, delivery and withheld) for each taste, as well as swallow, VAS periods and head motion parameters. B) in this analysis each run was modelled separately with the general linear model and therefore individual contrast images for each run are generated.

7.7.3 Whole brain group level analysis

A second level factorial model was constructed to examine the main effect of run within treatment. To answer this question a paired t-test was created for the whole cohort (n=25) to look for differences between runs for each contrast of interest individually.

Furthermore, for each contrast, 1st level contrast images for each run were entered into a repeated measures factorial model (SPM-12, 'flexible factorial model') with three factors; subject, drug and group, to look for main effects of drug as well as interaction effects. For both of the whole brain analyses the cluster forming threshold was set to $p < 0.001$ uncorrected. As before, clusters with $p < 0.05$ following FWE - Bonferroni correction for multiple comparisons (using the cluster extent criterion), were reported as significant.

7.7.4 ROI analysis

The main interest of this study is to interrogate the effects of insulin on this complex paradigm. An ROI analysis was performed within each BMI group to look at main drug effects, main run effects and also interaction effects. Mean values were extracted from subject contrast images created at the 1st level using 3dmaskave (AFNI) for each contrast, drug session and run. The ROIs used in this analysis of drug and run were identical to the ROIs previously defined. Similarly, the bilateral ACC, vmPFC, mOFC and NAcc ROI masks were used to assess dug and run differences during cue presentation conditions. For delivery contrasts the amygdala, anterior insula ,CPu and NAcc ROI masks were used to assess both drug and run differences.

The main aim of this analysis is to explore drug effects within these ROIs from individual runs that may have been missed or unable to be teased apart in the previous analysis in which the runs were combined. To increase the power to detect these drug effects, a within group analysis was conducted in OW and lean groups separately to look at the main effects of drug and run as well as the associated

interaction effects. This was done by constructing a factorial repeated measures ANOVA model for each contrast with the factors drug and run. Main effects of drug, main effects of run and interaction effects were assessed for significance using a p value of 0.05 from the ANOVA. Following significant main drug effects, planned comparison paired t-tests were conducted within run and similarly, following main run effects, paired t-tests were conducted within drug, as a post-hoc analysis judged to $p < 0.025$ significance to correct for multiple planned comparisons. Significant Interaction effects were interrogated using a Tukey post-hoc test, judged to $p < 0.05$ significance.

7.8 SECTION C. Results

7.8.1 VAS ratings

Effects of likeness over time for the whole cohort for sucrose and stevia are presented in Figure 7.8.1.

7.8.1.1 Whole Group – likeness ratings

Under placebo conditions, no differences in likeness ratings for stevia or sucrose between runs were identified following placebo administration (Figure 7.8.1.A).

Following insulin administration subjective VAS ratings showed significant differences between runs for likeness ratings of the stevia solution. Ratings of how much stevia was liked, decreased over time (run 1: 73.28 ± 11.99, run 2: 67.28 ± 13.55, p = 0.015, paired t-test) (Figure 7.8.1.B).

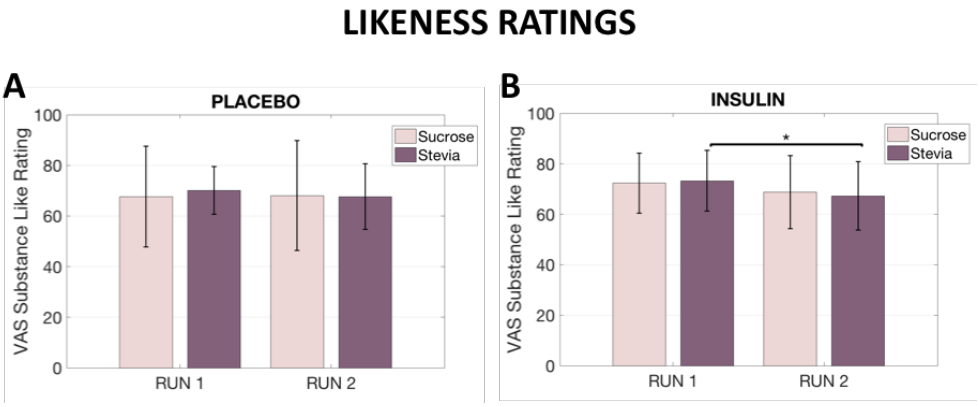

Figure 7.8.1 Whole group VAS likeness ratings for sucrose and stevia recorded during run and run 2 for placebo and insulin conditions. A) No difference between how much these two tastes are liked for either run under placebo, however, note the greater variability in the sucrose ratings as seen by the larger error bars compared to stevia scores. B) under insulin conditions there was a significant difference between likeness ratings over time for stevia. Stevia likeness ratings decreased over time (paired t-test). Data is showing mean ± SD, * p < 0.025, paired t-test, n=25 (whole group).

7.8.1.2 Whole Group – sweetness ratings

Whole group analysis (n=25) of subjective VAS scores showed that **under placebo conditions** the VAS sweetness ratings for stevia significantly decreased from run 1 to run 2 (run 1: 74.96 ± 10.59, run 2: 69.32 ± 15.74, p = 0.021, paired t-test) (Figure 7.8.2). Sucrose sweetness ratings on the other hand did not change over time.

Under insulin conditions, ratings of sweetness, were different between runs for both sucrose and stevia solutions but only stevia differences survived multiple testing correction. Sucrose solution increased in sweetness over time, but was not significant (run 1: 74.60 ± 13.09, run 2: 80.32 ± 10.74, p = 0.031, paired t-test), whereas the stevia solution decreased in sweetness over time (run 1: 76.28 ± 11.99, run 2: 65.92 ± 14.69, $p < 0.001$, paired t-test) (Figure 7.8.2).

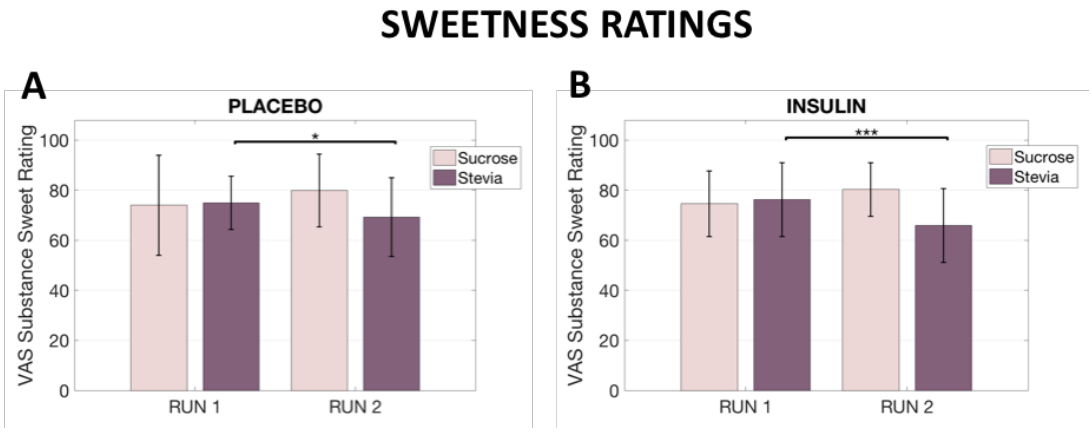

Figure 7.8.2 Sweetness VAS ratings for the whole group illustrating the effects of run over time for sucrose and stevia solution. A) Under placebo conditions stevia solution sweetness decreased over time. B) Under insulin conditions stevia solution sweetness decreased over time between runs. Data shown in mean ± SD, * $p < 0.025$, *** $p < 0.001$, using paired t-tests (n=25).

7.8.1.3 Lean Group – likeness and sweetness ratings

Within group and within drug comparisons of likeness and sweetness ratings were conducted to look for effects between substance's (i.e. sucrose or stevia) and also runs using repeated measure ANOVA models.

Within the lean group likeness and sweetness ratings for either sucrose or stevia did not change between run 1 ratings and run 2 ratings **under placebo conditions.**

Within the lean group, there were no effects on likeness for either of the two substances (sucrose and stevia) **under insulin conditions**. In terms of sweetness there was a significant main substance effect for sweetness ($F_{1,39}$ = 4.32, p = 0.045, ANOVA). This effect was driven by the sweetness of sucrose solution being rated greater than stevia in the second run. This comparison however did not the survive multiple comparison correction threshold (sucrose: 75.00 ± 8.01, stevia: 60.70 ± 17.22, t(9) = 2.50, p = 0.034, paired t-test).

7.8.1.4 OW Group – likeness and sweetness ratings

For the OW group, there were no differences between any of the likeness ratings **under placebo conditions**. However, there was a significant main effect of substance sweetness ($F_{1,59}$ = 5.10, p = 0.028, ANOVA), driven by a significantly higher rating of sweetness for sucrose compared to stevia solution only in the second run (sucrose: 81.2 ± 13.28, stevia: 71.33 ± 14.55, t(14) = 4.48, p < 0.001, paired t-test) **under placebo conditions** (Figure 7.8.3.A).

Within the OW, there were no effects on likeness ratings **following insulin administration**. For sweetness ratings an interaction effect was seen (run*substance $F_{1,39}$ = 11.12, p = 0.0015, ANOVA). Tukey test post-hoc analysis showed that this interaction effect was driven by a significant difference in sweetness between sucrose and stevia solution in the second run (sucrose: 83.87 ± 11.08, stevia: 69.4 ± 12.13, p = 0.008, Tukey test)(Figure 7.8.3.B).

Figure 7.8.3 VAS sweetness ratings in the OW group. A) Under placebo there was a significant difference between sweetness ratings for stevia and sucrose solutions, which was also seen under insulin conditions (B). ** $p < 0.01$, *** $p < 0.001$, paired t-tests, data shown is mean ± SD, n=15 (OW).

A summary table of all the significant results highlighted from the VAS analysis are presented in Table 7.8.1 below.

Summary of significant results: VAS scores				
Group	**INS / PLA**	**Like/sweet**	**Effect**	***p* value (test)**
Whole	INS	Likeness	Stevia ↓ overtime (run 1 > run 2)	$p = 0.015$ (paired t)
Whole	PLA	Sweetness	Stevia ↓ overtime (run 1 > run 2)	$p = 0.021$ (paired t)
Whole	INS	Sweetness	Stevia ↓ overtime (run 1 > run 2)	$p < 0.001$ (paired t)
OW	PLA	Sweetness	Sucrose > Stevia (Run 2)	$p < 0.001$ (paired t)
OW	INS	Sweetness	Sucrose > Stevia (Run 2)	$p = 0.008$ (Tukey)

Table 7.8.1 Summary of significant results from the VAS score analysis.

7.8.2 Whole brain analysis

Second level within treatment paired t-tests showed no differences in BOLD responsivity for either placebo or insulin conditions for any of the contrast comparisons tested.

Furthermore, within run repeated measure ANOVA models that were designed to look for main drug effects and interaction effects within each run separately did not show any significant changes for any of the contrasts tested.

7.8.3 ROI analysis

The ROI analysis looked for drug related effects across runs for each contrast separately. This analysis was constrained to within group comparisons.

7.8.3.1 Sucrose > water cue

Within the lean group a main drug effect was seen within the ACC ($F_{1,39}$ = 5.50, p = 0.025, ANOVA) and vmPFC ($F_{1,39}$ = 4.27, p = 0.046, ANOVA). Planned comparison paired t-tests however did not reveal any drug related differences from either run 1 or run 2 BOLD estimates. The OW group did not show any significant effects for any of the ROIs tested for from this contrast.

7.8.3.2 Stevia > water cue

For both lean and OW groups, there were no significant effects seen for the stevia cue > water cue for any of the ROIs tested.

7.8.3.3 Sucrose > stevia cue

For the sucrose cue > stevia cue contrast a significant main effect of run was seen from beta estimates extracted from the NAcc ($F_{1,39}$ = 5.20, p = 0.029, ANOVA) in the lean group. Planned comparison analysis did not reveal any further drug related differences in the NAcc. No significant effects from any of the ROIs were seen from analysis performed in the OW group for this contrast.

7.8.3.4 Sucrose delivery > withheld delivery

Sucrose delivery > withheld delivery contrast did not provide any significant drug or run effects from any of the ROIs tested in either the lean or the OW group.

7.8.3.5 Stevia delivery > withheld delivery

Finally, ROI extracted parameter estimates from the stevia delivery > withheld delivery contrast showed a significant main effect of drug within the NAcc ($F_{1,39}$ = 4.58, p = 0.039, ANOVA) in the lean group. Planned comparison paired t-tests showed that NAcc BOLD estimates extracted from the second run contrast were significantly greater following insulin administration compared to placebo (placebo: -0.08 ± 0.21, insulin: 0.23 ± 0.27, t(9) = 5.32, p < 0.001, paired t-test) (Figure 7.8.4). This was the only ROI that produced any significant effects within the lean group.

In the OW group, significant main effects of drug were seen from the estimates extracted from the CPu (t(14) = 10.52, p = 0.002, ANOVA. This main effect of drug was driven by a decrease in response to insulin administration within the first run (placebo: 0.57 ± 0.31, insulin: 0.07 ± 0.43, t(14) = -2.76, p = 0.015, paired t-test) (Figure 7.8.4). No other ROIs tested produced any significant drug related or run effects.

A summary table of significant differences seen from the ROI analysis is not provided as the significant results are presented in Figure 7.8.4 below.

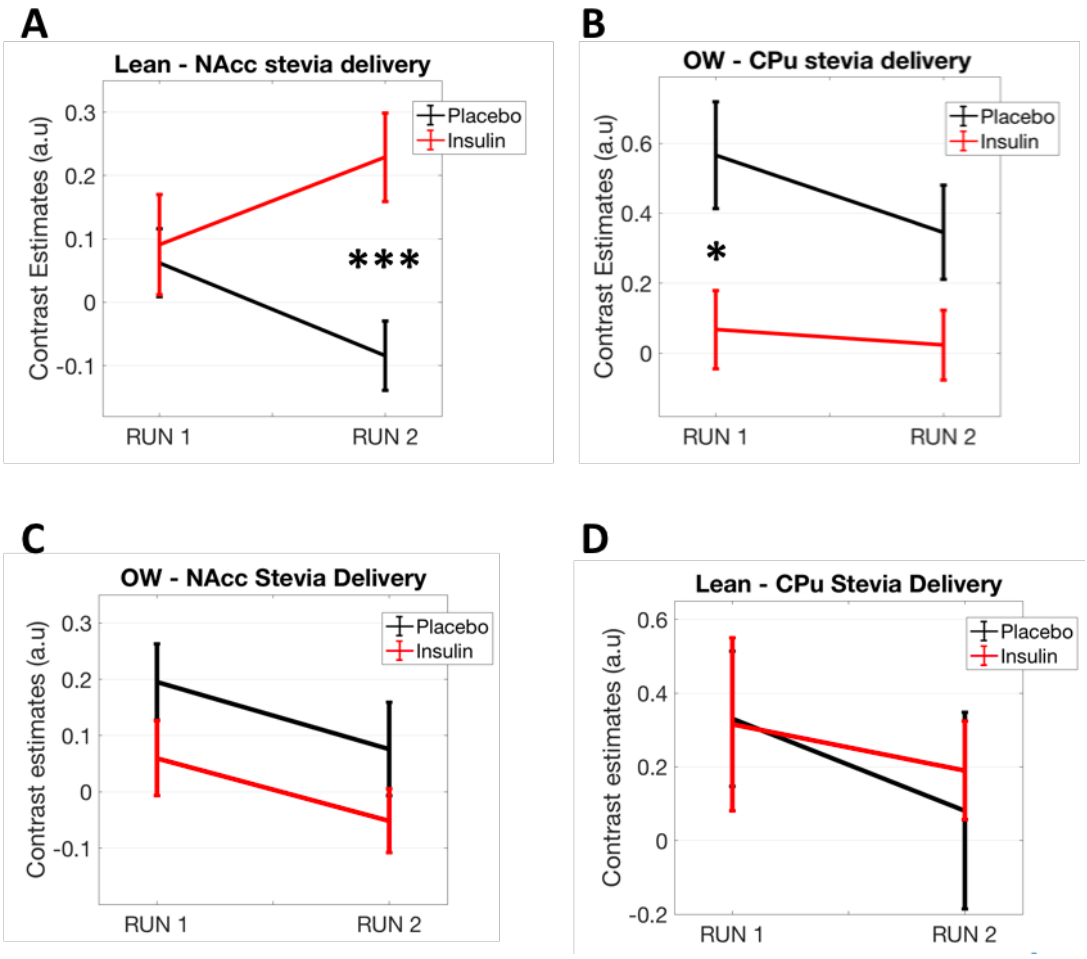

Figure 7.8.4 Contrast estimates extracted from the NAcc and the CPu regions from lean and OW groups for the stevia delivery contrast. A) ROI analysis within the lean group produced a significant increase for this contrast compared to placebo in the bilateral NAcc, which was observed in the second run only. NAcc contrast estimates were very similar for both conditions during the first run. B) The OW group displayed a reduced response in the CPu following insulin compared to placebo administration which showed a high contrast estimate. This difference was exclusive to the first run only. C) and D) illustrate contrast estimates for the OW and lean group for NAcc and CPu regions for reference. Differences were found from planned comparison paired t-tests. Data shown is mean ± SEM. * $p < 0.025$, *** $p < 0.001$, lean n=10, OW n=15.

7.9 Taste Paradigm Discussion

This study explored the neural mechanisms involved in primary reward processing from conditioned taste stimuli and how these systems are modulated by intranasal insulin administration. This study showed that the effects of insulin administration were (in general) most prominent upon receipt of stevia solution and that intranasal insulin displayed differential effects in the lean group compared with the overweight group. Insulin related effects were seen from regions of the prefrontal cortex and mesolimbic dopaminergic regions associated with reward evaluation (Fuster 2001) and reward processing (O'Doherty et al. 2004; Pagnoni et al. 2002), respectively, suggestive of an insulin related role on dopaminergic transmission. Additionally, this analysis has provided evidence for group effects upon cue presentation which are influenced by intranasal administration of insulin suggesting differential sensitivity to central insulin action, associated with BMI in prefrontal, cognitive functioning brain regions.

This is the first time that the primary effects of food (solution) taste and ingestion have been explored as part of a pharmacological investigation with intranasal insulin. Previous fMRI reports exploring the associations between elevated insulin and food related processing have largely focused on brain responsiveness to food cues/pictures (Guthoff et al. 2010; Kroemer et al. 2013) as a surrogate marker for food related neural processing. Food picture responsiveness fMRI experiments are useful for inferring the attractiveness or palatability of food under different homeostatic conditions (Goldstone et al. 2009) and in metabolic disease (Karra et al. 2013). However, these paradigms have limited scope for determining consummatory effects of food as the participant is not presented with a food stimulus to consume. This study, on the other hand, has made use of a primary reward paradigm that explored the effects of intranasal insulin on the anticipation and receipt of sweet tasting stimuli.

Furthermore, this is the first time that a BOLD functional imaging protocol has been implemented to explore brain responsiveness to the receipt of a non-nutritive sweetener, Stevia. The function of non-nutritive, zero calorie, sweeteners as an alternative to energy dense sweeteners such as sugar for weight loss and promotion of health is any area of considerable debate (Mattes and Popkin 2009). This work does not directly add knowledge to the literature regarding weight loss and health promotion but does help to address the acute effects that a popular non-nutritive sweetener has on brain responsiveness in comparison to sucrose.

On a primal level, all animal systems will ensure to attain key primary biological goals such as adequate nourishment and reproduction. Achieving these goals is facilitated through highly complex mechanisms (Goldstone 2006). Food intake is driven by three integrative systems, the homeostatic, hedonic and cognitive pathways, respectively. Homeostatic eating is largely controlled by the hypothalamus in response to peripheral signals regarding hunger, satiety and adiposity. Hedonic eating, on the other hand, is governed by the palatability and pleasure associated with eating certain foods and flavours. While the homeostatic system governs the body's metabolic needs, the pleasure that is coupled with eating makes energy intake worthwhile (Kringelbach 2015) and this pleasure has been proposed to be a key driver in the evolution of large primate brains (Kringelbach 2004). Hedonic eating and the pleasure associated from eating is a multi-faceted function that incorporates several distinct concepts involved in processing the pleasure induced by food administration. These are liking (palatability of food), wanting (motivation/drive for food) and learning (Berridge and Kringelbach 2008). Examinations of these components both individually and in combination has been one of the research goals of investigating food-related pleasure and consumption.

From the large body of relevant research, a number of models and theories relating to overconsumption of food in obesity and dysregulation of reward responsivity, have been suggested. One theory is the hypo-responsivity theory which suggests obese individuals show decreased activity within reward circuitry upon consumption, which in turn leads to repeated overeating to compensate for this deficit (Wang,

Volkow, and Fowler 2002; Blum et al. 1996). Alternatively, others have suggested that overeating associated with obesity stems from a hyper-responsivity to food stimuli leading to overall greater food intake (Stice et al. 2008; Davis, Strachan, and Berkson 2004). Both theories rely heavily on the effects of dopamine and its role in reward processing, specifically the pleasure aspect encoded within the striatum. More recently, an alternative interpretation of the literature has suggested that obese individuals display a reduction in reward-related cognitive inhibition rather than reward hypo or hyper-responsivity (Kroemer and Small 2016). Using links between obesity and drug addiction, *Volkow et al*., proposed a model of obesity that reflects an imbalance between circuits that drive pleasure seeking behaviour and circuits that regulate inhibitory control (Volkow, Wang, Fowler, et al. 2008). This discussion will address the circuits that contribute to reward motivated behaviours: reward saliency and learning, and how these circuits are affected in response to insulin administration and differ with regards to body weight (BMI). The cohort in this study are not obese, however this discussion intends to reference the relevant literature surrounding obesity related reward theory in support of the findings from this neuroimaging investigation. Furthermore, the effects of taste and consummatory responses to primary rewards with regards to natural and artificial sweeteners will also be discussed. The term 'reward' will be used throughout, which refers to the positive value assigned to a certain object, act or state (Schultz, Dayan, and Montague 1997). In this context, the term reward will be used to describe the value of the primary solution stimuli used in this task, unless stated otherwise.

The analysis for this task was separated into three sub-sections. This discussion will aim to bring the results of these sections together in an effort to harmonise the findings and complement the interpretation of this functional dataset. To aid the reader, the findings regarding the cue phase and delivery phase will be reported separately and then integrated for completion and to support or oppose reward and obesity based models and theories mentioned. The effects of intranasal insulin will be discussed thoroughly with reference to relevant literature first, followed by the interpretation of the effects seen as a consequence of BMI.

7.9.1 Anticipatory response

Experimental studies of reward processing often use conditioning paradigms to explore both the anticipatory phase as well as the consummatory phase. The presented cues used within this task were fractal images, not seen previously until the morning of each scan, and did not contain any patterns or characteristics that were predictive of the taste stimuli.

From whole brain maps that combined both functional scanning runs, there were no significant BOLD response increases seen when the water cue event was contrasted against either of the sweet solution presentation cues, in any group or treatment session. The lack of BOLD reactivity seen from this contrast suggest that the cue for water was less salient given its association with the water taste stimulus. VAS ratings averaged across the two runs show that the palatability of water stimulus, as measured by how much the water taste was liked, was significantly less than both the sweet stimuli.

These data showed significant increases in BOLD response activity common to both groups and treatment sessions upon presentation of both the sweet stimuli cues in comparison to the water stimulus cue. For all sweet > water cue contrasts and drug conditions regional BOLD activity was increased within both the left and right primary visual cortex. Previous work has shown that predictive cues coupled with higher value reward stimuli show greater activation within the primary visual and secondary (extrastriate) cortices (Anderson, Laurent, and Yantis 2014). The increased salience of greater reward-value cues, once learned, is thought to be augmented by dopaminergic activity, thus priming the brain to seek or find these learned rewards (Hickey, Chelazzi, and Theeuwes 2010). As mentioned previously, palatability scores were greater for sucrose and stevia over water stimuli so the increases in BOLD response in these visual regions for sweet > water cue contrasts is not surprising. The extrastriate cortex, makes up part of the secondary visual cortex, receiving inputs directly from the primary visual cortex and is involved with encoding shapes and edges (Okusa, Kakigi, and Osaka 2000; Vinberg and Grill-Spector 2008). The

complexity of shapes and patterns were similar for all the cues but with sufficient differences to permit visual differentiation. Cue and stimulus coupling were randomised amongst subjects to avoid any confounding effects of repeated cue and flavour across sessions thus the increased extrastriate response from these sweet cues is likely due to the increased likeness for sweet-tasting stimuli coupled with increased salience for those sweet cues.

BOLD response increases originating from the dorsal region of the cerebellum in the overweight group were seen following placebo administration when presented with the stevia paired cue vs water. Recent research in rodent models have shown neuronal responses from populations of granular cells within the VI region of the cerebellum during the anticipation of sucrose solution delivery (Wagner et al. 2017). Regions of the middle temporal gyrus showed increased BOLD responsiveness following cue presentation of stevia in comparison to water within lean and overweight groups following placebo administration. Although not directly related to food reward, fMRI results from a monetary reward paradigm (Manelis et al. 2016) highlighted the middle temporal gyrus as an area involved in the anticipation of winning in comparison to losing. Although, winning money is conceptually different to receiving a primary food reward, some similarities in neural organisation do exist (Simon et al. 2015) and so these responses in the temporal gyrus seen here could be common to both the anticipation of food stimuli and monetary reward.

Combining runs of functional data was conducted in an effort to increase statistical power in the first instance. Given that this paradigm examined the effects of three tastes: water, sucrose and stevia, it was important to collect sufficient functional data for each event for parametric general linear model based voxel wise analysis. Across both runs each participant was presented with 30 cue images for each taste and received the taste bolus following cue presentation 18 times, with 12 withheld delivery events. Whole brain, SVC and ROI analysis of combined run contrasts did not reveal any significant drug related effects for either sweet > water cue contrasts from combined run data. Observations of within treatment whole brain maps and SVC

analysis did, however, suggest that there were some subtle effects of both drug and BMI that were not detected from a whole brain voxel wise statistical comparison.
For all taste stimuli and drug sessions, the association between fractal cues and taste stimuli were learnt successfully during the course of the paradigm for each participant, tested by asking each participant out of the scanner. Thus presentation of the cue elicited an 'anticipatory' brain response, recruiting regions not just involved in visual processing, but those involved in higher level reward processing such as the vmPFC, ACC and mOFC, all commonly associated with evaluation and decision making in response to rewarding stimuli (Wallis and Kennerley 2011).

During the placebo session, SVC analysis did not show BOLD related increases from regions tested (ACC, vmPFC, NAcc, mOFC) for the sucrose > water cue presentation, in either BMI group. This was surprising given how much the sucrose solution was liked from VAS ratings and is in contrast to the results from *O'Doherty et al.,* who showed that during non-pharmacological challenges the mOFC is active during anticipation (O'Doherty et al. 2002). The likeness ratings for the whole group as seen from Figure 7.4.1.A following placebo administration showed that there was some variability in the VAS scores for sucrose solution, which may be reflected in the imaging data. More relevant perhaps is how this event was modelled. The cue presentation event modelled in the current taste paradigm was short (2s) and corresponded only to the period when the visual cue was present. Therefore, a limitation of this model approach could be the lack of imaging volumes used to capture the anticipatory phase fully, which may, arguably, begin post cue presentation. Despite this potential limitation, whole brain t-maps following insulin administration did show recruitment of regions commonly involved in anticipation (O'Doherty et al. 2002). These regions were highlighted by SVC results that showed BOLD responses for sucrose > water cues within the NAcc and the mOFC in the lean group suggestive of an anticipation effect, as well as an insulin related increase in anticipation recruitment. *Stouffer et al.* has shown in mice that increased central insulin concentrations act to enhance dopamine pre-synaptic neurotransmitter release in the NAcc and putamen (Stouffer et al. 2015) thereby acting as a reward signal. The mOFC is a region situated on the ventral surface of the prefrontal cortex.

The mOFC plays a role in reward evaluation, as well as the magnitude and probability of the related reward (Wallis and Miller 2003). As mentioned, *O'Doherty et al.* showed in humans that during the anticipation phase for sucrose solution stimulus there was an increased BOLD response in the mOFC when compared to the anticipation of a tasteless solution (O'Doherty et al. 2002). The mOFC acts as an integrative hub for many sensory inputs and is seen here in response to the cue presentation for sucrose stimulus in the lean group under insulin conditions but not placebo.

Activation due to the presentation of the stevia cue with respect to that for water, revealed BOLD related increases in pre-frontal regions (ACC, vmPFC and mOFC) as well as the NAcc region in the lean group, following placebo administration but were absent under insulin conditions. Despite these observable differences from within treatment analyses there was not any significant differences seen from whole brain or ROI analysis comparisons, but suggest a trend for a 'reward-reducing' effect of insulin. Experiments in mice have shown reduced anticipatory behaviour for sweet solutions following insulin injection into the VTA (Labouebe et al. 2013). In addition, central insulin injections to the VTA in mice are coupled with suppression of food cue salience via decreased dopamine release in the NAcc (Mebel et al. 2012). The opposing insulin response trend seen between 'sucrose > water' and 'stevia > water' cues is interesting. Particularly as there were no effects in either the placebo condition or insulin condition when comparing these two flavour-cue contrasts (sucrose > stevia) from whole brain analysis. Averaged sweetness ratings (run 1 and 2) for the whole group did show that, under insulin conditions only, sucrose was significantly sweeter than stevia but this did not affect how much these tastes were liked. It is worth stressing that ratings of sweetness are better related to the delivery or receipt of taste stimuli presentation as opposed to cue presentation.

Summary Box 1

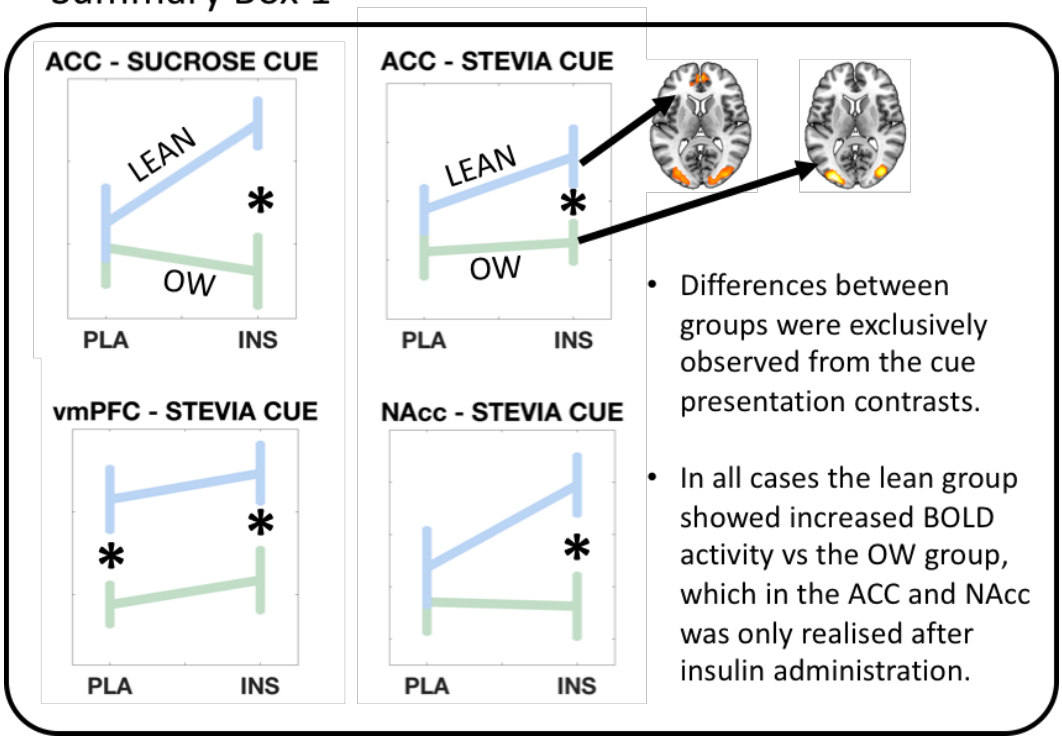

7.9.2 Group differences in cue reactivity

There were differences between groups which were only identified in the cue condition and were for observed upon presentation of both the sucrose and stevia cues vs water. The treatment dependent group differences were exclusively seen in response to insulin administration within the ACC and NAcc regions. The vmPFC also showed group wide BOLD signal differences under placebo conditions as well as following insulin administration. These group differences are highlighted in *Summary Box 1*.

These results suggest that the ACC and NAcc are both insulin sensitive and that BMI has an effect on regional insulin sensitivity. The NAcc BOLD increase seen in the lean group but not in overweight group in response to insulin administration follows a similar trend seen in pre-clinical work that shows insulin's lack of effectiveness as a reward signal in obese mice vs wild type littermates (Stouffer et al. 2015). Insulin receptors have been found within the NAcc (Schulingkamp et al. 2000; Werther et al.

1987) and exogenous insulin administration has been shown to modulate dopaminergic concentrations within this region (Jones et al. 2017; Stouffer et al. 2015). *Stouffer et al.* has shown in mice that increased central insulin concentrations enhanced dopamine synaptic neurotransmitter release in the NAcc and caudate-putamen (Stouffer et al. 2015) thereby acting as a reward signal, in support of the insulin induced increase in activity within the NAcc. Interestingly, from *Stouffer et al.,* the sensitivity of insulin related dopamine release from striatal neurons (NAcc, caudate-putamen) is diet dependent with obese rats displaying diminished insulin related dopamine synaptic concentrations (Stouffer et al. 2015). Although the participants involved in the current study are overweight and not obese, this result is in support of the notion that insulin may have a differential response in those with an increased BMI.

For both sucrose and stevia solution cue > water cue contrasts the ACC provided a distinguishable difference between the lean and OW groups in an insulin dependent manner. The fractal cue used in this paradigm informs the participant which taste may be delivered, but the cue does not inform the participant whether the taste will be delivered or not. Thus the cue itself is not predictive of whether the trial will be paired or unpaired. Therefore this raises a possibility that upon cue presentation the participant will observe the cue but also try and predict the probability of receiving the reward (taste bolus). The ACC has been previously shown to be involved in the prediction of rewarding outcomes (Silvetti, Seurinck, and Verguts 2013) and also has been recruited during assessing the probability of receiving primary rewards (Vassena et al. 2014). This study however limited in interpretation power given it is hard to know based on the data collected what the participant is actually thinking during these events. It is worth highlighting though that the process being carried out in the ACC is not taste dependent and is also modulated by insulin within the lean group, suggestive of a modulatory effect of insulin in the lean group that may lead these individuals to think and predict the probability of receiving the reward or not, which may be different in the OW group.

BOLD activity within the vmPFC was greater in lean individuals in response to the stevia cue for both the placebo and insulin sessions. The exploratory correlational analysis illustrated a relationship between placebo vmPFC activity in response to the stevia cue and BMI. This relationship showed that lower BMI is associated with greater BOLD activity in the vmPFC following placebo administration. A similar relationship was seen between vmPFC BOLD estimates and BMI following insulin administration but did not survive the statistical threshold. The vmPFC is associated with valuation of stimuli, both food and non-food related (Tiedemann et al. 2017) as well as decision making. *Halfmann et al*., showed that in older adults vmPFC activity was associated with gambling task performance and that greater activity within the vmPFC correlated well with better performance from the task, i.e. greater money won (Halfmann et al. 2016). This increase in vmPFC activity was predictive of better decision making and *Halfmann et al*., further suggested that the vmPFC could be important with regards to long term decision making and that this leads to effects on both wealth and health (Halfmann et al. 2016). As the task implemented in the SNIFAR study was passive, in that participants had no choice, the effects seen are hard to decipher and a decision making element introduced to this paradigm would be helpful to explore these effects seen and if these regions of interest translate to a more cognitively demanding reward paradigm.

These group differences do not fully support either the reward hyper-responsivity dopamine theory of obesity that has been suggested previously (Volkow, Wang, and Baler 2011; Burger and Stice 2011a). This is largely because of the lack of group differences seen following placebo administration within the NAcc. Furthermore, as the differences in cue responsivity within the NAcc were limited to stevia cue presentation the conclusions drawn are therefore not conclusive or applicable to all primary rewarding stimuli.

In light of this, these results suggest a hypo-responsivity of the NAcc, a key dopaminergic region, to centrally increased insulin in overweight compared to normal weight individuals in response to a predictive cue. Furthermore, prefrontal regions involved in cognitive processing, reward valuation and prediction were

unresponsive in the presence of central insulin in the OW group in comparison to the lean group who provided insulin related increases within these regions. Suggesting a BMI related differential sensitivity to central insulin which may be key to valuation and prediction prior to consumption of sweet foods.

7.9.3 Consummatory response

Whole brain functional images that corresponded to stimulus delivery events were contrasted against those that corresponded to the 'stimulus withheld' events for each taste. In both BMI groups the water taste revealed significant activations within the bilateral somatosensory cortex and anterior insula region for the both placebo and insulin conditions, using combined run data. It is well known that water is not 'tasteless' (Zald and Pardo 2000) and as these results show the taste of bottled mineral water elicits a reliable BOLD response irrespective of insulin or placebo challenge. Previous fMRI studies that investigated 'taste' often use either a tasteless artificial solution (Stice et al. 2008; O'Doherty et al. 2003) that mimics the ionic complexity saliva or distilled water (Szalay et al. 2012; Haase, Cerf-Ducastel, and Murphy 2009) as a control taste. In retrospect, incorporating water as a control solution has perhaps limited the functional contrasts that can be explored in the consummatory phase of the paradigm. For example, whole brain contrasts for the taste of sucrose vs water did not reveal any differences and likewise for stevia vs water, this data was not reported. Hence, for this investigation the taste responses were modelled as delivery minus withheld delivery for each taste. It has been possible to make inferences at both the whole brain level as well as from ROI analysis from these modelled events. In regards to the taste of water, formal drug related differences or group differences were not tested in this instance.

7.9.4 Sucrose and stevia delivery

Under placebo conditions, regions of common activation elicited in response to delivery of both sweeteners were the left and right somatosensory and motor cortical regions. The spatial location of this cortical activation along the lateral

surface coincides with areas functionally related to the lips, tongue and jaw (Miyamoto et al. 2006) and would be expected to be recruited by this paradigm for both these contrasts. By contrasting the delivery against the withheld event, these regions appear quite prominently from whole brain one sample t-tests. No statistically significant differences between whole brain t-maps for lean and OW groups for both sucrose delivery and stevia delivery under placebo conditions were observed. It is nevertheless instructive to review some of these differences. For example, under placebo conditions, the lean group showed a relatively reduced response in the somatosensory cortex in comparison to the overweight group for both the sucrose and stevia taste. So much so, that small volume correction did not result in any significant clusters within the lean group for the stevia delivery contrast and only provided a significant effect within the anterior insula from sucrose delivery. In contrast the OW group showed significant BOLD responses within the insula, amygdala, striatum and also cerebellum for stevia and sucrose delivery from small volume correction and whole brain interrogation, respectively.

The Insula has been well documented in its role of gustatory perception and processing (Frank, Kullmann, and Veit 2013) within the brain and is commonly referred also as part of the primary gustatory cortex. The dorsal surface of the tongue is scattered with raised projections known as papillae which are lined with taste buds. Each taste bud hosts a large number of taste receptor cells with afferent axons that carry information along cranial nerves to the brainstem and thalamus where relay neurons connect with the insula cortex, amygdala and hypothalamus (Breslin 2013). From the insula, projections to the striatum, OFC and ACC carry the oral sensory information where properties regarding reward valence and other cognitive processes are encoded (Breslin 2013). BOLD response increases were seen within the cerebellum from presentation of the stevia stimulus under placebo conditions. Activity within the cerebellum has been observed from previous fMRI studies looking at taste (Zald and Pardo 2000; Small et al. 2003). *Small et al.,* reported cerebellar activity associated with intensity of substances and suggested a role of the cerebellum to respond to taste intensity information and guide oral movements

(Small et al. 2003). The cerebellum was also involved following insulin administration for both sucrose and stevia delivery.

Following insulin administration whole brain t-maps were visually similar for the OW group in response to both sucrose and stevia delivery contrasts. Interestingly, BOLD increases were seen in the right putamen from stevia solution delivery which was absent following placebo conditions. Lean group whole brain maps for both sucrose and stevia delivery contrasts presented a more widespread spatial BOLD response, incorporating similar regions seen in the OW group, following insulin administration in comparison to placebo. In response to stevia administration, the lean group displayed activation within the supplementary motor area (SMA) under insulin conditions. The SMA is well known for its role in controlling movement actions (Nachev et al. 2007) and therefore this response seen could be due to preparation for swallowing. Why this region was only seen upon stevia delivery and not sucrose delivery, and why was limited to both the lean group and following insulin administration is hard to comprehend.

7.9.5 Insulin effects

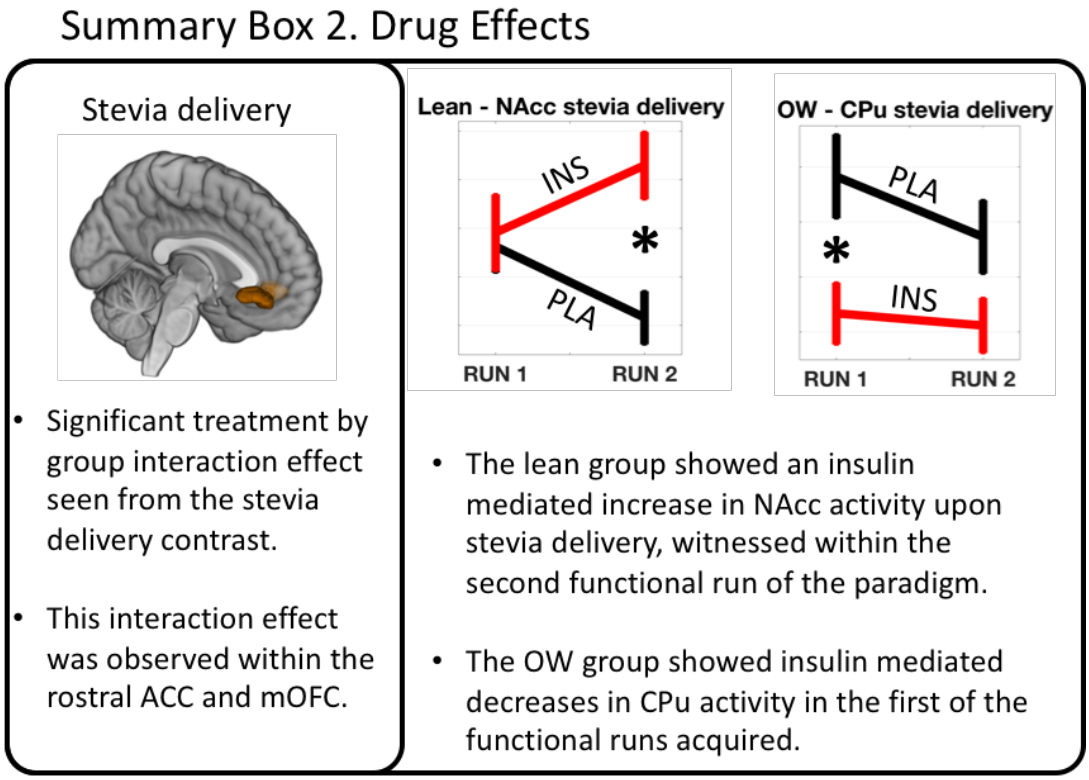

Whole brain parametric analysis provided a significant interaction effect between treatment and group in response to stevia delivery vs withheld delivery. Insulin administration vs placebo displayed a differential response in lean and overweight groups within the prefrontal cortex, localised to the rostral ACC and mOFC. The lean group showed an insulin-related BOLD increase within this region in contrast to the OW group who demonstrated an insulin-related BOLD decrease within this prefrontal region compared to placebo. Whole brain paired t-tests, conducted as *post hoc* analyses were not sensitive to detect significant insulin-induced changes for either group.

The interaction effect seen is anatomically interesting as the prefrontal cortex is heavily involved in cognitive functioning and decision making, as mentioned previously. In addition to the hedonic aspects associated with food consumption, the response to food taste and sight is highly dependent on higher level cognitive

processing. Cognitive control, via the prefrontal cortex, is key to both the enhancement and suppression of appetite and motivation to consume food (Dagher 2012). The prefrontal cortex is a region with known responses to changes in insulin concentration. For example, increases in endogenous insulin concentrations following glucose ingestion have been shown to induce reductions in prefrontal cortex activity upon food picture presentation (Heni, Kullmann, et al. 2014) suggesting that this cognitive hub is an insulin sensitive brain region. In relation to the current study, *Kullmann et al.,* showed an opposing interaction effect between intranasal insulin and group (lean and obese) for resting state cerebral blood flow (CBF) in the prefrontal cortex (Kullmann, Heni, Veit, Scheffler, Machann, Haring, et al. 2015). They showed that prefrontal cortex CBF was reduced in lean, insulin sensitive, individuals but was increased in obese, insulin resistant (HOMA-IR > 2.0), individuals in response to intranasal insulin administration compared to placebo (Kullmann, Heni, Veit, Scheffler, Machann, Häring, et al. 2015). The insulin induced reduction in the lean individuals correlated well with disinhibition measurements and thus the authors suggest a modulatory role for insulin within the prefrontal cortex (Kullmann, Heni, Veit, Scheffler, Machann, Häring, et al. 2015). On closer inspection, however, the origin of the CBF interaction effect observed by these authors was lateralised and more superior to that observed from this taste paradigm. The region reported in Kullmann *et al.* corresponded to the middle frontal gyrus (Kullmann, Heni, Veit, Scheffler, Machann, Häring, et al. 2015) as opposed to the more medial regions of the prefrontal cortex (rostral ACC and mOFC) seen from this current analysis and therefore similarities between these studies should not hold significant weight in support or opposition of these findings. Furthermore, the taste paradigm employed is a complex functional task that engages reward and learning circuitry as well as areas involved in taste anticipation and consumption rather than a resting state perfusion interrogation.

More relevant are studies that report activity within these regions in response to task based manipulation. For example, fMRI studies have shown the involvement of the vmPFC and rostral ACC (rACC) during encoding and predicting value of future rewards, particularly during decision making paradigms (Gläscher, Hampton, and

O'Doherty 2009). The ACC is a large anatomical structure, with the more frontal/rostral regions being closely linked to the cognitive evaluation of reward (Toda et al. 2012). The rACC in particular is known to be responsive upon receipt of hedonically relevant stimuli, whether the stimulus be oral or olfactory (de Araujo and Rolls 2004; de Araujo et al. 2005). The taste response to both fat and sucrose produce increases in the BOLD response within the rACC, irrespective of viscosity (de Araujo and Rolls 2004). Similarly, BOLD response magnitude in response to odour stimuli has been shown to be greater for stimuli labelled as 'appealing' (e.g. cheddar cheese) in comparison to the same odour labelled as 'unappealing' (e.g. body odour) (de Araujo et al. 2005). In the same vain, the rACC region has been shown to elicit a greater magnitude BOLD response to an umami taste stimulus labelled as appealing vs the same umami stimulus with a less appealing label (de Araujo et al. 2003). Thus the rACC has a cognitive modulatory effect on appealing and unappealing stimuli. In light of this involvement of the rACC in taste modulation and response, the participants were instructed to learn the association between cue and taste. Knowledge of each taste was not provided until completion of the entire study and so the response in this region could be attributed to or associated with trying to encode the taste.

The prefrontal cortex is an integrative hub with many roles and functions. The interaction effect observed from whole brain statistical maps for the stevia delivery contrast spans across multiple anatomical regions and slightly limits the interpretation power of this interesting result. As mentioned, whole paired t-tests within both groups did not reveal any significant drug related effects and thus power to speculate on this interaction effect is limited. Group related effects seen from the stevia cue, as mentioned previously, are seen within the same regions and also display lean related insulin increases in BOLD activity. Given the timing of events used in this paradigm and implemented within the 1st level model it could be argued that there is a carryover BOLD effect originating from the cue presentation to the bolus delivery.

Significant drug related effects of insulin were seen from the stevia delivery vs withheld contrast from ROI analyses that interrogated insulin related changes from

functional data acquired during the first and second run separately. Combining both runs was important for an initial analysis however the learning and sensitisation elements of this task may introduce temporal characteristics that warrants analyses of each run separately.

Ancillary VAS measures of how much each taste was liked and how sweet the participant found the taste bolus help to support the notion of temporal effects from this task. Following placebo administration, stevia solution was rated as significantly less sweet at the end of the second run compared to sweetness ratings made at the start of the first run but was not coupled with a change in likeness ratings. Under insulin conditions ratings of stevia sweetness also showed a strong decrease over time which was also coupled with a decrease in subjective liking. These results suggest that, firstly, there are dynamic changes in sweet taste sensitisation for stevia solution and secondly, that these changes are more prominent following insulin administration which also changed the how much stevia solution was liked. Stevia, as well as other non-nutritive sweeteners, activates sweet taste receptors and bitter taste receptors on the tongue simultaneously, in a concentration dependent manner (Hellfritsch et al. 2012). The decrease in stevia sweetness over time could be from an increase in bitterness following repeated exposure, however the bitterness of stevia was not assessed and therefore this cannot be confirmed. The decrease in subjective stevia sweetness was more pronounced following insulin administration compared to placebo. This pronounced decrease in sweetness was coupled by a decrease in likeness suggesting a decrease in the hedonic value over time, associated with central insulin concentrations.

ROI analysis employed to interrogate the data acquired during different independent runs for each BMI group separately, revealed interesting findings. No effects of drug or run were seen for any of the cue contrasts and no effects of drug or run were seen either for the sucrose delivery contrast. Effects were seen, however, within dopaminergic regions of the mesolimbic system for the stevia delivery contrast. Within lean individuals a significant increase in NAcc BOLD activity was seen in response to insulin compared to placebo, which was only apparent in the second run

(SUMMARY BOX 2). In contrast, in the overweight group insulin produced decreases in BOLD activity within the striatum (caudate and putamen) compared to placebo during the first run.

Work on reward processing has focused on the concept of reinforcement learning (classical conditioning) (Schultz 2001; Rescorla and Wagner 1972) and the involvement of the dopaminergic system in facilitating and reinforcing reward seeking and approach behaviours. Midbrain dopaminergic projections from the VTA and substantia nigra (SN) nuclei to the striatum and pre-frontal cortex are highly implicated in reward processing (Schultz 2001; Rolls 2004). Particular focus has been on the NAcc, a region commonly known for its role in pleasure and addiction (Adinoff 2004). With reference to cue conditioned reward paradigms the dopaminergic neuronal firing responses within the NAcc shift from the reward presentation stimulus (e.g. 0.5ml sweet bolus) to the cue presentation (e.g. fractal cue) during conditioning, known as temporal difference learning (Sutton 1988). A pattern similar to a temporal shift can be seen following placebo administration from the lean group NAcc plots in response to stevia delivery (Figure 7.8.4). The plot shows that over time (from run 1 to run 2) the NAcc activity decreases, as would be seen in the case of a temporal dopamine shift from reward stimulus to cue presentation, once the association had been learnt (Schultz 1998). Interestingly in response to increased central insulin concentrations in the lean group this pattern is reversed; NAcc activity increases over time. Insulin plays a dual role in the local mesolimbic regions. Firstly, insulin binds to insulin receptors on pre-synaptic striatal (NAcc and CPu) neurons and acts to increase pre-synaptic dopamine uptake via upregulated dopamine transporter activity (DAT) (Stouffer et al. 2015). Secondly, excitatory cholinergic interneurons that synapse onto striatal neurons display pre-synaptic insulin receptors. Successful binding of insulin upon these cholinergic interneurons increases excitability and action potential frequency thus increasing downstream dopaminergic release from striatal dopamine neurons (Stouffer et al. 2015). The latter effect is most prominent upon increased insulin concentrations and is sufficient to overcome the increased DAT uptake activity in response to increased striatal insulin concentrations. The increase in BOLD response seen from the NAcc from the

lean group may be explained by the excitatory effects of insulin on cholinergic interneurons associated with subsequent dopamine release. Cholinergic interneurons receive input from the thalamus and this mechanism is involved in directing attention, reinforcement and also learning (Smith et al. 2011). It could be suggested that the insulin related BOLD increase in this region is reflective of an informative signal, potentially due to a change in hedonic properties or valence. Perhaps the change in palatability and sweetness seen from VAS scores would be significant to elicit this attention signal.

One thing that has not been explored that would supplement this data is looking at the negative prediction error response that would occur during omission of the taste bolus. As the delivery event has been contrasted with the withheld delivery event the contrast images produced will have contributions from both beta estimates. This needs further exploration to help decipher the insulin related increases witnessed from the NAcc in the lean group.

In contrast, the OW group displayed an insulin related striatal (caudate and putamen) BOLD decrease in response to stevia presentation. Interestingly, from *Stouffer et al.,* the sensitivity of insulin related dopamine release from striatal neurons (NAcc, caudate-putamen) is diet dependent with obese rats displaying diminished insulin related dopamine synaptic concentrations (Stouffer et al. 2015). Although the participants involved in the current study are overweight and not obese, this result is in support of the notion that insulin may have a differential response in those with an increased BMI. Stouffer et al., and Jones et al., both showed that under chronic low basal insulin concentrations the caudate-putamen showed reduced insulin dependent DAT expression and activity, thus displaying an increase in net caudate-putamen dopamine release (Stouffer et al. 2015; Jones et al. 2017). Given that central insulin concentrations are decreased in those with a greater fat mass (i.e. BMI) (Kern et al. 2006) the greater BOLD response in the caudate-putamen seen in the OW group under placebo conditions vs insulin would be supported (see Summary Box 2). In turn, the presence of increased central insulin following intranasal insulin administration may reinstate DAT activity thus reducing caudate-putamen

dopaminergic activity as seen from the data. The lean group showed no insulin related changes in caudate-putamen activity which may suggest that the caudate-putamen is more sensitive to weight and fat induced changes in insulin related DAT sensitivity.

In conclusion this task has highlighted several interesting effects that intranasal insulin has on primary reward. The effects of centrally acting insulin are noticeably differently between lean and overweight groups for some of the contrasts interrogated in this task. In general, insulin acts to drive different neural responses between lean and overweight individuals. Interestingly, the effects of intranasal insulin were limited to the receipt of stevia, a non-nutritive sweetener. The reasoning behind this could be that stevia is novel to the taste buds and that this added novelty is sufficient to recruit and affect areas of the brain involved in higher level cognitive functions akin to the reward learning process. Insulin affects were seen within the striatum (NAcc, caudate-putamen) and this finding helps to support central insulin's role in dopaminergic signalling. Understanding the effects that this may have on energy related decision making and reward related deficiencies in obesity or insulin resistance is of great importance and continued research in this area is needed to support the findings reported here.

Chapter 8 Evaluation of the effects of intranasal insulin on resting functional connectivity

This chapter covers the resting state Blood Oxygen Level Dependent (BOLD) functional MRI component of the SNIFAR study that was employed to interrogate the effects of intranasal insulin administration on functional connectivity measures as well as effects of body mass index (BMI). Specific details regarding the acquisition parameters, pre-processing and analysis techniques employed for this component of the SNIFAR imaging study will be reported. For the analysis of these data, only 'seed based connectivity' inferences were made . The findings and results from this component are discussed with reference to previous fMRI based intranasal insulin pharmacological studies and also non-pharmacological resting state network literature.

8.1 Introduction

Centrally acting insulin has been shown to have an effect on a number of centrally controlled functions including memory, cognition, mood modulation, reward and appetite control (Kullmann, Heni, Fritsche, et al. 2015; Ott et al. 2012; Tiedemann et al. 2017; Stouffer et al. 2015). Key to understanding these modulatory effects has been the implementation of intranasal insulin administration coupled with a combination of multi-modal fMRI techniques (Kullmann, Heni, Fritsche, et al. 2015). Among these techniques, a body work has been conducted to investigate the effects of intranasal insulin on resting state functional activity (Kullmann et al. 2013; Kullmann, Heni, et al. 2017; Kullmann et al. 2018). The majority of this work has examined changes in BOLD signal dynamics using techniques known as Amplitude of Low-Frequency Fluctuations (ALFF) and Fractional Amplitude of Low-Frequency fluctuations (fALFF) (Zuo et al. 2010). Measures of ALFF and fALFF provide a view on resting, regional neuronal activity through quantifying the fraction of the total power of the BOLD signal that corresponds to the low frequency range (0.01 – 0.1 Hz) (Lv et al. 2018). Comparatively little work has been conducted to investigate the effects of intranasal insulin on network dynamics and functional connectivity through a seed-based model-driven approach, which was the main aim of this component of the SNIFAR protocol.

In this work, resting state BOLD data were acquired using a multi-echo (ME) EPI acquisition protocol combined with an image pre-processing and denoising methodology called multi-echo independent component analysis (ME-ICA). As described in Chapter 2 (section 2.3.4)**,** a multi-echo EPI acquisition acquires multiple whole brain EPI images (in this case three) at multiple TEs following spin excitation, in contrast to conventional EPI BOLD acquisitions which acquire a single EPI image (Howseman and Bowtell 1999). The benefits of the multi-echo acquisition approach are two-fold. Firstly, multiple EPI images can be combined using an optimally weighted summation approach to increase BOLD sensitivity throughout the entire brain (Posse et al. 1999). And secondly, the richness of the data per excitation (TR) permits the implementation of a denoising technique, ME-ICA (Kundu et al. 2012),

which was employed in this component of the SNIFAR investigation. The details of the ME-ICA methodology have been explained in detail in Chapter 2 (section 2.3.4).

Prior to SNIFAR study initiation, a study was conducted in a small number of healthy volunteers (n=8, 6M, 2F) to compare multi-echo denoising against a conventional single echo EPI acquisition (Wingrove et al. 2016). This work supported the use of ME-ICA for denoising functional timeseries compared to conventional single echo data, producing results that were similar to those obtained by *Kundu* et al., (Kundu et al. 2013; Kundu et al. 2012). Furthermore, using the multi-echo EPI methodology, data were collected to investigate two important issues: a) the optimum number of echo time-series to be used for denoising (3 echoes vs 4) (Wingrove, O'Daly, and Zelaya 2017b) and b) the differences between performing analysis on multi-echo data spatially normalised to standardised space (e.g. MNI), or in native subject space (Wingrove, O'Daly, and Zelaya 2017a). From this work, the use of three-echo data proved to be preferable to four-echo data with superior discrimination of BOLD and non-BOLD components. More specifically, four echo data in some occasions failed to identify non-BOLD components and therefore did not 'denoise' the dataset as efficiently as the three echo data. The data suggested that the fourth echo images, acquired with a long echo time (TE = 48ms) and with low signal to noise ratio (SNR), reduced the sensitivity of the denoising algorithm and thus three echoes turned out to be better in comparison (Wingrove, O'Daly, and Zelaya 2017b). Finally, analysis in subject space or MNI space did not show large amounts of differences as both performed comparatively well in terms of denoising. However, analysis conducted in native space is quicker and less computationally intensive due to a smaller number of voxels per image in the native space domain.

As a result of the above, the SNIFAR study was acquired using a three echo multi-echo sequence and analysed in native space, prior to normalisation of the final subject-level output.

8.2 Methods

In this resting state BOLD investigation, data from all subjects (n=27) were included. In total there were 12 lean participants (BMI = 22.40 ± 1.89 (mean ± standard deviation)) and 15 OW participants (BMI = 27.76 ± 1.92), (mean difference in BMI = 5.36, $p < 0.001$, two-tailed unpaired t-test). Groups did not differ significantly in age, as described in Chapter 5 (section 5.1.1)

8.2.1 Image acquisition

The resting state BOLD data were collected following the final anatomical image acquisition and were the first of the functional image series. This acquisition was approximately 25-30 minutes following intranasal insulin/placebo administration at a time when central insulin levels were close to their peak (Born et al. 2002).

Whole brain functional images were acquired using a custom-built, T2* weighted gradient echo multi-echo echo-planar imaging (ME-EPI) pulse sequence. A 32-channel receive only coil and 'array coil spatial sensitivity encoding slices' (ASSET) was employed for parallel imaging. Slices were acquired in a sequential top down direction in the near-axial plane parallel to the anterior-posterior commissure line (approximately 30° from the 'true axial' orientation) with the following parameters: TR = 2000 ms, TE = 12,28 and 44 ms, flip angle = 80°, acquisition matrix size = 64 x 64, FOV = 211 x 211, slice thickness = 3 mm, slice gap = 0.3 mm, no. of slices = 32, in plane voxel size = 3.30 x 3.30 mm^2. Four dummy acquisitions were used to achieve steady state magnetisation, which were discarded. The total number of imaging volumes was 192 acquired in 6:32 mins.

8.2.2 Image Processing

All resting state data pre-processing and seed based functional connectivity analyses was performed using AFNI, FSL and SPM functional imaging software packages. All data denoising processes were performed in subject specific space. Only for group

level seed-based connectivity analysis were images normalised and co-registered to MNI space.

Multi-echo EPI data was first split into individual echo times series (using the FSL function 'fslsplit'). In each echo time series, signal outliers were removed using the '3dDespike' routine found in the 'Analysis of Functional Neuroimages' (AFNI) software suite (Cox 1996). To correct for subject motion, the first echo (TE=12ms) timeseries were realigned to a base volume using '3dVolreg' (AFNI). Motion correction parameters were saved and applied to the second and third echo timeseries using '3Drotate' (AFNI). Individual echo time series were subsequently corrected for slice timing acquisition differences using '3dTshift' (AFNI). Brain extraction was performed to remove extra-cerebral signal from the first echo (using the 'BET' routine found in FSL). This 'skull-stripped' first echo image was then binarized and used as a mask to remove extra-cerebral signal from the other echo time series. All three 'skull-stripped' echo time series were concatenated along the z-axis for input into the ME-ICA denoising program (tedana.py, AFNI).

8.2.3 ME-ICA denoising

The ME-ICA denoising protocol has been previously described in Chapter 2 (section 2.3.4)**.** Output images from the ME-ICA processing consist of an optimally combined echo timeseries and a de-noised optimally combined echo timeseries. The latter de-noised timeseries was used for the functional connectivity analysis.

8.2.4 Spatial and temporal filtering

Prior to seed based connectivity analysis, additional filtering was applied; deep white matter and CSF signal regression, bandpass filtering and spatial smoothing.

Subject structural T1 images were segmented into grey matter (GM), white matter (WM) and cerebrospinal fluid (CSF) (FMRIB's Automated Segmentation Tool, *FAST,* FSL, (Zhang, Brady, and Smith 2001)). WM and CSF segmentations were eroded (fslmaths, FSL), for extraction of deep WM and CSF time series and to avoid

contamination of grey matter partial volume signal, and co-registered to the functional time series using the inverse registration affine parameters saved previously. WM and CSF signal timeseries were extracted from the denoised optimally combined dataset and combined with the six affine motion correction regressors which were then regressed from the denoised timeseries (fsl_glm, FSL)(a total of eight regressors; WM, CSF and 6 x head motion).

A temporal bandpass filter (0.01hz – 0.1hz) was applied (fslmaths, FSL) and images were spatially smoothed using a full width half maximum gaussian kernel of 8 x 8 x 8 mm^3.

Finally, denoised and filtered timeseries were normalised to MNI space by applying the saved transformation steps using Advanced Normalisation Tools (ANTs)(Avants et al. 2011; Avants et al. 2014).

8.2.5 Seed based connectivity analysis

Based on several previous publications, analysis of the resting state -BOLD (rs-BOLD) multi-echo data was conducted to examine insulin related functional connectivity changes using a seed based connectivity approach using two anatomical regions; the insula cortex and the hippocampus.

Mean signal time series data from denoised and filtered datasets were extracted for each subject from the defined seeds independently (3dROIstats, AFNI). A whole brain voxel-wise correlation was performed between the processed timeseries and the seed extracted time series (3dTcorr1D, AFNI) to produce a whole brain correlation maps (R values) for each subject. R values from these correlational maps were converted into z-scores using the Fisher Z-transformation (3dcalc, AFNI), to produce a seed specific Z-map for each subject in preparation for group level analysis.

8.2.5.1 Insula seeds

The insula has been shown to be responsive to intranasal insulin administration (Schilling et al. 2014) but little is known about the modulatory effects insulin may have on the regional functional connections of this substrate with other parts of the brain. Spherical seeds with a 5mm radius were created for both left and right anterior and posterior divisions of the insula, based on co-ordinates from *Taylor et al.,* (Taylor, Seminowicz, and Davis 2009)(displayed in Figure 8.2.1, coordinates in Table 8.2.1). The insula cortex is particularly large in volume and with known anatomical and functional segregations (Kurth, Zilles, et al. 2010; Stephani et al. 2011). This was taken into consideration in the design stage of the analysis and the seeds were created based on functional parcellations of the insula.

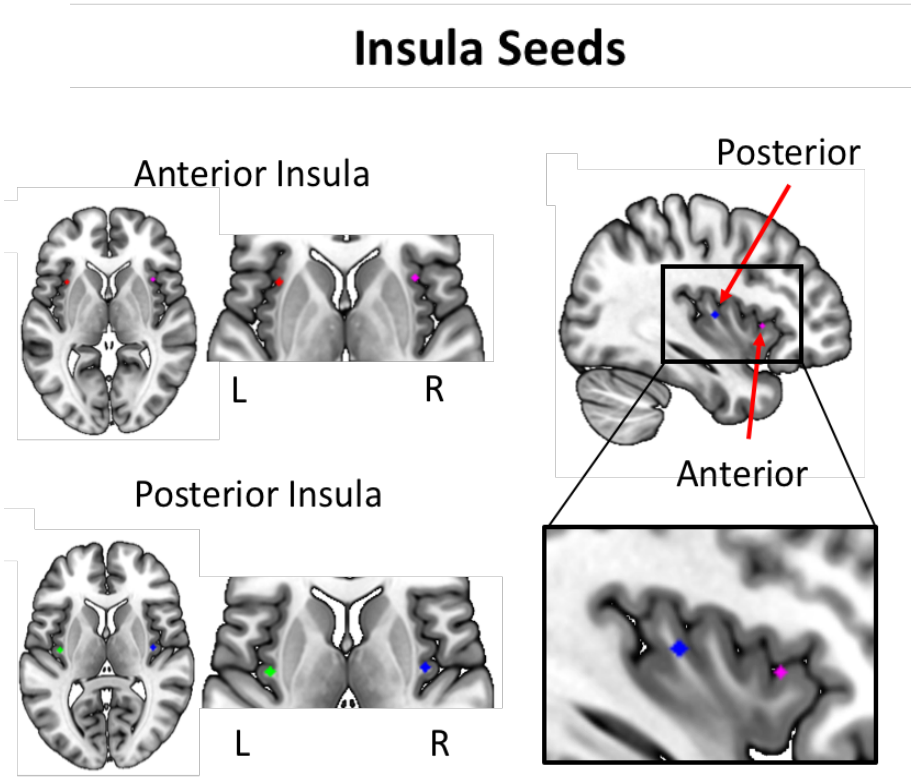

Figure 8.2.1 An image showing the locations of the four insula seeds used in this resting state analysis overlaid onto structural MNI image. The seeds in the images are smaller in volume than the 5mm spherical seeds employed in the analysis. The seeds correspond to the left and right anterior and posterior insula, respectively.

Insula seeds used for functional connectivity analysis	
Region	**MNI coordinates**
L Anterior Insula	-34 14 2
R Anterior Insula	36 16 2
L Posterior Insula	-38 -12 7
R Posterior Insula	38 -10 7

Table 8.2.1 Insula seed coordinates used in the resting state analysis.

8.2.5.2 Hippocampus Seeds

The hippocampus has an abundance of insulin receptors and is thought to be crucial in several memory related processes (Ott et al. 2012). Hippocampal seeds were defined by the creation of 5mm radius spheres within the left and right anterior and posterior regions of the hippocampus as defined by *Kahn et al.,* (Kahn et al. 2008)(displayed in Figure 8.2.2).

Hippocampus Seeds

Hippocampal seeds used for functional connectivity analysis	
Region	**MNI coordinates**
L Anterior Hippocampus	-24 -14 -20
R Anterior Hippocampus	24 -14 - 20
L Posterior Hippocampus	-26 -34 -4
R Posterior Hippocampus	26 -34 -4

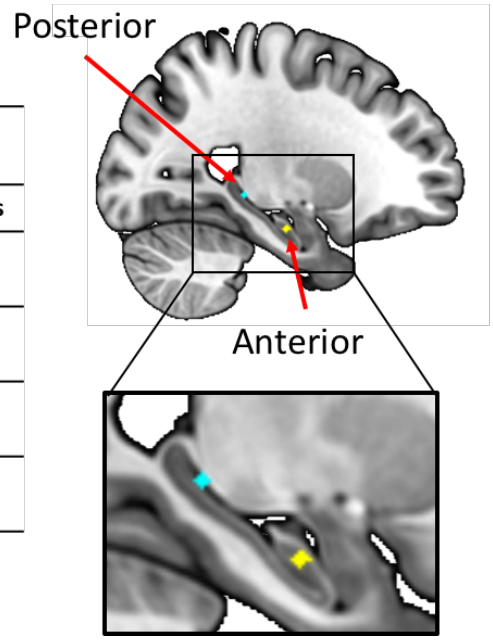

Figure 8.2.2 A table of hippocampus seed coordinates and the posterior and anterior hippocampus seed locations displayed onto a structural MNI image.

8.2.6 Group level analysis

A random effects group level analysis was conducted to explore insulin related functional connectivity effects and also within treatment group effects. For each seed, subject specific z-maps were entered into a second level repeated measures factorial model (SPM-12) with three factors; subject, drug (insulin, placebo) and group (lean, OW). Four linear contrasts of interest were created to explore for the main effects of drug and any drug by group interactions:

1. Insulin > Placebo (Main effect of insulin)
2. Insulin < Placebo (Main effect of placebo)
3. Lean Insulin > Placebo, OW Insulin < Placebo (Interaction 1)
4. Lean Insulin < Placebo, OW Insulin > Placebo (interaction 2)

The resulting statistical parametric t-maps created from this second level model were set to a cluster forming voxel threshold of $p < 0.001$ uncorrected. This seed based connectivity analysis was performed using a total of the eight seeds described earlier. The statistical threshold of the FWE correction for multiple comparisons was adjusted for multiple seeds and tests (0.05/8). The statistical cluster extent threshold was set to FWE $p < 0.0063$ to address the multiple seed/testing issue. Therefore, only clusters that survived the statistical threshold of $p < 0.0063$ (FWE-corrected) will be reported as significant.

The repeated measures ANOVA model employed at the second level (known in SPM as a flexible factorial model) is limited to interrogate treatment related effects and group by treatment interactions, but not main group effects. Significant clusters observed from either of the interaction contrasts tested were interrogated further in two ways.

Firstly, *group effects* were tested within treatment using whole brain unpaired (two-sample) t-tests. Linear contrasts for lean vs OW were created and tested. This whole

brain parametric analysis used a cluster forming voxel threshold of $p < 0.001$ and significant clusters were reported based on a $p < 0.05$, FWE-corrected statistical threshold. Furthermore, one sample t-tests within group for each treatment were conducted and presented to visualise the network structure generated from those seeds that were taken through to post-hoc analysis.

Secondly, *treatment effects* were tested within groups by creation of whole brain paired t-tests. Linear treatment contrasts (i.e. IN-INS > IN-PLA) within these paired t-tests were created and tested. Whole brain paired t-tests conducted in the lean group were performed both with and without the addition of the HOMA-IR score (calculated in Chapter 5, section 5.1.5) as an additional regressor of no interest (nuisance covariate) within the model. This regressor was added to help account for some of the physiological variance witnessed at baseline in the lean group (as detailed in Chapter 5, section 5.1.6). This methodological addition was only implemented in the lean group and not the OW group. In the OW group, one of the participants did not provide a full blood profile and therefore baseline HOMA-IR scores could not be used as a nuisance regressor in this OW group analysis.

For illustration purposes, all statistical t-maps are overlaid onto a T1 weighted MNI oriented image using MRIcroGL. Anatomical assignment of statistically significant clusters was done with the built-in probabilistic atlases within FSL (FMRIB Software Library version 4.1.9 www.fmrib.ox.ac.uk/fsl).

8.3 Results

8.3.1 Group level analysis

8.3.1.1 Anterior insula – *left and right*

Results from random effects group level repeated measures factorial model analysis did not reveal any main treatment effects or interaction effects of functional connectivity for either the left or right anterior insula seed correlations.

8.3.1.2 Posterior insula seed – *left and right*

For the right posterior insula, whole brain repeated measures analysis did not reveal any significant main treatment or interaction effects on functional connectivity.

Whole brain results from random effects group level analysis for the **l**eft posterior insula produced three large clusters from the interaction 1 contrast (Lean IN-INS > IN-PLA, OW IN-INS < IN-PLA) (see Figure 8.3.1 and Table 8.3.1). These clusters, were situated around the left dorsal medial prefrontal cortex (dmPFC), left lateral occipital cortex and left middle temporal gyrus with the left dmPFC cluster surviving multiple seed correction ($p < 0.05$, FWE – corrected).

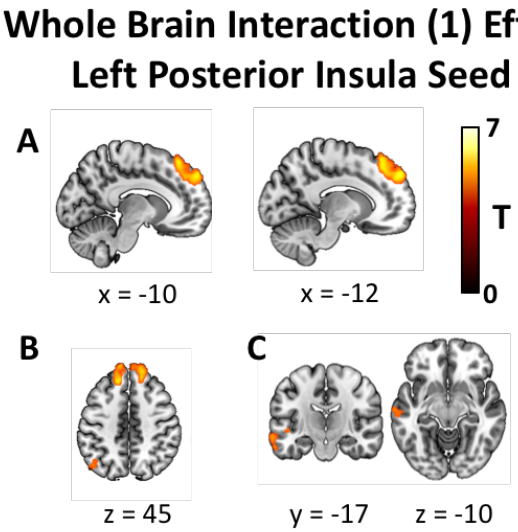

Figure 8.3.1 An image showing the left posterior insula seed interaction (1) effect t-map overlaid onto a structural MNI image. Maps contain only clusters that survived p < 0.05, FWE – corrected cluster extent statistical threshold. A) Sagittal slices show statistically significant cluster formations in the dmPFC region, which survived multiple seed correction. B) An axial slice illustrating the dmPFC significant cluster. C) Coronal and axial slices illustrating the middle temporal gyrus cluster which did not survive the multiple seed correction threshold.

Whole Brain Interaction Effect (1) statistics - Left PI seed				
Region	**P value (FWE-corrected)**	**Cluster Size**	**T-score**	**MNI coordinates**
Left Dorsal Medial Prefrontal Cortex	**0.000**	1488	5.71	-12 54 40
Left Lateral Occipital Cortex	0.037	325	4.71	-46 -72 56
Left Middle Temporal Gyrus	0.045	308	4.37	-66 -18 -14

Table 8.3.1 Whole brain statistic results from the interaction (1) effect observed from the repeated measures ANOVA analysis conducted for the left posterior insula seed. Cluster size refers to the number of voxels within the significant cluster. p values in BOLD correspond to those clusters that survived multiple seed correction threshold. Lean (n=12), OW (n=15).

8.3.1.3 Left posterior insula seed - group effects

Following this interaction effect whole brain unpaired t-tests were conducted to look for functional connectivity group differences, within treatment. This analysis did not reveal any significant between group effects for either the IN-PLA session or the IN-INS session.

8.3.1.4 Left posterior insula seed - treatment effects

Post hoc analysis whole brain paired t-tests were conducted for the left posterior insula seed correlation Z-maps to explore this interaction effect.
Paired t-tests performed in the OW group did not reveal any significant treatment effects.

The paired t-test conducted **without** the addition of the HOMA-IR regressor in the lean group (IN-INS > IN-PLA) revealed a large significant cluster (823 voxels, $p < 0.001$, FWE-corrected) situated over the left and right precuneus/posterior cingulate cortex (PCC) (see Figure 8.3.2 and Table 8.3.2).

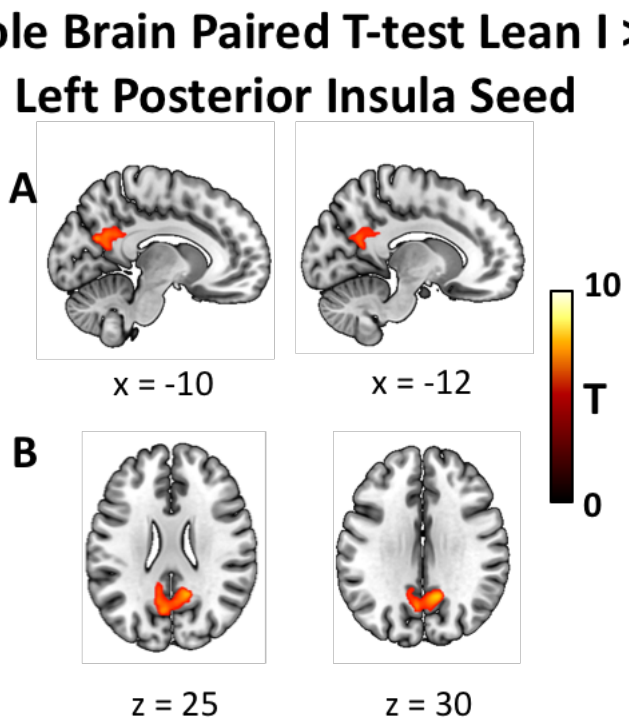

Figure 8.3.2 Whole brain paired t-test, t-map for the left posterior insula seed (IN-INS > IN-PLA) in the lean group overlaid onto a structural MNI template. A) sagittal and B) axials sections show increased functional connectivity between the left posterior insula seed and the PCC following IN-INS vs IN-PLA.

Whole Brain statistics – Lean: Insulin > placebo - Left PI seed				
Region	**P value (FWE-corrected)**	**Cluster Size**	**T-score**	**MNI coordinates**
Left and Right Precuneus Cortex	**0.000**	823	7.15	12 -56 28

Table 8.3.2 Whole brain statistics for the lean group left posterior insula seed connectivity paired t-test.

Similarly, the paired t-test conducted **with** HOMA-IR regressors (lean: IN-INS > IN-PLA) revealed two large significant clusters, that both survived the multiple seed correction threshold (see Figure 8.3.3 and Table 8.3.3),situated over the left and right precuneus/PCC and the dmPFC, respectively. These whole brain post hoc analyses IN-INS show an increase in functional connectivity between the left posterior insula seed and regions of the PCC and dmPFC when compared to IN-PLA.

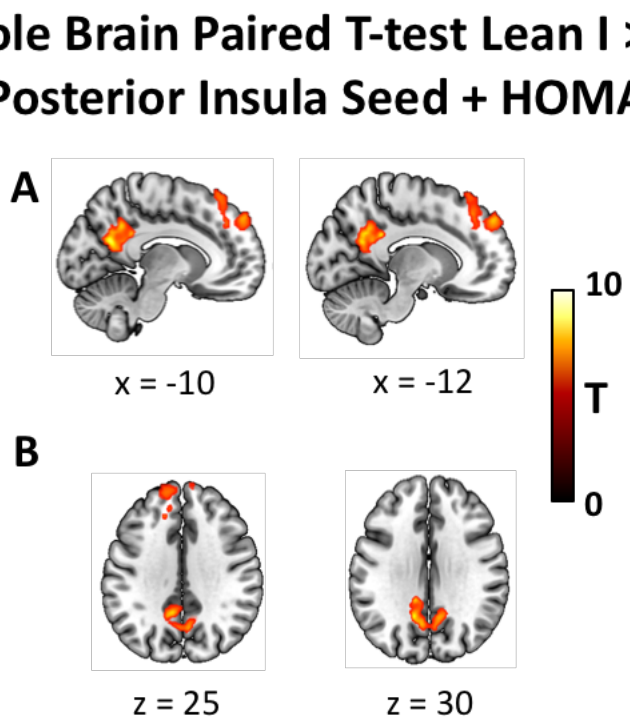

Figure 8.3.3 Whole brain paired t-test, t-map for the left posterior insula seed (IN-INS > IN-PLA) in the lean group, with the addition of HOMA-IR scores as a regressor of no interest overlaid onto a structural MNI template. A) sagittal and B) axials sections show increased functional connectivity between the left posterior insula seed with the PCC and dmPFC following IN-INS vs IN-PLA.

Whole Brain statistics – Lean: Insulin > placebo - Left PI seed + HOMA				
Region	**P value (FWE-corrected)**	**Cluster Size**	**T-score**	**MNI coordinates**
Left and Right Precuneus Cortex	**0.000**	1014	9.71	-8 -64 22
Left and Right Dorsal Medial Prefrontal Cortex	**0.000**	1066	7.16	-14 54 40

Table 8.3.3 Whole brain statistics for the lean group left posterior insula seed connectivity paired t-test, with additional HOMA-IR score regressor.

8.3.1.5 Anterior hippocampus – *left and right*

No significant effects were seen from whole brain analysis for either the left or the right anterior hippocampal seed correlations.

8.3.1.6 Posterior hippocampus – *left and right*

Using the right posterior hippocampus as a seed region, group level whole brain repeated measures analysis did not reveal any main treatment effects. From the interaction 1 contrast (Lean IN-INS > IN-PLA, OW IN-INS < IN-PLA), a cluster was identified in the right somatosensory cortex but did not survive multiple seed correction (335 voxels, $p = 0.043$). Therefore, post hoc analysis was not conducted for this seed.

Using the left posterior hippocampal seed, whole brain group level analysis showed that for the interaction 1 contrast (Lean IN-INS > IN-PLA, OW IN-INS < IN-PLA) revealed two large clusters (significant at $p < 0.05$, FWE) (see Figure 8.3.4 and Table 8.3.4), one of which survived multiple seed correction and one which did not. The significant cluster which survived multiple comparison correction (608 voxels) was situated around the right somatosensory cortex and the other (406 voxels) was situated around the left middle frontal gyrus.

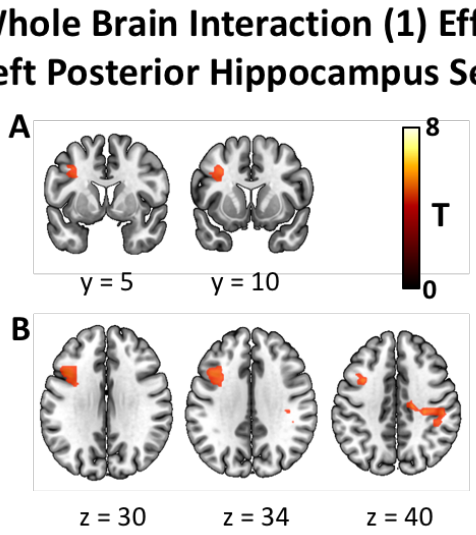

Figure 8.3.4 An image showing the left posterior hippocampus seed interaction (1) effect t-map overlaid onto a structural MNI image. Maps contain only clusters that survived $p < 0.05$, FWE – corrected cluster extent statistical threshold. A) Coronal slices show statistically significant clusters in the left middle frontal gyrus region, which did not survive multiple seed correction. B) Axial slices illustrating the left middle frontal gyrus cluster as well as the right somatosensory cortex significant cluster

Whole Brain Interaction Effect (1) statistics - Left PH seed				
Region	**P value (FWE-corrected)**	**Cluster Size**	**T-score**	**MNI coordinates**
Right Sensory Cortex	**0.004**	608	4.48	50 -26 42
Left Middle Frontal Gyrus	0.025	406	4.32	-34 8 40

Table 8.3.4 Whole brain statistic results from the interaction (1) effect observed from the repeated measures ANOVA analysis conducted for the left posterior hippocampus seed. Cluster size refers to the number of voxels within the cluster. p values in BOLD correspond to those clusters that survived multiple seed correction threshold. Lean (n=12), OW (n=15).

8.3.1.7 Left posterior hippocampus seed - group effects

Whole brain one sample t-tests are presented in Figure 8.3.5 for each group showing the spatial extent of the left posterior hippocampus functional connectivity maps, for display purposes.

Following IN-PLA there was a significant increase in functional connectivity seen between the left posterior hippocampus seed region and a region in the right primary sensory cortex in the OW group vs the lean group (see Figure 8.3.6 and Table 8.3.5). There were no significant increases in functional connectivity in the lean group when compared against the OW group for this seed following IN-PLA administration.

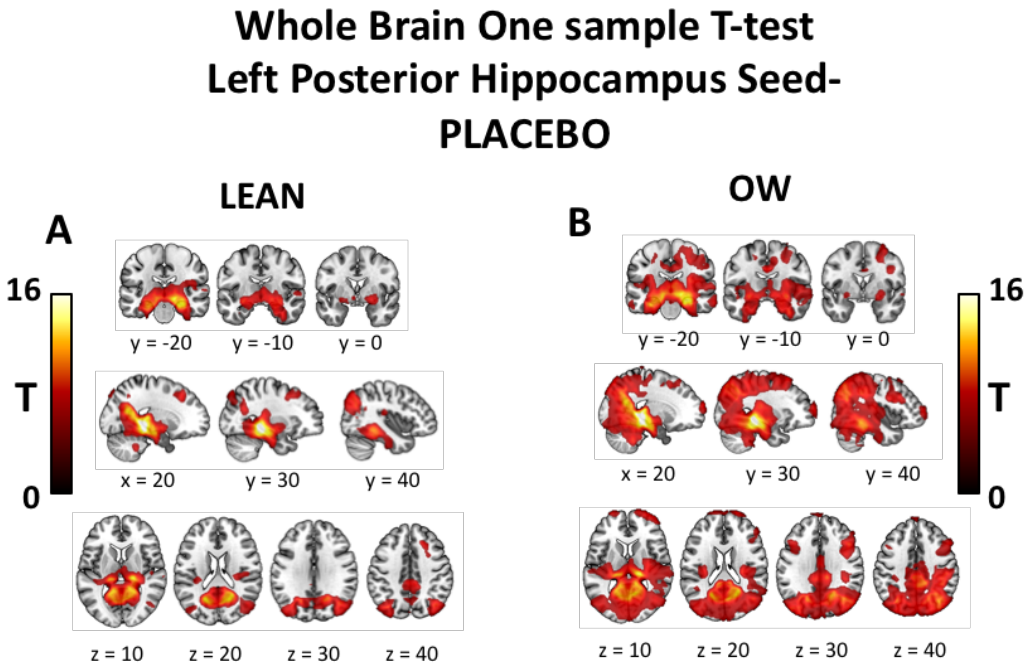

Figure 8.3.5 Whole brain one sample t-tests for each group for the left posterior hippocampus seed. A) lean and B) OW group functional connectivity maps, thresholded to $p < 0.05$, FWE-corrected level following IN-PLA administration

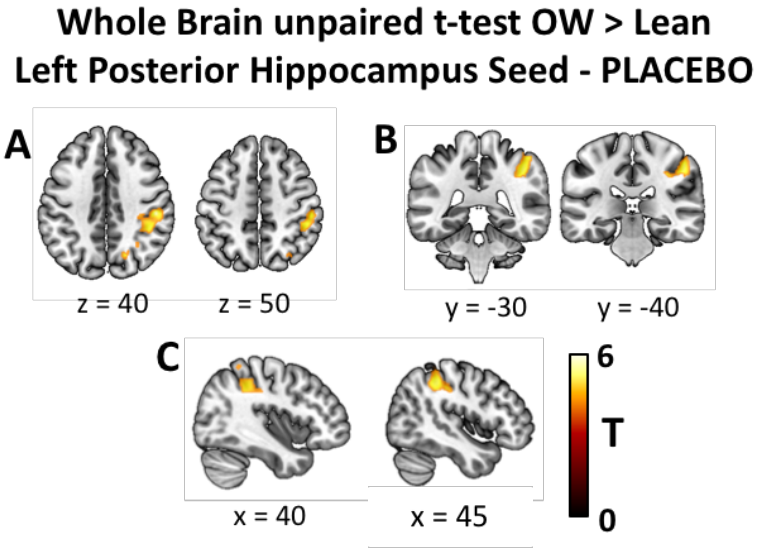

Figure 8.3.6 T-map overlaid onto a structural MNI showing group differences (OW > lean) for the left posterior hippocampus seed, following IN-PLA administration. A) axial, B) coronal and C) sagittal sections showing the right somatosensory cortex cluster.

PLACEBO: Whole Brain statistics - Left PH seed – L < O				
Region	**P value (FWE-corrected)**	**Cluster Size**	**T-score**	**MNI coordinates**
Right Sensory Cortex	**0.001**	883	5.62	50 -26 40

Table 8.3.5 Statistics from the left posterior hippocampus seed group differences OW > lean, IN-PLA.

Whole brain one sample t-test maps for both groups following IN-INS are presented in Figure 8.3.7. Following IN-INS there was a significant increase in functional connectivity seen between the hippocampus seed and a region corresponding to the right middle/superior frontal gyrus (Figure 8.3.7 and Table 8.3.6) in the lean group compared to the OW group. There were no other statistical group related differences seen for the IN-INS condition.

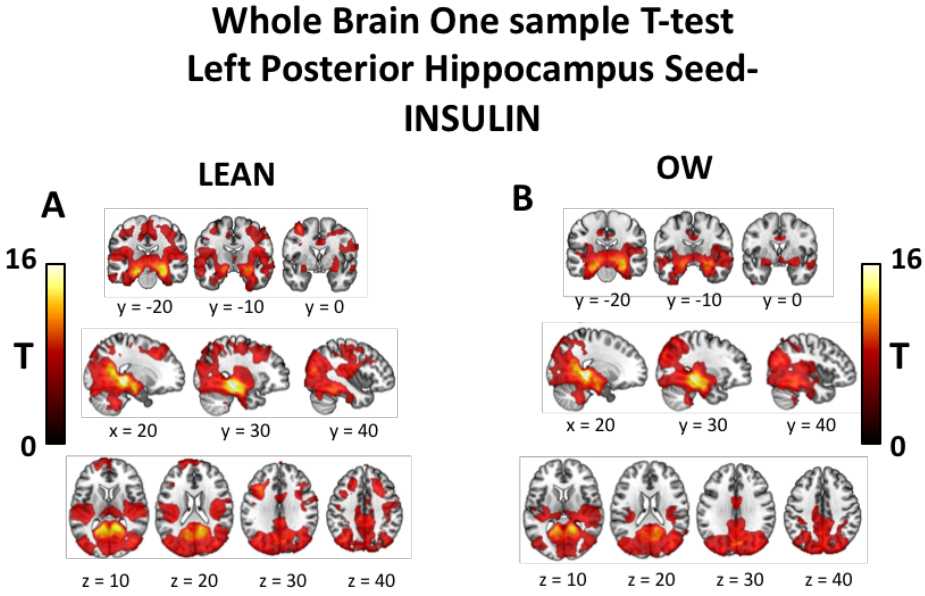

Figure 8.3.7 Whole brain one sample t-tests for each group for the left posterior hippocampus seed. A) lean and B) OW group functional connectivity maps, thresholded to $p < 0.05$, FWE-corrected level following IN-INS administration

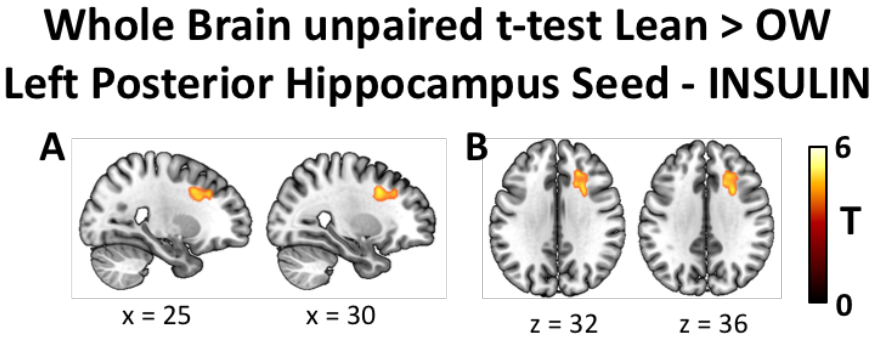

Figure 8.3.8 t-map overlaid onto a structural MNI showing group differences (Lean > OW) for the left posterior hippocampus seed, following IN-INS administration. A) Sagittal and B) axial sections showing the right middle frontal gyrus cluster.

INSULIN: Whole Brain statistics - Left PH seed – L > O				
Region	**P value (FWE-corrected)**	**Cluster Size**	**T-score**	**MNI coordinates**
Right Middle/superior frontal gyrus	**0.006**	550	5.43	28 12 36

Table 8.3.6 Statistics from the left posterior hippocampus seed group differences Lean > OW, IN-INS.

8.3.1.8 Left posterior hippocampus seed - treatment effects

Following the significant interaction effect seen from the whole group ANOVA model post hoc whole brain paired t-tests were then performed in the lean and OW group to look for within group treatment effects. Post hoc whole brain paired t-tests within the OW group did not reveal any significant treatment effects.

Post hoc whole brain paired t-tests within the lean group (IN-INS > IN-PLA) with no additional regressors provided a large significant cluster (526 voxels, $p = 0.001$, FWE-corrected) around the left fusiform gyrus (Figure 8.3.9 and Table 8.3.7).

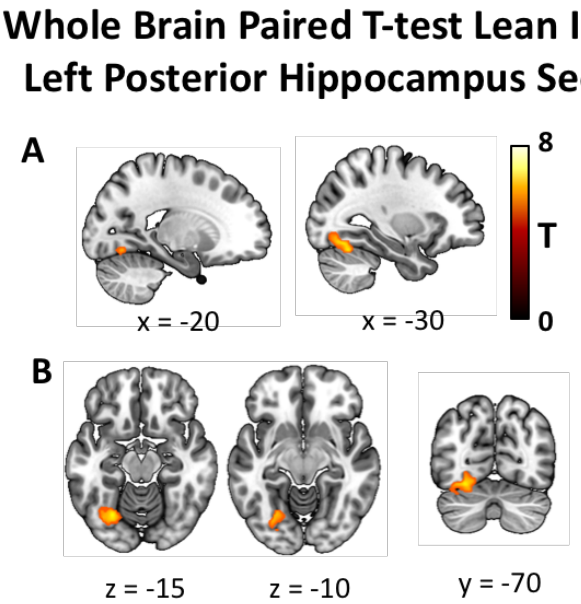

Figure 8.3.9 t-map overlaid onto structural MNI image from lean group IN-INS > IN-PLA (paired t-test). A) Sagittal and B) Axial and coronal sections showing IN-INS related increase in functional connectivity within the fusiform gyrus.

Whole Brain statistics – Lean Insulin > placebo - Left PH seed				
Region	**P value (FWE-corrected)**	**Cluster Size**	**T-score**	**MNI coordinates**
Left Fusiform Gyrus and Extrastriate Cortex	**0.001**	526	6.11	-28 -68 14

Table 8.3.7 Whole brain statistics for the lean group left posterior hippocampus seed connectivity paired t-test (IN-INS > IN-PLA).

With the addition of the HOMA-IR regressor into the paired t-test model, a significant cluster was obtained in the left fusiform gyrus (451 voxels, p = 0.002, FWE-corrected) (see Figure 8.3.10 and Table 8.3.8).

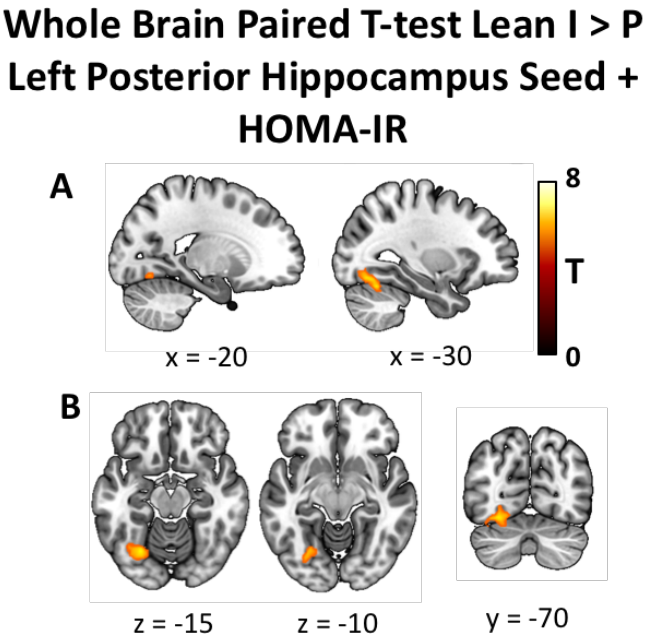

Figure 8.3.10 t-map overlaid onto structural MNI image from lean group IN-INS > IN-PLA (paired t-test) with the inclusion of HOMA-IR regressor into the model. A) Sagittal and B) Axial and coronal sections showing IN-INS related increase in functional connectivity within the fusiform gyrus.

Whole Brain statistics – Lean Insulin > placebo - Left PH seed + HOMA				
Region	**P value (FWE-corrected)**	**Cluster Size**	**T-score**	**MNI coordinates**
Left Fusiform Gyrus and Extrastriate Cortex	**0.002**	451	6.21	-28 -68 14

Table 8.3.8 Whole brain statistics for the lean group left posterior hippocampus seed connectivity paired t-test (IN-INS > IN-PLA) with the addition of HOMA-IR scores as a regressor of no interest.

8.3.2 Additional procedures to aid interpretation of treatment effects

Following formation of significant clusters from treatment effect contrasts within the post-hoc paired t-test analyses (with HOMA-IR regressors), there were additional steps taken to aid interpretation of these results for both the left posterior insula and hippocampus seeds.

Firstly, the significant clusters found from whole brain paired t-test models were used as masks to extract mean correlational values (Z-scores) from subject specific z-maps and plotted to evaluate the magnitude of the correlations. These values were plotted only and not used within any statistical tests to 'supplement' the whole brain statistics observed from the paired t-test analysis.

Secondly, a potential drawback of seed-based correlational analysis is that an increase in functional connectivity between two brain regions does not inform underlying BOLD activity, rather an increase in correlation. To aid interpretation of these functional connectivity changes seen, measures of low frequency fluctuations (ALFF), which are useful for detecting the regional intensity of spontaneous fluctuations in BOLD signal (Zou et al. 2008), were obtained from significant clusters (from paired t-tests) and seed ROIs. With these cluster and seed measures the effects of insulin on ALFF can be observed, providing a better and clearer understanding of the mechanisms underlying the insulin related functional connectivity increases witnessed.

This was done by, firstly creating whole brain ALFF maps for each lean participant and each session using AFNI's 3D resting state functional connectivity program (3DRSFC, AFNI). Denoised, filtered and smoothed timeseries (the final output from image pre-processing) were used to create a voxel-wise ALFF map (for an example ALFF map see Figure 8.3.11). The signal intensity from each voxel within these maps is equal to the total power of the BOLD signal within the range 0.01 and 0.1Hz measured from that voxel timeseries. Mean ALFF values were extracted from the significant clusters and respective seeds (using 3Dmaskave, AFNI) and the mean group value was plotted for each condition.

Similarly to the extracted z-values as mentioned above, no formal statistical testing was conducted on any of the mean values extracted. All values were calculated from a mask of significant change and therefore any statistical analysis conducted using these would be biased. Therefore, only summary statistics such as the group mean will be presented and plotted.

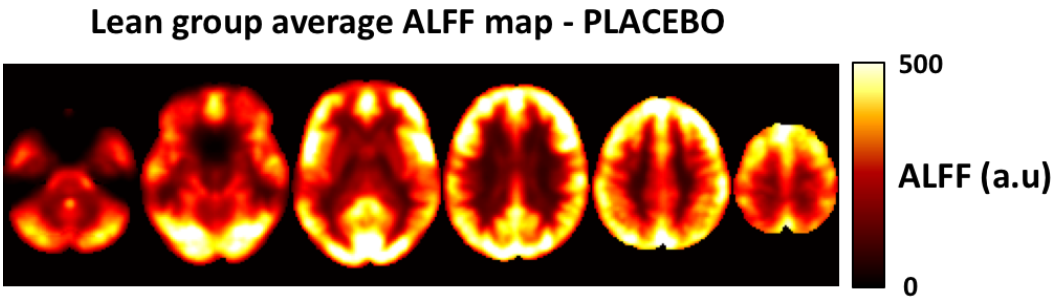

Figure 8.3.11 Axial sections of an example ALFF map made by averaging across the lean group IN-PLA session (n=12). ALFF is higher in cortical areas in comparison to sub-cortical and white matter regions.

8.3.3 Additional procedure analysis

8.3.3.1 Left posterior insula – extracted correlation values

Mean Z-scores were extracted from the significant bilateral PCC and dmPFC clusters obtained from the lean group post hoc paired t-test analysis with HOMA-IR covariate and plotted in Figure 8.3.12. From this plot it can be seen that following IN-PLA functional connectivity between these regions is negative, but in response to IN-INS, functional connectivity, as measured via correlation (Z-scores), increases from a negative value to a small positive value (mean z score IN-INS PCC = 0.04, mean z score IN-INS dmPFC = 0.09, respectively). This implies that under IN-PLA conditions the PCC and dmPFC are anti-correlated (negative z-score) with the left posterior insula seed but under IN-PLA the degree of anti-correlation changes and these regions become very slightly correlated (small positive z-score).

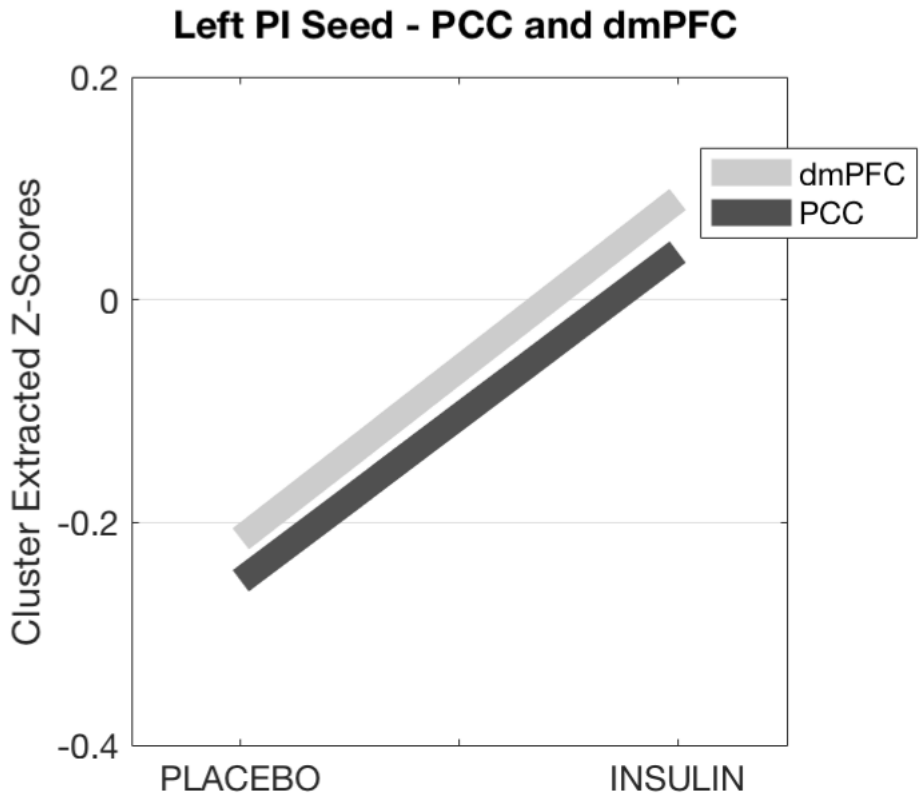

Figure 8.3.12 Line plot showing the mean Z-values from the PCC and dmPFC clusters extracted from the left posterior insula z-maps for the lean group.

Mean ALFF values extracted from the PCC, dmPFC and left posterior insula seed are plotted in Figure 8.3.13.These plots show that firstly under IN-PLA conditions that the ALFF measures between all regions are quite different, with the seed displaying the lowest ALFF measures and the dmPFC showing the greatest ALFF score. And secondly, these plots show that there is very little change between ALFF for any of these regions in response to IN-INS compared to IN-PLA.

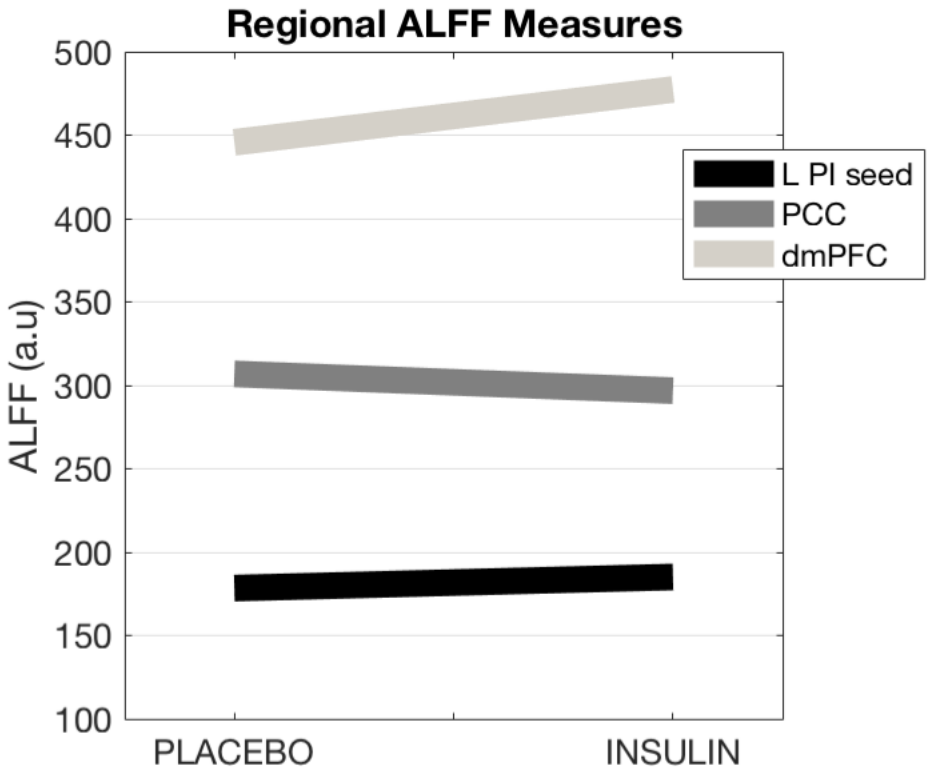

Figure 8.3.13 ALFF values extracted from the left posterior insula seed, PCC and dmPFC clusters from both IN-PLA and IN-INS ALFF maps.

For illustration and interpretation purposes, mean Z-scores were extracted from the left fusiform gyrus cluster (created from the lean paired t-test IN-INS > IN-PLA, with HOMA-IR covariate) from both IN-PLA and IN-INS sessions from the lean group only and plotted in Figure 8.3.14. From this plots it can be seen that there is an IN-INS related increase in functional connectivity between the left posterior hippocampus and the left fusiform gyrus cluster (mean z-score IN-PLA = 0.16, mean z-score IN-INS = 0.46).

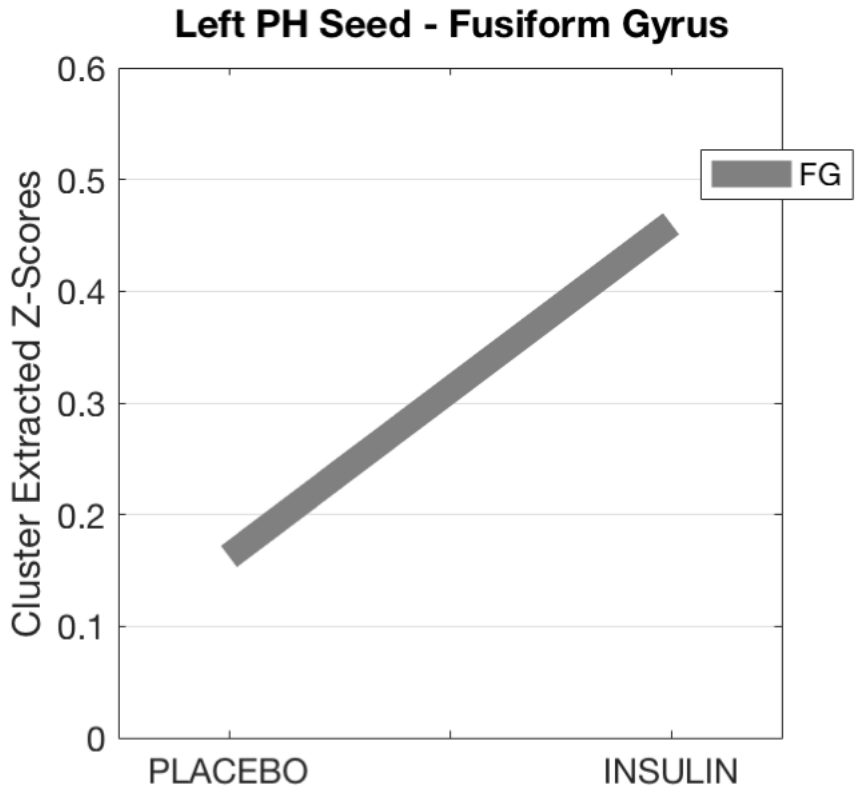

Figure 8.3.14 Line plot showing the mean Z-values from the fusiform gyrus cluster extracted from the left posterior hippocampus z-maps for the lean group.

Furthermore, mean ALFF scores were extracted from the same cluster and also from the left posterior hippocampus seed sphere for each treatment session and plotted in Figure 8.3.15. Furthermore, ALFF measurements were increased in the fusiform gyrus following IN-INS compared IN-PLA (mean ALFF IN-PLA = 401.71, mean ALFF IN-INS = 475.83). ALFF measures from the left posterior hippocampus seed were much smaller and a small increase in ALFF in response to IN-INS compared to placebo (mean ALFF IN-PLA = 127.62, mean ALFF IN-INS = 132.47) was observed. From these data, the IN-INS increase in functional connectivity between the left posterior hippocampus and a region of the left fusiform gyrus in the lean group can be clearly seen and that coupled with this increase in functional connectivity is an increase in ALFF within the fusiform gyrus region but not the posterior hippocampus seed.

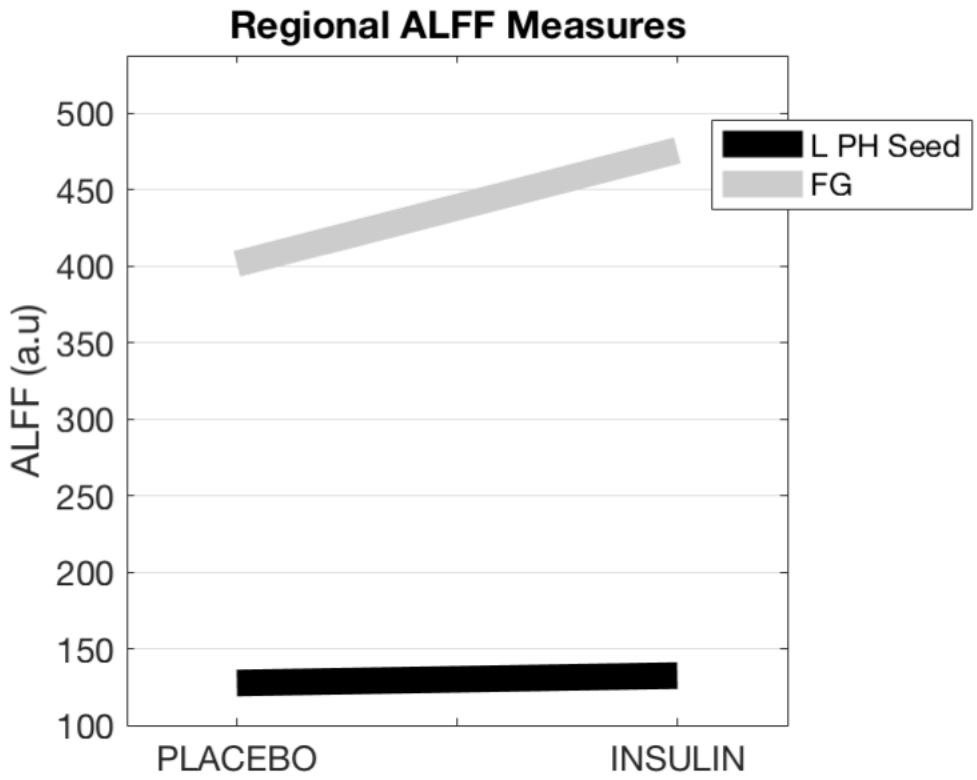

Figure 8.3.15 ALFF values extracted from the left posterior hippocampus seed, fusiform gyrus cluster from both IN-PLA and IN-INS ALFF maps.

8.4 Discussion

Seed-based connectivity analysis performed on multi-echo denoised BOLD data displayed intranasal insulin associated increases in functional connectivity between the left posterior hippocampus and the left fusiform gyrus, which was exclusive to the lean/normal weight individuals. Correlational measures between the left posterior insula and the precuneus and dmPFC were significantly modified by IN-INS, again exclusively in the lean group. Resting state neuronal information is carried by low frequency (<0.1Hz) oscillations from the time series frequency spectrum. An index of these fluctuations, in addition to the synchronicity measured as functional connectivity, is ALFF. Regional ALFF values extracted from regions significantly modulated by IN-INS were used as a supplementary information to describe the IN-INS results seen from this whole brain functional connectivity analysis.

Furthermore, group differences in the left posterior hippocampus functional connectivity was also observed. OW individuals displayed increased functional connectivity between the left posterior hippocampus seed and the right sensory cortex following IN-PLA, whereas the lean group displayed greater functional connectivity between the left posterior hippocampus and the middle frontal gyrus following IN-INS administration.

8.4.1 Relationships with insulin resistance as measured by HOMA-IR

For lean group treatment analyses, a 'default' whole brain paired t-test model was constructed as well as a paired t-test model that included the HOMA-IR score for each session as a regressor/covariate of no interest. These scores were added to the model in an attempt to explain some of the between session variability. For the left posterior hippocampus seed based analyses the addition of HOMA-IR scores had no effect on the parametric maps created when compared to the model without the added regressor. However, the addition of HOMA-IR regressor to the left posterior insula seed based analyses (lean paired t-test) provided the observation of a significant cluster formation in the region of the dmPFC, which was not observed in

the ‘default’ paired t-test model. From this observation the use of additional measures such as HOMA-IR proved beneficial in model fitting for this posterior insula seed analyses. The lack of effect seen from the posterior hippocampus seed may suggest that the effects seen in the fusiform gyrus were modelled well in the standard t-test and that the added attempt to explain any subject variability with HOMA-IR did not aid the model fitting.

This discussion will focus on interpreting each of the aforementioned results with reference to resting state as well as task based fMRI literature.

8.4.2 Insula

The insula is an anatomical substrate situated within the fold of the lateral sulcus within each hemisphere. The insula exhibits several features of functional specialisation and plays an important role in key actions such as gustatory processing (Frank, Kullmann, and Veit 2013), interoception, awareness and pain processing, providing a necessary link between sensory processing and affective system engagement (Craig 2009). The insula can be divided anatomically and functionally into the anterior and posterior sub-regions, which are bisected by the middle cerebral artery and are involved in functionally discrete processes (Flynn 1999). Furthermore, the anterior and posterior insula belong to distinct functional networks as described from seed based connectivity of resting state BOLD analysis with the anterior insula being connected with regions involved in emotional awareness and interoceptive functioning (Cauda et al. 2011). In comparison, the posterior insula is situated within a network involving sensorimotor hubs and has been thought to be involved in environmental monitoring and skeletal orientation (Cauda et al. 2011). The results from this present study showed a large effect of IN-INS on posterior insula connectivity and therefore the focus will be on this region and its associated connectivity profile.

From this multi-echo denoising data analysis it shows that, at the whole brain level, IN-INS increases functional connectivity between the posterior insula and two main hubs of the default mode network (DMN), the PCC and dmPFC, respectively (Buckner, Andrews-Hanna, and Schacter 2008). However, extracting Z-scores from the PCC and dmPFC from both sessions reveals anti-correlation (negative Z score) with the posterior insula seed timeseries following IN-PLA, but following IN-INS the degree of anti-correlation is decreased (Z score goes from negative to positive). Therefore, the effect observed at the whole brain level is not necessarily an IN-INS related increase in functional connectivity between the posterior insula seed and the PCC and dmPFC, but in fact a reduction in anti-correlation between the posterior insula and the PCC and dmPFC. The posterior insula is typically connected with the sensorimotor network (Deen, Pitskel, and Pelphrey 2011) and a large amount of task based research has also shown the posterior insula to be involved in pain related neural circuitry (Segerdahl et al. 2015). The sensorimotor network which typically involves the middle cingulate gyrus/supplementary motor area is known to be anti-correlated with the DMN at rest (Deen, Pitskel, and Pelphrey 2011). ALFF measures extracted from each of these regions do not suggest that there is any change in neural activity in either the PCC, dmPFC or posterior insula, implying that there are network level changes within the DMN and posterior insula-related sensorimotor connectivity that are causing this effect. From the analysis conducted, speculations as to why this affect is seen can be difficult and further analysis of DMN connectivity may have to be conducted to better understand this result.

8.4.3 Hippocampus

Using the posterior hippocampus as a seed region for this functional connectivity analysis permitted the observation that in response to IN-INS there was an increase in functional connectivity between this left posterior hippocampus and a region within the left fusiform gyrus. The fusiform gyrus forms part of the higher level visual cortex, residing within the ventral temporal cortex, and is well known for its involvement object recognition, face perception and processing (Downing et al. 2005). Task based fMRI studies involving the viewing of food pictures have shown the

involvement of both the fusiform gyrus and the hippocampus (Pelchat et al. 2004). Increased BOLD activity in both the fusiform gyrus and hippocampus are related to viewing of high and low calorie food pictures (Wallner-Liebmann et al. 2010) and have been associated with liking and craving for foods even from imagining and mental visualisation of different foods (Pelchat et al. 2004). In addition, the fusiform gyrus along with the hippocampus have previously been found to be modulated following IN-INS administration, within a task based food picture paradigm (Guthoff et al. 2010). *Guthoff* et al., showed that regions of both the hippocampus and fusiform gyrus displayed IN-INS related decreases in response to viewing food pictures compared to IN-PLA (Guthoff et al. 2010). They further speculate that the fusiform gyrus and hippocampus may form a circuitry that specialises in detection of food-related objects as there was no IN-INS related effects in these regions when viewing non-food pictures (Guthoff et al. 2010). Furthermore, increased central and peripheral insulin concentrations, via a hyperinsulinemic-euglycemic clamp technique, also showed bilateral fusiform gyrus decreases in BOLD activity in response to food pictures (Kroemer et al. 2013).

The fusiform gyrus has been termed an 'insulin sensitive' brain region from several reviews (Heni et al. 2015; Häring 2016; Kullmann et al. 2016). Within the current study it can be seen that there is an IN-INS related increase in connectivity between the left posterior hippocampus and fusiform gyrus, however whether this increase is driven by an overall increase or decrease in BOLD activity or neither is beyond seed based correlation analysis. From the seed based results alone one can speculate that in lean individuals, IN-INS increases connectivity between higher visual regions and memory related areas important for visual recognition or visual memory processing. Perhaps this increase in functional connectivity between these regions, seen in this analysis, is key to some of the reported cognitive and memory related benefits of IN-INS administration (Ott et al. 2012). As these data were collected during the resting state, or put another way, not during a cognitive engaging task, it is harder to interpret these findings and make fully supported claims on memory and cognitive effects in a direct manner. But the changes observed may underpin some of the

effects reported by other studies. Therefore, the interpretations of these results may be considered conjectural in the absence of data from cognitively-engaging periods. Whole brain ALFF maps were created in order to provide another perspective for the interpretation of the results from the seed based connectivity analyses. Mean ALFF values extracted from the fusiform gyrus cluster show an increase in response to IN-INS compared to IN-PLA (approximately 20%). However, for the left posterior hippocampus seed region the change in ALFF was not as pronounced as that of the fusiform, which would suggest that this increase in connectivity is driven by an insulin related increase in oscillatory BOLD signal in the fusiform gyrus as opposed to a dynamic change BOLD activity in the posterior hippocampus. *Rotte et al*., showed that participants presented increased bilateral fusiform gyrus BOLD activity in response to viewing unscrambled vs scrambled images during a hyperinsulinemic-euglycemic clamp, suggesting a role for insulin in modulating fusiform gyrus activity for imagery in general and not just food related pictures (Rotte et al. 2005). The increased connectivity seen here between these regions could be suggestive of fine tuning the visual system for object recognition.

Another speculation could be that insulin may act as a modulator to consolidate memories, particularly visual memories. Active learning of word pairs and also visualising those word pairs during memory recall increases BOLD activation within the fusiform gyrus and regions of the extra-striate visual network (Gais et al. 2007). Chronic IN-INS administration, over eight weeks showed that IN-INS treatment significantly improved word recall performance (Benedict et al. 2004). In light of this report, and coupled with fusiform gyrus involvement in memory recall paradigms, a suggestion that central insulin action within the fusiform gyrus coupled with an increased connection to the hippocampus may be key to these beneficial memory-associated effects. More research into both these regions would need to be conducted in order to supplement this suggestion. As mentioned previously, mentally visualising images of food also shows an increase in activation within the fusiform gyrus (Pelchat et al. 2004). An alternative, and final suggestion could be that during the resting state acquisition participants engaged in more imaginary and mental visualisation and perhaps this could be key to memory consolidation.

From observing the IN-PLA functional connectivity maps created using the left posterior hippocampus seed (Figure 8.3.5) the OW group display a widespread network that extends from the temporal lobe and covers a large region of the occipital lobe (visual association areas) and also prefrontal and frontal cortex regions. On the other hand, the lean group (following IN-PLA) display a much more constrained coverage comparatively to the OW group. The lean group seed based functional connectivity maps display much less cortical network connectivity. Formal whole brain comparisons revealed a statistically significant increase in connectivity between the posterior hippocampus and the right primary sensory cortex in the OW group vs the lean group.

Formal whole brain comparisons did reveal that following IN-INS administration there was a significant increase in connectivity seen between the left posterior hippocampus and the right superior medial frontal cortex/middle frontal gyrus in the lean group vs the OW group. This region has previously been shown to be insulin responsive in studies of cerebral blood flow (CBF) that have used IN-INS administration. Kullmann et al., previously showed that the right middle frontal gyrus CBF was decreased in insulin sensitive individuals (measured by HOMA-IR) but increased in insulin resistant individuals in response to IN-INS (Kullmann, Heni, Veit, Scheffler, Machann, Häring, et al. 2015). The CBF result mentioned above suggests that the right superior medial frontal cortex is an insulin sensitive region in both individuals with peripheral insulin sensitivity and resistance.

The results reported from this resting state analysis suggest a differential response within the superior medial frontal cortex and middle frontal gyrus to IN-INS administration which is in line with that seen previously (Kullmann, Heni, Veit, Scheffler, Machann, Häring, et al. 2015). However, clearly understanding the degree to which these effects share similarities, will require further interrogation. Given the anatomical location of this difference, however, one could speculate that this difference in connectivity could reflect a difference in attention as the superior medial frontal cortex is a key hub within the central executive network (Fang et al.

2016). The superior frontal cortex is recruited during working memory tasks with shapes (Yee, Roe, and Courtney 2010). A speculation could be that IN-INS increases general attention and focus that could be required for cognitive engagement, an effect which is more pronounced in the lean group, but not supported by any direct behavioural data.

As mentioned previously, the left posterior hippocampus functional connectivity maps for the lean and OW groups were visually different during IN-PLA but visually more similar following IN-INS. An observation such as this could demonstrate that under IN-PLA conditions the OW group show a high degree of functional connectivity within this network, which even when stimulated by IN-INS does not have capacity to change. On the other hand, the lean group showed a recruitment of a greater number of regions during IN-INS suggesting a potential for increased connectivity and potentially cognitive benefits. In keeping with this, the lean group may potentially have a more efficient resting state posterior hippocampal network capable of modulation, whereas the OW do not have this additional capability.

In a less speculative manner the absence of drug related effect in the OW group, could simply suggest the functional brain networks tested were not sensitive to the modulatory effects of central insulin. In a more pragmatic and critical approach it is necessary to remind the reader that this analyses was conducted exclusively at the whole brain level. In light of this simplistic approach, a more thorough region of interest based analysis approach would perhaps be more sensitive and appropriate to tease apart subtle insulin related changes in the OW group, and also additional effects in the lean group, if they exist.

Chapter 9 Discussion and Concluding Remarks

The goal of this thesis was to perform a thorough investigation into the acute functional effects of intra-nasally administered insulin in the brain. To this end, the study probed the central functional effects of insulin both at rest and during a paradigm designed to assess primary food related reward. The investigations at rest included resting state physiology (cerebral blood flow) and functional connectivity. The project was carried out in lean and overweight healthy male volunteers. Following a detailed analysis of these data, this thesis has provided new insights into the central role of insulin, which will hopefully contribute to an already extensive wealth of published data. The SNIFAR study has benefited from a range of newly developed functional imaging approaches, which have contributed to provide a collection of novel and interesting results. In this discussion, I will summarise the most pertinent findings presented in the thesis, their most relevant interpretations; and I will also present some limitations of the study and make recommendations for future research.

Main Significant Findings from the SNIFAR Study

Behavioral and Biological Analysis

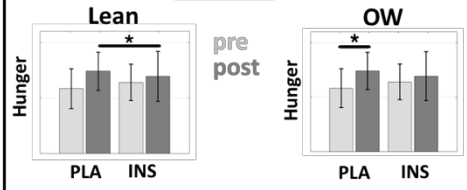

- Lean post scan hunger was significantly lower for IN-INS vs PLA
- OW hunger increased significantly overtime for PLA but not IN-INS

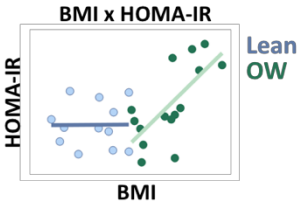

- None of the participants presented with peripheral insulin resistance. A correlation was seen between HOMA-IR and BMI in the overweight group only.

Cerebral Blood Flow Analysis

IN-INS ↓ resting CBF - OW

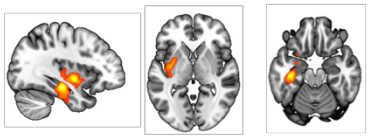

- IN-INS decreased CBF in the left posterior insula, left hippocampus, left putamen and left parrahippocampal gyrus in OW individuals.

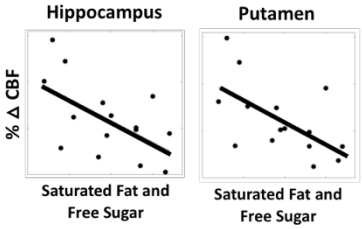

- Central INS responses in the hippocampus and putamen were lower in individuals with increased saturated fat and free sugar dietary intake.

Taste Task Analysis

Cue – anticipation (group effects)

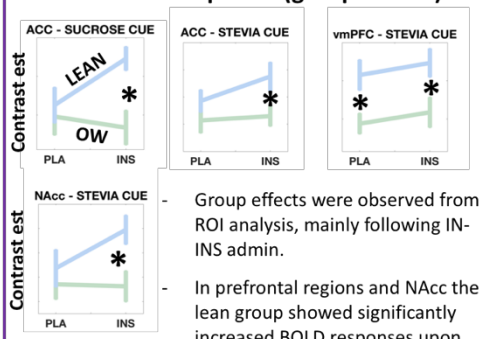

- Group effects were observed from ROI analysis, mainly following IN-INS admin.
- In prefrontal regions and NAcc the lean group showed significantly increased BOLD responses upon cue presentation.

Taste Effects

- Whole group analysis (lean + OW) showed that stevia sweetness decreased over time following both IN-PLA and INS.
- Following IN-INS admin the palatability (likeness) of stevia solution also significantly decreased.

Delivery – Consumption (drug effects)

- Whole brain drug X group interaction effect observed upon stevia delivery.

- The lean group showed an IN-INS related increase in NAcc BOLD response during second run of paradigm.

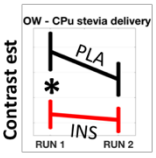

- The OW group showed an IN-INS related decrease in Caudate-putamen BOLD response during first run of paradigm.

Connectivity Analysis

IN-INS ↑ FC – left Post Hipp seed - Lean

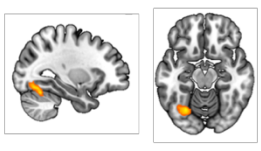

- IN-INS ↑ functional connectivity between Left Post Hippocampus seed and Left Fusiform Gyrus, in the lean group only.

Lean > OW FC – left Post Hipp seed - INS

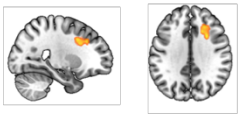

- Following IN-INS administration connectivity between Left Post Hippocampus and Right Middle frontal gyrus/dLPFC was significantly greater in lean vs OW individuals.

9.1 Analysis of Blood Samples and the Nasal Spray Device Employed

The results from the demography data were illuminating, particularly the blood analysis results. Mean fasting HOMA-IR did not differ between groups and for the lean group the HOMA-IR scores did not vary with BMI suggesting a homogeneity within the group, characteristic of an insulin sensitive phenotype. The overweight group did, on the other hand, display a positive relationship between HOMA-IR and BMI, suggestive of a relationship between markers of peripheral metabolism and body weight. In the OW data, a separation between individuals with a higher HOMA-IR and a low HOMA-IR (same range as the lean) at a BMI of 28 kg/m^2 was observed. These HOMA-IR score correlations suggest that stratification of these two groups could be made at a BMI of 28 m/kg^2. But given the small number of participants with a BMI > 28 m/kg^2 it was not possible to pursue this within the present dataset. Furthermore, HOMA-IR in this case, assessed fasting insulin resistance which is considered to be largely driven by insulin's suppressive effects on hepatic glucose release (Singh and Saxena 2010) and therefore does not reflect peripheral insulin-stimulated insulin resistance or skeletal muscle insulin resistance.

The study reported in this thesis utilised a commercial nasal spray device that was selected based after an analytical evaluation of nasal spray characteristics for nose to brain delivery of insulin. Characterisation of the pump was performed prior to the study initiation in an effort to optimise the study protocol. This is the first time that this type of characterisation and selection process has been conducted with insulin prior to a human pharmacological study. This characterisation and selection step should not be considered as just a complementary step, but rather, a critical consideration that should be encouraged for future research experiments using a less conventional administration procedure.

The use of intranasal administration to study the central effects of insulin was decided based on previous reports highlighting a short transport time into the brain

tissue (30-40 minutes (Born et al. 2002)), the limited effect this route has on peripheral blood glucose concentrations (Schmid et al. 2018; Heni et al. 2012; Heni, Wagner, et al. 2014; Kullmann et al. 2013; Kullmann et al. 2016; Kullmann, Heni, Veit, Scheffler, Machann, Häring, et al. 2015) coupled with a positive safety profile using high dose administration (i.e. 160 IU) (Schmid et al. 2018).

In this study the metabolic effects of intranasal insulin on peripheral blood measures were comparable to those previously reported (Guthoff et al. 2010), showing small decreases in plasma glucose concentration. Intranasal insulin did result in an increase in serum insulin concentrations that were significant in the overweight group, coupled with a decrease in C-peptide concentration, strongly suggesting an overspill effect of insulin into the peripheral circulation, coupled with an early counterregulatory suppression of endogenous insulin secretion. The small decrease in plasma glucose associated with the absorbed insulin was not significant in the overweight group and therefore illustrates a degree of peripheral insulin resistance within this overweight group. This reduced sensitivity to peripheral insulin was reflected in some of the imaging data, detailed below in the following sections. In the lean group, there was an increase in serum insulin associated with intranasal insulin administration, which was not significant. Surprisingly, there was a significant difference between pre-scan (fasting) serum insulin concentrations between visits which was unexpected and biologically difficult to disentangle, as serum C-peptide concentrations were comparable between visits. A potential drawback of using serum insulin levels for determining peripheral insulin resistance is that there is no standardised insulin assay but as the assay used was the same for all measures it seems odd that this group and this visit showed a high degree of serum insulin variability. Comparable to the significant trend seen in the overweight group there was a significant reduction in serum C-peptide over time which was more pronounced following intranasal insulin coupled with a small but insignificant decrease plasma glucose.

9.2 Taste Task

A major element of the SNIFAR study and a considerable component of this thesis was the acquisition of functional data during a task that delivered small amounts of liquid to the participant whilst in the scanner. The 'taste task' used in this study is a complex functional paradigm which combines elements of learning, memory, anticipation, consummation of primary rewards (liquid bolus) and also evaluation of these rewards, all within a single trial of the paradigm. Anticipating the oral delivery of sweet stimuli engaged cognitive prefrontal regions of the brain, as well as dopaminergic regions. This was the case for both lean and overweight groups. Pharmacologically challenging the central nervous system with insulin enhanced the responses to the task within these regions, but only in the lean group. In contrast, the responses to the task in the overweight group were either absent or in the opposite direction (decreases), which uncovered another potentially important functional difference between lean and overweight individuals. The prefrontal and dopaminergic regions consisted of the anterior cingulate cortex, ventromedial prefrontal cortex and the nucleus accumbens. The results presented suggest that these regions are insulin sensitive in lean individuals but show impaired insulin sensitivity with increased body weight. The ventromedial prefrontal cortex is known to be involved in encoding and performing valuations of upcoming stimuli (Hare, Camerer, and Rangel 2009); this region was also more active in the lean group under both insulin and placebo conditions. The anterior cingulate cortex, an anatomical neighbour of the ventromedial prefrontal cortex, is involved in decision making and assigning value to the outcome of decisions made (Vassena et al. 2014). Although this task did not involve subjective decision making, these insulin related modulations, as well as the ventromedial PFC activity, suggest that those with a lower BMI might be more cognitively engaged in this task, particularly during presentation of cues that occur prior to delivery of sweet stimuli. The group differences in the anterior cingulate cortex were witnessed in anticipation to both sucrose and stevia based sweet solutions, whereas the ventromedial prefrontal cortex and nucleus accumbens differences were observed only in anticipation to receiving the stevia solution.

According to classical conditioning literature, phasic dopaminergic neuron firing in the ventral tegmental area and the nucleus accumbens initially occurs in response to receipt of a primary sensory stimulus (Schultz 1998; Schultz, Dayan, and Montague 1997; Rescorla and Wagner 1972). If this stimulus is preceded by a cue, then this response is learnt (conditioned); and this phasic dopamine response shifts from being triggered by the stimulus to being triggered by cue presentation. This phenomenon is known as 'temporal difference learning' (O'Doherty et al. 2002; Schultz 2001). In lean individuals the BOLD response observed upon stevia cue presentation is greater compared to that from overweight subjects, following insulin administration. Coupled with increased prefrontal BOLD activity in the lean group, this finding would also provide support to the suggestion made on the previous page, that the lean group are more cognitively active and also more aware or alert to the stevia cue and its association with stevia taste over the combined runs (as seen from the increase in nucleus accumbens activity). In reference to reward deficiency theories of obesity (Stice et al. 2008; Burger and Stice 2011b), it could be argued that a central insulin challenge evokes a hypo-responsivity to food cues in overweight individuals, which is in contrary to classical dopamine obesity-reward theories which posit hyper-responsivity to food cues in obese individuals (Burger and Stice 2011b). Although not observed under placebo conditions, but only when challenged with central insulin, it could be argued that healthy overweight individuals respond as a 'reward deficient phenotype' when presented with predictive food related cues. Since both peripheral and central insulin levels normally rise endogenously after feeding, this finding could point to an aberrant postprandial response in the overweight but otherwise healthy population. Since this overweight group were not peripherally insulin resistant as measured by HOMA-IR, these results could be an example of an early stage dysregulation in appetite control and an early sign of prefrontal and dopaminergic central insulin resistance.

Investigation of the effect of the cerebral response to taste following intranasal insulin administration, has not been reported to date and therefore the results presented in this thesis have provided novel findings. Furthermore, the

implementation of oral stevia administration has not formed part of any functional taste investigations. Its inclusion in the SNIFAR study proved to be beneficial to further understand insulin-related and group related effects. Whole brain analysis revealed a significant drug by group interaction effect for the stevia delivery contrast within the ventromedial prefrontal cortex and rostral anterior cingulate cortex. The findings of this interaction consisted of insulin related increases and decreases in BOLD activity for lean and overweight groups, respectively. These regions have been shown to be more active to taste if the taste has been assigned a greater value (i.e. labelled as more appealing) (de Araujo et al. 2005). As previously mentioned, there was an insulin related increase in nucleus accumbens BOLD response upon the stevia cue presentation in the lean group. In keeping with this finding one could argue that the valence of this taste had been modulated under insulin conditions and therefore the taste carries increased appeal, coupled with increased BOLD responses in these regions. However, average (across run) palatability data (likeness score) did not show any changes between insulin or placebo and therefore, there is strictly no significant evidence to support this interpretation.

A set of interesting results from this taste task were discovered through region of interest analysis and given the complexity of the paradigm design, this dataset was analysed in several ways. This proved to be a worthwhile avenue that aided the understanding and interpretability of the results as a whole. Analysis of drug related effects was first performed with the two functional runs combined and secondly, for each individual run, to try and address the effects of conditioning, habituation to the taste stimuli and temporal changes in the BOLD response. This proved fruitful and revealed an insulin related increase in BOLD responsiveness within the nucleus accumbens upon receiving stevia solution during the second half of the paradigm in the lean group. This result was very interesting and opposed the effect of placebo, to which the observed nucleus accumbens BOLD response decreased over time (although not significantly). Under placebo conditions the reduced response over time would be expected, reflecting the temporal difference in the learning element of the paradigm (dopamine shift from stimulus delivery to cue presentation) (O'Doherty et al. 2004; O'Doherty et al. 2002). The nucleus accumbens responds to

salience, in the process of drawing attention to a stimulus and as a consequence, this additional attention contributes to learning. The palatability of stevia decreased over time in both groups for placebo conditions. However, following IN-INS, both the palatability (likeness) and sweetness of stevia decreased over time for both groups. This significant change in sweetness and palatability is perhaps salient and therefore the increase in BOLD activity is a reflection of encoding this salience. The change in palatability and sweetness could be of significance but how this change occurs in response to increased central insulin conditions is unknown.

Contrasts from both the stevia solution predictive cues and from the delivery of the bolus, were common to many of the statistically significant results observed. Stevia solution was employed as an alternative, low energy, but sweet tasting stimulus. Stevia is a non-nutritive sweetener that shows beneficial postprandial blood glucose effects in comparison to sucrose and other popular non-nutritive sweetener brands (Anton et al. 2010). The results reported have shown that the subjective sweetness of stevia solution decreases over time, an effect which was more pronounced following insulin administration and was coupled with a decrease in how much the stevia solution was liked over time also. This finding suggests a role for insulin in taste perception or perhaps a top down modulatory response on taste sweetness and an avenue of research that would be worthwhile pursuing. To date, only one study has looked at the effects of intranasal insulin on sensory perception. It focused on olfactory sensitivity and discrimination, highlighting an insulin related decrease in sensitivity to a non-food odorant (Brunner, Benedict, and Freiherr 2013). It would be interesting to explore olfaction and oral taste and the possible modulatory effects of insulin in a more thorough investigation with particular food odours and cues.

As the full title of the SNIFAR study suggests, one of the main aims of the investigation was to assess the modulatory effects of intranasal insulin on appetite control and reward. However, incorporating functional imaging data acquisition during periods of rest, permitted context-independent evaluation of the pharmacological effects. Additionally, interpretation on behaviour and function must however be restricted,

as the neurophysiological system being perturbed by the pharmacological agent during rest cannot, by itself, reflect behaviour.

9.3 Cerebral Blood Flow

A useful addition to the assessment of centrally acting agents are measures of regional cerebral perfusion, or blood flow (CBF) (Jenkins 2012; Mehta and O'Daly 2011; Zelaya et al. 2016). In this study, a pseudo-continuous arterial spin labelling (pCASL) sequence incorporating a long label duration, was employed to identify intranasal insulin related changes in CBF. From the unbiased, voxel-wise whole brain analysis, an intranasal insulin related decrease in CBF was witnessed within the left posterior insula, left hippocampus, left putamen and also left parahippocampal gyrus, which were all limited to the overweight group only. Another interesting observation from this assessment of CBF was that the insulin related change in hippocampal and putamen CBF showed a strong correlation with saturated fat intake and sugar intake scores assessed with questionnaires at screening. This work showed that diet composition is related to regional neuronal insulin sensitivity and supports the suggested relationship between high fat, high carbohydrate diets and reduced neuronal insulin sensitivity (von Frankenberg et al. 2017). Despite this illustrated relationship, the information gathered to make these observations is from overweight individuals who are by all accounts healthy (disease free) and this must be borne in mind when interpretating the data in a clinical context. With that caveat, these correlations do suggest that having an overweight BMI in combination with a diet high in saturated fat and sugar may lead to reduced insulin sensitivity within the hippocampus and putamen.

These are the first results to demonstrate evidence of changes in hippocampal resting activity in response to intranasal insulin. This result provides evidence that this agent affects the neuronal profile within this region, which, coupled with the reported beneficial effects of intranasal insulin on memory and cognition in Alzheimer's Disease, makes this a relevant and significant result (Craft et al. 2012; Benedict et al. 2004).

Furthermore, another important possible interpretation of these data relies on the assumption that brain insulin levels rise when peripheral insulin levels rise (Banks, Owen, and Erickson 2012; Gray, Meijer, and Barrett 2014). Hence, normal insulin sensitivity of these brain regions may be important to form memory of tastes and hence contribute to the control of feeding (Higgs 2005). For example, based on the framework set out by Higgs et al., the hippocampus works to form memories of food consumption and meals, to aid future decisions about what to eat, as well as when to next eat (Higgs et al. 2017). This was elegantly shown in amnesic individuals with impaired hippocampal-dependent memory formation function who consumed multiple meals in succession as a consequence of not remembering when they last ate (Higgs et al. 2008). These important results suggest that dysregulation of hippocampal insulin sensitivity serve as a precursor to dysregulated cognitive input to appetite control.

It is important to note that from the intranasal insulin literature, only one study has shown a significant effect of intranasal insulin on weight loss, predominantly fat tissue loss (Hallschmid et al. 2004). This study was part of an 8-week 'long term administration' study whereby intranasal insulin (160 IU) was administered daily. The acute intranasal insulin administration studies that have evaluated appetite and reward have not reported any significant changes in total food intake; or interrogated these variables using *ad libitum* food intake. Hallschmid et al., showed that intranasal insulin decreased postprandial snack intake for a certain palatable snack, but that overall calorie intake was not affected, but they consumed more of the other snacks (Hallschmid et al. 2012). This lack of empirical evidence highlights two things; firstly, studying intranasal insulin and *ad libitum* food intake is necessary for future work, and secondly, perhaps the weight loss effects of food intake are as a result of the delayed effects of insulin on possible cognitive mechanisms and top down control of food intake (Higgs and Spetter 2018; Higgs et al. 2017).

9.4 Resting State Connectivity

The resting state BOLD component of the SNIFAR study interrogated the effects of intranasal insulin on whole brain functional connectivity using a seed based connectivity approach and a newly developed denoising acquisition and processing methodology (multi-echo independent component analysis). The hippocampal region featured within this analysis, implemented as a seed region, divided into anterior and posterior subdivisions. Results from this analysis showed an insulin related increase in functional connectivity between the left posterior hippocampus and the left fusiform gyrus, which was limited to the lean group only. The fusiform gyrus is a component of the temporal visual system, typically involved in evaluating food pictures and tracking energy dense foods (van der Laan et al. 2011). The increase in connectivity between the posterior hippocampus and fusiform gyrus, observed following insulin administration, may underlie some of the memory associated benefits that were mentioned earlier in this discussion (Ott et al. 2012; Benedict et al. 2004). Furthermore, the lean group showed an increase in functional connectivity between the left posterior hippocampus and the right superior frontal gyrus in comparison to the overweight group under insulin conditions. The lean group presented with a connectivity network, (when using the left posterior hippocampus as a seed), which responded to insulin related modulation. The overweight group on the other hand presented with a similar network, under both placebo and insulin conditions, demonstrating a lack of modulation with increased central insulin. As the network seen in response to insulin in the lean group was similar to the overweight group under both conditions, it could be considered that this network is already upregulated in overweight individuals and therefore may explain the lack of insulin modulatory effect. This is of course an interesting 'observation' that requires greater interrogation.

9.5 Generalised Observations

From all of the experimental imaging chapters a common theme was observed. In most cases the analysis was kept uniform between the imaging studies employing a whole brain repeated measures factorial model to explore intranasal insulin vs placebo effects and interaction effects between group responsiveness. Not all of these models provided significant observations, however some did. In these cases, interaction effects were observed that showed intranasal insulin related increases in CBF and BOLD contrast in the lean group compared to placebo but displayed insulin related decreases in the overweight group. These observations were common occurrences throughout the results and highlight intrinsic differences between these two groups in central insulin responsiveness. This is suggestive of differential responding to intranasal insulin dependent on body mass index (BMI) alone and provides some evidence to support this basic measure as a useful tool to assess metabolic, hedonic and cognitive effects of appetite control.

9.6 Methodological Considerations and Future Work

In this multi-modal MRI study, two groups of healthy male individuals were studied. These groups were stratified based on a crude anthropometric measure (WHO 1995), BMI, and split into one group of normal weight (lean) and one group of overweight individuals (which also contained one individual who was classified as obese). BMI, essentially a ratio between mass and the square of a subject's height, was used as a recruitment and screening tool (Nuttall 2015). These individuals were stratified into two groups (lean and overweight) based on these BMI measures. It could be argued that those individuals at the BMI threshold between normal weight and overweight could be differentiated at all. This may explain why some of the group effects reported are not substantial, and this must be considered when interpreting the data. Upon reflection, splitting the two groups into BMI using a larger separation may have been a more suitable approach. Furthermore, a more comprehensive set of

measurements such as hip-waist ratio or adiposity measures such as plasma leptin concentration, may have provided additional information on body composition that may have enhanced the observed differences and aided the interpretation of the study results. Other than BMI the two groups were well matched for age and did not significantly differ on any of the screening questionnaires or measures of peripheral insulin resistance, assessed with the homeostatic model assessment of insulin resistance (Matthews, Hosker, et al. 1985; Wallace, Levy, and Matthews 2004).

This functional MRI study was conducted on a relatively small sample size. Unfortunately, there was additional exclusion of individuals from the analysis which made the sample size even more reduced. Given this, the results and data reported here must be largely considered exploratory rather than definitive. These results however, are very interesting and will inform future work and investigations into the effects of insulin administered via the nasal cavity on brain function.

The blood analysis results highlight a methodological limitation regarding the efficiency of nasal administration to selectively increase central concentrations with limited effect on peripheral blood glucose and insulin concentrations (Reger and Craft 2006). More recent options have been devised further to limit the systemic effects of insulin, such as bespoke devices and insulin formulations designed for nose to brain delivery such as those reviewed in (Warnken et al. 2016).

Regarding the nasal administration methodology used, a few considerations must be acknowledged. Firstly, the placebo treatment used in this study was a saline solution, and although appropriate in this instance, a better placebo treatment would have been a formulation derived from the vehicle constituents of the insulin solution, which has been previously reported (Schilling et al. 2014). Secondly, the study was conducted from September through to April. One concern is that during the winter period (November, December, January, February) the cold weather may have bought about extra congestion within the nasal cavity associated with the common cold (Sanu and Eccles 2008). Efforts to only scan when the participants were healthy and attempts to decongest prior to commencing the nasal administration protocol were

made; but ridding all congestion effects is perhaps unattainable. On the other hand, nasal congestion resulting from allergic rhinitis (hay fever) during the spring and summer seasons may have had a similar effect on nasal flow, which was avoided entirely by not scanning during the high pollen seasons.

In line with seasonal effects are the effects of food and alcohol consumption during the holiday periods. Several studies have shown significant weight gain and increases in fat mass over the winter holiday period (e.g. Christmas and New Year) (Hull, Hester, and Fields 2006; Diaz-Zavala et al. 2017). This is something worth considering as this may lead to some additional inter-subject variability, and perhaps a temporal physiological change reflective of a deviation from the normal baseline of certain participants. In reality avoiding these issues is difficult and one must hope that implementing short inter-scan intervals into the protocol would help prevent any major intra-subject variability.

From an acquisition and interpretation perspective (of functional imaging data), one must be aware that the changes or effects witnessed are made based on surrogate markers of neuronal activity, i.e. neuro-vascular changes that give rise to changes in CBF and BOLD contrast. Inferences based on these changes must therefore be restricted or limited as it is not possible to interpret these data in terms of *direct* changes in neuronal activity, neurotransmission or receptor-substrate activity. In terms of vasoactive effects of insulin, Grichisch et al., reported no effects of intranasal insulin (160 IU) vs placebo on visual cortex CBF during rest and also during visual stimulation (checkerboard task) (Grichisch et al. 2012). This study was limited to a single occipital region and so cannot confirm vasoactive effects on other regions where insulin receptors are more dense, or present.

The central effects of intranasal insulin reported in this thesis are made upon an assumption that exogenous insulin substrate is active within the brain tissue and it is these interactions that are driving the effects seen from imaging data analysis. This assumption is present, although not explicitly mentioned, within the published human intranasal insulin literature (Kullmann et al. 2016; Reger and Craft 2006), and

is based on work published by Born and colleagues in 2002 that showed increased concentration in cerebrospinal fluid (CSF) following intranasal insulin administration (Born et al. 2002). This work shows that CSF concentrations are increased following nasal administration. There is no denying that this description of nose to brain delivery of insulin has changed the landscape of insulin research in the brain. However, during the recent surge in intranasal insulin use as a research tool there has been very little focus on the effects of intranasal insulin on insulin receptor transmission within the olfactory bulb. This is an area of research that requires some consideration in the future.

The cohort recruited for this study were healthy male volunteers who had a range of different weights and associated BMI scores. Those individuals stratified into the overweight group did not however show a peripheral insulin resistance phenotype as measured from HOMA-IR scores. This overweight group of volunteers were healthy as attained from the screening protocol, did not smoke excessively or drink excessively (as per the exclusion criteria) and were relatively young. As insulin resistance develops over time it could be suggested that it is for these reasons that this cohort did not display signs of peripheral insulin resistance as measured by the HOMA-IR model. For future work, it would be important to investigate a group of overweight individuals who display peripheral insulin resistance, thus using insulin resistance as an inclusion criteria for recruitment. Understanding the transition phase or identifying neural correlates associated with a phenotype of non-obese but insulin resistant group of individuals would be paramount to understanding what neural responses might pre-dispose certain individuals to weight gain or development of metabolic disease.

Simulating real-life situations in a laboratory environment is a major limitation for research, especially in the investigation of food-driven reward. From the point of view of brain function, during food consumption in the 'real world' is no trivial action. Rather, it is a complex decision making process that takes into account an number of factors such as meal cost, predicted reward, logistics, convenience, mood, arousal, alcohol intake and appetite suppressant intake (nicotine, caffeine), to name but a

few (Guyenet and Schwartz 2012). This study may have benefitted from a decision making element in combination with anticipation, to better try and replicate the processes that govern food consumption (Gluck, Viswanath, and Stinson 2017) and explore in more detail the cognitive effects central insulin may potentially have.

From a methodological standpoint the 'taste task' posed some challenges. Incorporating three taste stimuli into the design of this paradigm required a balance between overall scan duration, number of events/epochs for each taste stimuli, having an appropriate inter-trial interval and time between cue and delivery events whilst taking into account taste habituation effects, participant compliance and performance. In spite of having implemented a design that balanced all those factors, a retrospective examination of this paradigm showed that there are features that could be changed or optimised in future investigations. Firstly, the use of just two tastes, one control and one rewarding, would be better suited to this style of design as it would permit both a greater number of trials for each taste and also allow for greater separation of events in time. For example, a long anticipation period, (5-7s), prior to stimulus delivery would be advantageous and would permit adequate sampling of the BOLD response associated with this anticipatory phase. This was not the case in the current work. Although an apparatus was developed and used to minimise the need for movement during the reception of the taste solutions, participant head movements occurred during swallowing periods which were modelled in the first level analysis. Standard motion correction and regression at the first level was implemented and the whole brain results generated were in line with previous literature (O'Doherty et al. 2004; O'Doherty et al. 2002; van Bloemendaal et al. 2015) and as expected. Previous research using a similar study design made use of an EEG-like cap with a single copper node attached to the neck as a fiducial marker (O'Doherty et al. 2004). Swallowing-related movements were detected and a timeseries for this fiducial marker was regressed from the time series. This seems like an easily implementable addition. Finally, this paradigm only probes taste initiated by activation of taste receptors on the tongue and does not assess the response associated with the 'flavour' experience of the stimulus. To better understand the effect of 'flavour', which is a multi-modal perception requiring the combination of

taste, aroma and also other sensory systems, the paradigm should be modified to fully model the BOLD response that follows swallowing, i.e. the post ingestion phase. This could be achieved by incorporating an 'immediate swallow', whereby the participant swallows the delivered bolus as soon as it is delivered, much like how you would drink normally (Eldeghaidy et al. 2011) This event would be followed by a sufficient consummatory phase, well after the swallow event, which incorporates the retro-nasal aroma that is produced following swallowing thus integrating taste and aroma to help create flavour perception (Eldeghaidy et al. 2011). By using this approach the movement from receiving the stimulus delivery plus swallowing would be combined into a single event thus reducing the number of motion provoking events in the design.

Finally, the external environmental factors that interact and contribute to food processing and appetite are hard to simulate and also hard to control. Overnight fasting perturbs the homeostatic system and has been shown to alter the salience of food pictures (Dagher 2012) and also increases the preference for energy dense foods over low energy food pictures (Goldstone et al. 2009). The future of functional imaging for metabolic research will require a better understanding of the environmental factors that contribute to overeating and overconsumption of energy dense, 'rewarding' foods, coupled with an understanding of the decisions made to seek out these food types as opposed to the response upon consumption. The anticipation of food is a driver of hedonic reward and one which is largely controlled by cognitive top down modulators. How does the interplay of circulating hormones such as insulin, environmental factors, and past experiences converge and how does this multi-faceted system become dysregulated or vulnerable to dysregulation in certain individuals?

9.7 Final Concluding Statements

This thesis presented work that employed a commercial nasal pump to increase central insulin concentrations via the nose to brain delivery route. The manifestations of these increased insulin concentrations were observed through the

use of both resting and task based functional imaging techniques. This work has added knowledge to the field of intranasal insulin and presented some thought provoking results. It is clear from these findings alongside the previously reported literature that the role of insulin in appetite control and subsequent food intake is multi-factorial and has implications for the homeostatic, hedonic and cognitive systems that ultimately govern food intake.

9.8 Bibliography

Adinoff, Bryon. 2004. 'Neurobiologic Processes in Drug Reward and Addiction', *Harvard review of psychiatry*, 12: 305-20.

Agrawal, Mukta, Swarnlata Saraf, Shailendra Saraf, Sophia G. Antimisiaris, Mahavir Bhupal Chougule, Sunday A. Shoyele, and Amit Alexander. 2018. 'Nose-to-brain drug delivery: An update on clinical challenges and progress towards approval of anti-Alzheimer drugs', *Journal of Controlled Release*, 281: 139-77.

Ahn, C. B., J. H. Kim, and Z. H. Cho. 1986. 'High-speed spiral-scan echo planar NMR imaging-I', *IEEE Trans Med Imaging*, 5: 2-7.

Air, E. L., M. Z. Strowski, S. C. Benoit, S. L. Conarello, G. M. Salituro, X. M. Guan, K. Liu, S. C. Woods, and B. B. Zhang. 2002. 'Small molecule insulin mimetics reduce food intake and body weight and prevent development of obesity', *Nat Med*, 8: 179-83.

Akintola, Abimbola A., Anna M. van Opstal, Rudi G. Westendorp, Iris Postmus, Jeroen van der Grond, and Diana van Heemst. 2017. 'Effect of intranasally administered insulin on cerebral blood flow and perfusion; a randomized experiment in young and older adults', *Aging (Albany NY)*, 9: 790-802.

Allen, G. V., C. B. Saper, K. M. Hurley, and D. F. Cechetto. 1991. 'Organization of visceral and limbic connections in the insular cortex of the rat', *J Comp Neurol*, 311: 1-16.

Alsop, D. C., J. A. Detre, X. Golay, M. Gunther, J. Hendrikse, L. Hernandez-Garcia, H. Lu, B. J. Macintosh, L. M. Parkes, M. Smits, M. J. van Osch, D. J. Wang, E. C. Wong, and G. Zaharchuk. 2014. 'Recommended implementation of arterial spin-labeled perfusion MRI for clinical applications: A consensus of the ISMRM perfusion study group and the European consortium for ASL in dementia', *Magn Reson Med*.

Amaro, E., Jr., and G. J. Barker. 2006. 'Study design in fMRI: basic principles', *Brain Cogn*, 60: 220-32.

Anderson, Brian A., Patryk A. Laurent, and Steven Yantis. 2014. 'Value-Driven Attentional Priority Signals in Human Basal Ganglia and Visual Cortex', *Brain Res*, 1587: 88-96.

Anton, Stephen D., Corby K. Martin, Hongmei Han, Sandra Coulon, William T. Cefalu, Paula Geiselman, and Donald A. Williamson. 2010. 'Effects of stevia, aspartame, and sucrose on food intake, satiety, and postprandial glucose and insulin levels', *Appetite*, 55: 37-43.

Arnold, Steven E., Irwin Lucki, Bethany R. Brookshire, Gregory C. Carlson, Caroline A. Browne, Hala Kazi, Sookhee Bang, Bo-Ran Choi, Yong Chen, Mary F. McMullen, and Sangwon F. Kim. 2014. 'High fat diet produces brain insulin resistance, synaptodendritic abnormalities and altered behavior in mice', *Neurobiology of disease*, 67: 79-87.

Asllani, I., A. Borogovac, and T. R. Brown. 2008. 'Regression algorithm correcting for partial volume effects in arterial spin labeling MRI', *Magn Reson Med*, 60: 1362-71.

Atlas, IDF Diabetes. 2017. 'Brussels, Belgium: international diabetes federation; 2013', *International Diabetes Federation (IDF)*.

Attwell, D., and C. Iadecola. 2002. 'The neural basis of functional brain imaging signals', *Trends Neurosci*, 25: 621-5.

Attwell, David, Alastair M. Buchan, Serge Charpak, Martin Lauritzen, Brian A. MacVicar, and Eric A. Newman. 2010. 'Glial and neuronal control of brain blood flow', *Nature*, 468: 232-43.

Avants, B. B., N. J. Tustison, M. Stauffer, G. Song, B. Wu, and J. C. Gee. 2014. 'The Insight ToolKit image registration framework', *Front Neuroinform*, 8: 44.

Avants, Brian B., Nicholas J. Tustison, Gang Song, Philip A. Cook, Arno Klein, and James C. Gee. 2011. 'A reproducible evaluation of ANTs similarity metric performance in brain image registration', *NeuroImage*, 54: 2033-44.

Balin, B. J., R. D. Broadwell, M. Salcman, and M. el-Kalliny. 1986. 'Avenues for entry of peripherally administered protein to the central nervous system in mouse, rat, and squirrel monkey', *J Comp Neurol*, 251: 260-80.

Bandettini, P. A., E. C. Wong, R. S. Hinks, R. S. Tikofsky, and J. S. Hyde. 1992. 'Time course EPI of human brain function during task activation', *Magn Reson Med*, 25: 390-7.

Bandettini, P. A., E. C. Wong, A. Jesmanowicz, R. S. Hinks, and J. S. Hyde. 1994. 'Spin-echo and gradient-echo EPI of human brain activation using BOLD contrast: a comparative study at 1.5 T', *NMR Biomed*, 7: 12-20.

Banks, William A., Abba J. Kastin, and Weihong Pan. 1999. 'Uptake and degradation of blood-borne insulin by the olfactory bulb', *Peptides*, 20: 373-78.

Banks, William A., Joshua B. Owen, and Michelle A. Erickson. 2012. 'Insulin in the brain: There and back again', *Pharmacology & Therapeutics*, 136: 82-93.

Barker, Carl. 2018. *Obesity Statistics: Briefing Paper* (Commons Library: House of Commons Library).

Baskin, D. G. 2015. 'A Historical Perspective on the Identification of Cell Types in Pancreatic Islets of Langerhans by Staining and Histochemical Techniques', *J Histochem Cytochem*, 63: 543-58.

Begley, D. J., and M. W. Brightman. 2003. 'Structural and functional aspects of the blood-brain barrier', *Prog Drug Res*, 61: 39-78.

Benedict, C., M. Hallschmid, A. Hatke, B. Schultes, H. L. Fehm, J. Born, and W. Kern. 2004. 'Intranasal insulin improves memory in humans', *Psychoneuroendocrinology*, 29: 1326-34.

Benedict, C., W. Kern, B. Schultes, J. Born, and M. Hallschmid. 2008. 'Differential sensitivity of men and women to anorexigenic and memory-improving effects of intranasal insulin', *J Clin Endocrinol Metab*, 93: 1339-44.

Berridge, K. C. 2004. 'Motivation concepts in behavioral neuroscience', *Physiol Behav*, 81: 179-209.

———. 2009. ''Liking' and 'wanting' food rewards: brain substrates and roles in eating disorders', *Physiol Behav*, 97: 537-50.

Berridge, K. C., and M. L. Kringelbach. 2008. 'Affective neuroscience of pleasure: reward in humans and animals', *Psychopharmacology (Berl)*, 199: 457-80.

Berthoud, Hans-Rudolf. 2006. 'Homeostatic and Non-homeostatic Pathways Involved in the Control of Food Intake and Energy Balance', *Obesity*, 14: 197S-200S.

Biswal, B., F. Z. Yetkin, V. M. Haughton, and J. S. Hyde. 1995. 'Functional connectivity in the motor cortex of resting human brain using echo-planar MRI', *Magn Reson Med*, 34: 537-41.

Blázquez, Enrique, Esther Velázquez, Verónica Hurtado-Carneiro, and Juan Miguel Ruiz-Albusac. 2014. 'Insulin in the Brain: Its Pathophysiological Implications for States Related with Central Insulin Resistance, Type 2 Diabetes and Alzheimer's Disease', *Frontiers in Endocrinology*, 5.

Bloch, F. 1946. 'Nuclear Induction', *Physical Review*, 70: 460-74.

Bloembergen, N., E. M. Purcell, and R. V. Pound. 1948. 'Relaxation Effects in Nuclear Magnetic Resonance Absorption', *Physical Review*, 73: 679-712.

Blum, Kenneth, John G. Cull, Eric R. Braverman, and David E. Comings. 1996. 'Reward Deficiency Syndrome', *American Scientist*, 84: 132-45.

Boghossian, Stéphane, Karalee Lemmon, MieJung Park, and David A. York. 2009. 'High-fat diets induce a rapid loss of the insulin anorectic response in the amygdala', *American Journal of Physiology-Regulatory, Integrative and Comparative Physiology*, 297: R1302-R11.

Born, J., T. Lange, W. Kern, G. P. McGregor, U. Bickel, and H. L. Fehm. 2002. 'Sniffing neuropeptides: a transnasal approach to the human brain', *Nat Neurosci*, 5: 514-6.

Braak, H., E. Braak, D. Yilmazer, and J. Bohl. 1996. 'Functional anatomy of human hippocampal formation and related structures', *J Child Neurol*, 11: 265-75.

Braude, L., and R. J. Stevenson. 2014. 'Watching television while eating increases energy intake. Examining the mechanisms in female participants', *Appetite*, 76: 9-16.

Breslin, P. A. 2013. 'An evolutionary perspective on food and human taste', *Curr Biol*, 23: R409-18.

Bruning, J. C., D. Gautam, D. J. Burks, J. Gillette, M. Schubert, P. C. Orban, R. Klein, W. Krone, D. Muller-Wieland, and C. R. Kahn. 2000. 'Role of brain insulin receptor in control of body weight and reproduction', *Science*, 289: 2122-5.

Brunner, Y. F., C. Benedict, and J. Freiherr. 2013. 'Intranasal insulin reduces olfactory sensitivity in normosmic humans', *J Clin Endocrinol Metab*, 98: E1626-30.

Bryant, E. J., N. A. King, and J. E. Blundell. 2008. 'Disinhibition: its effects on appetite and weight regulation', *Obes Rev*, 9: 409-19.

Buckner, R. L., J. R. Andrews-Hanna, and D. L. Schacter. 2008. 'The brain's default network: anatomy, function, and relevance to disease', *Ann N Y Acad Sci*, 1124: 1-38.

Burger, K. S., and E. Stice. 2011a. 'Relation of dietary restraint scores to activation of reward-related brain regions in response to food intake, anticipated intake, and food pictures', *NeuroImage*, 55: 233-9.

———. 2011b. 'Variability in reward responsivity and obesity: evidence from brain imaging studies', *Curr Drug Abuse Rev*, 4: 182-9.

Buxton, R. B. 2005. 'Quantifying CBF with arterial spin labeling', *J Magn Reson Imaging*, 22: 723-6.

———. 2013. 'The physics of functional magnetic resonance imaging (fMRI)', *Reports on Progress in Physics*, 76: 096601.

Buxton, R. B., L. R. Frank, E. C. Wong, B. Siewert, S. Warach, and R. R. Edelman. 1998. 'A general kinetic model for quantitative perfusion imaging with arterial spin labeling', *Magn Reson Med*, 40: 383-96.

Buxton, R. B., K. Uludag, D. J. Dubowitz, and T. T. Liu. 2004. 'Modeling the hemodynamic response to brain activation', *NeuroImage*, 23 Suppl 1: S220-33.

Caballero-Gaudes, César, and Richard C. Reynolds. 2017. 'Methods for cleaning the BOLD fMRI signal', *NeuroImage*, 154: 128-49.

Cabrera, O., D. M. Berman, N. S. Kenyon, C. Ricordi, P. O. Berggren, and A. Caicedo. 2006. 'The unique cytoarchitecture of human pancreatic islets has implications for islet cell function', *Proc Natl Acad Sci U S A*, 103: 2334-9.

Cahill, G. F., Jr. 1970. 'Starvation in man', *N Engl J Med*, 282: 668-75.

Carlson, Joseph J., Amy A. Turpin, Gail Wiebke, Steven C. Hunt, and Ted D. Adams. 2009. 'Pre- and post- prandial appetite hormone levels in normal weight and severely obese women', *Nutrition & metabolism*, 6: 32-32.

Cauda, F., F. D'Agata, K. Sacco, S. Duca, G. Geminiani, and A. Vercelli. 2011. 'Functional connectivity of the insula in the resting brain', *NeuroImage*, 55: 8-23.

Caumo, A., and L. Luzi. 2004. 'First-phase insulin secretion: does it exist in real life? Considerations on shape and function', *Am J Physiol Endocrinol Metab*, 287: E371-85.

Chang, J. C., M. C. Wu, I. M. Liu, and J. T. Cheng. 2005. 'Increase of insulin sensitivity by stevioside in fructose-rich chow-fed rats', *Horm Metab Res*, 37: 610-6.

Chang, Louise, Shian-Huey Chiang, and Alan R. Saltiel. 2004. 'Insulin Signaling and the Regulation of Glucose Transport', *Molecular Medicine*, 10: 65-71.

Chappell, M. A., A. R. Groves, B. J. MacIntosh, M. J. Donahue, P. Jezzard, and M. W. Woolrich. 2011. 'Partial volume correction of multiple inversion time arterial spin labeling MRI data', *Magn Reson Med*, 65: 1173-83.

Chaudhri, O. B., J. R. Parkinson, Y. T. Kuo, M. R. Druce, A. H. Herlihy, J. D. Bell, W. S. Dhillo, S. A. Stanley, M. A. Ghatei, and S. R. Bloom. 2006. 'Differential hypothalamic neuronal activation following peripheral injection of GLP-1 and oxyntomodulin in mice detected by manganese-enhanced magnetic resonance imaging', *Biochem Biophys Res Commun*, 350: 298-306.

Chechlacz, M., P. Rotshtein, S. Klamer, K. Porubska, S. Higgs, D. Booth, A. Fritsche, H. Preissl, H. Abele, N. Birbaumer, and A. Nouwen. 2009. 'Diabetes dietary management alters responses to food pictures in brain regions associated with motivation and emotion: a functional magnetic resonance imaging study', *Diabetologia*, 52: 524-33.

Cheesman, Katherine, and Edward Burdett. 2011. 'Anatomy of the nose and pharynx', *Anaesthesia & Intensive Care Medicine*, 12: 283-86.

Chen, J. J., H. D. Rosas, and D. H. Salat. 2011. 'Age-associated reductions in cerebral blood flow are independent from regional atrophy', *NeuroImage*, 55: 468-78.

Cheng, Y. S., T. D. Holmes, J. Gao, R. A. Guilmette, S. Li, Y. Surakitbanharn, and C. Rowlings. 2001. 'Characterization of nasal spray pumps and deposition pattern in a replica of the human nasal airway', *J Aerosol Med*, 14: 267-80.

Cipolla, M. J. 2009. 'Integrated Systems Physiology: From Molecule to Function.' in, *The Cerebral Circulation* (Morgan & Claypool Life Sciences

Clegg, D. J., L. M. Brown, S. C. Woods, and S. C. Benoit. 2006. 'Gonadal hormones determine sensitivity to central leptin and insulin', *Diabetes*, 55: 978-87.

Cole, David M., Stephen M. Smith, and Christian F. Beckmann. 2010. 'Advances and Pitfalls in the Analysis and Interpretation of Resting-State FMRI Data', *Frontiers in Systems Neuroscience*, 4: 8.

Coll, Anthony P., I. Sadaf Farooqi, and Stephen O'Rahilly. 2007. 'The hormonal control of food intake', *Cell*, 129: 251-62.

Comings, D. E., and K. Blum. 2000. 'Reward deficiency syndrome: genetic aspects of behavioral disorders', *Prog Brain Res*, 126: 325-41.

Cox, Robert W. 1996. 'AFNI: Software for Analysis and Visualization of Functional Magnetic Resonance Neuroimages', *Computers and Biomedical Research*, 29: 162-73.

Craft, S., L. D. Baker, T. J. Montine, S. Minoshima, G. S. Watson, A. Claxton, M. Arbuckle, M. Callaghan, E. Tsai, S. R. Plymate, P. S. Green, J. Leverenz, D. Cross, and B. Gerton. 2012. 'Intranasal insulin therapy for Alzheimer disease and amnestic mild cognitive impairment: a pilot clinical trial', *Arch Neurol*, 69: 29-38.

Craft, S., E. Peskind, M. W. Schwartz, G. D. Schellenberg, M. Raskind, and D. Porte, Jr. 1998. 'Cerebrospinal fluid and plasma insulin levels in Alzheimer's disease: relationship to severity of dementia and apolipoprotein E genotype', *Neurology*, 50: 164-8.

Craig, A. D. 2009. 'How do you feel — now? The anterior insula and human awareness', *Nature Reviews Neuroscience*, 10: 59.

Creasey, H., and S. I. Rapoport. 1985. 'The aging human brain', *Ann Neurol*, 17: 2-10.

Cullmann, M., A. Hilding, and C. G. Ostenson. 2012. 'Alcohol consumption and risk of pre-diabetes and type 2 diabetes development in a Swedish population', *Diabet Med*, 29: 441-52.

Dagher, Alain. 2012. 'Functional brain imaging of appetite', *Trends in Endocrinology & Metabolism*, 23: 250-60.

Dai, W., D. Garcia, C. de Bazelaire, and D. C. Alsop. 2008. 'Continuous flow-driven inversion for arterial spin labeling using pulsed radio frequency and gradient fields', *Magn Reson Med*, 60: 1488-97.

Dai, W., P. M. Robson, A. Shankaranarayanan, and D. C. Alsop. 2012. 'Reduced resolution transit delay prescan for quantitative continuous arterial spin labeling perfusion imaging', *Magn Reson Med*, 67: 1252-65.

Dai, W., A. Shankaranarayanan, and D. C. Alsop. 2013. 'Volumetric measurement of perfusion and arterial transit delay using hadamard encoded continuous arterial spin labeling', *Magn Reson Med*, 69: 1014-22.

Damadian, R. 1971. 'Tumor detection by nuclear magnetic resonance', *Science*, 171: 1151-3.

Davis, C., S. Strachan, and M. Berkson. 2004. 'Sensitivity to reward: implications for overeating and overweight', *Appetite*, 42: 131-8.

Dawe, S., and N. J. Loxton. 2004. 'The role of impulsivity in the development of substance use and eating disorders', *Neurosci Biobehav Rev*, 28: 343-51.

Dayal, Pankaj, Madhu Sudhan Shaik, and Mandip Singh. 2004. 'Evaluation of different parameters that affect droplet-size distribution from nasal sprays using the Malvern Spraytec®', *Journal of Pharmaceutical Sciences*, 93: 1725-42.

de Araujo, I. E., M. L. Kringelbach, E. T. Rolls, and P. Hobden. 2003. 'Representation of umami taste in the human brain', *J Neurophysiol*, 90: 313-9.

de Araujo, I. E., E. T. Rolls, M. I. Velazco, C. Margot, and I. Cayeux. 2005. 'Cognitive modulation of olfactory processing', *Neuron*, 46: 671-9.

de Araujo, Ivan E., and Edmund T. Rolls. 2004. 'Representation in the Human Brain of Food Texture and Oral Fat', *The Journal of Neuroscience*, 24: 3086.

de Lauzon, B., M. Romon, V. Deschamps, L. Lafay, J. M. Borys, J. Karlsson, P. Ducimetiere, and M. A. Charles. 2004. 'The Three-Factor Eating Questionnaire-R18 is able to distinguish among different eating patterns in a general population', *J Nutr*, 134: 2372-80.

Deen, B., N. B. Pitskel, and K. A. Pelphrey. 2011. 'Three systems of insular functional connectivity identified with cluster analysis', *Cereb Cortex*, 21: 1498-506.

Deichmann, R., J. A. Gottfried, C. Hutton, and R. Turner. 2003. 'Optimized EPI for fMRI studies of the orbitofrontal cortex', *NeuroImage*, 19: 430-41.

Desikan, R. S., F. Segonne, B. Fischl, B. T. Quinn, B. C. Dickerson, D. Blacker, R. L. Buckner, A. M. Dale, R. P. Maguire, B. T. Hyman, M. S. Albert, and R. J. Killiany. 2006. 'An automated labeling system for subdividing the human cerebral cortex on MRI scans into gyral based regions of interest', *NeuroImage*, 31: 968-80.

Detre, J. A., J. S. Leigh, D. S. Williams, and A. P. Koretsky. 1992. 'Perfusion imaging', *Magn Reson Med*, 23: 37-45.

Dhuria, S. V., L. R. Hanson, and W. H. Frey, 2nd. 2010. 'Intranasal delivery to the central nervous system: mechanisms and experimental considerations', *J Pharm Sci*, 99: 1654-73.

Diaz-Zavala, R. G., M. F. Castro-Cantu, M. E. Valencia, G. Alvarez-Hernandez, M. M. Haby, and J. Esparza-Romero. 2017. 'Effect of the Holiday Season on Weight Gain: A Narrative Review', *J Obes*, 2017: 2085136.

Dipasquale, Ottavia, Arjun Sethi, Maria Marcella Laganà, Francesca Baglio, Giuseppe Baselli, Prantik Kundu, Neil A. Harrison, and Mara Cercignani. 2017. 'Comparing resting state fMRI de-noising approaches using multi- and single-echo acquisitions', *PLoS ONE*, 12: e0173289.

Djupesland, P. G. 2013. 'Nasal drug delivery devices: characteristics and performance in a clinical perspective-a review', *Drug Deliv Transl Res*, 3: 42-62.

Doughty, Diane V., Carrie Vibbert, Anupama Kewalramani, Mary E. Bollinger, and Richard N. Dalby. 2011. 'Automated actuation of nasal spray products: determination and comparison of adult and pediatric settings', *Drug Development and Industrial Pharmacy*, 37: 359-66.

Downing, Paul E, AW-Y Chan, MV Peelen, CM Dodds, and N Kanwisher. 2005. 'Domain specificity in visual cortex', *Cerebral Cortex*, 16: 1453-61.

Drewnowski, Adam. 2007. 'The Real Contribution of Added Sugars and Fats to Obesity', *Epidemiologic Reviews*, 29: 160-71.

Edelstein, W. A., J. M. S. Hutchison, G. Johnson, and T. Redpath. 1980. 'Spin warp NMR imaging and applications to human whole-body imaging', *Physics in Medicine & Biology*, 25: 751.

Eldeghaidy, Sally, Luca Marciani, Johann C. Pfeiffer, Joanne Hort, Kay Head, Andrew J. Taylor, Robin C. Spiller, Penny A. Gowland, and Susan Francis. 2011. 'Use of an Immediate Swallow Protocol to Assess Taste and Aroma Integration in fMRI Studies', *Chemosensory Perception*, 4: 163-74.

Epstein, L. H., S. J. Salvy, K. A. Carr, K. K. Dearing, and W. K. Bickel. 2010. 'Food reinforcement, delay discounting and obesity', *Physiol Behav*, 100: 438-45.

Erbsloh, F., A. Bernsmeier, and H. Hillesheim. 1958. '[The glucose consumption of the brain & its dependence on the liver]', *Arch Psychiatr Nervenkr Z Gesamte Neurol Psychiatr*, 196: 611-26.

Erdmann, Johannes, Florian Lippl, Stefan Wagenpfeil, and Volker Schusdziarra. 2005. 'Differential Association of Basal and Postprandial Plasma Ghrelin With Leptin, Insulin, and Type 2 Diabetes', *Diabetes*, 54: 1371-78.

Evans, J.D. 1995. *Straightforward Statistics for the Behavioral Sciences: Instructor's Manual* (Brooks/Cole).

Faber, William M. 1937. 'The nasal mucosa and the subarachnoid space', *American Journal of Anatomy*, 62: 121-48.

Fang, Xiaojing, Yuanchao Zhang, Yuan Zhou, Luqi Cheng, Jin Li, Yulin Wang, Karl J. Friston, and Tianzi Jiang. 2016. 'Resting-State Coupling between Core Regions within the Central-Executive and Salience Networks Contributes to Working Memory Performance', *Frontiers in Behavioral Neuroscience*, 10.

Faul, Franz, Edgar Erdfelder, Albert-Georg Lang, and Axel Buchner. 2007. 'G*Power 3: A flexible statistical power analysis program for the social, behavioral, and biomedical sciences', *Behavior Research Methods*, 39: 175-91.

FDA, U.S. Food and Drug Administration. 2003. 'Guidance for industry: Bioavailability and Bioequivalence Studies for Nasal Aerosols and Nasal Sprays for Local Action.'.

Ferreira de Sa, D. S., A. Schulz, F. E. Streit, J. D. Turner, M. S. Oitzl, T. D. Blumenthal, and H. Schachinger. 2014. 'Cortisol, but not intranasal insulin, affects the central processing of visual food cues', *Psychoneuroendocrinology*, 50: 311-20.

Figlewicz, D. P., and S. C. Benoit. 2009. 'Insulin, leptin, and food reward: update 2008', *Am J Physiol Regul Integr Comp Physiol*, 296: R9-r19.

Figlewicz, D. P., S. B. Evans, J. Murphy, M. Hoen, and D. G. Baskin. 2003. 'Expression of receptors for insulin and leptin in the ventral tegmental area/substantia nigra (VTA/SN) of the rat', *Brain Res*, 964: 107-15.

Figlewicz, D. P., A. MacDonald Naleid, and A. J. Sipols. 2007. 'Modulation of food reward by adiposity signals', *Physiol Behav*, 91: 473-8.

Finlayson, G., N. King, and J. E. Blundell. 2007. 'Is it possible to dissociate 'liking' and 'wanting' for foods in humans? A novel experimental procedure', *Physiol Behav*, 90: 36-42.

Flint, A., A. Raben, J. E. Blundell, and A. Astrup. 2000. 'Reproducibility, power and validity of visual analogue scales in assessment of appetite sensations in single test meal studies', *Int J Obes Relat Metab Disord*, 24: 38-48.

Flynn, Frederick G. 1999. 'Anatomy of the insula functional and clinical correlates', *Aphasiology*, 13: 55-78.

Fowler, Michael J. 2008. 'Microvascular and Macrovascular Complications of Diabetes', *Clinical Diabetes*, 26: 77-82.

Fox, P. T., and M. E. Raichle. 1986. 'Focal physiological uncoupling of cerebral blood flow and oxidative metabolism during somatosensory stimulation in human subjects', *Proc Natl Acad Sci U S A*, 83: 1140-4.

Francis, H. M., and R. J. Stevenson. 2011. 'Higher reported saturated fat and refined sugar intake is associated with reduced hippocampal-dependent memory and sensitivity to interoceptive signals', *Behav Neurosci*, 125: 943-55.

Francis, H., and R. Stevenson. 2013. 'Validity and test–retest reliability of a short dietary questionnaire to assess intake of saturated fat and free sugars: a preliminary study', *Journal of Human Nutrition and Dietetics*, 26: 234-42.

Frank, Sabine, Stephanie Kullmann, and Ralf Veit. 2013. 'Food related processes in the insular cortex', *Frontiers in Human Neuroscience*, 7.

Freiherr, J., M. Hallschmid, W. H. Frey, 2nd, Y. F. Brunner, C. D. Chapman, C. Holscher, S. Craft, F. G. De Felice, and C. Benedict. 2013. 'Intranasal insulin as a treatment for Alzheimer's disease: a review of basic research and clinical evidence', *CNS Drugs*, 27: 505-14.

Fu, Zhuo, Elizabeth R. Gilbert, and Dongmin Liu. 2013. 'Regulation of Insulin Synthesis and Secretion and Pancreatic Beta-Cell Dysfunction in Diabetes', *Current diabetes reviews*, 9: 25-53.

Fulop, T., A. Larbi, and N. Douziech. 2003. 'Insulin receptor and ageing', *Pathol Biol (Paris)*, 51: 574-80.

Fung, Man Chiu, Kiao Inthavong, William Yang, Petros Lappas, and Jiyuan Tu. 2013. 'External Characteristics of Unsteady Spray Atomization from a Nasal Spray Device', *Journal of Pharmaceutical Sciences*, 102: 1024-35.

Fuster, J. M. 2001. 'The prefrontal cortex--an update: time is of the essence', *Neuron*, 30: 319-33.

Gais, Steffen, Geneviève Albouy, Mélanie Boly, Thien Thanh Dang-Vu, Annabelle Darsaud, Martin Desseilles, Géraldine Rauchs, Manuel Schabus, Virginie Sterpenich, Gilles Vandewalle, Pierre Maquet, and Philippe Peigneux. 2007. 'Sleep transforms the cerebral trace of declarative memories', *Proceedings of the National Academy of Sciences*, 104: 18778-83.

Garcia, D. M., G. Duhamel, and D. C. Alsop. 2005. 'Efficiency of inversion pulses for background suppressed arterial spin labeling', *Magn Reson Med*, 54: 366-72.

Geurkink, N. 1983. 'Nasal anatomy, physiology, and function', *J Allergy Clin Immunol*, 72: 123-8.

Ghasemi, R., A. Haeri, L. Dargahi, Z. Mohamed, and A. Ahmadiani. 2013. 'Insulin in the brain: sources, localization and functions', *Mol Neurobiol*, 47: 145-71.

Ghori, Muhammad U., Mohammed H. Mahdi, Alan M. Smith, and Barbara R. Conway. 2015. 'Nasal Drug Delivery Systems: An Overview', *American Journal of Pharmacological Sciences*, 3: 110-19.

Giovannucci, Edward, David M. Harlan, Michael C. Archer, Richard M. Bergenstal, Susan M. Gapstur, Laurel A. Habel, Michael Pollak, Judith G. Regensteiner, and Douglas Yee. 2010. 'Diabetes and cancer: a consensus report', *Diabetes Care*, 33: 1674-85.

Girouard, H., and C. Iadecola. 2006. 'Neurovascular coupling in the normal brain and in hypertension, stroke, and Alzheimer disease', *J Appl Physiol (1985)*, 100: 328-35.

Gläscher, Jan, Alan N. Hampton, and John P. O'Doherty. 2009. 'Determining a Role for Ventromedial Prefrontal Cortex in Encoding Action-Based Value Signals During Reward-Related Decision Making', *Cerebral Cortex*, 19: 483-95.

Glover, G. H. 2012. 'Spiral imaging in fMRI', *NeuroImage*, 62: 706-12.

Glover, Gary H. 2011. 'Overview of Functional Magnetic Resonance Imaging', *Neurosurgery clinics of North America*, 22: 133-39.

Gluck, M. E., P. Viswanath, and E. J. Stinson. 2017. 'Obesity, Appetite, and the Prefrontal Cortex', *Curr Obes Rep*, 6: 380-88.

Goke, B. 2008. 'Islet cell function: alpha and beta cells--partners towards normoglycaemia', *Int J Clin Pract Suppl*: 2-7.

Goldstone, A. P. 2006. 'The hypothalamus, hormones, and hunger: alterations in human obesity and illness', *Prog Brain Res*, 153: 57-73.

Goldstone, A. P., C. G. Prechtl, S. Scholtz, A. D. Miras, N. Chhina, G. Durighel, S. S. Deliran, C. Beckmann, M. A. Ghatei, D. R. Ashby, A. D. Waldman, B. D. Gaylinn, M. O. Thorner, G. S. Frost, S. R. Bloom, and J. D. Bell. 2014. 'Ghrelin mimics fasting to enhance human hedonic, orbitofrontal cortex, and hippocampal responses to food', *Am J Clin Nutr*, 99: 1319-30.

Goldstone, A. P., C. G. Prechtl de Hernandez, J. D. Beaver, K. Muhammed, C. Croese, G. Bell, G. Durighel, E. Hughes, A. D. Waldman, G. Frost, and J. D. Bell. 2009. 'Fasting biases brain reward systems towards high-calorie foods', *Eur J Neurosci*, 30: 1625-35.

Gonzalez-At, J. B., D. C. Alsop, and J. A. Detre. 2000. 'Cerebral perfusion and arterial transit time changes during task activation determined with continuous arterial spin labeling', *Magn Reson Med*, 43: 739-46.

Gonzalez-Castillo, J., P. Panwar, L. C. Buchanan, C. Caballero-Gaudes, D. A. Handwerker, D. C. Jangraw, V. Zachariou, S. Inati, V. Roopchansingh, J. A. Derbyshire, and P. A. Bandettini. 2016. 'Evaluation of multi-echo ICA denoising for task based fMRI studies: Block designs, rapid event-related designs, and cardiac-gated fMRI', *NeuroImage*, 141: 452-68.

Gonzalez-Muniesa, P., M. A. Martinez-Gonzalez, F. B. Hu, J. P. Despres, Y. Matsuzawa, R. J. F. Loos, L. A. Moreno, G. A. Bray, and J. A. Martinez. 2017. 'Obesity', *Nat Rev Dis Primers*, 3: 17034.

González-Muniesa, Pedro, Miguel-Angel Mártinez-González, Frank B. Hu, Jean-Pierre Després, Yuji Matsuzawa, Ruth J. F. Loos, Luis A. Moreno, George A. Bray, and J. Alfredo Martinez. 2017. 'Obesity', *Nature Reviews Disease Primers*, 3: 17034.

Gottfried, J. A., J. O'Doherty, and R. J. Dolan. 2003. 'Encoding predictive reward value in human amygdala and orbitofrontal cortex', *Science*, 301: 1104-7.

Goyal, S. K., Samsher, and R. K. Goyal. 2010. 'Stevia (Stevia rebaudiana) a bio-sweetener: a review', *Int J Food Sci Nutr*, 61: 1-10.

Gray, Sarah M., Rick I. Meijer, and Eugene J. Barrett. 2014. 'Insulin Regulates Brain Function, but How Does It Get There?', *Diabetes*, 63: 3992-97.

Grichisch, Y., M. Cavusoglu, H. Preissl, K. Uludag, M. Hallschmid, N. Birbaumer, H. U. Haring, A. Fritsche, and R. Veit. 2012. 'Differential effects of intranasal insulin and caffeine on cerebral blood flow', *Hum Brain Mapp*, 33: 280-7.

Guastella, A. J., I. B. Hickie, M. M. McGuinness, M. Otis, E. A. Woods, H. M. Disinger, H. K. Chan, T. F. Chen, and R. B. Banati. 2013. 'Recommendations for the standardisation of oxytocin nasal administration and guidelines for its reporting in human research', *Psychoneuroendocrinology*, 38: 612-25.

Gundersen, H., H. van Wageningen, and R. Gruner. 2013. 'Alcohol-induced changes in cerebral blood flow and cerebral blood volume in social drinkers', *Alcohol Alcohol*, 48: 160-5.

Gunther, M. 2007. "Efficient Accelerated Acquisition of Perfusion Inflow Series by Cycled Aterial Spin Labelling " In *Proceedings of the 15th Annual International Society for Magentic Resonance in Medicine*, p380. Berlin, Germany.

Guthoff, M., Y. Grichisch, C. Canova, O. Tschritter, R. Veit, M. Hallschmid, H. U. Haring, H. Preissl, A. M. Hennige, and A. Fritsche. 2010. 'Insulin modulates food-related activity in the central nervous system', *J Clin Endocrinol Metab*, 95: 748-55.

Guyenet, S. J., and M. W. Schwartz. 2012. 'Clinical review: Regulation of food intake, energy balance, and body fat mass: implications for the pathogenesis and treatment of obesity', *J Clin Endocrinol Metab*, 97: 745-55.

Haase, L., B. Cerf-Ducastel, and C. Murphy. 2009. 'Cortical activation in response to pure taste stimuli during the physiological states of hunger and satiety', *NeuroImage*, 44: 1008-21.

Hahn, E. L. 1950. 'Spin Echoes', *Physical Review*, 80: 580-94.

Haight, J. S., and P. Cole. 1983. 'The site and function of the nasal valve', *Laryngoscope*, 93: 49-55.

Halfmann, K., W. Hedgcock, J. Kable, and N. L. Denburg. 2016. 'Individual differences in the neural signature of subjective value among older adults', *Soc Cogn Affect Neurosci*, 11: 1111-20.

Hallschmid, M., C. Benedict, B. Schultes, J. Born, and W. Kern. 2008. 'Obese men respond to cognitive but not to catabolic brain insulin signaling', *Int J Obes (Lond)*, 32: 275-82.

Hallschmid, M., C. Benedict, B. Schultes, H. L. Fehm, J. Born, and W. Kern. 2004. 'Intranasal insulin reduces body fat in men but not in women', *Diabetes*, 53: 3024-9.

Hallschmid, Manfred, Suzanne Higgs, Matthias Thienel, Volker Ott, and Hendrik Lehnert. 2012. 'Postprandial Administration of Intranasal Insulin Intensifies Satiety and Reduces Intake of Palatable Snacks in Women', *Diabetes*, 61: 782-89.

Hare, T. A., C. F. Camerer, and A. Rangel. 2009. 'Self-control in decision-making involves modulation of the vmPFC valuation system', *Science*, 324: 646-8.

Hargrave, S. L., T. L. Davidson, W. Zheng, and K. P. Kinzig. 2016. 'Western diets induce blood-brain barrier leakage and alter spatial strategies in rats', *Behav Neurosci*, 130: 123-35.

Häring, Hans-Ulrich. 2016. 'Novel phenotypes of prediabetes?', *Diabetologia*, 59: 1806-18.

Harris, J. J., C. Reynell, and D. Attwell. 2011. 'The physiology of developmental changes in BOLD functional imaging signals', *Dev Cogn Neurosci*, 1: 199-216.

Hellfritsch, C., A. Brockhoff, F. Stahler, W. Meyerhof, and T. Hofmann. 2012. 'Human psychometric and taste receptor responses to steviol glycosides', *J Agric Food Chem*, 60: 6782-93.

Heni, M., S. Kullmann, C. Ketterer, M. Guthoff, M. Bayer, H. Staiger, F. Machicao, H. U. Haring, H. Preissl, R. Veit, and A. Fritsche. 2014. 'Differential effect of glucose ingestion on the neural processing of food stimuli in lean and overweight adults', *Hum Brain Mapp*, 35: 918-28.

Heni, M., S. Kullmann, C. Ketterer, M. Guthoff, K. Linder, R. Wagner, K. T. Stingl, R. Veit, H. Staiger, H. U. Haring, H. Preissl, and A. Fritsche. 2012. 'Nasal insulin changes peripheral insulin sensitivity simultaneously with altered activity in homeostatic and reward-related human brain regions', *Diabetologia*, 55: 1773-82.

Heni, M., S. Kullmann, H. Preissl, A. Fritsche, and H. U. Haring. 2015. 'Impaired insulin action in the human brain: causes and metabolic consequences', *Nat Rev Endocrinol*, 11: 701-11.

Heni, M., R. Wagner, S. Kullmann, R. Veit, H. Mat Husin, K. Linder, C. Benkendorff, A. Peter, N. Stefan, H. U. Haring, H. Preissl, and A. Fritsche. 2014. 'Central insulin administration improves whole-body insulin sensitivity via hypothalamus and parasympathetic outputs in men', *Diabetes*, 63: 4083-8.

Heni, Martin, Patricia Schöpfer, Andreas Peter, Tina Sartorius, Andreas Fritsche, Matthis Synofzik, Hans-Ulrich Häring, Walter Maetzler, and AnitaM Hennige. 2014. 'Evidence for altered transport of insulin across the blood–brain barrier in insulin-resistant humans', *Acta Diabetologica*, 51: 679-81.

Henkin, R. I. 2010. 'Inhaled insulin-intrapulmonary, intranasal, and other routes of administration: mechanisms of action', *Nutrition*, 26: 33-9.

Hennig, J. 1999. 'K-space sampling strategies', *European Radiology*, 9: 1020-31.

Hennig, J., A. Nauerth, and H. Friedburg. 1986. 'RARE imaging: A fast imaging method for clinical MR', *Magnetic Resonance in Medicine*, 3: 823-33.

Herbert, B. M., and O. Pollatos. 2014. 'Attenuated interoceptive sensitivity in overweight and obese individuals', *Eat Behav*, 15: 445-8.
Herscovitch, P., and M. E. Raichle. 1985. 'What is the correct value for the brain--blood partition coefficient for water?', *J Cereb Blood Flow Metab*, 5: 65-9.
Hickey, Clayton, Leonardo Chelazzi, and Jan Theeuwes. 2010. 'Reward Guides Vision when It's Your Thing: Trait Reward-Seeking in Reward-Mediated Visual Priming', *PLoS ONE*, 5: e14087.
Higgs, S. 2005. 'Memory and its role in appetite regulation', *Physiol Behav*, 85: 67-72.
Higgs, S., and M. S. Spetter. 2018. 'Cognitive Control of Eating: the Role of Memory in Appetite and Weight Gain', *Curr Obes Rep*, 7: 50-59.
Higgs, S., M. S. Spetter, J. M. Thomas, P. Rotshtein, M. Lee, M. Hallschmid, and C. T. Dourish. 2017. 'Interactions between metabolic, reward and cognitive processes in appetite control: Implications for novel weight management therapies', *J Psychopharmacol*, 31: 1460-74.
Higgs, S., A. C. Williamson, P. Rotshtein, and G. W. Humphreys. 2008. 'Sensory-specific satiety is intact in amnesics who eat multiple meals', *Psychol Sci*, 19: 623-8.
Higgs, Suzanne. 2016. 'Cognitive processing of food rewards', *Appetite*, 104: 10-17.
Hogenkamp, P. S., W. Zhou, L. S. Dahlberg, J. Stark, A. L. Larsen, G. Olivo, L. Wiemerslage, E. M. Larsson, M. Sundbom, C. Benedict, and H. B. Schiöth. 2016. 'Higher resting-state activity in reward-related brain circuits in obese versus normal-weight females independent of food intake', *International Journal Of Obesity*, 40: 1687.
Hoult, D. I., and R. E. Richards. 1975. 'Critical Factors in the Design of Sensitive High Resolution Nuclear Magnetic Resonance Spectrometers', *Proceedings of the Royal Society of London. Series A, Mathematical and Physical Sciences*, 344: 311-40.
Howseman, A. M., and R. W. Bowtell. 1999. 'Functional magnetic resonance imaging: imaging techniques and contrast mechanisms', *Philos Trans R Soc Lond B Biol Sci*, 354: 1179-94.
Hu, F. B., R. M. van Dam, and S. Liu. 2001. 'Diet and risk of Type II diabetes: the role of types of fat and carbohydrate', *Diabetologia*, 44: 805-17.
Hu, X., and E. Yacoub. 2012. 'The story of the initial dip in fMRI', *NeuroImage*, 62: 1103-8.
Hull, Holly R., Casey N. Hester, and David A. Fields. 2006. 'The effect of the holiday season on body weight and composition in college students', *Nutrition & metabolism*, 3: 44-44.
Hussain, Syed, Errol Richardson, Yue Ma, Christopher Holton, Ivan De Backer, Niki Buckley, Waljit Dhillo, Gavin Bewick, Shuai Zhang, David Carling, Steve Bloom, and James Gardiner. 2015. 'Glucokinase activity in the arcuate nucleus regulates glucose intake', *The Journal of Clinical Investigation*, 125: 337-49.
Ichimura, T., P. A. Fraser, and H. F. Cserr. 1991. 'Distribution of extracellular tracers in perivascular spaces of the rat brain', *Brain Res*, 545: 103-13.
Inthavong, K., Z. F. Tian, H. F. Li, J. Y. Tu, W. Yang, C. L. Xue, and C. G. Li. 2006. 'A Numerical Study of Spray Particle Deposition in a Human Nasal Cavity', *Aerosol Science and Technology*, 40: 1034-45.
Inthavong, K., Z. F. Tian, J. Y. Tu, W. Yang, and C. Xue. 2008. 'Optimising nasal spray parameters for efficient drug delivery using computational fluid dynamics', *Comput Biol Med*, 38: 713-26.
Irarrazabal, P., and D. G. Nishimura. 1995. 'Fast three dimensional magnetic resonance imaging', *Magn Reson Med*, 33: 656-62.
Ishimaru, H., M. Ochi, M. Morikawa, H. Takahata, Y. Matsuoka, T. Koshiishi, T. Fujimoto, A. Egawa, K. Mitarai, T. Murakami, and M. Uetani. 2007. 'Accuracy of pre- and postcontrast 3D time-of-flight MR angiography in patients with acute ischemic stroke: correlation with catheter angiography', *AJNR Am J Neuroradiol*, 28: 923-6.

Jansson, B., and E. Bjork. 2002. 'Visualization of in vivo olfactory uptake and transfer using fluorescein dextran', *J Drug Target*, 10: 379-86.

Jauch-Chara, K., A. Friedrich, M. Rezmer, U. H. Melchert, G. Scholand-Engler H, M. Hallschmid, and K. M. Oltmanns. 2012. 'Intranasal insulin suppresses food intake via enhancement of brain energy levels in humans', *Diabetes*, 61: 2261-8.

Jauch-Chara, Kamila, and Kerstin M Oltmanns. 2014. 'Obesity–a neuropsychological disease? Systematic review and neuropsychological model', *Prog Neurobiol*, 114: 84-101.

Jenkins, Bruce G. 2012. 'Pharmacologic magnetic resonance imaging (phMRI): Imaging drug action in the brain', *NeuroImage*, 62: 1072-85.

Jenkinson, M., P. Bannister, M. Brady, and S. Smith. 2002. 'Improved optimization for the robust and accurate linear registration and motion correction of brain images', *NeuroImage*, 17: 825-41.

Jenkinson, M., and S. Smith. 2001. 'A global optimisation method for robust affine registration of brain images', *Med Image Anal*, 5: 143-56.

Jin, Z., Y. Jin, S. Kumar-Mendu, E. Degerman, L. Groop, and B. Birnir. 2011. 'Insulin reduces neuronal excitability by turning on GABA(A) channels that generate tonic current', *PLoS ONE*, 6: e16188.

Jones, K. T., C. Woods, J. Zhen, T. Antonio, K. D. Carr, and M. E. Reith. 2017. 'Effects of diet and insulin on dopamine transporter activity and expression in rat caudate-putamen, nucleus accumbens, and midbrain', *J Neurochem*, 140: 728-40.

Kahn, I., J. R. Andrews-Hanna, J. L. Vincent, A. Z. Snyder, and R. L. Buckner. 2008. 'Distinct cortical anatomy linked to subregions of the medial temporal lobe revealed by intrinsic functional connectivity', *J Neurophysiol*, 100: 129-39.

Kaiyala, K. J., R. L. Prigeon, S. E. Kahn, S. C. Woods, and M. W. Schwartz. 2000. 'Obesity induced by a high-fat diet is associated with reduced brain insulin transport in dogs', *Diabetes*, 49: 1525-33.

Kamel, H. A. M., and J. Toland. 2001. 'Trigeminal Nerve Anatomy', *American Journal of Roentgenology*, 176: 247-51.

Kanoski, Scott E., Yanshu Zhang, Wei Zheng, and Terry L. Davidson. 2010. 'The Effects of a High-Energy Diet on Hippocampal Function and Blood-Brain Barrier Integrity in the Rat', *Journal of Alzheimer's disease : JAD*, 21: 207-19.

Karakelides, Helen, Brian A. Irving, Kevin R. Short, Peter O'Brien, and K. Sreekumaran Nair. 2010. 'Age, Obesity, and Sex Effects on Insulin Sensitivity and Skeletal Muscle Mitochondrial Function', *Diabetes*, 59: 89-97.

Karlsson, H. K., J. J. Tuulari, L. Tuominen, J. Hirvonen, H. Honka, R. Parkkola, S. Helin, P. Salminen, P. Nuutila, and L. Nummenmaa. 2015. 'Weight loss after bariatric surgery normalizes brain opioid receptors in morbid obesity', *Molecular Psychiatry*, 21: 1057.

Karra, E., K. Chandarana, and R. L. Batterham. 2009. 'The role of peptide YY in appetite regulation and obesity', *J Physiol*, 587: 19-25.

Karra, E., O. G. O'Daly, A. I. Choudhury, A. Yousseif, S. Millership, M. T. Neary, W. R. Scott, K. Chandarana, S. Manning, M. E. Hess, H. Iwakura, T. Akamizu, Q. Millet, C. Gelegen, M. E. Drew, S. Rahman, J. J. Emmanuel, S. C. Williams, U. U. Ruther, J. C. Bruning, D. J. Withers, F. O. Zelaya, and R. L. Batterham. 2013. 'A link between FTO, ghrelin, and impaired brain food-cue responsivity', *J Clin Invest*, 123: 3539-51.

Kern, W., C. Benedict, B. Schultes, F. Plohr, A. Moser, J. Born, H. L. Fehm, and M. Hallschmid. 2006. 'Low cerebrospinal fluid insulin levels in obese humans', *Diabetologia*, 49: 2790-92.

Kido, Y., J. Nakae, and D. Accili. 2001. 'Clinical review 125: The insulin receptor and its cellular targets', *J Clin Endocrinol Metab*, 86: 972-9.

Kim, Dongjoo, Young Hyo Kim, and Soonjo Kwon. 2018. 'Enhanced nasal drug delivery efficiency by increasing mechanical loading using hypergravity', *Scientific Reports*, 8: 168.

Kim, Jason K. 2009. 'Hyperinsulinemic–Euglycemic Clamp to Assess Insulin Sensitivity In Vivo.' in Claire Stocker (ed.), *Type 2 Diabetes: Methods and Protocols* (Humana Press: Totowa, NJ).

Kleinridders, André, Heather A. Ferris, Weikang Cai, and C. Ronald Kahn. 2014. 'Insulin Action in Brain Regulates Systemic Metabolism and Brain Function', *Diabetes*, 63: 2232-43.

Kleinridders, André, Hans PMM Lauritzen, Siegfried Ussar, Jane H Christensen, Marcelo A Mori, Peter Bross, and C Ronald Kahn. 2013. 'Leptin regulation of Hsp60 impacts hypothalamic insulin signaling', *The Journal of Clinical Investigation*, 123: 4667-80.

Korbonits, M., P. J. Trainer, J. A. Little, R. Edwards, P. G. Kopelman, G. M. Besser, F. Svec, and A. B. Grossman. 1997. 'Leptin levels do not change acutely with food administration in normal or obese subjects, but are negatively correlated with pituitary-adrenal activity', *Clin Endocrinol (Oxf)*, 46: 751-7.

Korol, S. V., A. Tafreshiha, A. K. Bhandage, B. Birnir, and Z. Jin. 2018. 'Insulin enhances GABAA receptor-mediated inhibitory currents in rat central amygdala neurons', *Neurosci Lett*, 671: 76-81.

Kreymann, B., G. Williams, M. A. Ghatei, and S. R. Bloom. 1987. 'Glucagon-like peptide-1 7-36: a physiological incretin in man', *Lancet*, 2: 1300-4.

Kringelbach, M. L. 2004. 'Food for thought: hedonic experience beyond homeostasis in the human brain', *Neuroscience*, 126: 807-19.

Kringelbach, Morten L. 2015. 'The pleasure of food: underlying brain mechanisms of eating and other pleasures', *Flavour*, 4: 20.

Kristensson, Krister, and Yngve Olsson. 1971. 'Uptake of exogenous proteins in mouse olfactory cells', *Acta Neuropathologica*, 19: 145-54.

Kroemer, N. B., L. Krebs, A. Kobiella, O. Grimm, S. Vollstadt-Klein, U. Wolfensteller, R. Kling, M. Bidlingmaier, U. S. Zimmermann, and M. N. Smolka. 2013. '(Still) longing for food: insulin reactivity modulates response to food pictures', *Hum Brain Mapp*, 34: 2367-80.

Kroemer, N. B., and D. M. Small. 2016. 'Fuel not fun: Reinterpreting attenuated brain responses to reward in obesity', *Physiol Behav*, 162: 37-45.

Kullmann, S., S. Frank, M. Heni, C. Ketterer, R. Veit, H. U. Haring, A. Fritsche, and H. Preissl. 2013. 'Intranasal insulin modulates intrinsic reward and prefrontal circuitry of the human brain in lean women', *Neuroendocrinology*, 97: 176-82.

Kullmann, S., A. Fritsche, R. Wagner, S. Schwab, H. U. Haring, H. Preissl, and M. Heni. 2017. 'Hypothalamic insulin responsiveness is associated with pancreatic insulin secretion in humans', *Physiol Behav*, 176: 134-38.

Kullmann, S., M. Heni, A. Fritsche, and H. Preissl. 2015. 'Insulin Action in the Human Brain: Evidence from Neuroimaging Studies', *Journal of Neuroendocrinology*, 27: 419-23.

Kullmann, S., M. Heni, M. Hallschmid, A. Fritsche, H. Preissl, and H. U. Haring. 2016. 'Brain Insulin Resistance at the Crossroads of Metabolic and Cognitive Disorders in Humans', *Physiol Rev*, 96: 1169-209.

Kullmann, S., M. Heni, R. Veit, K. Scheffler, J. Machann, H. U. Haring, A. Fritsche, and H. Preissl. 2015. 'Selective insulin resistance in homeostatic and cognitive control brain areas in overweight and obese adults', *Diabetes Care*, 38: 1044-50.

Kullmann, S., R. Veit, A. Peter, R. Pohmann, K. Scheffler, H. U. Haring, A. Fritsche, H. Preissl, and M. Heni. 2018. 'Dose-Dependent Effects of Intranasal Insulin on Resting-State Brain Activity', *J Clin Endocrinol Metab*, 103: 253-62.

Kullmann, Stephanie, Martin Heni, Ralf Veit, Klaus Scheffler, Jürgen Machann, Hans-Ulrich Häring, Andreas Fritsche, and Hubert Preissl. 2015. 'Selective Insulin Resistance in

Homeostatic and Cognitive Control Brain Areas in Overweight and Obese Adults', *Diabetes Care*, 38: 1044-50.

———. 2017. 'Intranasal insulin enhances brain functional connectivity mediating the relationship between adiposity and subjective feeling of hunger', *Scientific Reports*, 7: 1627.

Kundu, P., S. J. Inati, J. W. Evans, W. M. Luh, and P. A. Bandettini. 2012. 'Differentiating BOLD and non-BOLD signals in fMRI time series using multi-echo EPI', *NeuroImage*, 60: 1759-70.

Kundu, Prantik, Noah D. Brenowitz, Valerie Voon, Yulia Worbe, Petra E. Vértes, Souheil J. Inati, Ziad S. Saad, Peter A. Bandettini, and Edward T. Bullmore. 2013. 'Integrated strategy for improving functional connectivity mapping using multiecho fMRI', *Proceedings of the National Academy of Sciences*, 110: 16187-92.

Kundu, Prantik, Valerie Voon, Priti Balchandani, Michael V. Lombardo, Benedikt A. Poser, and Peter Bandettini. 2017. 'Multi-Echo fMRI: A Review of Applications in fMRI Denoising and Analysis of BOLD Signals', *NeuroImage*.

Kurth, Florian, Simon B. Eickhoff, Axel Schleicher, Lars Hoemke, Karl Zilles, and Katrin Amunts. 2010. 'Cytoarchitecture and Probabilistic Maps of the Human Posterior Insular Cortex', *Cerebral Cortex (New York, NY)*, 20: 1448-61.

Kurth, Florian, Karl Zilles, Peter T. Fox, Angela R. Laird, and Simon B. Eickhoff. 2010. 'A link between the systems: functional differentiation and integration within the human insula revealed by meta-analysis', *Brain structure & function*, 214: 519-34.

LaBar, K. S., D. R. Gitelman, T. B. Parrish, Y. H. Kim, A. C. Nobre, and M. M. Mesulam. 2001. 'Hunger selectively modulates corticolimbic activation to food stimuli in humans', *Behav Neurosci*, 115: 493-500.

Labouebe, G., S. Liu, C. Dias, H. Zou, J. C. Wong, S. Karunakaran, S. M. Clee, A. G. Phillips, B. Boutrel, and S. L. Borgland. 2013. 'Insulin induces long-term depression of ventral tegmental area dopamine neurons via endocannabinoids', *Nat Neurosci*, 16: 300-8.

Lauterbur, P. C. 1973. 'Image Formation by Induced Local Interactions: Examples Employing Nuclear Magnetic Resonance', *Nature*, 242: 190.

le Roux, C. W., R. L. Batterham, S. J. Aylwin, M. Patterson, C. M. Borg, K. J. Wynne, A. Kent, R. P. Vincent, J. Gardiner, M. A. Ghatei, and S. R. Bloom. 2006. 'Attenuated peptide YY release in obese subjects is associated with reduced satiety', *Endocrinology*, 147: 3-8.

Levy, J. C., D. R. Matthews, and M. P. Hermans. 1998. 'Correct homeostasis model assessment (HOMA) evaluation uses the computer program', *Diabetes Care*, 21: 2191-2.

Li, Xiaodong, Lena Staszewski, Hong Xu, Kyle Durick, Mark Zoller, and Elliot Adler. 2002. 'Human receptors for sweet and umami taste', *Proceedings of the National Academy of Sciences*, 99: 4692-96.

Liao, J. R., J. M. Pauly, T. J. Brosnan, and N. J. Pelc. 1997. 'Reduction of motion artifacts in cine MRI using variable-density spiral trajectories', *Magn Reson Med*, 37: 569-75.

Liau, J., J. E. Perthen, and T. T. Liu. 2008. 'Caffeine reduces the activation extent and contrast-to-noise ratio of the functional cerebral blood flow response but not the BOLD response', *NeuroImage*, 42: 296-305.

Linder, K., F. Schleger, C. Ketterer, L. Fritsche, I. Kiefer-Schmidt, A. Hennige, H. U. Haring, H. Preissl, and A. Fritsche. 2014. 'Maternal insulin sensitivity is associated with oral glucose-induced changes in fetal brain activity', *Diabetologia*, 57: 1192-8.

Linder, K., F. Schleger, I. Kiefer-Schmidt, L. Fritsche, S. Kummel, M. Bocker, M. Heni, M. Weiss, H. U. Haring, H. Preissl, and A. Fritsche. 2015. 'Gestational Diabetes Impairs Human Fetal Postprandial Brain Activity', *J Clin Endocrinol Metab*, 100: 4029-36.

Liu, Peiying, Jinsoo Uh, and Hanzhang Lu. 2011. 'Determination of spin compartment in arterial spin labeling MRI', *Magn Reson Med*, 65: 120-27.

Lochhead, Jeffrey J., and Robert G. Thorne. 2012. 'Intranasal delivery of biologics to the central nervous system', *Advanced Drug Delivery Reviews*, 64: 614-28.

Logothetis, N. K., and J. Pfeuffer. 2004. 'On the nature of the BOLD fMRI contrast mechanism', *Magn Reson Imaging*, 22: 1517-31.

Logothetis, N. K., and B. A. Wandell. 2004. 'Interpreting the BOLD signal', *Annu Rev Physiol*, 66: 735-69.

Lombardo, M. V., B. Auyeung, R. J. Holt, J. Waldman, A. N. Ruigrok, N. Mooney, E. T. Bullmore, S. Baron-Cohen, and P. Kundu. 2016. 'Improving effect size estimation and statistical power with multi-echo fMRI and its impact on understanding the neural systems supporting mentalizing', *NeuroImage*.

Lu, H., C. Clingman, X. Golay, and P. C. van Zijl. 2004. 'Determining the longitudinal relaxation time (T1) of blood at 3.0 Tesla', *Magn Reson Med*, 52: 679-82.

Lutter, Michael, and Eric J. Nestler. 2009. 'Homeostatic and Hedonic Signals Interact in the Regulation of Food Intake', *J Nutr*, 139: 629-32.

Lv, H., Z. Wang, E. Tong, L.M. Williams, G. Zaharchuk, M. Zeineh, A.N. Goldstein-Piekarski, T.M. Ball, C. Liao, and M. Wintermark. 2018. 'Resting-State Functional MRI: Everything That Nonexperts Have Always Wanted to Know', *American Journal of Neuroradiology*.

Macdonald, I. A. 2016. 'A review of recent evidence relating to sugars, insulin resistance and diabetes', *European Journal of Nutrition*, 55: 17-23.

MacIntosh, B. J., N. Filippini, M. A. Chappell, M. W. Woolrich, C. E. Mackay, and P. Jezzard. 2010. 'Assessment of arterial arrival times derived from multiple inversion time pulsed arterial spin labeling MRI', *Magn Reson Med*, 63: 641-7.

Manelis, A., J. R. Almeida, R. Stiffler, J. C. Lockovich, H. A. Aslam, and M. L. Phillips. 2016. 'Anticipation-related brain connectivity in bipolar and unipolar depression: a graph theory approach', *Brain*, 139: 2554-66.

Manning, Joshua, Gretchen Reynolds, Zeynep M. Saygin, Stefan G. Hofmann, Mark Pollack, John D. E. Gabrieli, and Susan Whitfield-Gabrieli. 2015. 'Altered Resting-State Functional Connectivity of the Frontal-Striatal Reward System in Social Anxiety Disorder', *PLoS ONE*, 10: e0125286.

Mansfield, P. 1977. 'Multi-planar image formation using NMR spin echoes', *Journal of Physics C: Solid State Physics*, 10: L55.

Manson, J. E., U. A. Ajani, S. Liu, D. M. Nathan, and C. H. Hennekens. 2000. 'A prospective study of cigarette smoking and the incidence of diabetes mellitus among US male physicians', *Am J Med*, 109: 538-42.

Martín-Timón, Iciar, Cristina Sevillano-Collantes, Amparo Segura-Galindo, and Francisco Javier Del Cañizo-Gómez. 2014. 'Type 2 diabetes and cardiovascular disease: Have all risk factors the same strength?', *World Journal of Diabetes*, 5: 444-70.

Massa, M. L., J. J. Gagliardino, and F. Francini. 2011. 'Liver glucokinase: An overview on the regulatory mechanisms of its activity', *IUBMB Life*, 63: 1-6.

Mattes, R. D., and B. M. Popkin. 2009. 'Nonnutritive sweetener consumption in humans: effects on appetite and food intake and their putative mechanisms', *Am J Clin Nutr*, 89: 1-14.

Matthews, D. R., J. P. Hosker, A. S. Rudenski, B. A. Naylor, D. F. Treacher, and R. C. Turner. 1985. 'Homeostasis model assessment: insulin resistance and beta-cell function from fasting plasma glucose and insulin concentrations in man', *Diabetologia*, 28: 412-9.

Matthews, D. R., A. S. Rudenski, M. A. Burnett, P. Darling, and R. C. Turner. 1985. 'The half-life of endogenous insulin and C-peptide in man assessed by somatostatin suppression', *Clin Endocrinol (Oxf)*, 23: 71-9.

McKeown, Martin J., Lars Kai Hansen, and Terrence J. Sejnowsk. 2003. 'Independent component analysis of functional MRI: what is signal and what is noise?', *Current Opinion in Neurobiology*, 13: 620-29.

Mebel, D. M., J. C. Wong, Y. J. Dong, and S. L. Borgland. 2012. 'Insulin in the ventral tegmental area reduces hedonic feeding and suppresses dopamine concentration via increased reuptake', *Eur J Neurosci*, 36: 2336-46.

Mehta, M. A., and O. G. O'Daly. 2011. 'Pharmacological application of fMRI', *Methods Mol Biol*, 711: 551-65.

Menon, R. S., S. Ogawa, X. Hu, J. P. Strupp, P. Anderson, and K. Ugurbil. 1995. 'BOLD based functional MRI at 4 Tesla includes a capillary bed contribution: echo-planar imaging correlates with previous optical imaging using intrinsic signals', *Magn Reson Med*, 33: 453-9.

Mergenthaler, Philipp, Ute Lindauer, Gerald A. Dienel, and Andreas Meisel. 2013. 'Sugar for the brain: the role of glucose in physiological and pathological brain function', *Trends Neurosci*, 36: 587-97.

Mielke, J. G., C. Taghibiglou, L. Liu, Y. Zhang, Z. Jia, K. Adeli, and Y. T. Wang. 2005. 'A biochemical and functional characterization of diet-induced brain insulin resistance', *J Neurochem*, 93: 1568-78.

Miyamoto, J. J., M. Honda, D. N. Saito, T. Okada, T. Ono, K. Ohyama, and N. Sadato. 2006. 'The representation of the human oral area in the somatosensory cortex: a functional MRI study', *Cereb Cortex*, 16: 669-75.

Morris, J. S., and R. J. Dolan. 2001. 'Involvement of human amygdala and orbitofrontal cortex in hunger-enhanced memory for food stimuli', *J Neurosci*, 21: 5304-10.

Murphy, K., R. M. Birn, and P. A. Bandettini. 2013. 'Resting-state fMRI confounds and cleanup', *NeuroImage*, 80: 349-59.

Murphy, Susannah E., and Clare E. Mackay. 2010. 'Using MRI to measure drug action: caveats and new directions', *Journal of Psychopharmacology*, 25: 1168-74.

Myers, Martin G., Jr., Rudolph L. Leibel, Randy J. Seeley, and Michael W. Schwartz. 2010. 'Obesity and leptin resistance: distinguishing cause from effect', *Trends in endocrinology and metabolism: TEM*, 21: 643-51.

Nachev, Parashkev, Henrietta Wydell, Kevin O'Neill, Masud Husain, and Christopher Kennard. 2007. 'The role of the pre-supplementary motor area in the control of action', *NeuroImage*, 36: T155-T63.

Newman, S. P., F. Moren, and S. W. Clarke. 1988. 'Deposition pattern of nasal sprays in man', *Rhinology*, 26: 111-20.

Nordestgaard, Børge G, Tom M Palmer, Marianne Benn, Jeppe Zacho, Anne Tybjærg-Hansen, George Davey Smith, and Nicholas J Timpson. 2012. 'The effect of elevated body mass index on ischemic heart disease risk: causal estimates from a Mendelian randomisation approach', *PLoS medicine*, 9: e1001212.

Nuttall, Frank Q. 2015. 'Body Mass Index: Obesity, BMI, and Health: A Critical Review', *Nutrition today*, 50: 117-28.

O'Doherty, J., P. Dayan, J. Schultz, R. Deichmann, K. Friston, and R. J. Dolan. 2004. 'Dissociable roles of ventral and dorsal striatum in instrumental conditioning', *Science*, 304: 452-4.

O'Doherty, J. P., R. Deichmann, H. D. Critchley, and R. J. Dolan. 2002. 'Neural responses during anticipation of a primary taste reward', *Neuron*, 33: 815-26.

O'Doherty, John P., Peter Dayan, Karl Friston, Hugo Critchley, and Raymond J. Dolan. 2003. 'Temporal Difference Models and Reward-Related Learning in the Human Brain', *Neuron*, 38: 329-37.

O'Malley, Dervla, and Jenni Harvey. 2007. 'MAPK-dependent actin cytoskeletal reorganization underlies BK channel activation by insulin', *European Journal of Neuroscience*, 25: 673-82.

O'Malley, Dervla, Lynne J. Shanley, and Jenni Harvey. 2003. 'Insulin inhibits rat hippocampal neurones via activation of ATP-sensitive K+ and large conductance Ca2+-activated K+ channels', *Neuropharmacology*, 44: 855-63.

Ogawa, S., T. M. Lee, A. S. Nayak, and P. Glynn. 1990. 'Oxygenation-sensitive contrast in magnetic resonance image of rodent brain at high magnetic fields', *Magn Reson Med*, 14: 68-78.

Ogawa, S., D. W. Tank, R. Menon, J. M. Ellermann, S. G. Kim, H. Merkle, and K. Ugurbil. 1992. 'Intrinsic signal changes accompanying sensory stimulation: functional brain mapping with magnetic resonance imaging', *Proc Natl Acad Sci U S A*, 89: 5951-5.

Oh, H., S. Boghossian, D. A. York, and M. Park-York. 2013. 'The effect of high fat diet and saturated fatty acids on insulin signaling in the amygdala and hypothalamus of rats', *Brain Res*, 1537: 191-200.

Ohman, A. 2005. 'The role of the amygdala in human fear: automatic detection of threat', *Psychoneuroendocrinology*, 30: 953-8.

Ojemann, J. G., E. Akbudak, A. Z. Snyder, R. C. McKinstry, M. E. Raichle, and T. E. Conturo. 1997. 'Anatomic localization and quantitative analysis of gradient refocused echo-planar fMRI susceptibility artifacts', *NeuroImage*, 6: 156-67.

Okusa, T., R. Kakigi, and N. Osaka. 2000. 'Cortical activity related to cue-invariant shape perception in humans', *Neuroscience*, 98: 615-24.

Opstal, Anna M. van, Abimbola A. Akintola, Marjan van der Elst, Rudi G. Westendorp, Hanno Pijl, Diana van Heemst, and Jeroen van der Grond. 2017. 'Effects of intranasal insulin application on the hypothalamic BOLD response to glucose ingestion', *Scientific Reports*, 7: 13327.

Ott, V., C. Benedict, B. Schultes, J. Born, and M. Hallschmid. 2012. 'Intranasal administration of insulin to the brain impacts cognitive function and peripheral metabolism', *Diabetes Obes Metab*, 14: 214-21.

Pagnoni, G., C. F. Zink, P. R. Montague, and G. S. Berns. 2002. 'Activity in human ventral striatum locked to errors of reward prediction', *Nat Neurosci*, 5: 97-8.

Paloyelis, Y., O. M. Doyle, F. O. Zelaya, S. Maltezos, S. C. Williams, A. Fotopoulou, and M. A. Howard. 2014. 'A Spatiotemporal Profile of In Vivo Cerebral Blood Flow Changes Following Intranasal Oxytocin in Humans', *Biol Psychiatry*.

Pardeshi, Chandrakantsing Vijaysing, and Veena Shailendra Belgamwar. 2013. 'Direct nose to brain drug delivery via integrated nerve pathways bypassing the blood–brain barrier: an excellent platform for brain targeting', *Expert Opin Drug Deliv*, 10: 957-72.

Parent, Marise B. 2016. 'Dorsal hippocampal–dependent episodic memory inhibits eating', *Current Directions in Psychological Science*, 25: 461-66.

Parkes, L. M. 2005. 'Quantification of cerebral perfusion using arterial spin labeling: two-compartment models', *J Magn Reson Imaging*, 22: 732-6.

Parkes, L. M., W. Rashid, D. T. Chard, and P. S. Tofts. 2004. 'Normal cerebral perfusion measurements using arterial spin labeling: reproducibility, stability, and age and gender effects', *Magn Reson Med*, 51: 736-43.

Parkes, L. M., and P. S. Tofts. 2002. 'Improved accuracy of human cerebral blood perfusion measurements using arterial spin labeling: accounting for capillary water permeability', *Magn Reson Med*, 48: 27-41.

Pasinetti, G. M., and J. A. Eberstein. 2008. 'Metabolic syndrome and the role of dietary lifestyles in Alzheimer's disease', *J Neurochem*, 106: 1503-14.

Pecina, S., and K. C. Berridge. 2005. 'Hedonic hot spot in nucleus accumbens shell: where do mu-opioids cause increased hedonic impact of sweetness?', *J Neurosci*, 25: 11777-86.

Pelchat, M. L., A. Johnson, R. Chan, J. Valdez, and J. D. Ragland. 2004. 'Images of desire: food-craving activation during fMRI', *NeuroImage*, 23: 1486-93.

Persidsky, Y., S. H. Ramirez, J. Haorah, and G. D. Kanmogne. 2006. 'Blood-brain barrier: structural components and function under physiologic and pathologic conditions', *J Neuroimmune Pharmacol*, 1: 223-36.

Perthen, J. E., A. E. Lansing, J. Liau, T. T. Liu, and R. B. Buxton. 2008. 'Caffeine-induced uncoupling of cerebral blood flow and oxygen metabolism: a calibrated BOLD fMRI study', *NeuroImage*, 40: 237-47.

Petersen, E. T., I. Zimine, Y. C. Ho, and X. Golay. 2006. 'Non-invasive measurement of perfusion: a critical review of arterial spin labelling techniques', *Br J Radiol*, 79: 688-701.

Phalen, R. F. 1976. 'Inhalation exposure of animals', *Environ Health Perspect*, 16: 17-24.

Plum, Leona, Markus Schubert, and Jens C. Brüning. 2005. 'The role of insulin receptor signaling in the brain', *Trends in Endocrinology & Metabolism*, 16: 59-65.

Posse, S., S. Wiese, D. Gembris, K. Mathiak, C. Kessler, M. L. Grosse-Ruyken, B. Elghahwagi, T. Richards, S. R. Dager, and V. G. Kiselev. 1999. 'Enhancement of BOLD-contrast sensitivity by single-shot multi-echo functional MR imaging', *Magn Reson Med*, 42: 87-97.

Posse, Stefan. 2012. 'Multi-echo acquisition', *NeuroImage*, 62: 665-71.

Poulsen, P., K. O. Kyvik, A. Vaag, and H. Beck-Nielsen. 1999. 'Heritability of type II (non-insulin-dependent) diabetes mellitus and abnormal glucose tolerance--a population-based twin study', *Diabetologia*, 42: 139-45.

Power, J. D., M. Plitt, S. J. Gotts, P. Kundu, V. Voon, P. A. Bandettini, and A. Martin. 2018. 'Ridding fMRI data of motion-related influences: Removal of signals with distinct spatial and physical bases in multiecho data', *Proc Natl Acad Sci U S A*, 115: E2105-e14.

Pruim, R. H. R., M. Mennes, D. van Rooij, A. Llera, J. K. Buitelaar, and C. F. Beckmann. 2015. 'ICA-AROMA: A robust ICA-based strategy for removing motion artifacts from fMRI data', *NeuroImage*, 112: 267-77.

Pu, Yu, Adrian P. Goodey, Xiuhua Fang, and Kuriakose Jacob. 2014. 'A Comparison of the Deposition Patterns of Different Nasal Spray Formulations Using a Nasal Cast', *Aerosol Science and Technology*, 48: 930-38.

Purcell, E. M., H. C. Torrey, and R. V. Pound. 1946. 'Resonance Absorption by Nuclear Magnetic Moments in a Solid', *Physical Review*, 69: 37-38.

Qiu, Maolin, R. Paul Maguire, Jagriti Arora, Beata Planeta-Wilson, David Weinzimmer, Jinghua Wang, Yuenan Wang, Hyeonjin Kim, Nallakkandi Rajeevan, Yiyun Huang, Richard E. Carson, and R. Todd Constable. 2010. 'Arterial Transit Time Effects in Pulsed Arterial Spin Labeling CBF Mapping: Insight From a PET and MR Study in Normal Human Subjects', *Magnetic resonance in medicine : official journal of the Society of Magnetic Resonance in Medicine / Society of Magnetic Resonance in Medicine*, 63: 374-84.

Ramsay, S. C., K. Murphy, S. A. Shea, K. J. Friston, A. A. Lammertsma, J. C. Clark, L. Adams, A. Guz, and R. S. Frackowiak. 1993. 'Changes in global cerebral blood flow in humans: effect on regional cerebral blood flow during a neural activation task', *The Journal of Physiology*, 471: 521-34.

Ranganath, L. R., J. M. Beety, L. M. Morgan, J. W. Wright, R. Howland, and V. Marks. 1996. 'Attenuated GLP-1 secretion in obesity: cause or consequence?', *Gut*, 38: 916-19.

Reger, M. A., and S. Craft. 2006. 'Intranasal insulin administration: a method for dissociating central and peripheral effects of insulin', *Drugs Today (Barc)*, 42: 729-39.

Renehan, Andrew G, Isabelle Soerjomataram, Margaret Tyson, Matthias Egger, Marcel Zwahlen, Jan Willem Coebergh, and Iain Buchan. 2010. 'Incident cancer burden attributable to excess body mass index in 30 European countries', *International journal of cancer*, 126: 692-702.

Rescorla, Robert A, and Allan R Wagner. 1972. 'A theory of Pavlovian conditioning: Variations in the effectiveness of reinforcement and nonreinforcement', *Classical conditioning II: Current research and theory*, 2: 64-99.

Ressler, Kerry J. 2010. 'Amygdala Activity, Fear, and Anxiety: Modulation by Stress', *Biological Psychiatry*, 67: 1117-19.

Richardson, C. C., K. Hussain, P. M. Jones, S. Persaud, K. Löbner, A. Boehm, A. Clark, and M. R. Christie. 2007. 'Low levels of glucose transporters and channels in human pancreatic beta cells early in development', *Diabetologia*, 50: 1000-05.

Robbins, David C, Lennart Andersen, Ron Bowsher, Ron Chance, Bo Dinesen, Bruce Frank, Ron Gingerich, David Goldstein, Hsaio-Mei Widemeyer, Steven Haffner, C Nick Hales, Leonard Jarett, Kenneth Polonsky, Daniel Porte, Jay Skyler, George Webb, and Kathy Gallagher. 1996. 'Report of the American Diabetes Association's Task Force on Standardization of the Insulin Assay', *Diabetes*, 45: 242-56.

Roder, P. V., B. Wu, Y. Liu, and W. Han. 2016. 'Pancreatic regulation of glucose homeostasis', *Exp Mol Med*, 48: e219.

Rolls, Barbara J, Edmund T Rolls, Edward A Rowe, and Kevin Sweeney. 1981. 'Sensory specific satiety in man', *Physiol Behav*, 27: 137-42.

Rolls, E. T. 2004. 'The functions of the orbitofrontal cortex', *Brain Cogn*, 55: 11-29.

———. 2006. 'Brain mechanisms underlying flavour and appetite', *Philos Trans R Soc Lond B Biol Sci*, 361: 1123-36.

Rosqvist, F., D. Iggman, J. Kullberg, J. Cedernaes, H. E. Johansson, A. Larsson, L. Johansson, H. Ahlstrom, P. Arner, I. Dahlman, and U. Riserus. 2014. 'Overfeeding polyunsaturated and saturated fat causes distinct effects on liver and visceral fat accumulation in humans', *Diabetes*, 63: 2356-68.

Rothemund, Y., C. Preuschhof, G. Bohner, H. C. Bauknecht, R. Klingebiel, H. Flor, and B. F. Klapp. 2007. 'Differential activation of the dorsal striatum by high-calorie visual food stimuli in obese individuals', *NeuroImage*, 37: 410-21.

Rotte, M., C. Baerecke, G. Pottag, S. Klose, E. Kanneberg, H. J. Heinze, and H. Lehnert. 2005. 'Insulin affects the neuronal response in the medial temporal lobe in humans', *Neuroendocrinology*, 81: 49-55.

Rui, L. 2014. 'Energy metabolism in the liver', *Compr Physiol*, 4: 177-97.

Ryan, A. S. 2000. 'Insulin resistance with aging: effects of diet and exercise', *Sports Med*, 30: 327-46.

Salimi-Khorshidi, G., G. Douaud, C. F. Beckmann, M. F. Glasser, L. Griffanti, and S. M. Smith. 2014. 'Automatic denoising of functional MRI data: combining independent component analysis and hierarchical fusion of classifiers', *NeuroImage*, 90: 449-68.

Santiago, João C. P., and Manfred Hallschmid. 2017. 'Central Nervous Insulin Administration before Nocturnal Sleep Decreases Breakfast Intake in Healthy Young and Elderly Subjects', *Frontiers in Neuroscience*, 11.

Sanu, A., and R. Eccles. 2008. 'The effects of a hot drink on nasal airflow and symptoms of common cold and flu', *Rhinology*, 46: 271-5.

Sartorius, T., A. Peter, M. Heni, W. Maetzler, A. Fritsche, H. U. Haring, and A. M. Hennige. 2015. 'The brain response to peripheral insulin declines with age: a contribution of the blood-brain barrier?', *PLoS ONE*, 10: e0126804.

Schilling, T. M., D. S. Ferreira de Sa, R. Westerhausen, F. Strelzyk, M. F. Larra, M. Hallschmid, E. Savaskan, M. S. Oitzl, H. P. Busch, E. Naumann, and H. Schachinger. 2014. 'Intranasal insulin increases regional cerebral blood flow in the insular cortex in men independently of cortisol manipulation', *Hum Brain Mapp*, 35: 1944-56.

Schmid, V., S. Kullmann, W. Gfrorer, V. Hund, M. Hallschmid, H. P. Lipp, H. U. Haring, H. Preissl, A. Fritsche, and M. Heni. 2018. 'Safety of intranasal human insulin: A review', *Diabetes Obes Metab*, 20: 1563-77.

Schulingkamp, R. J., T. C. Pagano, D. Hung, and R. B. Raffa. 2000. 'Insulin receptors and insulin action in the brain: review and clinical implications', *Neuroscience & Biobehavioral Reviews*, 24: 855-72.

Schultz, W. 1998. 'Predictive reward signal of dopamine neurons', *J Neurophysiol*, 80: 1-27.

———. 2001. 'Reward signaling by dopamine neurons', *Neuroscientist*, 7: 293-302.

Schultz, Wolfram, Peter Dayan, and P. Read Montague. 1997. 'A Neural Substrate of Prediction and Reward', *Science*, 275: 1593-99.

Schwartz, M. W., A. Sipols, S. E. Kahn, D. F. Lattemann, G. J. Taborsky, Jr., R. N. Bergman, S. C. Woods, and D. Porte, Jr. 1990. 'Kinetics and specificity of insulin uptake from plasma into cerebrospinal fluid', *Am J Physiol*, 259: E378-83.

Seaquist, Elizabeth R., John Anderson, Belinda Childs, Philip Cryer, Samuel Dagogo-Jack, Lisa Fish, Simon R. Heller, Henry Rodriguez, James Rosenzweig, and Robert Vigersky. 2013. 'Hypoglycemia and Diabetes: A Report of a Workgroup of the American Diabetes Association and The Endocrine Society', *Diabetes Care*.

Sears, D. D., G. Hsiao, A. Hsiao, J. G. Yu, C. H. Courtney, J. M. Ofrecio, J. Chapman, and S. Subramaniam. 2009. 'Mechanisms of human insulin resistance and thiazolidinedione-mediated insulin sensitization', *Proceedings of the National Academy of Sciences*, 106: 18745-50.

Segerdahl, Andrew R., Melvin Mezue, Thomas W. Okell, John T. Farrar, and Irene Tracey. 2015. 'The dorsal posterior insula subserves a fundamental role in human pain', *Nat Neurosci*, 18: 499.

Sellaro, Roberta, and Lorenza S. Colzato. 2017. 'High body mass index is associated with impaired cognitive control', *Appetite*, 113: 301-09.

Silvetti, Massimo, Ruth Seurinck, and Tom Verguts. 2013. 'Value and prediction error estimation account for volatility effects in ACC: A model-based fMRI study', *Cortex*, 49: 1627-35.

Simon, Joe J., Mandy Skunde, Mudan Wu, Knut Schnell, Sabine C. Herpertz, Martin Bendszus, Wolfgang Herzog, and Hans-Christoph Friederich. 2015. 'Neural dissociation of food- and money-related reward processing using an abstract incentive delay task', *Social Cognitive and Affective Neuroscience*, 10: 1113-20.

Singh, Bhawna, and Alpana Saxena. 2010. 'Surrogate markers of insulin resistance: A review', *World Journal of Diabetes*, 1: 36-47.

Small, D. M., M. Jones-Gotman, and A. Dagher. 2003. 'Feeding-induced dopamine release in dorsal striatum correlates with meal pleasantness ratings in healthy human volunteers', *NeuroImage*, 19: 1709-15.

Small, Dana M., Michael D. Gregory, Y. Erica Mak, Darren Gitelman, M. Marsel Mesulam, and Todd Parrish. 2003. 'Dissociation of Neural Representation of Intensity and Affective Valuation in Human Gustation', *Neuron*, 39: 701-11.

Smeets, P. A., C. de Graaf, A. Stafleu, M. J. van Osch, and J. van der Grond. 2005. 'Functional MRI of human hypothalamic responses following glucose ingestion', *NeuroImage*, 24: 363-8.

Smeets, P. A., S. Vidarsdottir, C. de Graaf, A. Stafleu, M. J. van Osch, M. A. Viergever, H. Pijl, and J. van der Grond. 2007. 'Oral glucose intake inhibits hypothalamic neuronal

activity more effectively than glucose infusion', *Am J Physiol Endocrinol Metab*, 293: E754-8.

Smith, Stephen M., Diego Vidaurre, Christian F. Beckmann, Matthew F. Glasser, Mark Jenkinson, Karla L. Miller, Thomas E. Nichols, Emma C. Robinson, Gholamreza Salimi-Khorshidi, Mark W. Woolrich, Deanna M. Barch, Kamil Uğurbil, and David C. Van Essen. 2013. 'Functional connectomics from resting-state fMRI', *Trends Cogn Sci*, 17: 666-82.

Smith, Yoland, D. James Surmeier, Peter Redgrave, and Minoru Kimura. 2011. 'Thalamic contributions to Basal Ganglia-related behavioral switching and reinforcement', *J Neurosci*, 31: 16102-06.

Song, W. J., P. Mondal, Y. Li, S. E. Lee, and M. A. Hussain. 2013. 'Pancreatic β-Cell Response to Increased Metabolic Demand and to Pharmacologic Secretagogues Requires EPAC2A', *Diabetes*, 62: 2796-807.

Spetter, M. S., and M. Hallschmid. 2015. 'Intranasal Neuropeptide Administration To Target the Human Brain in Health and Disease', *Mol Pharm*, 12: 2767-80.

Sridhar, Gumpeny R., Gumpeny Lakshmi, and Gumpeny Nagamani. 2015. 'Emerging links between type 2 diabetes and Alzheimer's disease', *World Journal of Diabetes*, 6: 744-51.

Stears, A., S. O'Rahilly, R. K. Semple, and D. B. Savage. 2012. 'Metabolic insights from extreme human insulin resistance phenotypes', *Best Pract Res Clin Endocrinol Metab*, 26: 145-57.

Stephani, C., G. Fernandez-Baca Vaca, R. Maciunas, M. Koubeissi, and H. O. Lüders. 2011. 'Functional neuroanatomy of the insular lobe', *Brain structure & function*, 216: 137-49.

Stice, E., S. Spoor, C. Bohon, M. G. Veldhuizen, and D. M. Small. 2008. 'Relation of reward from food intake and anticipated food intake to obesity: a functional magnetic resonance imaging study', *J Abnorm Psychol*, 117: 924-35.

Stoeckel, Luke E, James E Cox, Edwin W Cook III, and Rosalyn E Weller. 2007. 'Motivational state modulates the hedonic value of food images differently in men and women', *Appetite*, 48: 139-44.

Stouffer, M. A., C. A. Woods, J. C. Patel, C. R. Lee, P. Witkovsky, L. Bao, R. P. Machold, K. T. Jones, S. C. de Vaca, M. E. Reith, K. D. Carr, and M. E. Rice. 2015. 'Insulin enhances striatal dopamine release by activating cholinergic interneurons and thereby signals reward', *Nat Commun*, 6: 8543.

Stunkard, A. J., and S. Messick. 1985. 'The three-factor eating questionnaire to measure dietary restraint, disinhibition and hunger', *J Psychosom Res*, 29: 71-83.

Suman, J. D., B. L. Laube, T. C. Lin, G. Brouet, and R. Dalby. 2002. 'Validity of in vitro tests on aqueous spray pumps as surrogates for nasal deposition', *Pharm Res*, 19: 1-6.

Sutton, Richard S. 1988. 'Learning to Predict by the Methods of Temporal Differences', *Machine Learning*, 3: 9-44.

Szalay, C., M. Aradi, A. Schwarcz, G. Orsi, G. Perlaki, L. Nemeth, S. Hanna, G. Takacs, I. Szabo, L. Bajnok, A. Vereczkei, T. Doczi, J. Janszky, S. Komoly, P. Ors Horvath, L. Lenard, and Z. Karadi. 2012. 'Gustatory perception alterations in obesity: an fMRI study', *Brain Res*, 1473: 131-40.

Takei, H., S. Fujita, T. Shirakawa, N. Koshikawa, and M. Kobayashi. 2010. 'Insulin facilitates repetitive spike firing in rat insular cortex via phosphoinositide 3-kinase but not mitogen activated protein kinase cascade', *Neuroscience*, 170: 1199-208.

Tataranni, P. Antonio, Jean-François Gautier, Kewei Chen, Anne Uecker, Daniel Bandy, Arline D. Salbe, Richard E. Pratley, Michael Lawson, Eric M. Reiman, and Eric Ravussin. 1999. 'Neuroanatomical correlates of hunger and satiation in humans using positron

emission tomography', *Proceedings of the National Academy of Sciences of the United States of America*, 96: 4569-74.

Taylor, K. S., D. A. Seminowicz, and K. D. Davis. 2009. 'Two systems of resting state connectivity between the insula and cingulate cortex', *Hum Brain Mapp*, 30: 2731-45.

Thomas, Jason M, Suzanne Higgs, Colin T Dourish, Peter C Hansen, Catherine J Harmer, and Ciara McCabe. 2015. 'Satiation attenuates BOLD activity in brain regions involved in reward and increases activity in dorsolateral prefrontal cortex: an fMRI study in healthy volunteers–', *Am J Clin Nutr*, 101: 697-704.

Tiedemann, Lena J., Sebastian M. Schmid, Judith Hettel, Katrin Giesen, Paul Francke, Christian Büchel, and Stefanie Brassen. 2017. 'Central insulin modulates food valuation via mesolimbic pathways', *Nature Communications*, 8: 16052.

Toda, Koji, Yasuko Sugase-Miyamoto, Takashi Mizuhiki, Kiyonori Inaba, Barry J. Richmond, and Munetaka Shidara. 2012. 'Differential Encoding of Factors Influencing Predicted Reward Value in Monkey Rostral Anterior Cingulate Cortex', *PLoS ONE*, 7: e30190.

Trevisan, Maurizio, Jian Liu, Fadlalla Bahsas Bahsas, Alessandro Menotti, Risk Factor, and Life Expectancy Research Group. 1998. 'Syndrome X and mortality: a population-based study', *American journal of epidemiology*, 148: 958-66.

Trows, S., K. Wuchner, R. Spycher, and H. Steckel. 2014. 'Analytical challenges and regulatory requirements for nasal drug products in europe and the u.s', *Pharmaceutics*, 6: 195-219.

Turner, R., Alastair Howseman, Geraint E. Rees, Oliver Josephs, and Karl Friston. 1998. 'Functional magnetic resonance imaging of the human brain: data acquisition and analysis', *Experimental Brain Research*, 123: 5-12.

Turner, R., D. Le Bihan, C. T. Moonen, D. Despres, and J. Frank. 1991. 'Echo-planar time course MRI of cat brain oxygenation changes', *Magn Reson Med*, 22: 159-66.

Unnikrishnan, Ranjit, Rajendra Pradeepa, Shashank R. Joshi, and Viswanathan Mohan. 2017. 'Type 2 Diabetes: Demystifying the Global Epidemic', *Diabetes*, 66: 1432-42.

van Bloemendaal, L., D. J. Veltman, J. S. Ten Kulve, P. F. Groot, H. G. Ruhe, F. Barkhof, J. H. Sloan, M. Diamant, and R. G. Ijzerman. 2015. 'Brain reward-system activation in response to anticipation and consumption of palatable food is altered by glucagon-like peptide-1 receptor activation in humans', *Diabetes Obes Metab*, 17: 878-86.

van der Laan, L. N., D. T. de Ridder, M. A. Viergever, and P. A. Smeets. 2011. 'The first taste is always with the eyes: a meta-analysis on the neural correlates of processing visual food cues', *NeuroImage*, 55: 296-303.

van Zijl, P. C., J. Hua, and H. Lu. 2012. 'The BOLD post-stimulus undershoot, one of the most debated issues in fMRI', *NeuroImage*, 62: 1092-102.

Vassena, E., R. M. Krebs, M. Silvetti, W. Fias, and T. Verguts. 2014. 'Dissociating contributions of ACC and vmPFC in reward prediction, outcome, and choice', *Neuropsychologia*, 59: 112-23.

Verhagen, J. V. 2007. 'The neurocognitive bases of human multimodal food perception: consciousness', *Brain Res Rev*, 53: 271-86.

Vidyasagar, Rishma, Arno Greyling, Richard Draijer, Douglas R. Corfield, and Laura M. Parkes. 2013. 'The effect of black tea and caffeine on regional cerebral blood flow measured with arterial spin labeling', *Journal of Cerebral Blood Flow & Metabolism*, 33: 963-68.

Vinberg, J., and K. Grill-Spector. 2008. 'Representation of shapes, edges, and surfaces across multiple cues in the human visual cortex', *J Neurophysiol*, 99: 1380-93.

Vogeser, M., D. Konig, I. Frey, H. G. Predel, K. G. Parhofer, and A. Berg. 2007. 'Fasting serum insulin and the homeostasis model of insulin resistance (HOMA-IR) in the monitoring of lifestyle interventions in obese persons', *Clin Biochem*, 40: 964-8.

Volkow, N. D., J. S. Fowler, and G. J. Wang. 2002. 'Role of dopamine in drug reinforcement and addiction in humans: results from imaging studies', *Behav Pharmacol*, 13: 355-66.

Volkow, N. D., G. J. Wang, and R. D. Baler. 2011. 'Reward, dopamine and the control of food intake: implications for obesity', *Trends Cogn Sci*, 15: 37-46.

Volkow, N. D., G. J. Wang, F. Telang, J. S. Fowler, R. Z. Goldstein, N. Alia-Klein, J. Logan, C. Wong, P. K. Thanos, Y. Ma, and K. Pradhan. 2009. 'Inverse association between BMI and prefrontal metabolic activity in healthy adults', *Obesity (Silver Spring)*, 17: 60-5.

Volkow, Nora D., Gene-Jack Wang, Joanna S. Fowler, and Frank Telang. 2008. 'Overlapping neuronal circuits in addiction and obesity: evidence of systems pathology', *Philosophical Transactions of the Royal Society B: Biological Sciences*, 363: 3191-200.

Volkow, Nora D., Gene-Jack Wang, Frank Telang, Joanna S. Fowler, Panayotis K. Thanos, Jean Logan, David Alexoff, Yu-Shin Ding, Christopher Wong, Yeming Ma, and Kith Pradhan. 2008. 'Low dopamine striatal D2 receptors are associated with prefrontal metabolism in obese subjects: possible contributing factors', *NeuroImage*, 42: 1537-43.

von Frankenberg, A. D., A. Marina, X. Song, H. S. Callahan, M. Kratz, and K. M. Utzschneider. 2017. 'A high-fat, high-saturated fat diet decreases insulin sensitivity without changing intra-abdominal fat in weight-stable overweight and obese adults', *Eur J Nutr*, 56: 431-43.

Wagner, Mark J., Tony Hyun Kim, Joan Savall, Mark J. Schnitzer, and Liqun Luo. 2017. 'Cerebellar granule cells encode the expectation of reward', *Nature*, 544: 96.

Wallace, Tara M., Jonathan C. Levy, and David R. Matthews. 2004. 'Use and Abuse of HOMA Modeling', *Diabetes Care*, 27: 1487-95.

Wallis, J. D., and S. W. Kennerley. 2011. 'Contrasting reward signals in the orbitofrontal cortex and anterior cingulate cortex', *Ann N Y Acad Sci*, 1239: 33-42.

Wallis, J. D., and E. K. Miller. 2003. 'Neuronal activity in primate dorsolateral and orbital prefrontal cortex during performance of a reward preference task', *Eur J Neurosci*, 18: 2069-81.

Wallner-Liebmann, S., K. Koschutnig, G. Reishofer, E. Sorantin, B. Blaschitz, R. Kruschitz, H. F. Unterrainer, R. Gasser, F. Freytag, C. Bauer-Denk, A. Schienle, A. Schafer, and H. Mangge. 2010. 'Insulin and hippocampus activation in response to images of high-calorie food in normal weight and obese adolescents', *Obesity (Silver Spring)*, 18: 1552-7.

Wallum, B. J., G. J. Taborsky, Jr., D. Porte, Jr., D. P. Figlewicz, L. Jacobson, J. C. Beard, W. K. Ward, and D. Dorsa. 1987. 'Cerebrospinal fluid insulin levels increase during intravenous insulin infusions in man', *J Clin Endocrinol Metab*, 64: 190-4.

Wan, Q., Z. G. Xiong, H. Y. Man, C. A. Ackerley, J. Braunton, W. Y. Lu, L. E. Becker, J. F. MacDonald, and Y. T. Wang. 1997. 'Recruitment of functional GABA(A) receptors to postsynaptic domains by insulin', *Nature*, 388: 686-90.

Wang, Danny J. J., Yufen Chen, María A. Fernández-Seara, and John A. Detre. 2011a. 'Potentials and Challenges for Arterial Spin Labeling in Pharmacological Magnetic Resonance Imaging', *The Journal of Pharmacology and Experimental Therapeutics*, 337: 359-66.

———. 2011b. 'Potentials and Challenges for Arterial Spin Labeling in Pharmacological Magnetic Resonance Imaging', *Journal of Pharmacology and Experimental Therapeutics*, 337: 359-66.

Wang, G. J., T. Dardo, A. Convit, N. D. Volkow, J. Logan, C. Wong, E. Shumay, and J. S. Fowler. 2013. 'Peripheral insulin resistance affects brain dopaminergic signaling after glucose ingestion', *Journal Nuclear Medicine*, 54: 29.

Wang, G. J., N. D. Volkow, and J. S. Fowler. 2002. 'The role of dopamine in motivation for food in humans: implications for obesity', *Expert Opin Ther Targets*, 6: 601-9.

Wang, G. J., N. D. Volkow, J. Logan, N. R. Pappas, C. T. Wong, W. Zhu, N. Netusil, and J. S. Fowler. 2001. 'Brain dopamine and obesity', *Lancet*, 357: 354-7.

Wang, J., D. J. Licht, G. H. Jahng, C. S. Liu, J. T. Rubin, J. Haselgrove, R. A. Zimmerman, and J. A. Detre. 2003. 'Pediatric perfusion imaging using pulsed arterial spin labeling', *J Magn Reson Imaging*, 18: 404-13.

Wang, Y Claire, Klim McPherson, Tim Marsh, Steven L Gortmaker, and Martin Brown. 2011. 'Health and economic burden of the projected obesity trends in the USA and the UK', *The Lancet*, 378: 815-25.

Warnken, Zachary N., Hugh D. C. Smyth, Alan B. Watts, Steve Weitman, John G. Kuhn, and Robert O. Williams. 2016. 'Formulation and device design to increase nose to brain drug delivery', *Journal of Drug Delivery Science and Technology*, 35: 213-22.

Washburn, Edward W. 1921. 'The Dynamics of Capillary Flow', *Physical Review*, 17: 273-83.

Weller, R. E., E. W. Cook, 3rd, K. B. Avsar, and J. E. Cox. 2008. 'Obese women show greater delay discounting than healthy-weight women', *Appetite*, 51: 563-9.

Wells, J. A., M. F. Lythgoe, D. G. Gadian, R. J. Ordidge, and D. L. Thomas. 2010. 'In vivo Hadamard encoded continuous arterial spin labeling (H-CASL)', *Magn Reson Med*, 63: 1111-8.

Werther, G. A., A. Hogg, B. J. Oldfield, M. J. McKinley, R. Figdor, A. M. Allen, and F. A. Mendelsohn. 1987. 'Localization and characterization of insulin receptors in rat brain and pituitary gland using in vitro autoradiography and computerized densitometry', *Endocrinology*, 121: 1562-70.

WHO. 1995. 'Physical status: the use and interpretation of anthropometry. Report of a WHO Expert Committee', *World Health Organ Tech Rep Ser*, 854: 1-452.

Wilcox, G. 2005. 'Insulin and Insulin Resistance', *Clin Biochem Rev*, 26: 19-39.

Williams, D. S., J. A. Detre, J. S. Leigh, and A. P. Koretsky. 1992. 'Magnetic resonance imaging of perfusion using spin inversion of arterial water', *Proceedings of the National Academy of Sciences of the United States of America*, 89: 212-16.

Wilson, M. M., D. R. Thomas, L. Z. Rubenstein, J. T. Chibnall, S. Anderson, A. Baxi, M. R. Diebold, and J. E. Morley. 2005. 'Appetite assessment: simple appetite questionnaire predicts weight loss in community-dwelling adults and nursing home residents', *Am J Clin Nutr*, 82: 1074-81.

Wingrove, JO. , O. O'Daly, and FO. Zelaya. 2017a. "Identification of BOLD and non-BOLD components using Multi-Echo ICA analysis: is native space better than MNI space?" In *ISMRM 25th Annual Meeting and Exhibition*. Honolulu, HI, USA: ISMRM.

———. 2017b. "Less may be better: comparison of multi-echo ICA de-noising for three and four echo EPI acquisitions in studies of seed-based functional connectivity." In *International Society for Magnetic Resonance in Medicine Meeting* Honolulu, HI, USA: ISMRM.

Wingrove, JO. , S. Wastling, P. Kundu, G. J. Barker, D. Hill, O. O'Daly, and FO. Zelaya. 2016. "Single vs Multi-Echo EPI: a Head-to-Head, within-session cross over comparison for Task Evoked and Seed Based Connectivity Analysis." In *ISMRM 24th Annual Meeting & Exhibition* Singapore.

Wingrove, JO., O. O'Daly, M. Lebel, and FO. Zelaya. 2015. "High Spatial Resolution 3D Arterial Spin Labelling Combined With Long Duratoin Labelling Pulses." In *21st British Chapter International Society for Magentic Resonance in Medicine Annual Meeting*. UCL, London, UK.

Winocur, G., M. Moscovitch, and B. Bontempi. 2010. 'Memory formation and long-term retention in humans and animals: convergence towards a transformation account of hippocampal-neocortical interactions', *Neuropsychologia*, 48: 2339-56.

Worsley, K. J., and K. J. Friston. 1995. 'Analysis of fMRI Time-Series Revisited—Again', *NeuroImage*, 2: 173-81.

Ye, F. Q., K. F. Berman, T. Ellmore, G. Esposito, J. D. van Horn, Y. Yang, J. Duyn, A. M. Smith, J. A. Frank, D. R. Weinberger, and A. C. McLaughlin. 2000. 'H(2)(15)O PET validation of steady-state arterial spin tagging cerebral blood flow measurements in humans', *Magn Reson Med*, 44: 450-6.

Ye, F. Q., J. A. Frank, D. R. Weinberger, and A. C. McLaughlin. 2000. 'Noise reduction in 3D perfusion imaging by attenuating the static signal in arterial spin tagging (ASSIST)', *Magn Reson Med*, 44: 92-100.

Yee, Lydia T. S., Katherine Roe, and Susan M. Courtney. 2010. 'Selective involvement of superior frontal cortex during working memory for shapes', *J Neurophysiol*, 103: 557-63.

Ying, Weihai. 2008. 'The nose may help the brain: intranasal drug delivery for treating neurological diseases', *Future Neurology*, 3: 1-4.

Zald, D. H., and J. V. Pardo. 2000. 'Cortical activation induced by intraoral stimulation with water in humans', *Chem Senses*, 25: 267-75.

Zelaya, F. O., M. Fernandez-Seara, K. Black, S. C. R. Williams, and M. Metha. 2016. *MR and CT Perfusion and Pharmacokinetic Imaging: Clinical Applications and Theoretical Principles, Chapter 72: Perfusion in Pharmacologic Imaging* (Lippincott Williams and Wilkins; 1 Har/Psc edition).

Zhang, Y., M. Brady, and S. Smith. 2001. 'Segmentation of brain MR images through a hidden Markov random field model and the expectation-maximization algorithm', *IEEE Trans Med Imaging*, 20: 45-57.

Ziauddeen, Hisham, Naresh Subramaniam, Victoria C. Cambridge, Nenad Medic, Ismaa Sadaf Farooqi, and Paul C. Fletcher. 2014. 'Studying food reward and motivation in humans', *Journal of visualized experiments : JoVE*: 51281.

Zimmerman, A. R., A. Mason, P. J. Rogers, and J. M. Brunstrom. 2017. 'Obese and overweight individuals are less sensitive to information about meal times in portion-size judgements', *International Journal Of Obesity*, 42: 905.

Zou, Qi-Hong, Chao-Zhe Zhu, Yihong Yang, Xi-Nian Zuo, Xiang-Yu Long, Qing-Jiu Cao, Yu-Feng Wang, and Yu-Feng Zang. 2008. 'An improved approach to detection of amplitude of low-frequency fluctuation (ALFF) for resting-state fMRI: fractional ALFF', *Journal of neuroscience methods*, 172: 137-41.

Zun, Zungho, M Lebel, A Shankaranarayana, and Zahrachuk G. 2014. "What is the Ideal Labelling Duration for Pseudocontinuosu Arterial Spin Labelling?" In *International Society for Magnetic Resonance in Medicine*. Milan, Italy.

Zuo, Xi-Nian, Adriana Di Martino, Clare Kelly, Zarrar E. Shehzad, Dylan G. Gee, Donald F. Klein, F. Xavier Castellanos, Bharat B. Biswal, and Michael P. Milham. 2010. 'The oscillating brain: Complex and reliable', *NeuroImage*, 49: 1432-45.